Author/s:
Chen, Qianyu

Title:
Organotypic airway epithelial cultures in modelling inflammation and infection

Date:
2021

Persistent Link:
https://hdl.handle.net/11343/297353

ORGANOTYPIC AIRWAY EPITHELIAL CULTURES IN MODELLING INFLAMMATION AND INFECTION

Qianyu Chen

ORCID: 0000-0001-9048-2004

Doctor of Philosophy

August 2021

Department of Biochemistry and Pharmacology
Faculty of Medicine, Dentistry and Health Sciences
The University of Melbourne

Supervisor:

Professor Alastair Stewart (Principal supervisor)

Dr Yuxiu Connie Xia (Co-supervisor)

Submitted in total fulfilment of the requirements of the degree of Doctor of Philosophy

ABSTRACT

Respiratory diseases, including severe asthma and chronic obstructive pulmonary disease (COPD), are conditions with significant unmet need. However, many drug developments have failed, despite showing impressive efficacy in pre-clinical models. Biomechanical characteristics of the preclinical in vitro models have been highlighted as important influences on cell morphology, proliferation, and other physiological functions. The majority of pre-clinical research is carried out in conventional plastic culture systems, which is an environment much stiffer than human tissues. Matrix stiffness in respiratory system as a biomechanical characteristic has been highlighted for its contribution to therapies and pathogenesis in fibroblasts and airway smooth muscle cells. Airway epithelial cells reside on basement membrane, which becomes thicker in the remodelled airway. The influence of matrix stiffness on airway epithelium remains to be established.

Airway epithelium plays critical roles in the pathogenesis of inflammatory and allergic diseases, such as asthma, COPD, and respiratory infections. The Coronavirus disease 2019 (COVID-19) caused by infection with the severe acute respiratory syndrome coronavirus 2 (SARS-CoV-2) is an acute respiratory disease with systemic complications. Therapeutic strategies for COVID-19, including repurposing (partially) developed drugs are urgently needed, regardless of the increasingly successful vaccination outcomes. Over the past decades, the development of organotypic cellular cultures has enabled researchers to not only recapitulate the *in vivo* architecture and cell diversities, but also provide cells a physio(patho)logically relevant mechanical environment.

The data presented in this thesis have provided evidence that matrix stiffness has an influence on airway epithelial cell biology. Soft environments protected airway epithelial cells from transforming growth factor (TGF-β) induced production of fibrotic proteins and epithelial-mesenchymal transition. Our data highlighted the marked induction of epithelial sodium channel α (ENaCα) by soft environments. Matrix stiffness also has a potential influence on ENaCα activity.

Within this thesis, airway organoid droplet culture was applied and modified with a silicone mask, enabling standardization and potential industrialization. The culture medium and cell conditions are critical for mucociliary differentiation in air-liquid interface (ALI) and airway organoid culture. This thesis systematically compared the utility of airway epithelial cultures, from two-dimensional to three-dimensional, submerged to organotypic, in modelling

inflammation and infection. Our data suggested that air-liquid interface culture and airway organoid culture are the most promising models in SARS-CoV-2 infection. The relevance of these findings is supported by observations that ALI cultures are susceptible to SARS-CoV-2, whereas submerged airway epithelial cells are not. Our data also highlighted the lack of cytokine induction responses in SARS-CoV-2 infected ALI cultures, that appears to be consistent with the overwhelmingly asymptomatic transmission of COVID-19.

This thesis has demonstrated the importance of matrix stiffness to be considered in studying airway epithelial cells, which may provide insights into new therapeutic targets for fibrosis. Through the systematic comparison of airway epithelial cultures in modelling inflammation and infection, this thesis has provided evidence that organotypic, and particularly ALI airway cultures are valid tools for investigation of SARS-CoV-2 infection and evaluating the clinical potential of therapeutics for COVID-19.

DECLARATION

This is to certify that

a) This thesis comprises only my original work towards the PhD except where indicated in the preface;
b) Due acknowledgement has been made in the text to all other material used;
c) This thesis is fewer than 100,000 word limit in length, exclusive of tables, maps, bibliographies and appendices.

Qianyu Chen, MSc

Date: August 2021

PREFACE

I acknowledge that specific contributions to the experiments carried out in this thesis were performed by others:

- The microtome cutting of human airway biopsies from the Melbourne Epidemiological Study of Childhood Asthma (MESCA) and air-liquid interface culture paraffin blocks were performed by Ms Shenna Langenbach.
- The immunohistochemistry staining of ACE2 on MESCA paraffin sections was conducted by Ms Shenna Langenbach.
- Preparation of rat-tail collagen for establishing air-liquid interface cultures was assisted by Ms Trudi Harris.
- The air-liquid interface culture generated from asthmatic and COPD patient derived primary bronchial epithelial cells were conducted by Dr. Meina Li, Dr. Danica Prodanovic, Dr. Connie Xia, and Ms Trudi Harris.
- The silicone mask for airway organoid culture was prepared by Dr. Bryan Gao.
- The SARS-CoV-2 infection was performed by Dr. Elizabeth Pharo, Dr. Sinéad Williams, Mr Shawn Todd, Dr. Michelle Baker, Dr. Matthew Gartner, and Dr. Kanta Subbarao.

I acknowledge that the relationship of ENaC and matrix stiffness hasn't been fully addressed in this thesis, due to COVID-19 pandemic. In response to COVID-19, the work presented in Chapter 6 was generated to enable timely completion.

The Chapter 6 of this thesis is in preparation to submit for publication.

This thesis was supported by grants from NHMRC [1181637] and ARC [IC170100016] Industry Transformation Training Centre for Personalised Therapeutics Technologies and the Melbourne Research Scholarship/Australia Government Research Training Program Scholarship.

ETHICS STATEMENT

All experiments using cells and tissues from animal or human origin were conducted in accordance with the Australian Code of Practice for the Care and Use of Animals for Scientific Purposes, and the National Statement on Ethical Conduct in Human Research.

ACKNOWLEDGEMENTS

First and foremost, I would like to express my sincere appreciation and gratitude to my principal supervisor, Professor Alastair Stewart. Thank you for all the support throughout the years. Your imaginative ideas, fascinating enthusiasm, and creative suggestions have facilitated my research and helped me to complete my PhD life. I would also like to thank you for giving me opportunities and supports to attend national and international conferences and symposium, participate in various studies, and most importantly devote in studying SARS-CoV-2. It is a challenging ending year of my PhD with COVID-19 restrictions. Your optimistic gratitude, patience, and virtual greetings have greatly encouraged me to conquer all the challenges. Above all, thank you for having me in the Stewart lab and mentoring me.

I would like to thank my co-supervisor, Dr. Yuxiu Connie Xia, for sharing me all your "little tricks" in experiments and inspiring me in my research and life. I really appreciate your accompanying in the lab and respect your determination.

I would also like to thank my supervisory committee members Dr. Michael Lew, Dr. Jonathan Mangum, Dr. Susan Northfield for their invaluable advice and encouragement throughout my candidature. Special thanks to Dr. Meina Li and Ms Shenna Langenbach for instructing and demonstrating me in the laboratory work and supporting me throughout my candidature. Special thanks to Dr. Bryan Gao for his assistance in making silicone mask and all the engineering modifications.

I must also acknowledge the contribution of Dr. Mathew Gartner and Prof. Kanta Subbarao on SARS-CoV-2 infection work. I am also thankful for Dr. Elizabeth Pharo, Dr. Sinéad Williams, and Dr. Michelle Baker for sharing the experience in air-liquid interface culture and contributing to SARS-CoV-2 infection work.

Thank you to all the lovely past and present members of Stewart lab: Trudi Harris, Shenna Langenbach, Danica Prodanović, Asres Berhan Mitke, Yan Tu, Fernando Jativa, Mehdi Zia, Bryan Gao, Meina Li, Tianhong Tina Cheng, Yanqi Wu, Wenjia Lu, Xin Li, and Stephanie Zhang. You have all immensely contributed to my personal and professional time throughout my PhD studies. I enjoyed my lab life with all of you and our lunch time filled with jokes and laughs. Special thanks to Bryan and Shenna for your supportive companions in the lab during COVID-19 lockdown. Special mention must also be made to Tina and Yanqi for your support and companions outside the lab during COVID-19 time.

Thank you to all the members of the Department of Biochemistry and Pharmacology. I would like to thank Dr. Mark Habgood and Netzie Bebing for giving me the opportunity to develop my teaching and demonstrating skills in practical classes. Big thank you to all the Students of Pharmacology (StOP) members, particularly Nithya Fernandopulle, Amna Mazeh, Zachery Moore, and Irene Lin, for all the support and overall great times in the past four years.

I would like to thank my friend Vivian Guo for all your support. I would not have decided to come to Australia without you. I sincerely feel lucky to be friend with you and Fiona Liu since our high school. I would like to thank Yuehan Zhao for offering me a warm home in Australia and our friendship. Thanks to Xianhui Chen and Tianyu He for your international support throughout the four years and our happy time in Los Angeles.

Special and sincere thanks go to my mum and dad for their continuous support and encouragement. It is painful not able to see them but also comforting that we all stay healthy since COVID-19. The unconditional love from my parents is the driving force for me to finish this wonderful journey.

COMMUNICATIONS

Publications:

1. Prodanovic, D., Keenan, C.R., Langenbach, S., Li, M., **Chen, Q.**, Lew, M.J., and Stewart, A.G. (2017). Cortisol limits selected actions of synthetic glucocorticoids in the airway epithelium. The FASEB Journal, fj. 201700730R.

2. Keenan, C.R., Langenbach, S.Y., Jativa, F., Harris, T., Li, M., **Chen, Q.**, Xia, Y., Gao, B., Schuliga, M.J., Jaffar, J., et al. (2018). Casein Kinase 1delta/epsilon Inhibitor, PF670462 Attenuates the Fibrogenic Effects of Transforming Growth Factor-beta in Pulmonary Fibrosis. Front Pharmacol, 9, 738.

3. Li, M., Keenan, C.R., Lopez-Campos, G., Mangum, J.E., **Chen, Q.**, Prodanovic, D., Xia, Y.C., Langenbach, S.Y., Harris, T., Hofferek, V., et al. (2019). A Non-canonical Pathway with Potential for Safer Modulation of Transforming Growth Factor-beta1 in Steroid-Resistant Airway Diseases. iScience, 12, 232-246.

4. Fustin, J.M., Li, M., Gao, B., **Chen, Q.**, Cheng, T., and Stewart, A.G. (2019). Rhythm on a chip: circadian entrainment in vitro is the next frontier in body-on-a chip technology. Curr Opin Pharmacol, 48, 127-136.

5. Wu, Y., Cheng, T., **Chen, Q.**, Gao, B., Stewart, A.G., and Lee, P.V.S. (2020). On-chip surface acoustic wave and micropipette aspiration techniques to assess cell elastic properties. Biomicrofluidics, 14, 014114.

Conference presentations

1. The Thoracic Society of Australia & New Zealand (TSANZ) Annual Scientific Meeting 2018, Adelaide, Australia
   Poster discussion
   Chen, Q., Li, M., Wu, Y., Xia, Y., Langenbach, S., Lee, P.V.S., Stewart, A.G. Physiological stiffness is critical for emulation of glucocorticoid responses.

2. American Thoracic Society (ATS) International Conference 2018, San Diego, USA
   Poster discussion
   Chen, Q., Li, M., Wu, Y., Xia, Y., Langenbach, S., Lee, P.V.S., Stewart, A.G.
   Culture of epithelial cells on unphysiologically stiff plastic perturbs baseline and glucocorticoid induced gene expression.

3. ARC centre for Personalised Therapeutics Technologies 2019 Training, Melbourne, Australia
   Oral presentation
   Chen, Q..
   Airway organoids: cilia beating inside-out and inside-in.

4. 11st Young Investigator Meeting on Airway Smooth Muscle, 2019, Sydney, Australia
   Oral presentation
   Chen, Q., Gao, B., Clarke, N., Ranganathan, S.C., Stewart, A.G.
   Matrix is critical for emulation of airway epithelial cell biological behaviour.

5. Cutting Edge Symposia: Challenges and Opportunities for "ex vivo" Model Systems, 2020, Geelong, Australia
   Oral presentation
   Chen, Q., Clarke, N., Ranganathan, S.C., Stewart, A.G.
   A comparison of airway organoids and air-liquid interface as tools in respiratory research.

6. 2020 ARC centre for Personalised Therapeutics Technologies Training Forum Symposium, Melbourne, Australia
   Oral presentation
   Chen, Q..
   Organotypic airway cultures for SARS-COV-2 research.

TABLE OF CONTENTS

LIST OF TABLES

LIST OF FIGURES

ABBREVIATIONS

18s	18s ribosomal RNA
2D	Two-dimensional
3D	Three-dimensional
ACE2	Angiotensin converting enzyme 2
ACF	Animal component-free
ALF	The Alfred hospital
ALI	Air-liquid interface
ANOVA	Analysis of variance
AO media	Airway organoid media
ASL	Airway surface liquid
ATI	Alveolar epithelial type I
ATII	Alveolar epithelial type II
BEGM	Bronchial epithelial growth medium
BPE	Bovine pituitary extract
BSA	Bovine serum albumin
Bud	Budesonide
Cas9	CRISPR associated protein 9
CBF	Cilia beating frequency
CC10	Club cell protein 10
CDKN1C	Cyclin-dependent kinase inhibitor 1C
cDNA	Complementary deoxyribonuclieic acid
CF	Cystic fibrosis
CFTR	Cystic fibrosis transmembrane conductance regulator

COL1A	Collagen type I alpha
COPD	Chronic obstructive pulmonary disease
COVID-19	Coronavirus disease 2019
COX-2	Cyclooxygenase-2
CRISPR	Clustered regularly interspaced short palindromic repeats
CT	Cycle threshold
DAB	3,3'-diaminobenzidine
DAPI	4’,6-diamidino-2-phenylindole
DEG	Degenerin
DEPC	Diethylpyrocarbonate
Dex	Dexamethasone
DMEM	Dulbecco's modified Eagles medium
DMSO	Dimethylsulphoxide
DNA	Deoxyribonucleic acid
DNAH1	Dynein heavy chain 1
DNAH5	Dynein heavy chain 5
E-Cad	E-Cadherin
ECM	Extracellular matrix
EDTA	Ethylenediaminetetraacetic acid
EGF	Epidermal growth factor
EGFR	Epidermal growth factor receptor
EIPA	5-(N-Ethyl-N-isopropyl) amiloride
ELISA	Enzyme-linked immunosorbent assay
EMT	Epithelial-mesenchymal transition
ENaC	Epithelial sodium channel

ERK	Extracellular signal-regulated kinase
F-actin	Filamentous actin
FCS	Fetal calf serum
FEV_1	Forced expiratory volume in one second
FGF	Fibroblast growth factor
FIS assay	Forskolin-induced
Form	Formoterol
FOXJ1	Forkhead box protein J1
G-actin	Globular actin
GA	Gentamicin
GC	Glucocorticoid
GFR	Growth factor reduced
GILZ	Glucocorticoid-induced leucine zipper
GM-CSF	Granulocyte macrophage colony-stimulating factor
H&E staining	Hematoxylin and eosin stain
HBEB	Human bronchial epithelial brushing cell
HBEC	Human bronchial epithelial cell
HC	Hydrocortisone
HEPES	4-(2-hydroxyethyl)-1-piperazineethanesulfonic acid
HIFCS	Heat inactivated fetal calf serum
HRP	Horseradish peroxidase
ICS	Inhaled corticosteroid
IF	Immunofluorescence
IFN	Interferon
Ig	Immunoglobulin

IHC	Immunohistochemistry
IL	Interleukin
IPF	Idiopathic pulmonary fibrosis
iPSC	Induced pluripotent stem cell
ITGA6	Integrin alpha 6
IκB	Inhibitor of nuclear factor kappa B
KRT5	Keratin 5
LABA	Long-acting β_2-agonist
LDH	Lactate dehydrogenase
LHC-9	Laboratory of human carcinogenesis medium #9
LPS	Lipopolysaccharides
MAPK	Mitogen-activated protein kinase
MESCA	Melbourne epidemiological study of childhood asthma
MKP-1	MAP kinase phosphatase 1
mRNA	Messenger RNA
MRTFs	Myocardin-related transcription factors
MUC5AC	Mucin 5AC
MUC5B	Mucin 5B
N-Cad	N-Cadherin
NBF	Neutral buffered formalin
NF-κB	Nuclear factor kappa B
NHBE	Normal human bronchial epithelial cell
P-ALI	PneumaCult™ ALI medium
PAI-1	Plasminogen activator inhibitor-1
PBS	Phosphate buffered saline

PCL	Periciliary layer
PDMS	Polydimethylsiloxane
PGE_2	Prostaglandin E_2
Poly I:C	Polyinosinic:polycytidylic acid
Poly-HEMA	Poly (2-hydroxyethyl methacrylate)
PSC	Pluripotent stem cell
PTHLH	Parathyroid hormone like hormone
PTHrP	Parathyroid hormone-related protein
RA	Retinoid acid
RFU	Relative fluorescence units
RNA	Ribonucleic acid
ROCK	Rho kinase
RSV	Respiratory syncytial virus
RT-qPCR	Real time quantitative polymerase chain reaction
SARS-COV-2	Severe acute respiratory syndrome coronavirus 2
SEM	Standard error of mean
SMAD	SMA and MAD related proteins
SRF	Serum response factor
TAZ	Transcriptional coactivator with PDZ-binding motif
TEAD	TEA domain family member
TEER	Transepithelial electrical resistance
TFF3	Trefoil factor 3
TGF-β	Transforming growth factor beta
TLR	Toll-like receptor
TMB	3,3',5,5'-tetramethylbenzidine

TMPRSS2	Transmembrane protease, serine 2
TNF-α	Tumour necrosis factor alpha
TNS	Trypsin neutralising solution
vRNA	Viral RNA
YAP	Yes-associated protein
ZO-1	Tight junction protein 1
α-SMA	Alpha smooth muscle actin

CHAPTER 1

GENERAL INTRODUCTION

1.1 Lessons from clinical trial failure

1.1.1 Drug efficacy in clinical trials

Drug development undergoes 3 main steps: discovery, preclinical research, and clinical trial. Clinical trials follow a series from early, small-scale, Phase I safety-related studies to late-stage, large-scale, Phase III efficacy-related studies. Recent data indicated an increased probability of success of late stage development, from phase III to market (Dowden and Munro, 2019). However, the probability of success from drug discovery to enter the market remains below 10%. Analysis of the reasons for clinical trial failure from 2007 to 2015 have been nearly unchanged (**Figure 1.1**) (Arrowsmith, 2011; Cook et al., 2014; Harrison, 2016). Among these reasons, over 50% were due to lack of efficacy; about 25% were due to lack of safety; 15% were resulted from strategic realignment; 6-7% were for commercial reasons; last 1-3% were because of operational or technical shortcomings (Graul et al., 2019; Graul et al., 2018; Graul et al., 2017; Graul et al., 2020; Graul and Sorbera, 2021).

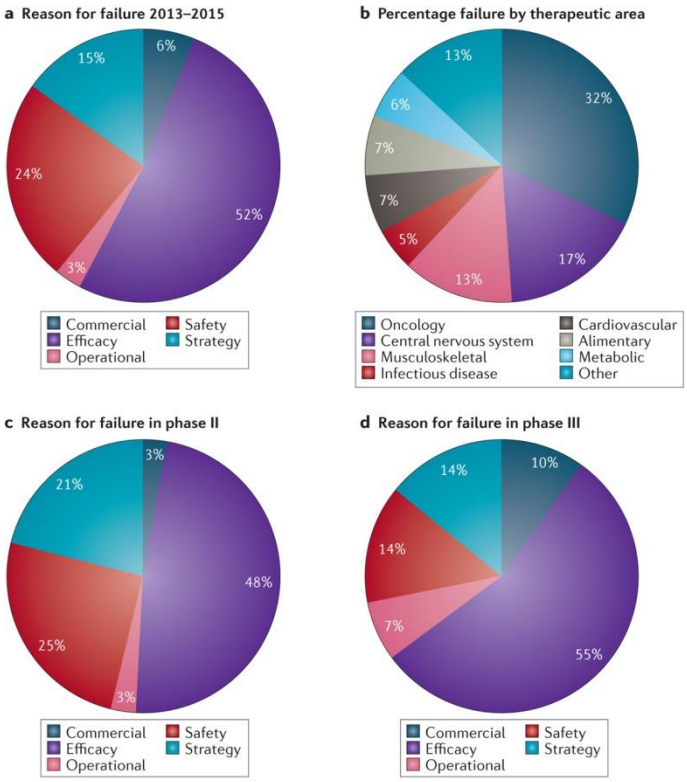

Figure 1.1 Reasons for failure in clinical trials

Reproduced from (Harrison, 2016) with the permission of Springer Nature.

1.1.2 Tissue mechanics

The gap between unphysiological plastic and human body could be one of the reasons to explain the fact that preclinical successful drugs failed in clinical trial. It is clear that these *in vitro* models have contributed to the progression of the drug developments. However, many drugs failed to have efficacy, even though they are effective in these models. For instance, epidermal growth factor receptor (EGFR) pathway regulates airway mucus cell hyperplasia and mucus production (Vallath et al., 2014). BIBX 1522, a selective inhibitor of EGFR tyrosine kinase (TKI), can prevent mucin upregulation in *Pseudomonas aeruginosa* stimulated human airway epithelial cells, which was performed in conventional plastic cell culture plates (Kohri et al., 2002). However, safety and efficacy trial of BIBW 2948, a more potent EGFR TKI, found that this antagonist had no significant efficacy in reducing mucin stores in airway epithelial cells of chronic obstructive pulmonary disease (COPD) patients and there was a dose-related increase in adverse events (Woodruff et al., 2010). Another example is that imatinib was shown to be excellent in inhibiting transforming growth factor beta (TGF-β) induced fibrosis but ineffective in patients with idiopathic pulmonary fibrosis, albeit it succeeded in mouse model (Daniels et al., 2010; Daniels et al., 2004).

Human tissues are complex materials that can exhibit nonlinear, time-dependent, inhomogeneous and anisotropic behaviours (Yohan Payan, 2017). The term “cell microenvironment” describes these complex, heterotypic, and dynamic set of biochemical and biophysical cues (Huang et al., 2017). Generally, there are four key common features of cell microenvironment, including neighbouring cells, soluble factors, extracellular matrix (ECM), and biophysical factors. Among these, ECM not only provides structural support for cells but also regulates cell behaviours through its biomechanical properties, which is of interest to our group. Since the mechanical properties of living tissues have been systematically described (Fung, 1993), many research groups have proposed biomechanical models to study their physiology and mechanical behaviours (Keeratichamroen et al., 2018; Meng, 2010; Narkhede et al., 2018). The mechanical interactions between cells and ECM have been reported to be essential in biological behaviours, like migration (Narkhede et al., 2018), differentiation (Engler et al., 2006), morphogenesis (Linde-Medina and Marcucio, 2018), and proliferation (Keeratichamroen et al., 2018; Narkhede et al., 2018). “Stiffness” is a term used to describe the force needed to achieve a certain deformation of a structure (Baumgart, 2000). External forces transfer from ECM to cell and the cell would generate forces within itself to affect its overall deformability and stiffness, called “outside-in” forces

and “inside-out” forces (Discher et al., 2005b; Krishnan et al., 2016). Cells grown on hard or soft substrates could regulate cellular stiffness and traction force, respectively, with the cell responding constantly to its external microenvironment (Discher et al., 2009). Our lab has previously highlighted the importance of prostaglandin E_2 (PGE_2) in feedback on tissue stiffening (Berhan et al., 2020; Stewart et al., 2018). Tissue stiffening in response to injury and repair activates TGF-β, causing further stiffening. PGE_2 can soften myofibroblasts. Therefore, repressed PGE_2 synthesis may result in further stiffening.

1.1.3 Cell type diversity

In drug development, preclinical research begins before clinical trials, and includes pharmacodynamics, pharmacokinetics, and toxicology testing. Both *in vitro* and *in vivo* studies will be conducted to guide dosing for clinical trial and assess potential toxicity of the product. In most circumstances, only single cell type is used in *in vitro* studies. The lack of cell type diversity may not fully reflect their functions in multicellular organisms. Human body has an estimated number of 10^{12} to 10^{13} cells (Alberts et al., 2015; Sender et al., 2016). Over 400 cell types have been identified in normal healthy human body (Vickaryous and Hall, 2006). Among them, not all the cell types can be maintained *in vitro*. Many cells even change their morphology and function when established into *in vitro* culture. Chondrocytes in culture lose their differentiated phenotype and produce type I procollagen and fibronectin, instead of producing type II collagen (Alberts B, 2002; Aulthouse et al., 1989). Different cell types require different culture conditions, especially for stem cells. Essential growth factors for one cell type often will interfere the growth or function of other cell type, which create more challenges for co-culture. Serum-free medium for primary human bronchial epithelial cells cannot support fibroblast proliferation, albeit supplemented with bovine pituitary extract. Recently, more serum-free medium for fibroblasts have been developed, potentially providing tools to break the boundary for co-culture of these cells with epithelia. Moreover, organotypic culture and organ-on-chip also offer a system with multiple cell types to comprehensively study cell physiology and pathology (da Silva da Costa et al., 2021; Huh et al., 2010; Lu et al., 2021).

1.2 Mechanopharmacology

In 2004, “mechanophamacology” was used to describe the study of the mechanics of individual proteins that modulation of membrane proteins by amphipathic peptides involving not only the protein itself but also the surrounding lipids (Suchyna et al., 2004). Mechanotransduction describes the overall process of how cells sense a mechanical stimulus and converts it into a biochemical, intracellular response (Jansen et al., 2017). It requires “mechanosensor” to sense the external forces of mechanical properties and then “mechanotransducers” transduce this information through specific “mechanosignalling” to induce a series of reactions.

Currently, the term of “mechanopharmacology” is a subdiscipline that applies biomechanically appropriate settings *in vitro* and *in vivo* to reflect the relevant (patho)physiology with a view to improved identification of new drugs and drug targets. (Krishnan et al., 2016). For example, several therapeutic strategies against chemoresistant pancreatic cancer failed to meet their preclinical expectation. Researchers then turned attention to novel experimental avenues, such as elastic micropillar arrays that provide fresh insights for the development of mechanopharmacology (Coppola et al., 2017). To build such an ideal microenvironment, methodologies that expose drugs to mediators while cells are maintained in a three-dimensional (3D) condition with appropriate mechanical properties need to be improved. Recently, a high-throughput mechanopharmacological drug screening platform for stroma-reprogrammed combinatorial therapy (SRCT) was established based on biomechanically primed hepatic stromal stellate cells, leading to reduced “barrier effects” and increased tissue-infiltration of chemotherapy drug (Zhu et al., 2017a). Therefore, providing cells with microenvironment that mimics actual mechanical extracellular environment would enable researchers to improve the relevance of drug discovery and screening models to human tissues.

1.2.1 Mechanosensor

Every cell in a living body will be facing a myriad of mechanical forces, including internal pulling forces, dictated by the tension and organization of the cytoskeleton, and counterbalancing external forces, such as the topology and rigidity of the surrounding extracellular matrix and other cells (Panciera et al., 2017). It has been accepted that stretch-activated ion channels, adhesion complexes, cell-cell junctions and cytoskeletal components

can function as mechanosensitive elements (Ali and Schumacker, 2002; Murthy et al., 2017; Ross et al., 2013).

Ion channels are recognized as potential mechanosensors because they locate at the plasma membrane and can ideally convert the mechanical forces into electrical or ion-dependent cellular signal (Gillespie and Walker, 2001). As reviewed by Ben-Shahar, the function of degenerin/epithelial sodium channels (DEG/ENaC) have been implicated in mechanosensation, as well as chemosensory transduction pathways (Ben-Shahar, 2011). K^+ and Ca^+ channels can transduce shear stress and mechanical strain in endothelium (Ali and Schumacker, 2002). Piezos, the largest known pore-forming multimeric and *bona fide* mechanically activated ion channels, can also be activated by various physiologically relevant physical forces to serve as mechanosensors (Murthy et al., 2017).

There are complex plasma membrane-associated macromolecular cell-cell and cell-ECM adhesions. These adhesions engage via integrin receptors and physically connect with F-actin cytoskeleton. Since the composition of these adhesions change reacted to the physical forces of the integrin-associated adhesion sites, they are therefore categorized as mechanosensors (Jansen et al., 2017; Kuo, 2014; Sun et al., 2016).

Interestingly, the nucleus has now also been viewed as a cellular mechanosensor. Recent findings indicating that external mechanical forces trigger changes in nuclear envelope structure and composition, chromatin organization and gene expression, support a direct role of the nucleus in cellular mechanosensing (Athirasala et al., 2017; Kirby and Lammerding, 2018).

1.2.2 Mehcanotransducers and mechanosignaling

The myocardin-related transcription factors (MRTFs)-serum response factor (SRF) and YAP (Yes-associated protein)/TAZ (transcriptional coactivator with PDZ-binding motif)-TEAD (TEA domain family member) are thought to be involved in the mechanosignaling as mechanotransducers. There is evidence supporting a contribution of MRTF-SRF circuit to endothelial-to-mesenchymal transition in cardiac fibrosis (Sharma et al., 2017) and protection of lung fibrosis (Zhou et al., 2013) when YAP/TAZ can promote myofibroblast activation by matrix stiffness (Liu et al., 2015; Liu et al., 2010). There is growing support for the suggestion that the MRTFs and YAP/TAZ functionally interact each other (Foster et al., 2017; Kim et al., 2017; Olivia et al., 2016; Speight et al., 2016). However, the mechanosignaling

sensed by ion channels is still unclear (Ben-Shahar, 2011; Murthy et al., 2017). Novel models are needed for understanding how they exert their mechanotransduction influence and to establish their more general importance in regulating biological processes.

1.2.2.1 MRTF-SRF signalling

MRTF-A and MRTF-B, also known as MAL and MKL2, are most widely expressed MRTF family members (Wang et al., 2002). Under physiological conditions, nuclear MRTF is complexed by nuclear globular actin (G-actin), which inhibits MRTF-mediated stimulation of SRF-dependent transcription and facilitates MRTF nuclear export (Vartiainen et al., 2007). Tracing back the activation of MRTF nuclear translocation, the well-known signalling is through the activation of Rho GTPases by diverse extracellular stimulation and then the actin polymerization of incorporating G-actin into the filamentous actin (F-actin) polymer (Allingham et al., 2006; Pollard, 2007). As reviewed by Olson, the activity of Rho GTPase activity can be modulated by several types of plasma membrane receptors, G protein-coupled receptors (GPCRs), receptor Tyr kinases (RTKs), integrins as structural mediators of focal adhesions, transforming growth factor-β receptors (TGFβRs), E-cadherins at *adherens* junctions, and Frizzled, the non-canonical Wnt-planar cell polarity (PCP) pathway (**Figure 1.2**) (Olson and Nordheim, 2010). The activation of MRTF-SRF would lead to the expression of genes (e.g., actin), effectors of actin turnover (e.g., Cofilin1), and regulators of actin dynamics (e.g., Talin1) (Olson and Nordheim, 2010). Increased matrix stiffness drives MRTF-A/B nuclear translocation and activation of pro-fibrotic gene expression, which including α smooth muscle actin (α-SMA) (Johnson et al., 2013; Velasquez et al., 2013).

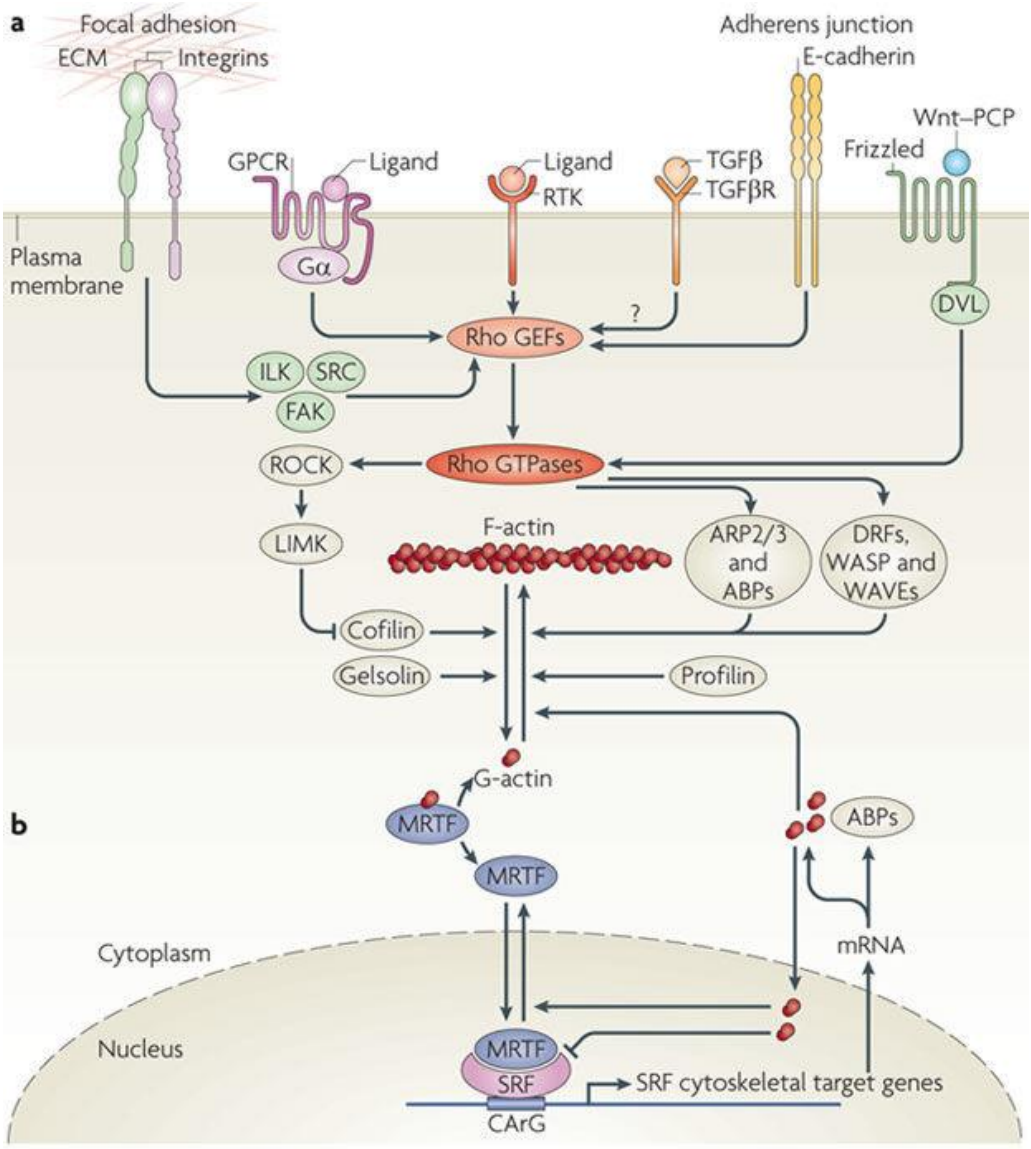

Figure 1.2 Receptors affecting actin dynamics and MRTF-mediated regulation of SRF target genes

Reproduced from (Olson and Nordheim, 2010) with the permission of Springer Nature.

1.2.2.2 YAP/TAZ-TEAD signalling

YAP and TAZ are transcriptional co-regulators that bind to TEAD factors. They are best understood in the evolutionarily conserved Hippo signalling pathway that controls organ size by regulating cell proliferation, apoptosis, and stem cell self-renewal (Pan, 2010; Piccolo et al., 2014; Yu et al., 2015). The upstream kinases MST1 and MST2 trigger phosphorylation and activation of the kinases LATS1/2, which in turn phosphorylate and inhibit YAP/TAZ nuclear translocation to interact with TEAD. However, currently there is evidence from

various systems indicating that YAP/TAZ mechanosignaling is independent of Hippo signalling (Aragona et al., 2013; Dupont et al., 2011; Feng et al., 2014).

Similarly, the activation of YAP/TAZ of nuclear translocation is regulated by cell shape, rigidity and topology of ECM, and shear stress (**Figure 1.3**) (Calvo et al., 2013; Dupont et al., 2011; Halder et al., 2012; Wang et al., 2016). Once the mechanical forces are detected by mechanosensors, like integrins, *adherens* junctions, focal adhesion kinase (FAK) and SRC-family kinases (a family of tyrosine kinases having impact on phosphotyrosine proteome and diverse cell behaviours), the information would be passed to activate YAP/TAZ (Panciera et al., 2017; Tzima et al., 2001). Interestingly, the Rho GTPases signalling is also essential for YPA/TAZ transduction (Aragona et al., 2013; Tzima et al., 2001). Till now, YAP/TAZ has been implicated in atherosclerosis and cardiovascular diseases, tissue fibrosis, inflammatory responses, muscular dystrophy, and cancer (Panciera et al., 2017). Specifically, they can promote fibroblast activation by regulating pro-fibrotic gene expression, such as type I collagen and αSMA (Liang et al., 2017; Liu et al., 2015).

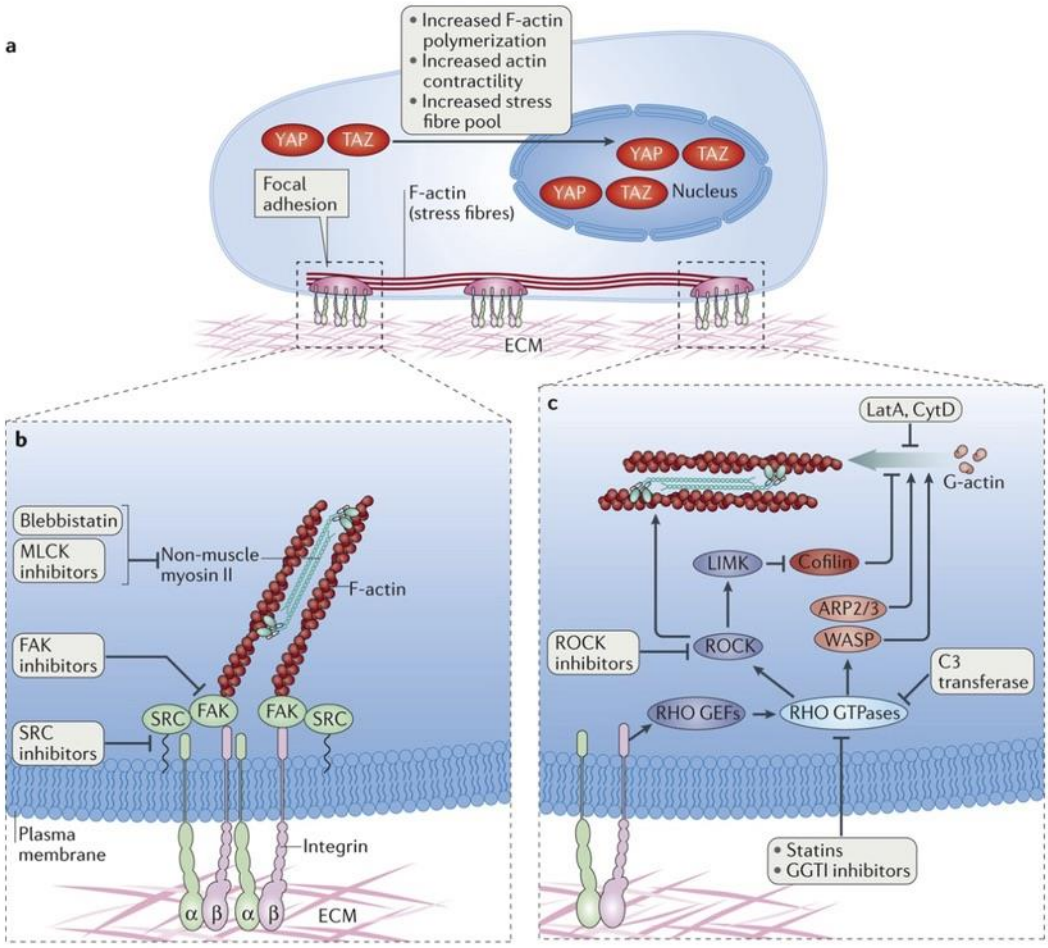

Figure 1.3 Molecular players involved in YAP and TAZ mechanotransduction signalling

Reproduced from (Panciera et al., 2017) with the permission of Springer Nature.

1.2.3 Physiological models in mechanopharmacology

To mimic a physiological microenvironment, there are two key factors needed: a dynamic environment that is biomechanically similar to the target organs or cells; a structure of quantitative measurable biomechanical activity (Krishnan et al., 2016).

Conventionally, the tissue culture plastic is coated by polystyrene for its excellent optical clarity and can be easily molded and sterilized by irradiation. However, it possesses a Young's modulus ranging from 2 to 4 GPa (Butcher et al., 2009), while human tissue stiffness ranging from around 1kPa (as in lung) (Goss et al., 2006) to very rigid of 6.9-31.6 GPa (as in bone) (Thurner, 2009), suggesting that most cells cultured on it will experience a much stiffer surface (**Figure 1.4**).

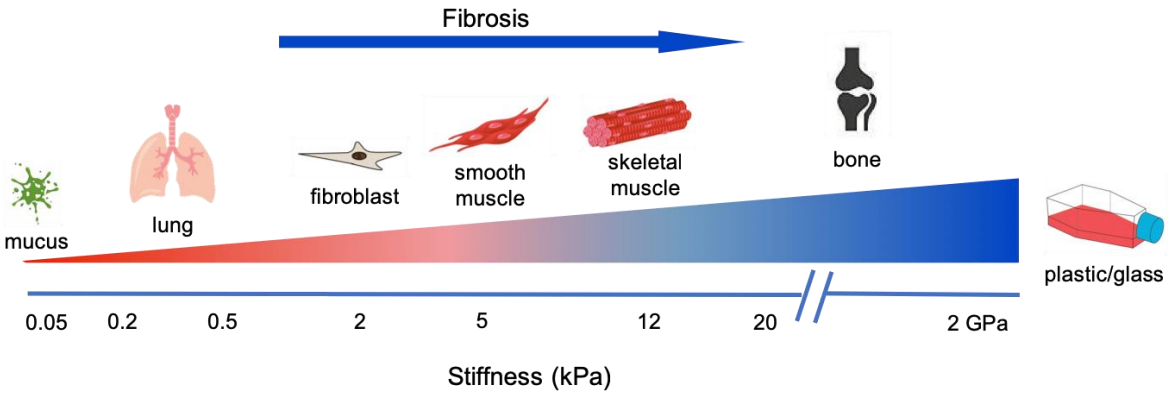

Figure 1.4 Stiffness of human tissues and culture plastic

1.2.3.1 Stiffness tuneable substrate

In 2001, Cukierman et al. compared the composition and function of adhesions between two-dimensional (2D) substrates and 3D-matrix, indicating that there were distinctive differences in structure, localization and function *in vivo* 3D-matrix adhesions that would be more biologically relevant to living organisms (Cukierman et al., 2001). Now the most widely used strategy is to synthesize stiffness tuneable hydrogel. By modulating the intensity of UV light exposure of polyacrylamide substrate, hydrogel with mechanical compliance gradients was used to study migration of vascular smooth muscle cells (Wong et al., 2003). A rapid fabrication process for multiwall platforms with polyacrylamide hydrogels ranging from 0.3 to 55 kPa was established for routine screening of stiffness-dependent cell biology (Mih et al., 2011). Defined stiffness collagen-conjugated polyacrylamide hydrogels was achieved by controlling the molar ratio between *N,N'*-methylenebis-(acrylamide) and acrylamide (Shkumatov et al., 2015).

1.2.3.2 Decellularized matrices

Although the approaches mentioned above are more appropriate than culturing cells on plastic plates, they are limited in lacking the variability of the complex ECM of organs *in situ*. Some investigators turned to rely on acellular matrices. Ott et al. and colleagues demonstrated an ability to regenerate functional lungs (Ott et al., 2010; Petersen et al., 2010) and heart (Ott et al., 2008) by repopulating acellular matrices with various cell types. Further, Booth et al. used this decellularized human lung matrices to address how ECM influences fibroblast phenotype in a disease-specific manner (Booth et al., 2012).

1.2.3.3 Three-dimensional spheroids

3D cultures are regarded as an effective method to reflect *in vivo* microenvironment for cancer research and toxicological studies (Meng, 2010; Ramaiahgari et al., 2014). 3D spheroid is thought to able to better replicate cell-cell communications as well as cell-autonomous and cell non-autonomous contributions than 2D cell culture (Lancaster and Knoblich, 2014). 3D pulmospheres, composed by cells derived exclusively from primary lung biopsy tissues of patients, were developed to exploit the invasive phenotype of idiopathic pulmonary fibrosis (IPF) lung tissue to evaluate anti-fibrotic drugs (Surolia et al., 2017). 3D spheroid is also believed to be more effective for mimicking tumour behaviour than 2D culture and has been applied in high throughput high-content imaging and analysis methods to characterize phenotypic changes in response to compound treatment (Sirenko et al., 2015). Our lab has used spheroids to demonstrate the therapeutic potential of casein kinase 1 delta and epsilon (CK1δ/ε) inhibitor PF670462 for IPF (Keenan et al., 2018) and emphasize the dysregulation of prostanoid biosynthesis and signalling pathways in fibroblasts from IPF patients (Berhan et al., 2020), which provide subtle structure with realistic cell density than those in hydrogels that preclude cell-cell contact (Bourke et al., 2011; Fustin et al., 2019; Schuliga et al., 2010; Schuliga et al., 2009).

1.2.3.4 Organoids

"Organoids" have been conferred as a self-organizing 3D structure grown from stem cells which mimics the *in vivo* architecture and multi-lineage differentiation of the original tissue in mammal (Dutta et al., 2017). The emulation of microarchitecture and functional characteristics of human tissues give organoids great potential in multiple clinical applications such as organoid biobanking, disease modelling, drug toxicity testing, personalized therapy, host-microbe interaction studies, and omics analysis as well as targeted gene therapy using the CRISPR/Cas9 system (**Figure 1.5**) (Dutta et al., 2017; Lancaster and Knoblich, 2014; Rossi et al., 2018). The organoid culture bloomed after the publication of intestine organoids generated from $Lgr5^+$ stem cells (Sato et al., 2009). To date, organoids have been seen succeeded in mimicking brain (Hubert et al., 2016; Lancaster et al., 2013), lung (Sachs et al., 2019; Zhou et al., 2018), mammary (Linnemann et al., 2015; Mroue and Bissell, 2012), liver (Jin et al., 2018; Sorrentino et al., 2020), pancreas (Broutier et al., 2016; Yang et al., 2020), intestine, colon (Crespo et al., 2017; Sato et al., 2011), ovarian and

fallopian tube (Hoffmann et al., 2020a; Kessler et al., 2015), prostate (Chua et al., 2014; Drost et al., 2016), and kidney (Freedman et al., 2015; Takasato et al., 2015). Although attractive, there are still challenges in applying organoids. The formation of organoids is highly dependent on complex extracellular matrix to support formation of 3D structure. Commonly used Matrigel® has heterogeneous composition, which increases the burden in manipulating and manufacturing. Microengineering techniques have been utilized to address this problem (Demers et al., 2016; Wang et al., 2018b). The variability of organoid morphology and function leads to reproducibility issue, which is a major issue that limits the application of organoids in drug screening and transplantation (Yin et al., 2016). Automated digital microfluidic platforms have provided opportunities to achieve high-throughput manipulation and analysis of organoids (Au et al., 2014; Jin et al., 2014; Wang et al., 2018a; Zhu et al., 2017b). Nevertheless, organoid culture is a robust model in recapitulating *in vivo* architecture and function with promising potential in therapeutics.

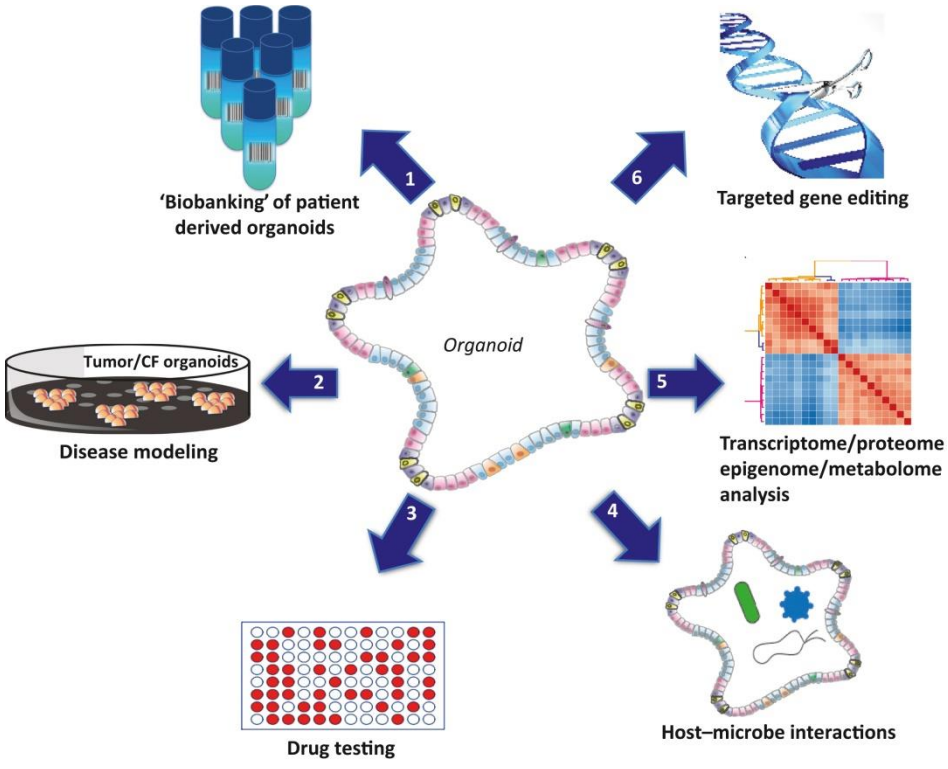

Figure 1.5 Multiple applications of organoid technology

Reproduced from (Dutta et al., 2017) with the permission of Elsevier.

1.3 Airway

1.3.1 Airway structure and airway remodelling

The bronchial airway is made up of mucosa, smooth muscle, submucosa and *lamina propria* (Ball et al., 2020; Jeffery et al., 1997). The bronchial mucosa is constituted by ciliated epithelium, goblet cells and basal cells. The *lamina propria* is a thin layer of connective tissue and has been characterized to include fibroblasts, lymphocytes, macrophages, eosinophilic leukocytes, and mast cells (Wiseman et al., 2003). ECM is a collection of extracellular molecules that supports surrounding cells structurally and functionally. In human airway, the most recognizable ECM structure is the subepithelial basement membrane (BM) (Fernandes et al., 2006), primarily consisting of collagen I (which provides tensile strength), elastins (which provide elasticity), and laminins and collagen IV (which constitutes the bulk of alveolar and airway basement membranes) (Booth et al., 2012).

The most typical structural change in airway is airway remodelling (**Figure 1.6**). It includes loss of epithelial integrity, thickening of basement membrane, subepithelial fibrosis, goblet cell and submucosal gland enlargement, increased smooth muscle mass, decreased cartilage integrity, and increased airway vascularity (Bergeron et al., 2009). Airway remodelling has been evident in asthma and COPD. In asthma, airway smooth muscle (ASM) cells hypertrophy (cell volume increase) and hyperplasia (cell number increase) increase the thickness of ASM layer (Ebina et al., 1993a; James et al., 2012; Woodruff et al., 2004). Chronic airway inflammation is also associated with airway remodelling in allergic asthma (Jeffery and Haahtela, 2006; Lloyd and Robinson, 2007), which is supported by finding that steroid treatment has beneficial effect on airway remodelling in asthmatic patients (Chetta et al., 2003; Hoshino et al., 2001; Sont et al., 1999). Airway remodelling in COPD is similar to asthma but not the same (Jones et al., 2016). In COPD patient, the lung function only changed 225 mL from a baseline forced expiratory volume in the first second (FEV_1) of 1,500 mL, suggesting the airway narrowing is limited as it has already been narrowed (Du Toit et al., 1986; Jones et al., 2016; Woolcock et al., 1984). The increase in ECM proteins have been shown in asthma (Amin et al., 2005; Huang et al., 1999; Westergren-Thorsson et al., 2002) but few in COPD. In asymptomatic smokers, tenascin and laminin were reported to be increased (Amin et al., 2003; Ekberg-Jansson et al., 2005). Remodelled airway becomes stiffer compared to healthy airway (Khan et al., 2010). The airway stiffness can be indicated by the distensibility of the airway, which is generally increased in asthma (Brackel et al.,

2000a; Ward et al., 2001; Wilson et al., 1993a) but seems to be reduced in COPD (Baldi et al., 2010; Diaz et al., 2012; Scichilone et al., 2008). Nevertheless, abnormal airway wall can be viewed as a mechanical cue to regulate airway cell behaviours.

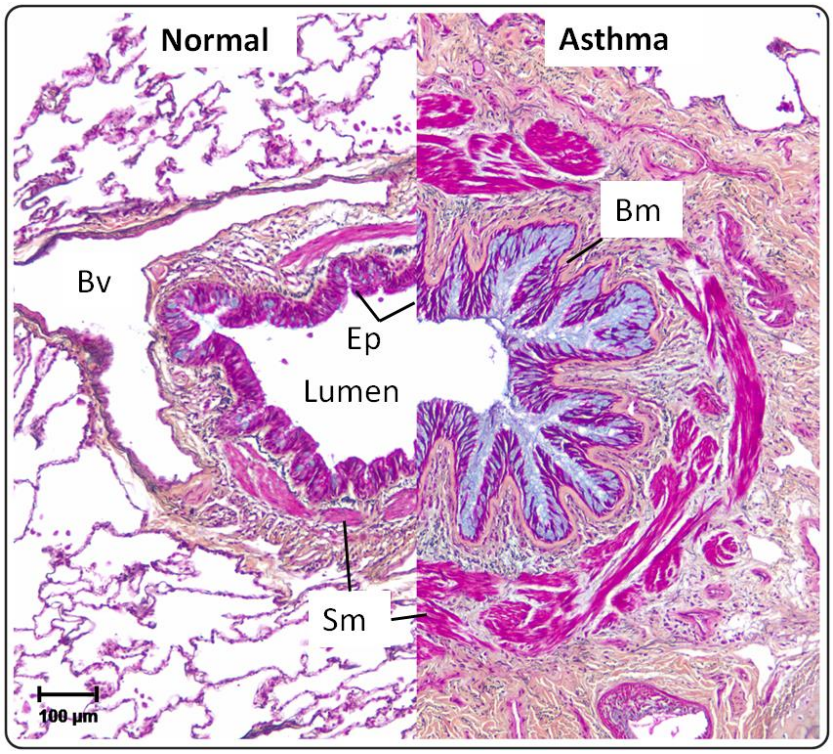

Figure 1.6 The airways in asthma undergo significant structural remodelling

Bm = basement membrane. Bv = blood vessel. Ep = epithelium. Sm = smooth muscle. Reproduced from (Wadsworth et al., 2012) with Licensee IntechOpen.

1.3.2 Mechanical interactions between matrix stiffness and lung fibroblast and airway smooth muscle cells

To date, increasing efforts have been put to the interactions between ECM and lung fibroblasts and airway smooth muscle cells. Pulmonary fibrogenesis involves remodelling of the parenchyma (e.g., in IPF) and airways (e.g., in asthma) of lung, and is characterized by excessive extracellular matrix deposition and accumulation of apoptosis-resistant myofibroblasts (Hardie et al., 2009). Researchers have made extensive efforts to illustrate the role that soluble inflammatory and fibrogenic mediators, like cytokines and TGF-β, play in the initiation and progression of fibrosis (Wynn, 2008). The evidence that variations of

matrix stiffness altered fibroblast morphology, proliferation, TGF-β signalling, and myofibroblast activation (Asano et al., 2017; El-Mohri et al., 2017; Wang et al., 2000; Wipff et al., 2007) re-positioned matrix stiffness from merely the outcome of fibrosis to an involvement in the stage of initiating fibrosis. The finding that the fibrotic extracellular matrix is both a cause and consequence of fibroblast activation in pathological fibrosis (Liu et al., 2015) further confirmed this idea.

It is widely accepted that the total amount of airway smooth muscle is increased in airway remodelling (Joubert and Hamid, 2005). In principle, the hyperplasia and cell volume (hypertrophy) of airway smooth muscle cells are responsible for the thickening of asthmatic airway (Ebina et al., 1993b; Fehrenbach et al., 2017; Hirst et al., 2004). During airway smooth muscle cell contraction, cytoskeletal events are orchestrated by macromolecular protein complexes that associated with the cytoplasmic domains of integrin proteins at the adhesion junctions between muscle cells and the extracellular matrix (Zhang and Gunst, 2008). ECM composition and rigidity can differentially affect mechanical reactivity of the airway smooth muscle cell (An et al., 2009). Human airway smooth muscle cells increasingly produce a variety of ECM components after exposure to atopic asthmatic serum (Johnson et al., 2000). Apart from its contractile properties, airway smooth muscle cells also produce inflammatory cytokines, proteases, and growth factors, which may contribute to the remodelling process and induce phenotypic changes of the muscle (Chung, 2005).

1.4 Airway Epithelium

1.4.1 Airway epithelium structure

The epithelium has been regarded as a barrier between the air and the internal milieu when processing exogenous inhaled particles in order to elicit a highly regulated response ranging from the easiest (mucus clearance) to the most complex (synergistic innate and adapted immune responses) (Gras et al., 2013). Fully differentiated epithelium comprises different cell types, defined by their morphological appearance (**Figure 1.7**). Most recent classification using single-cell RNA sequencing identified specific cell-type sub-clusters according to their molecular states, such as suprabasal cells (intermediate between basal and club cell), deuterosomal cells (precursor of ciliated cell), mucous-ciliated cells (intermediate between goblet and ciliated cell) (Deprez et al., 2020; Hewitt and Lloyd, 2021; Vieira Braga et al., 2019). Single-cell transcriptomics have shown advantages in revealing cellular heterogeneity and identifying rare cell populations (Haque et al., 2017). However, it is not always necessary to distinguish these rare cell types as they are often low expressed or in a transition state. Thus, we will be focusing on the three abundant airway epithelium phenotypes: ciliated, columnar, secretory columnar, and basal cells.

Ciliated epithelial cells account for over 50% of all epithelial cells and effect unidirectional transport of mucus from the lung to the throat (Knight and Holgate, 2003). The crucial defence mechanism of human airway for removing inhaled pathogens is achieved by mucociliary transport. Cilia beat in a rhythmic and rotating metachromic ascending movement to prevent the epithelium from being blocked in mucus (Matsui et al., 1998) and move the periciliary liquid layer surrounding the epithelial surface.

Goblet cell numbers stay at a steady state in health but undergo hyperplasia in most chronic airway diseases. They are categorized as secretory cells because of their ability to release mucus, an aqueous solution of liquid, proteins, and mucous glycoproteins (mucins) (Rogers, 2007). Mucus exists as a liquid bilayer: an upper “gel” layer traps inhaled airborne particles and pathogens, which is moved by the cilia of airway epithelial ciliated cells, and beneath this is a watery layer that “lubricates” cilia and ensures that mucus spreads over the epithelium (Evans et al., 2009; Ha and Rogers, 2016). Club cells, previously known as Clara cells, are low columnar/cuboidal cells with short microvilli located in the small airways (Boers et al., 1999; Massaro et al., 1994; Plopper et al., 1980). Club cells stimulated by adrenergic transmitters secrete a number of substances, including its primary product

uteroglobin/blastokinin, glycoproteins, lipids (Reynolds and Malkinson, 2010; Rokicki et al., 2016). They are progenitor cells in small airway (Akram et al., 2013; Reynolds et al., 2000; Reynolds and Malkinson, 2010). Interestingly, Club cells have been shown to be critical in maintaining circadian oscillations in lung tissue (Gibbs et al., 2009).

Basal cells attach the ciliated and goblet cells to the basement membrane via specialized adhesion structures. They are multipotent stem/progenitor cells of airway epithelium, which are capable of regeneration and differentiation into specialized cell populations of ciliated and goblet cells (Hackett et al., 2008; Hajj et al., 2007; Rock et al., 2009).

The classic intercellular adhesion of airway epithelium includes tight junctions, desmosomes, gap junctions, and hemidesmosomes (Roche et al., 1993). The tight junction protein-1 (ZO-1) demonstrated that the tight junctions seal the lateral apices of the columnar epithelial cell whereas the E-cadherin extended inferiorly along the lateral cell membranes mediate *adherens* junctions of columnar cells, regulating paracellular transport and the permeability of epithelium (Roche et al., 1993). Desmosomes, with a laminar arrangement of intercellular glycoproteins, plaque proteins, and radiating tonofilaments (Miller et al., 1987), are present along the lateral borders of the basal cells and particularly at the junction of the basal and columnar cell layer (Roche et al., 1993). Hemidesmosomes bond the basal epithelium to the laminin of the basement membrane. Integrins heterodimers comprising alpha and beta subunits, can link the contractile machinery of the cell cytoskeletal network to the extracellular matrix. The α_6- and β_4- integrin molecules in the hemidesmosome are distributed along the inferior border of the basal cell (Stepp et al., 1990).

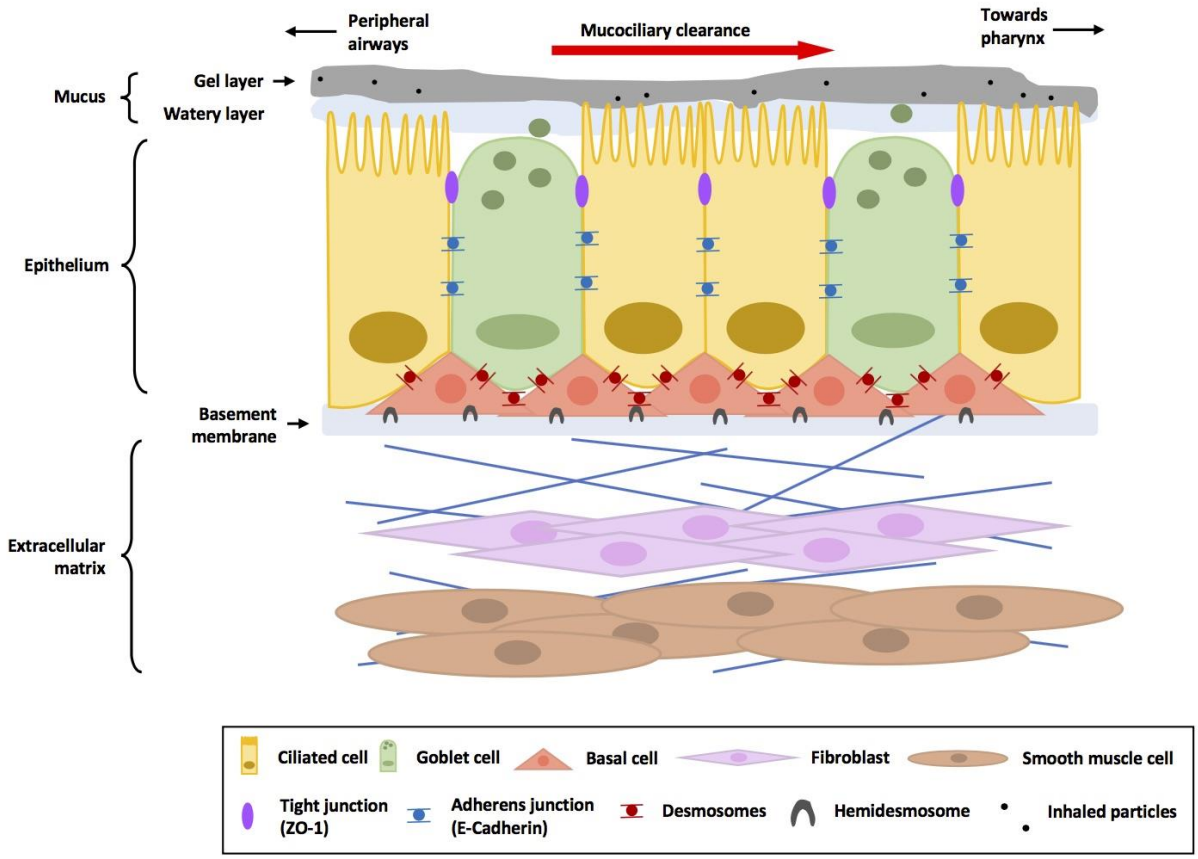

Figure 1.7 Structure of airway epithelium

Adapted from *(Ha and Rogers, 2016; Rock and Hogan, 2011; Wadsworth et al., 2012)*.

1.4.2 Mechanical environment of airway epithelium

1.4.2.1 Basement membrane thickening and extracellular matrix stiffness

The basement membrane thickening is suggested to be pathognomonic of asthma (Jeffery, 2004) and has been reported to occur not only in asthma but also cystic fibrosis (CF) and COPD patients in both children and adult (Fehrenbach et al., 2017). As described above, fibroblasts and airway smooth muscle cell could contribute to the deposition of extracellular matrix in airway diseases, which make the ECM more stiff than usual. The native normal human lung possessed a mean (± SEM) Young's modulus of 1.96 ± 0.13 kPa arranged in a relatively homogeneous pattern whilst the mean (± SEM) stiffness of IPF tissue was 16.52 ± 2.25 kPa (Booth et al., 2012). ECM deposition and basement membrane thickening weakened intracellular attachments between cell-cell and cell-ECM which led to the shedding of

columnar cells. However, there are no direct observations on how the epithelium reacts to stiff matrix.

1.4.2.2 Mucus hypersecretion and cilia beating dysfunction

"Mucus" is defined as the extracellular mixture of mucins that have been secreted or released by hydrolysis of a membrane anchor, other macromolecules such as proteoglycans and antimicrobial proteins, water, ions, and cellular debris (Evans et al., 2009). The gel layer is approximately 5-50 μm thick and the watery layer is 7 μm in depth (Tarran et al., 2006; Widdicombe, 1997). Under pathological conditions, airway mucins may be secreted by surface goblet cells in increased quantities, which is called mucus hypersecretion. The large amounts of mucus (sputum) may lead to airway closure.

Cilia beat within the watery layer propels the gel layer to the pharynx where it is swallowed with particles and pathogens. To be effective in transporting secretions out of the lung, the mucociliary transport apparatus must exhibit a cohesive beating of all ciliated epithelial cells that line the upper and lower respiratory tract (Yaghi and Dolovich, 2016). The dysfunction of cilia beating leads to serious respiratory issues, like airflow obstructions and increased airway hyperactivity. Cilia beating frequency (CBF) has been reported to vary from 6 to 15 Hz depending on the species and the anatomic location of the epithelium (Nakahari, 2007). CBF can response to a variety of endogenous and exogenous stimulations, including mechanical stimulation. Shear stress, the force generated by ciliary motion and fluid flow on the mucociliary escalator at the mucosal surface, with caudal flow causes a large increase in CBF from 10 to 25-35 Hz in mouse trachea (Winters et al., 2007). Cilia function is intertwined with viscosity of mucus. Tracheal mucus velocity (TMV) was significantly less (6.3 ± 2.3 mm per min, mean ± SEM, n=6) in asymptomatic asthmatic patients than in normal subjects (11.6 ± 3.6 mm per min, mean ± SEM, n=7) (Mezey et al., 1978). Mucus velocity in mice (0.7 mm per mine, n=4-9 mice) can be reduced by cilia-beating inhibitor bupivacaine.

1.4.2.3 Epithelial –mesenchymal transition

Epithelial-mesenchymal transition (EMT), first observed by Elizabeth Hay (Greenburg and Hay, 1982), is a biological process in cohort epithelial cells lose their cell polarity and cell-cell adhesion and gain migratory and invasive properties to become mesenchymal (fibroblast-

like) cells (**Figure 1.8**). The EMT starts from the loss of cell-cell junctions, such as ZO-1 and E-cadherin, accompanied with the simultaneous gain of N-cadherin, and then the increasing expression of specific cell-surface markers characteristic for myofibroblasts, α-SMA (Zeisberg and Neilson, 2009). Finally, cells begin to synthesize ECM components like fibronectin and collagen type 1 (Kim et al., 2006). Obviously, EMT induced ECM deposition would impact the structure and function of epithelium. Interestingly, Wei et al. suggested two concepts: first, that the matrix stiffness could regulate EMT to facilitate tumour dissemination; and second, that mechanical cues could signal in concert with biochemical signals to regulate EMT (Wei and Yang, 2016). Therefore, the connection between EMT and matrix stiffness promotes the requirement of introducing mechanical factors into airway epithelial related studies.

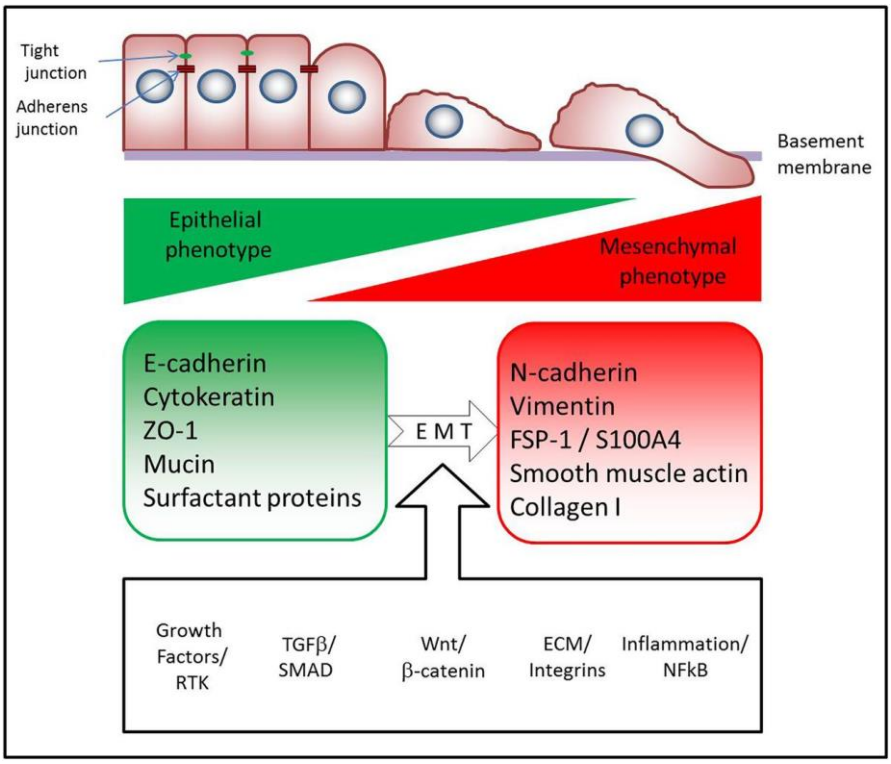

Figure 1.8 The most important features of epithelial-mesenchymal transition

Reproduced from (Bartis et al., 2014) with the permission of BMJ Publishing Group Ltd.

1.4.3 Conventional airway epithelial cell cultures

From large airways to small airways, pseudostratified airway epithelial cells become columnar and cuboidal (Crystal et al., 2008). The large airway epithelial cells are composed

by ciliated and secretory cells primarily adapted to facilitate mucociliary clearance of exogenous particles and pathogens in the air. The small airway region is lined by alveolar epithelial type I (ATI) cells, providing a surface for gas exchange, and alveolar epithelial type II (ATII) cell, secreting pulmonary surfactant to prevent alveolar collapse (Mason and Crystal, 1998).

In airway epithelial cell related studies, continuous cell lines as 2D cellular models are normally the first choice. They possess advantages over primary epithelial cells for their extendable life span, easy handling, and reproductivity. The most widely used cell lines include immortalized human bronchial epithelial cell line BEAS-2B, human bronchial epithelial cell line 16HBE14o-, non-small-cell lung cancer cell line Calu-3, and type II alveolar epithelium-derived adenocarcinoma cell line A549.

BEAS-2B cell line was immortalized by infecting normal human bronchial epithelium with adenovirus 12-SV40 virus hybrid (Reddel et al., 1988). They have a predominantly polygonal appearance typical of epithelial cells. BEAS-2B cells have been extensively uses as an *in vitro* cellular model in variety areas, including mechanism studies (Li et al., 2019; Prodanovic et al., 2017), infection studies (Xia et al., 2017), and drug screening (Wagner et al., 2019).

The 16HBE14o- is a $SV40^{o-}$ transformed cell line from human bronchial epithelial cells (Cozens et al., 1994). They have a cobblestone appearance and display ion transport, supporting the original purpose for study of the cystic fibrosis transmembrane conductance (CFTR) regulator. 16HBE14o- cells also have a wide use in studying COPD, asthma, and lung cancer, but the barrier function was influenced by CFTR-dependent transcellular conductance (Callaghan et al., 2020).

The Calu-3 cell line is derived from human bronchial epithelial submucosal glands, which are a major source of mucins and airway surface liquid (Zhu et al., 2010). Interestingly, Calu-3 cells in air-liquid interface culture expresses mucin, but only contain sparse numbers of ciliated cells (Grainger et al., 2006; Stewart et al., 2012b). Calu-3 cells are mostly used in cancer research (Kreft et al., 2015) and drug development (Haghi et al., 2010). Most recently, Calu-3 cells have shown to be a cell line infectable with SARS-COV-2, although with lower virus production than Vero cells (Park et al., 2021).

The A549 cell line was established in 1972 by D. J. Giard, et al through explant culture of lung carcinomatous tissue (Lieber et al., 1976). They appear to be squamous in nature and

grow as adherent monolayers *in vitro*. Primary ATII cells rapidly differentiate into ATI cells *in vitro* (Beers and Moodley, 2017), can only be maintained in culture for a limited period, and cannot be expanded. The A549 cell line as a model for alveolar basal epithelial cells has become a critical tool for studying alveolar epithelial cell biology, albeit acknowledged that it has myriad genetic abnormalities.

1.5 Hypothesis and main aims

The airway epithelial cells reside in an environment with altered stiffness in response to pathological changes. However, little is known about the influence of matrix stiffness on airway epithelial cell biology. We have observed the regulatory effects of matrix stiffness on fibroblasts using 3D setting. Organoid culture not only can restore the diversity of airway epithelial cell types, but also provide cells extracellular matrix. Thus, we hypothesize that airway organoid culture may be superior to other airway epithelial cellular models in drug screening and for investigating disease mechanisms.

The main aims of this study were to:

1. To investigate the influence of stiffness on morphological change, TGF-β actions, and glucocorticoid responsiveness in airway epithelial cells.
2. To generate airway organoid cultures.
3. To compare the airway organoid with other cellular models for its application in pre-clinical inflammation and infection study.

CHAPTER 2

GENERAL METHODS

2.1 General cell line culture

2.1.1 Culture of immortalized human bronchial epithelial cell line BEAS-2B and human adenocarcinoma cell line A549

2.1.1.1 Propagation method

The immortalized normal human AD12-SV40-hybrid virus-transformed human bronchial epithelial cell line BEAS-2B (American Type Culture Collection (ATCC), VA, USA) was cultured in LHC-9 medium (12680013, Life Technologies, NY, USA), supplemented with 2% (v/v) heat-inactivated fetal calf serum (HIFCS) (12003C, Sigma, MO, USA), 2 mM L-glutamine (59202C, Sigma), 100 IU/mL penicillin and 50 µg/mL streptomycin (P4458, Sigma). The type II alveolar epithelium-derived adenocarcinoma cell line A549 (ATCC) was cultured in phenol red-free Dulbecco's modified Eagle's medium (DMEM) (31053036, Life Technologies), supplemented with 10% (v/v) HIFCS, 2 mM L-Glutamine, 1% (v/v) non-essential amino acids (M7145, Sigma), 1% (v/v) sodium pyruvate (S8636, Sigma), 0.2% (v/v) sodium bicarbonate (S8761, Sigma), 15 mM HEPES (H0887, Sigma), 100 IU/mL penicillin and 50 µg/mL streptomycin. The cells were kept at 37°C in a humidified atmosphere containing 5% CO_2. Cells were passaged twice a week by washing confluent cell monolayers twice with sterile phosphate-buffered saline (PBS) (14190250, Life Technologies), followed by incubating with trypsin-EDTA (0.12% w/v) (59430C, Sigma) for 2-3 minutes to detach the cells. Cell suspension was re-seeded at a density of 8,000 cells/cm^2.

2.1.1.2 Starvation method

Unless otherwise indicated, BEAS-2B cells and A549 cells were serum-starved 24 h prior to drug treatments, using incomplete DMEM medium, supplemented with 0.25% (w/v) BSA (A8412, Sigma), 2 mM L-Glutamine, 1% (v/v) non-essential amino acids, 1% (v/v) sodium pyruvate, 0.2% (v/v) sodium bicarbonate, 15 mM HEPES, 100 IU/mL penicillin and 50 µg/mL streptomycin. The cells were kept at 37°C in a humidified atmosphere containing 5% CO_2. Given our interest in steroid responses, the presence of hydrocortisone in LHC-9 medium is a confounder as has been shown in our previous work (Keenan et al., 2014; Prodanovic et al., 2017). Thus, incomplete DMEM medium was chosen to starve BEAS-2B cells instead of LHC-9 medium.

2.1.2 Culture of immortalized primary human bronchial epithelial cell line BCis

2.1.2.1 Propagation method

The immortalized primary human epithelial cell line BCi NS 1.1 was provide by Dr. Mathew Walters and Dr. Ron Crystal (Weill Cornell Medical College, New York, USA). After lentiviral transduction with Cas9 expressing construct, the stable polyclonal population was expanded in culture and termed BCi Cas9 cells. The BCi Cas9 cells were generated and kindly provided by Dr. Li Eon Kuek and Dr. Graham A Mackay (The University of Melbourne). The BCi NS1.1 and BCi Cas9 cells were cultured in the Clonetics™ BEGM™ Bronchial Epithelial Cell Growth Medium Bulletkit™ (Lonza, Mt Waverley, Australia) consisting of bronchial epithelial cell basal medium (CC-3171, Lonza) supplemented with SingleQuots™ (CC-4174, Lonza) as shown in **Table 2.1**. Cells were kept at 37°C in a humidified atmosphere containing 5% CO_2 and passaged from a single T25 flask using method recommended by the manufacturer. Briefly, 70-80% confluent cell monolayers were washed with PBS, incubated with 1 mL trypsin/EDTA (CC-5012, Lonza), and then neutralized with 2 mL trypsin neutralizing solution (TNS) (CC-50002, Lonza). Cells were collected by centrifugation at 220 g for 8 minutes at room temperature. Viable cell count was performed using haemocytometer with Trypan Blue. Cells were then re-seeded at a density of 5,000 cells/cm^2. Medium was renewed three time a week.

Table 2.1 Composition of 1x BEGM, 1x minimal, and 2x BEGM medium

Reagents	1x BEGM	1x minimal	2x BEGM
BPE	52 µg protein contents/mL	×	104 µg/mL
rhEGF	0.5 ng/mL	×	1 ng/mL
Hydrocortisone	1.4 µM	0.1 µM	2.8 µM
Insulin	5 µg/mL	1 µg/mL	10 µg/mL
Transferrin	10 µg/mL	10 µg/mL	20 µg/mL
Epinephrine	0.5 µg/mL	0.5 µg/mL	1 µg/mL

Triiodothyronine	6.5 ng/mL	6.5 ng/mL	13 ng/mL
GA	50 µg/mL	50 µg/mL	100 µg/mL
RA (add fresh)	50 nM	50 nM	100 nM
BSA	×	1.5 µg/mL	3 µg/mL

BPE: bovine pituitary extract; GA: gentamicin/amphotericin B; RA: retinoic acid.

2.1.2.2 Starvation method

Unless otherwise indicated, BCis cells were starved 24 h prior to drug treatments, using 1x minimal medium as shown in **Table 2.1**.

2.1.3 Primary bronchial epithelial cell culture

Unless otherwise indicated, the primary bronchial epithelial cells were maintained under identical culture conditions to BCis cells.

2.1.3.1 Rat-tail collagen preparation and surface coating

Rat tails, obtained from the animals euthanized for other studies, were used for preparation of the fibrillar, type I collagen. The tails were soaked in 70% (v/v) ethanol for 15 minutes, after which the tail skin was removed, exposing tendons for dissection and subsequent digestion in 0.1% (v/v) sterile acetic acid at 4°C for 72 hours. Digested collagen was centrifuged every 24 hours at 2,000 rpm for 2 hours at room temperature, after which the supernatant was collected, and fresh acid was added to further digest insoluble collagen fibres. Supernatant was dialysed against sterile, endotoxin-free water at 4°C for 24 hours and the concentration of the protein was determined by Bradford protein assay, as described in Section 2.4.3. The rat tail collagen was diluted to 30 mg/mL in sterile water for culture surface coating. Following 45 minutes incubation at 37°C, collagen solution was aspirated, and the culture surface was washed once with PBS to remove unbound matrix solution. The culture surface was then left to air-dry. Collagen coated flasks and plate can be stored at 4°C for one month.

2.1.3.2 Culture of primary human bronchial epithelial cells

Primary human bronchial epithelial cells were purchased commercially from Lonza. The characteristics of donors are shown in **Table 2.2**.

Table 2.2 Main characteristics of donors of primary human bronchial epithelial cells

TAN	Diagnosis	Age	Sex	Alcohol	Smoking
27434	Normal	57	Female	Yes	No
33652	Normal	56	Male	No	No
32958	Normal	30	Female	Yes	Yes
26520	Normal	69	Female	Yes	No
29734	Asthmatic	55	Female	No	No
28043	COPD	59	Male	Yes	Yes

2.1.3.3 Establishment of primary human bronchial epithelial cells from bronchial brushing

Paediatric cystic fibrosis (CF) patients and non-CF participants were recruited at the Murdoch Children's Research Institute, The Royal Children's Hospital (Melbourne, VIC, Australia). The clinical characteristics of the CF patients are shown in **Table 2.3**. The research ethics committees of the Royal Children's Hospital Melbourne (approval no. HREC 25054) and The University of Melbourne (approval no. HREC 2056658) approved the study. Written consent was obtained from the parents of the children enrolled into the study.

The bronchial epithelial brushing cells were obtained in conjunction with bronchoalveolar lavage by using cytology brushes (BC-203D-2006, Olympus, PA, USA). The freshly brushed cells were seeded on collagen coated T25 cell culture flasks in BEGM medium supplemented with 250 ng/mL Amphotericin B (15290018, Life Technologies). Cells were cultured at 37°C in a humidified atmosphere containing 5% CO_2. Once reached 80% confluency, the cells were propagated as BCi NS1.1 cells, described in Section 2.1.2.1.

Table 2.3 Characteristics of donors of primary human bronchial epithelial brushing cell cultures

ID	CF/Non-CF	Age	Sex	CFTR mutation 1	CFTR mutation 2	Modulator use
M1C130	CF	4.9	Male	deltaF508	G551D	Ivacaftor
M1C154	CF	3.2	Male	deltaF508	deltaF508	No
M1C175	CF	1.0	Female	c.1521_1523 (delCTT)	c.1521_1523 (delCTT)	No
M1C134	CF	5.0	Male	delta F508	delta F508	No
M1C172	CF	2.0	Male	delta F508	delta F508	No
M1C151	CF	4.0	Male	delta F508	delta F508	No
M1C123	CF	6.0	Female	delta F508	delta F508	Lumacaftor-ivacaftor
M1C126	CF	5.9	Female	p.F508del	p.F508del	No
M1C129	CF	5.9	Male	delta F508	p.G551D	Yes
M1C158	CF	3.9	Female	p.Arg1158Ter	p.Arg1158Ter	No
M1C176	CF	1.9	Male	p.Phe508del	p.Phe508del	No
M1C155	CF	3.9	Male	p.Phe508del	p.G551D	Yes
M1C184	CF	0.5	Female	p.1507del	p.F508del	No
M1N050	Non-CF	8.4	Female	N/A	N/A	N/A
M1N055	Non-CF	1.1	Male	N/A	N/A	N/A
M1N056	Non-CF	5.9	Female	N/A	N/A	N/A
M1N057	Non-CF	3.7	Male	N/A	N/A	N/A

CFTR: cystic fibrosis transmembrane conductance regulator.

2.1.3.4 Establishment of primary human bronchial epithelial cells from bronchial scraping

Primary human bronchial epithelial cells were established from bronchi of lung resection specimens derived from donors without chronic respiratory disease as previously described (Schuliga et al., 2009). Samples were obtained with approval from the University of Melbourne (approval no. HREC 1750014) and Alfred Hospital (approval no. 336/13; Alfred Hospital, Melbourne, VIC, Australia). The characteristics of donors are shown in **Table 2.4**.

The bronchial epithelial cells were obtained by scraping the inner surface of airway with no. 23 scalpel blade. The scalpel blade was rinsed in RPMI 1640 medium (11835055, Life Technologies) supplemented with 10% (v/v) HIFCS. The cell suspension was centrifuged at 150 g for 5 minutes at room temperature. The cell pellet was resuspended in pre-warmed BEGM medium and seeded on collagen coated T25 cell culture flasks. Cells were cultured at 37°C in a humidified atmosphere containing 5% CO2. Once reached 80% confluency, the cells were propagated as BCi NS1.1 cells, described in Section 2.1.2.1.

Table 2.4 Donor characteristics for human bronchial epithelial cell cultures

ID	Age	Sex
ALF051	27	Male
ALF052	31	Male
ALF053	41	Female
IK	30	Unknown

2.1.4 Cryopreservation

Cells were dissociated as described above. The BEAS-2B and A549 cells were harvested by centrifugation at 500 g for 5 minutes. The cell pellet was resuspended in ice-cold 90% (v/v) HIFCS with 10% (v/v) dimethylsulphoxide (DMSO). The BCi cells and primary epithelial cells were harvested by centrifugation at 220 g for 8 minutes. The cell pellet was resuspended in ice-cold 80% (v/v) BEGM with 10% (v/v) HIFCS and 10% (v/v) DMSO. The cell suspension was then transferred into cryogenic tubes (Thermo Fisher Scientific, Waltham,

USA) and put into Mr. Frosty™ freezing container (Thermo Fisher Scientific) filled with room temperature isopropanol. The container was left in a -80°C freezer. After 24 hours, the cryogenic tubes were transferred into a liquid nitrogen cryopreservation vessel for long term storage.

2.1.5 Mycoplasma detection

Mycoplasma contamination was routinely tested in all cell cultures, using the Mycoalert™ PLUS Mycoplasma detection kit (LT07-701, Lonza) according to manufacturer's instruction.

2.2 Two-dimensional cell culture

2.2.1 2D stiff and 2D soft environment

The conventional polystyrene coated tissue culture plastic is defined as "2D stiff" environment, which possess a Young's modulus ranging from 2 to 4 GPa. The "2D soft" environment is used to describe a tissue culture surface coated with collagen hydrogel. The collagen coating solution was prepared by mixing 4 mg/mL Rat Tail Type I Collagen (#5153, Advanced BioMatrix, CA, USA) with sterile water and 4x DMEM (12100061, Life Technologies) at a ratio of 3:3:2. The 24-well flat bottom plate was coated with 200 µL collagen solution at 37°C for 45-60 minutes to allow collagen gelling. The Young's modulus of collagen hydrogel ranges from 0.2 to 2 kPa (Berhan et al., 2020).

2.2.2 Gelatin coating

The gelatin solution (G1393, Sigma) was filter sterilized through 0.22 µM filter and applied 500 µL into the 24-well plate. The plate was incubated at 37°C for no less than 30 minutes to allow gelatin polymerizing, after which the excessive gelatin solution was aspirated and left dry overnight in a bio-cabinet.

2.2.3 Stiffness gradient *Cytosoft*® plate

The *CytoSoft*® discovery kit (#5190-7EA, Advanced BioMatrix) contains six silicone gel coated plates with different elastic moduli of 0.2, 0.5, 2, 8,16, 32, and 64 kPa. The Rat Tail Type I Collagen was diluted as 1:30 in PBS and dispensed 3 mL of solution into each well of the *CytoSoft*® plates. The plates were incubated at room temperature for 1 hour. The remaining material was aspirated and rinsed immediately two times with PBS. The plate was left with PBS until the cells been added in.

2.3 Three-dimensional cell culture

2.3.1 Air-liquid interface culture (ALI)

2.3.1.1 Coating of transwell inserts with rat-tail collagen

Rat-tail collagen was prepared as described in section 2.1.3.1. 100 µL of 30 mg/mL rat-tail collagen was used to coat Corning® Transwell® inserts containing 0.4 µM pore polyester membrane (CLS3470-48EA, Sigma). Following 45 minutes incubation at 37°C, collagen solution was carefully aspirated, and membranes were washed once with 150 µL PBS. The transwells were left to air-dry. Collagen coated transwells can be stored at 4°C and used within one month.

2.3.1.2 Preparation of ALI medium

The BEGM medium system and PneumaCult™ medium system (STEMCELL Technologies, BC, Canada) were used to develop ALI cultures. The medium was applied according to submerge culture phase, ALI expansion phase and maintenance phase.

In the BEGM system, the 1x BEGM medium was used in submerge culture phase and ALI expansion phase. In ALI maintenance phase, the differentiation medium was prepared out of 1:1 (v/v) mixture of 2x BEGM (**Table 2.1**) and DMEM, supplemented with 0.2% (v/v) sodium bicarbonate, 15 mM HEPES, 2 mM L-glutamine, 1% (v/v) non-essential amino acids, 1% (v/v) sodium pyruvate, 100 IU/mL penicillin and 50 µg/mL streptomycin. The mixture of 2x BEGM and DMEM was made freshly.

In the PneumaCult™ system, the PneumaCult™ Ex Plus medium was used in submerge culture phase and ALI expansion phase. The PneumaCult™ ALI medium was used in ALI

maintenance phase. The medium composition is shown in **Table 2.5**. The complete medium can be stored at 4°C for 2 weeks.

Table 2.5 Composition of PneumaCult™ Ex Plus and PneumaCult™ ALI medium

	Reagents	Storage
PneumaCult™ Ex Plus (05040, STEMCELL Technologies)	PneumaCult™ Ex Plus base medium	4°C
	50x Supplement	-20°C
	100 nM Hydrocortisone (07925, STEMCELL Technologies)	-20°C
PneumaCult™ ALI (P-ALI) (05001, STEMCELL Technologies)	PneumaCult™ ALI base medium	4°C
	10x Supplement	-20°C
	100x Maintenance Supplement	-20°C
	1 µM Hydrocortisone	-20°C
	0.2% (v/v) Heparin Solution (07980, STEMCELL Technologies)	4°C

2.3.1.3 Differentiation of primary bronchial epithelial cells by ALI culture

At Day 0, submerge primary bronchial epithelial cells cultured in BEGM were harvested as described in section 2.1.2.1. For cell cultured in PneumaCult™ Ex Plus medium, 80% confluent cells were dissociated using the animal component-free (ACF) cell dissociation kit (05426, STEMCELL Technologies). Specifically, cells were washed once with PBS. 2 mL ACF Enzymatic Dissociation Solution was added into T25 flask and incubated at 37°C for 7 minutes, followed by 2 mL ACF Enzyme Inhibition Solution. Cells were collected by centrifugation at 350 g for 5 minutes. Viable cell count was performed using hemocytometer with Trypan Blue. The cells were seeded onto collagen-coated transwell inserts at 75,000 cells/well in 100 µL 1x BEGM or PneumaCult™ Ex Plus medium. Additional 350 µL 1x BEGM or PneumaCult™ Ex Plus medium was added to the basal chamber and cells were incubated at 37°C in a humidified atmosphere containing 5% CO_2. The medium was replaced with pre-warmed medium for both apical and basal chamber. At Day 4, cells were "air-lifted"

by aspirating medium from both apical and basal chamber and only adding 350 µL mixture of 2x BEGM and DMEM or P-ALI medium to basal chamber. Cells were then re-fed three times a week over a period of 4 weeks by aspirating medium from basal chamber and refilling with fresh medium. Apical liquid was removed post air-lifting if there was any. From Day 14, excess mucus was removed from apical surface once a week (or every time before medium refresh). Briefly, 150 µL pre-warmed PBS was added to apical chamber and incubated at 37°C for 30 minutes, after which the mucus wash was aspirated and stored at -80°C. Differentiation of the cells was confirmed through visualisation of the beating cilia under Olympus IX53 microscope equipped with QImaging optiMOS high speed camera at 100 frames/sec. Alternatively, the trans-epithelial electrical resistance (TEER) was measured using an EVOM2 Volt ohmmeter (WPI, FL, USA). Sterilisation of the electrode was carried out by submerging the electrode in 80% ethanol for 5 minutes, following its air drying and rinsing in PBS. A 100 µL of pre-warmed PBS was added to the apical surface of the transwells. The measurement was carried out by holding the electrode vertically and as steady as possible until the reading (Ω) was stabilised, and the process was then repeated for each transwell (Srinivasan et al., 2015).

2.3.2 Airway organoids culture

2.3.2.1 Preparation of silicone mask

The silicone mask was fabricated with Polydimethylsiloxane (PDMS) for its biocompatibility and hydrophobicity. Briefly, PDMS base and curing agent from SYLGARD® 184 kit (761036, Sigma) was mixed at a ratio of 10:1. A thin PDMS layer of 150 µM in thickness was made by spin coating at 200 rpm for 2 min on the back of a clean Ø15 mm plastic petri dish. Curing was then achieved by incubating at 60°C for 24 h. Specific mask layouts were cut to shape by Accu-punch (69038, Electron Microscopy Sciences, USA): 8 mm + 5 mm for 48-well plate, 10 mm + 6 mm for 24-well plate.

2.3.2.2 Preparation of airway organoid medium

The airway organoid medium was adapted from previous reported protocols (Broutier et al., 2016; Sachs et al., 2019). The medium components are shown in **Table 2.6**. The basal medium, containing Penicillin/Streptomycin, HEPES, Primocin, and Glutamax, was stored at

4°C for 1 month. The working medium containing all the other components was stored at 4°C and used within two weeks.

Table 2.6 Components of airway organoid medium

Media Component	Final concentration
R-Spondin 1 (120-38, Peprotech, NJ, USA)	500 ng/mL
FGF 7 (100-19, Peprotech)	25 ng/mL
FGF 10 (100-26, Peprotech)	100 ng/mL
Noggin (120-10C, Peprotech)	100 ng/mL
A83-01 (2939, Tocris, UK)	500 nM
Y-27632 (Y0503, Sigma)	5 mM
SB202190 (S7067, Sigma)	500 nM
B27 supplement (17504044, Life Technologies)	1x
N-Acetylcysteine (A9165, Sigma)	1.25 mM
Nicotinamide (N0636, Sigma)	5 mM
GlutaMax 100x (35050061, Life Technologies)	1x
HEPES	10 mM
Penicillin/Streptomycin	100 U/mL/100 mg/mL
Primocin (Ant-pm-1, Invivogen, CA, USA)	50 mg/mL
Advanced DMEM/F12 (12634010, Life Technologies)	1x

FGF: fibroblast growth factor.

2.3.2.3 Differentiation of primary bronchial epithelial cells by airway organoids culture

The Growth Factor Reduced Matrigel® (356231, Corning) was thawed at 4°C for overnight. Once thawed, the vial was gently swirled to disperse the Matrigel® evenly and then 1 mL

Matrigel® was aliquoted out and kept in -80°C for storage. The Matrigel® was kept on ice for all the steps.

At Day 0, the silicone masks were sticked to the bottom of culture plate wells by flat tip tweezer. The centre area of the mask was coated with 1% (w/w) BSA in PBS. Following 45 minutes incubation at 37°C, BSA solution was aspirated, and coating area was washed once with PBS. The plate was left to air-dry. Before use, pre-warm the plate in 37°C.

Submerge primary bronchial epithelial cells cultured in BEGM were harvested as described in section 2.1.2.1. Volume of cell suspension was calculated as 5,000 cells/well for 24-well plate or 3,000 cells/well for 48-well plate. The desired volume of cell suspension was transferred to a 15 mL falcon tube. After centrifugation at 220 g for 8 min, the supernatant was carefully removed. The airway organoids working medium was added to resuspend the cell pellet as 20 µL/well for 24-well plate or 12.5 µL/well for 48-well plate. The tube was then put on ice to add the Matrigel® as the same volume of working medium to form a 50% (w/w) Matrigel® mixture. A 40 µL or 25 µL drop of cell mixture was then seeded to the centre of the silicone mask in 24-well plate or 48-well plate. Following solidification of the droplet by incubating at 37°C for 10-20 min, 500 µL or 250 µL of pre-warmed airway organoid working medium was added to each well. The cells were incubated at 37°C in a humidified atmosphere containing 5% CO_2 and the medium was replaced three times a week for 3 to 4 weeks. Differentiation of the cells was confirmed through visualisation of the beating cilia under Olympus IX53 microscope equipped with QImaging optiMOS high speed camera at 100 frames/sec.

2.4 General analytical techniques

2.4.1 Real-time quantitative polymerase chain reaction (RT-qPCR)

2.4.1.1 Total mRNA extraction

Total RNA was extracted using Illustra™ RNAspin Mini RNA Isolation Kit (25-0500-72, GE Healthcare, UK) and performed at room temperature. Initially, cells were lysed in 350 µL lysis solution with 1% β-mercaptoethanol (M6250, Sigma) and each sample was transferred into corresponding RNAspin Mini Filter Units (violet ring). Clear lysates were collected by centrifugation at 11,000 g for 1 min. Adjustment of RNA binding condition was carried out through addition of 350 µL 70% Ethanol in diethylpyrocarbonate (DEPC)-H_2O, mixing by

vortexing twice for 5 sec and centrifuging the solution in RNAspin Mini Column Units at 8,000 g for 30 sec. After desalting the silica membrane with 350 µL desalting buffer followed by centrifugation at 11,000 g for 1 min, DNA was digested by 15 min incubation with reconstituted DNase I, diluted 10x in DNase reaction buffer. 200 µL of wash buffer I was added to inactivate DNase and columns were centrifuged at 11,000 g for 1 min. Then the columns were washed twice with 600 µL and 250 µL wash buffer II by centrifuging at 11,000 g for 1 min and 2 min respectively. Finally, highly purified RNA was eluted in 40 µL of RNase-free H_2O by centrifuging at 11,000 g for 1 min. Quantification of RNA concentration was performed by the NanoDrop 1000. Samples were stored at -80℃.

2.4.1.2 Reverse transcription

Total RNA was reversely transcribed to cDNA using High Capacity cDNA reverse transcription kit (4387406, Thermo Fisher Scientific) following manufacturer's instructions. The total reaction volume was 5 µL, consisting of 2 µL of total RNA (100 ng RNA), 2.5 µL 2x RT buffer, and 0.5 µL 20x RT enzyme mix, with one additional control sample (without RT enzyme mix). Thermal conditions applied for the reaction were 37℃ for 60 min and then 95 °C for 5 min in Eppendorf Mastercycler Pro. cDNA was diluted with 145 µL DEPC-H_2O and stored at -20°C.

2.4.1.3 RT-qPCR

RT-qPCR was performed in triplicate for each gene in a 384-well plate using QuantStudio™ 6 Flex Real-Time PCR System (Thermo Fisher Scientific). The RT-qPCR reaction was done by 6 µL reaction consisting of 2 µL diluted cDNA, 2.5 µL iTaq™ Universal SYBR® Green Supermix (1725125, Bio-Rad, CA, USA) and 1.5 µL mixture of the relevant 100 nM forward and reverse human primers (**Table 2.7**). Primers were obtained from either previously published references or from pre-validated KiCqStart® SYBR® Green Primers (KSPQ12012, Sigma). PCR amplification was done as following thermal protocol: 50°C for 2 min, 95℃ for 10 min followed by 40 cycles of 95℃ for 15 sec, and 60℃ for 1 min. The threshold cycle detected for each gene was normalized to house-keeping gene 18S ribosomal RNA. Relative gene expression was calculated using cycle threshold (CT) values of target genes and 18S according to $2^{-\Delta CT}$ method ($-\Delta CT = CT_{\text{target gene}} - CT_{18S}$). Logarithmic (log2) scale was used to display expression levels and was chosen because the higher the value the higher is the

expression level, and it allows the comparison of absolute levels of gene expression in different cultures and conditions.

Table 2.7 Human primer sequences for RT-qPCR

Gene product	Forward primer	Reverse primer	Supplier
18S	CGC CGC TAG AGG TGA AAT TC	TTG GCA AAT GCT TTC GCT C	Invitrogen
ACE2	GTT TGT AAC CCA GAT AAT CCA C	AAT GAT TTG CTC TTG CCA TC	Sigma
CFTR	CAT TTG GAT CCA GTA ACA TAC C	ATT GCT TCT ATC CTG TGT TC	Sigma
COL1A	GTG CTA AAG GTG CCA ATG GT	ACC AGG TTC ACC GCT GTT AC	Invitrogen
DNAH1	ACT AGT ACA AGA GGT CAT TAG G	CAC AGT ATT GTT GTA CAG GC	Sigma
DNAH5	CTT GAA AAA TGT TGT GAC CC	GTC ACC TTT ACA AAC AGA GAT C	Sigma
E-Cadherin	ACC ACA AAT CCA GTG AAC AAC G	CAA GCC CTT TGC TGT TTT CAA	Invitrogen
FOXJ1	GTG AAG CCT CCC TAC TC	AAT TCT GCC AGG TGG G	Sigma
GILZ	TCC TGT CTG AGC CCT GAA GAG	AGC CAC TTA CAC CGC AGA AC	Sigma
IFNA	GTG AGG AAA TAC TTC CAA AGA ATC AC	TCT CAT GAT TTC TGC TCT GAC AA	Invitrogen
IFNB	CAG CAA TTT TCA GTG TCA GAA GC	TCA TCC TGT CCT TGA GGC AGT	Invitrogen
IFNG	ACA ATT GGA AAG AGG AGA GTG ACA G	AGG AGA CAA TTT GGC TCT GGA	Invitrogen
IL-11	CTC CTG GCG GAC ACG C	GCT GGG AAT TTG TCC CTC AG	Invitrogen
IL-28A	ACA TAG CCC AGT TCA AGT C	GAC TCT TCT AAG GCA TCT TTG	Sigma

ITGA6	CAA GGT CGT GAC ATG TGC TCA	TTC GTA TTA ACA TGC TGC CTT TTT T	Invitrogen
Iκβα	TAG CCA TGG ATA GAG GCT AAG TGT AGA	TAC CAA CTA CAA TGG CCA CAC G	Invitrogen
KRT5	AGT TTG TGA TGG TGA AGA AG	GTT AAT CTC ATC CAT CAG TGC	Sigma
MKP-1	CCA CAA GGC AGA CAT CAG CTC	TCT ATG AAG TCA ATG GCC TCG TT	Invitrogen
MUC5AC	GGA ACT GTG GGG ACA GCT CTT	GTC ACA TTC CTC AGC GAG GTC	Invitrogen
MUC5B	TAC GTT CTG TCC AAG AAA TG	TAG ATG GAG TTG AGG AAC AC	Invitrogen
N-Cadherin	CCA CAA GGC AGA CAT CAG CTC	TCT ATG AAG TCA ATG GCC TCG TT	Invitrogen
PAI-1	TCA GGC TGA CTT CAC GAG TCT TT	CTG CGC GAC GTG GAG AG	Sigma
PTHLH	GCT ATT ATT TCA GAG GAA GCG	CTC GGG ACT TAT TTA GCA AC	Sigma
SARSCOV2-1	GCC TCT TCT CGT TCC TCA TCA C	AGC AGC ATC ACC GCC ATT G	Sigma
SARSCOV2-2	AGC CTC TTC TCG TTC CTC ATC AC	CCG CCA TTG CCA GCC ATT C	Sigma
SCNN1A	AGC ACA ACC GCA TGA AGA C	TGA GGT TGA TGT TGA GGC TG	Invitrogen
SCNN1B	CTG GTC CTT ATT GAT GAA CG	ATA GTC TCA TGG CCA TTT TG	Sigma
SCNN1G	CTT CTA TAC TGT CTC TCA GTT TCC	TGT ACT TGT AGG GGT TGA TG	Sigma
Tektin 1	ATT ACA GCT CTT GAA AAG GC	GGG CTA AAG TTT CCT TCA ATC	Invitrogen
TFF3	AGA ATG CAC CTT CTG AGG	AAA AGC TGA GAT GAA CAG TG	Sigma

TLR1	CCC TAC AAA AGG AAT CTG TAT C	TGC TAG TCA TTT TGG AAC AC	Sigma
TLR2	CTT TCA ACT GGT AGT TGT GG	GGA ATG GAG TTT AAA GAT CCT	Sigma
TLR3	AGA TTC AAG GTA CAT CAT GC	CAA TTT ATG ACG AAA GGC AC	Sigma
TLR4	GAT TTA TCC AGG TGT GAA ATC C	TAT TAA GGT AGA GAG ACG TGG C	Sigma
TLR5	ATC TTT CAC ATG GGT TTG TC	TTC CCC CAG AAG GTT ATA TG	Sigma
TLR6	AGA GAT CTT GAA TTT GGA CTC	TGT CTT TGG TCA TGA TGT TG	Sigma
TLR7	AGA TAT AGG ATC ACT CCA TGC	CTT CCA AAA TGG AAT GTA GAG	Sigma
TLR8	TGG AAA ACA TGT TCC TTC AG	TGC TTT TTC TCA TCA CAA GG	Sigma
TLR9	AAA TCC CTC ATA TCC CTG TC	TTG TAA TAA CAG TTG CCG TC	Sigma
TLR10	CAT CTG TAA GGG TTT TGA GC	CTT TCT TAG AGA CAT GTT GGA G	Sigma
TMPRSS2	CAG GTC ATA TTG AAC ATT CCA G	CTG AGT TCA AAG CCA TCT TG	Sigma
TP63	CAG CCT ATA TGT TCA GTT CAG	CAG TCC ATG CAT GCT AAT CTC AAT C	Sigma

2.4.2 Detection of proteins from cell culture supernatant

2.4.2.1 Supernatant collection

The conditioned cell culture media were transferred from wells to Eppendorf tubes. After centrifugation at 250 g for 5 min, the supernatant was collected and stored at -20°C until further analysis.

2.4.2.2 Enzyme-linked immunosorbent assay (ELISA)

Supernatants were assayed for IL-6 (555220), IL-8 (555244), and GM-CSF (555126) levels using OptEIA ELISA Set (BD Biosciences, NJ, USA). Flat bottom medium binding ELISA 96-well plates (655001, Greiner Bio-One, Austria) were coated with specific capture antibodies (diluted in coating buffer (0.1 M sodium carbonate, pH 9.8)) overnight. After three times of washing with 0.1% (v/v) Tween 20 in PBS, the plates were blocked with 10% (v/v) HIFCS in PBS for 1 h at room temperature. The standards and supernatants were then incubated for 2 h at room temperature. Detection antibody and HRP-conjugated streptavidin complex diluted in 10% HIFCS was applied for 1 h at room temperature. Washing process was repeated four times between each step and a final wash of five times, after which the visualization was carried out using 3,3',5,5'-tetramethylbenzidine (TMB) substrate (1:1 of A and B, 555214, BD Bioscience) until sufficient colour developed.

IL-11 (DY218) and PAI-1 (DY1786) levels were measured using DuoSet® ELISA kit (R&D systems, MN, USA). Briefly, flat bottom medium binding plate for PAI-1 and high binding plate (655061, Greiner Bio-One) for IL-11 were coated for overnight. After washing, the plate was blocked by 1% BSA in PBS for 1 h. Standards and samples were incubated for 2 h, followed by 2 h incubation of detection antibodies diluted in 1% BSA in PBS and 40 min incubation of HRP-conjugated streptavidin complex diluted in 1% BSA in PBS. Plates were then finally washed five times and applied with TMB to allow colour development.

The reaction was stopped by 2 M sulphuric acid and the absorbance was measured at 450 nm on a Multiskan™ FC Microplate Photometer (Thermo Fisher Scientific). The concentration of cytokines and proteins was determined using the absorbance of the standards and 4 parameter logistic curve fitting.

2.4.2.3 Bio-Plex Pro™ Cytokine, Chemokine, and Growth Factor Assay

High throughput cytokines measurement was done by using Bio-Plex Pro™ Human Cytokine Grp I Panel 27-Plex (M500KCAF0Y, Bio-Rad). The assay was carried out following the manufacturer's instruction. Briefly, the magnetic beads were mixed thoroughly and added to the plate. After two times wash with washing buffer, standards, samples, and medium blank were incubated for 30 min at room temperature. The plate was washed three times and then incubated with detection antibody for 30 min. After another three times wash, streptavidin-PE was applied and incubated for 10 min. Following three washes, the beads were resuspended in assay buffer. All the incubation was done by shaking at 850 rpm on an orbital shaker and covered with foil. The washing steps were done by the plate washer with magnetic components or manually on EpiMag HT (96-Well) Magnetic Separator (Q10002-1, Epigentek, NY, USA) to avoid losing the magnetic beads. The plate was read on Bio-Plex system (Bio-Rad). The concentration of cytokines and proteins was determined using the fluorescence intensity of the standards and 4 parameter logistic curve fitting.

2.4.3 Bradford protein assay

Bradford protein assay were applied to determine the protein concentration in samples. Briefly, BSA standards were prepared at final concentrations of 0; 2.5; 5.0; 7.5;10; 15; 20 µg/mL. 100 µL PBS-diluted samples or BSA standards were vortexed and incubated with 100 µL 0.2 M NaOH. After 15 min incubation at room temperature, 600 µL water and 200 µL Protein Assay Dye Reagent Concentrate (5000006, Bio-Rad) were added. Tubes were vortexed thoroughly and 200 µL of the solution was transferred to a 96-well plate to be measured at 595 nm on Multiskan™ FC Microplate Photometer. The standard curve generated from the absorbance of BSA standards was used to calculate the concentration of proteins in the samples.

2.4.4 Immunohistochemistry

2.4.4.1 Melbourne Epidemiological Study of Childhood Asthma (MESCA)

The MESCA study began in 1964 with the specific aims to define clinical syndromes involved in the range of wheezing in children and to estimate the prevalence of asthma and examine the differences in outcomes later in life (Oswald et al., 1994). Approximately 400

seven years old children were randomly chosen out of 30,000 living in Melbourne (Victoria, Australia) and initially this cohort was divided into 4 groups as following: non-asthmatic control, mild wheezy bronchitis, wheezy bronchitis, and asthma. The cohort was reviewed at the subsequent ages of 10, 14, 21, 28, 35 and 42. At the age 42 review (from May 1999 to September 2000), 94 subjects out of 380 subjects examined consented to further examinations for lung function and bronchoscopy with airway biopsies (approved by Royal Melbourne Hospital Ethics Committee).

2.4.4.2 Bronchoscopy and processing of mucosal biopsies

Bronchoscopy was performed trans-nasally using a fiberoptic Pentax FB 15P bronchoscopy. All patients received local anaesthesia with 2% lignocaine applied topically to the upper airway and nares. Two mucosal biopsies were taken from the sub-carina of the right lower and right-middle lobes, using Pentax fenestrated non-toothed biopsy forceps. Biopsies were fixed in 10% (v/v) neutral buffered formalin (NBF, Trajan) for 2 h and placed in 70% ethanol for overnight prior paraffin processing (Ward et al., 2008).

2.4.4.3 Three-layer immunoperoxidase staining

The three-layer immunoperoxidase staining was applied in this project. Paraffin embedded human airway blocks were cut into 2 µM or 3 µM sections. The sections were dewaxed by immersing in histolene (2 x 5 min), rehydrated through 100%, 100%, and 70% ethanol (5 min each), and washed in PBS (2 x 5 min) at room temperature. Antigen retrieval was performed using citric acid in oven at 85°C for 30 min if needed. After cooling down, the sections were washed in PBS (2 x 5 min). Sections were then dehydrated through 70%, 100%, and 100% ethanol and immersed in 0.3% H_2O_2 in methanol for 10 min to block endogenous peroxidase. Following rehydration through 100%, 100%, and 70% ethanol, 1.5% normal goat serum was applied for 20 min to block non-specific sites. Primary antibodies (**Table 2.8**) diluted in 0.25% BSA in PBS was incubated overnight at 4°C. Matched concentration of isotype control was used as the negative control and rabbit monoclonal pan-actin antibody (#8456, Cell Signaling, MA, USA) was used at 1:100 as positive control. On the second day, after washing in PBS (2 x 5 min), Vectastain® biotinylated goat anti-rabbit secondary antibody (PK4001, Vector Laboratories, CA, USA) was incubated at 1:200 for 30 min. Sections were then incubated with Vectastain® ABC reagents (equal volume of A (avidin) and B (biotinylated enzyme) in

PBS) for 30 min after PBS wash. Subsequent specific staining was visualized by applying stable peroxidase substrate buffer DAB (K346811, Agilent, CA, USA). After washing in tap water, the sections were counterstained in Mayer's haematoxylin (MH, Trajan, VIC, Australia), differentiated in 1% acid alcohol, blued in Schott's reagent (SCOT, Trajan), and dehydrated through 70%, 100%, 100% ethanol. Finally, the sections were coverslipped with DPX Mountant for Histology (44581, Sigma) and imaged by Olympus BX51 (Olympus, Japan).

2.4.5 Immunofluorescence

In general, the cells were washed in PBS two times and then fixed in 10% NBF. After washing three times in PBS, the cells were stained or kept in PBS at 4°C for future staining. Cells were blocked in 5% normal goat serum (G9023, Sigma) diluted in 0.1% Triton X-100 in 1% BSA in PBS for 1 h at room temperature. Primary antibodies (**Table 2.8**) diluted in 0.1% Triton X-100 in 1% BSA in PBS was incubated overnight at 4°C. Antibody diluent was used as negative control. At the following day, cells were washed three times in PBS and incubated with secondary antibodies (**Table 2.8**) diluted in 1% BSA in PBS for 1 h at room temperature. Cells were then stained with Alexa Fluor® 488 Phalloidin (8878S, Cell Signaling) for 20 min to stain actin filaments and DAPI (3598, Santa Cruz, TX, USA) for 10 min to stain nuclei. Cells were finally coverslipped using DAKO fluorescence anti-fade mounting medium (S3023, DAKO, Denmark). The confocal images were acquired using Zeiss LSM880 Airyscan Fast confocal microscope (Biological Optical Microscopy Platform, University of Melbourne) and analysed using Imaris 9.2 and FIJI Image J.

Table 2.8 Antibodies for Immunohistochemistry and Immunofluorescence

Name	Species	Dilution	Supplier
alpha-ENaC	Rabbit polyclonal	1:4000	PA1-920A, Invitrogen
Anti- Mucin 5AC [45M1]	Mouse monoclonal	1:200	ab3649, Abcam
Anti-ACE2	Rabbit polyclonal	1:200 (IF); 1:3000 (IHC)	ab15348, Abcam
Anti-Acetylated Tubulin	Mouse monoclonal	1:4000	T7451, Sigma
Anti-Cytokeratin 5	Rabbit polyclonal	1:1000	ab53121, Abcam
E-Cadherin (24E10)	Rabbit monoclonal	1:200	3195, Cell Signaling
Human Uteroglobin/SCGB1A1	Rat monoclonal	1:100	MAB4218, R&D Systems
Anti-ZO-1	Rabbit polyclonal	1:100	61-7300, Invitrogen
Anti-dsRNA [J2]	Mouse monoclonal	1:200	Ab01299-2.0, Australian Bioresearch
Anti-Cytokeratin, pan antibody	Mouse monoclonal	1:400	C2931, Sigma
IgG polyclonal isotype control	Rabbit polyclonal		ab37415, Abcam
Alexa Fluor® 488 Phalloidin		1:50	8878S, Cell Signaling
Alexa Fluor® 594 DNase		1:400	D12372, Invitrogen
DAPI		1:100	3598, Santa Cruz
Goat anti-Mouse IgG (H+L) Cross-Adsorbed Secondary Antibody, Alexa Fluor 647		1:500	A21235, Invitrogen

Goat anti-Rabbit IgG (H+L) Cross-Adsorbed Secondary Antibody, Alexa Fluor 568	1:500	A11011, Invitrogen
Goat anti-Rat IgG (H+L) Cross-Adsorbed Secondary Antibody, Alexa Fluor 488	1:500	A11006, Invitrogen

2.4.6 FLIPR® Membrane Potential Assay

The epithelial sodium channel activity was measured by FLIPR® Membrane Potential Assay Kits (R8128 & R8042, Molecular Devices, CA, USA) according to manufacturer's instruction. Briefly, the cells were seeded in 96-well plate. The supernatant was removed and replaced with Tyrode's Buffer (T2145, Sigma). The blue dye diluted in assay buffer was added as same volume of Tyrode's Buffer and incubated for 40 min at room temperature. A drug plate was prepared by adding serial concentrations of Amiloride (A7410, Sigma) or 5-(N-Ethyl-N-isopropyl) amiloride (EIPA, A3085, Sigma) into 96-well plate. After incubation, the plate was then read in FlexStation® 3 Benchtop Multi-Mode Microplate Reader (Molecular Devices) with following parameters (**Table 2.9**).

Table 2.9 FlexStation® 3 setup parameters for FLIPR® Membrane Potential Assay

	Parameters
Excitation wavelength (nm)	530
Emission wavelength (nm)	565
Emission cut-off (nm)	550
Addition Speed (Rate)	1

2.5 Statistical analysis

All data were statistically analysed by GraphPad Prism 7.0 (GraphPad, San Diego, CA, USA) and presented as the mean ± standard error of mean (SEM) for n individual experiments in cell lines, n individual donors of primary epithelial cell culture or median ± interquartile

range for n individual donors of MESCA samples. For one independent variable, one-way analysis of variance (ANOVA) with the Dunnett's *post-hoc* test, non-parametric Kruskal-Wallis test, and non-parametric Mann-Whitney test were used. Two-way ANOVA with Bonferroni post-hoc tests were used for two independent variables. $P<0.05$ was considered to be statistically significant.

CHAPTER 3

UNPHYSIOLOGICALLY STIFF PLASTIC PERTURBS AIRWAY EPITHELIAL CELL BIOLOGY

3.1 Introduction

Airway epithelium is well known as a physical barrier between external environment and internal *milieu* and a component of host defence interacting with immune system to maintain homeostasis while facilitating immune reactions (Iwasaki et al., 2017). The airway epithelial responses play critical roles in the pathogenesis of inflammatory and allergic diseases, such as asthma, chronic obstructive pulmonary disease (COPD), cystic fibrosis (CF), and respiratory infection (Calvén et al., 2020; De Rose et al., 2018; Vareille et al., 2011). Glucocorticoids (GC) as one of the most efficacious treatments against inflammation are widely used in acute and chronic respiratory diseases, especially inhaled corticosteroids (ICSs). As the initial cell type that in contact with ICSs, airway epithelial cells are more likely to be exposed to higher concentrations of GCs and therefore can be viewed as one of the targets for glucocorticoid therapy.

In airway epithelial cells, it is evident that GCs have profound functional effects in inhibiting pro-inflammatory cytokines, chemokines, peptides, and lipid mediators (Woodruff et al., 2007). GCs initiate their anti-inflammatory actions by regulating gene expression, from early signalling events to nuclear, transcriptional mechanisms, and to post-transcriptional regulatory events in the cytoplasm (Stellato, 2007). Upon ligand binding, the glucocorticoid receptor (GR) homodimers interact with DNA at glucocorticoid response elements (GREs), resulting in increased transcription of targeted genes, including glucocorticoid inducible leucine zipper (GILZ), MAP kinase phosphatase 1 (MKP-1), and inhibitor of nuclear factor kappa B (NF-κB) (IκBα) (Vandevyver et al., 2013). Monomeric ligand-bound GR can bind to DNA-bound proinflammatory transcription factors, NF-κB and activating protein-1 (AP-1), repressing the transcription of their target pro-inflammatory genes (Keenan et al., 2012; Scheinman et al., 1995). GCs also act through non-genomic mechanisms to mediate gene transcription (Surjit et al., 2011). Particularly in airway epithelial cells, dexamethasone at low concentrations rapidly regulates intracellular pH, Ca^{2+}, and protein kinase A (PKA) activity and inhibits Cl^- secretion via non-genomic mechanism (Urbach et al., 2006).

Despite the proven efficacy in controlling inflammation, GC insensitivity in patients with severe disease remains a clinical challenge. Currently, the combination of ICS and short-acting β_2-agonist (SABA) are used for controlling and relieving symptoms for mild asthmatic patients (GINA, 2020). Increased concentration of ICS in combination with long-acting β_2-agonist (LABA) is mostly for moderate and severe asthma patients. Severe asthma patients

remain uncontrolled despite high-dose treatment or can only be controlled with continual high-dose treatment (Holguin et al., 2019). For COPD patients, LABA/ICS are recommended for patients with exacerbations and moderate to severe COPD (GOLD, 2020). However, the use of glucocorticoid in COPD remains controversial (Agusti et al., 2018; Suissa et al., 2013). Evidence showed that ICS use is associated with higher prevalence of oral candidiasis, hoarse voice, skin bruising and pneumonia (Yang et al., 2012).

The molecular mechanisms of GC insensitivity vary depending on the context and cell phenotype (Keenan et al., 2015). Of the mechanisms investigated to date, the GC insensitivity induced by transforming growth factor-β (TGF-β) attracts our attention. Previously, we have reported that TGF-β at 40 pM impairs glucocorticoid inhibition on IL-1α induced IL-6 and IL-8 production in A549 cell line. This impairment was associated with reduced GRE-dependent transactivation and induction of IκBα, GILZ, and the epithelial sodium channel α subunit (ENaCα) (Salem et al., 2012). The impairment of TGF-β on glucocorticoid transactivation was also observed in BEAS-2B cell line and human primary epithelial cells under air-liquid interface (ALI) culture (Keenan et al., 2014). Additionally, we have identified that TGF-β is a key mediator in viral-induced glucocorticoid-insensitivity (Xia et al., 2017). Most recently, we have elucidated a non-canonical TGF-β1 signalling pathway, providing potential drug targets for chronic inflammatory diseases (Li et al., 2019).

The TGF-β superfamily has more than 30 members including the TGF-βs, bone morphogenetic proteins (BMPs), and growth differentiation factors (GDFs) (Poniatowski et al., 2015). The TGF-βs are well-studied and identified in many cellular activities including proliferation, differentiation, migration, adhesion, extracellular matrix (ECM) synthesis, and cell death. Beyond GC-insensitivity, TGF-β has also been extensively evident in lung diseases (Lachapelle et al., 2018). TGF-β is fundamental to the pathogenesis of pulmonary fibrosis by promoting epithelial mesenchymal transition of alveolar epithelial type II (ATII) cells to fibroblasts (Willis and Borok, 2007), ATII cell apoptosis (Thannickal and Horowitz, 2006), deposition of ECM (Verrecchia and Mauviel, 2002), and differentiation of myofibroblasts (Wipff et al., 2007). In CF patients, increased TGF-β levels in blood and bronchoalveolar lavage fluid (BAL) were associated with pulmonary exacerbations, severity of lung disease, and bacterial infection (Harris et al., 2011; Harris et al., 2009). The potential mechanisms of TGF-β in CF include down-regulating epithelial chloride transport, driving goblet cell hyperplasia, suppressing innate immune responses, and promoting fibrosis (reviewed in (Kramer and Clancy, 2018)). In COPD patients, plasma TGF-β levels were

significantly elevated and inversely correlated with forced expiratory volume in one second (FEV_1) (% predicted) and forced vital capacity (FVC) (% predicted) (Mak et al., 2009). Among smokers and patients with COPD, TGF-β levels were positively correlated with the extent of smoking history and the degree of small airway obstruction (Takizawa et al., 2001), and this was influenced by a disturbed intracellular feedback mechanism involving inhibitory Smad 6 and 7 (Springer et al., 2004). Similarly, elevated levels of TGF-β and activation of TGF-β/Smad pathways have also been observed in patients with asthma (Bossé and Rola-Pleszczynski, 2007; Redington et al., 1997). Increased TGF-β in asthmatic patients may contribute to the adhesion of inflammatory cells to airway epithelial cells (Gagliardo et al., 2013) and stimulate structural cells to release pro-inflammatory cytokines (Li et al., 2006). The up-regulation of TGF-β2 may increase airway mucin production and mediate IL-13 induced mucin expression (Chu et al., 2004; Feldman et al., 2019). Furthermore, TGF-β promotes airway remodelling by inducing epithelial cell apoptosis, epithelial-mesenchymal transition (EMT), ECM deposition, and airway smooth muscle cell remodelling (Halwani et al., 2011; Tang et al., 2006).

Emerging interests have been focussed on the relationship of matrix stiffness and TGF-β. Decreasing matrix rigidity promoted TGF-β induced tumour cell apoptosis, whereas increasing rigidity resulted in EMT (Leight et al., 2012). Matrix stiffening can co-operate with TGF-β to elicit excessive collagen deposition and support a role of the FAK/Akt pathway (Gimenez et al., 2017). Interestingly, TGF-β has also been regarded as an extracellular mechanosensory, as it can be activated by matrix stiffening increased mechanical resistance to cell contractile force (Hinz, 2015).

The matrix stiffness, as an important factor of the microenvironment, has been proven to play critical role in airway smooth muscle cells and fibroblasts, as demonstrated in Chapter 1. However, little was known about its influence on airway epithelial cells. In this chapter, we used two-dimensional settings to first investigate the influence of matrix stiffness on airway epithelial cell morphology and functionality. Fibrogenic protein levels were measured to evaluate whether matrix stiffening activates TGF-β in airway epithelial cells. Glucocorticoid transactivation and inhibition on pro-inflammatory cytokines and TGF-β induced GC insensitivity were examined to assess the influence of matrix stiffness in therapeutic research.

3.2 Methods

3.2.1 Cell culture

3.2.1.1 Cell lines

BEAS-2B, A549, and BCi NS1.1 cell cultures were established in 2D stiff, 2D soft and gelatin coating settings as described in Section 2.2. Cells were seeded at 75,000 cells/well in 24-well plate in complete LHC-9, DMEM, and BEGM medium, supplemented as described in Section 2.1.1.1 and 2.1.2.1. On the second day, cells were serum-starved in incomplete DMEM medium or 1x minimal medium, supplemented as described in Section 2.1.1.2 and 2.1.2.2. Following 24 h starvation, cells were treated with drugs according to experiment requirements or cell lysates collected for gene expression measurements.

3.2.1.2 Primary human bronchial epithelial brushing cells

Primary human bronchial epithelial brushing cell (HBEB) cultures were seeded on collagen-coated T25 cell culture flasks and propagated as described in Section 2.1.3.3.

3.2.2 3D spheroid of A549 and MRC-5 cells

3.2.2.1 Culture of normal human lung fibroblast cell line MRC-5

The normal human lung fibroblast cell line MRC-5 (ATCC) was cultured in ATCC-formulated Eagle's Minimum Essential Medium (EMEM, 30-2003, ATCC), supplemented with 10% (v/v) HIFCS, 100 IU/mL penicillin and 50 µg/mL streptomycin. The cells were kept at 37°C in a humidified atmosphere containing 5% CO_2. Cells were passaged once a week by washing confluent cell monolayers twice with sterile PBS, followed by incubating with trypsin-EDTA for 2-3 minutes to detach the cells. Cells were collected by centrifugation at 250 g for 5 minutes at room temperature. Cells were then re-seeded at a density of 6,000 cells/cm^2.

3.2.2.2 Preparation of low adherence plates

Low adherence plates were prepared by coating round-bottom 96-well plates (3799, Corning) with 50 µL poly (2-hydroxyethyl methacrylate) (poly-HEMA, P3932, Sigma) solution. Poly-

HEMA was dissolved at 0.5% (w/v) in 95% ethanol. Coated plates were incubated at 37°C for at least 3 days to allow ethanol evaporation. Poly-HEMA coated plates can be then stored at 4°C until use.

3.2.2.3 Preparation of 3D spheroid from A549 and MRC-5 cells

A549 and MRC-5 cells were mixed at ratios of 5:1, 10:1, and 20:1. Mixed cells were added into low adherence plates. The spheroids were formed by centrifugation at 1,000g for 10min. The cells were imaged using brightfield microscopy every day for 4 days. Spheroid diameter was measured using Image J.

3.2.3 Lactate dehydrogenase activity assay (LDH assay)

The percentage release of the cytosolic enzyme LDH into the supernatant indicates plasma membrane damage. After collecting supernatants from 3D spheroid, the LDH level was measured using Pierce™ LDH Cytotoxicity Assay Kit (88954, Thermo Fisher Scientific) according to the manufacturer's instructions. Briefly, 10% (v/v) sterile ultrapure water and 10% (v/v) lysis buffer (10X) were added into supernatants as spontaneous LDH activity control and maximum LDH activity control. After 45 min incubation at 37°C, 50 µL samples were transferred to flat-bottom 96-well plates in triplicate wells. Samples were incubated with 50 µL reaction mixture at room temperature for 30 min, protected from light. After which, the reaction was stopped by adding 50 µL stop solution and the absorbance was measured at 492 nm and 690 nm. To determine LDH activity, the 690 nm absorbance value (background signal from instrument) was subtracted from the 492 nm absorbance. The percentage of cytotoxicity was then calculated using the following formula.

$$\%Cytotoxicity = \frac{LDH\ activity\ in\ supernatant - Spontaneous\ LDH\ activity}{Maximum\ LDH\ activity - Spontaneous\ LDH\ activity} \times 100\%$$

3.2.4 F-G actin staining

2D stiff, 2D soft, and gelatin coating was prepared in µ-Slide Angiogenesis (81506, Ibidi, Germany) slide as described in Section 2.2, except that the volume of collagen mixture and gelatin solution was 10 µL. BEAS-2B cells were seeded into the slide and left overnight.

Cells were then starved in incomplete DMEM for 48 h prior fixation. The cells were washed twice with pre-cold PBS, fixed in 10% NBF for 15 min, and washed three times in PBS. Cell permeabilization was achieved by incubation with 0.2% Triton X-100 in PBS for 5 min at room temperature. Cells were blocked in 0.1% Triton X-100 in 1% BSA/PBS solution for 15 min at room temperature. After blocking, Alexa Fluor® 488 Phalloidin (1:40) and Alexa Fluor® 594 DNase 1 (1: 400) in 1% BSA/PBS were incubated for 20 min, followed by DAPI (1:100) for 10 min. Three PBS washes were carried out between every incubation. Cells were finally cover-slipped using DAKO fluorescence anti-fade mounting medium. The confocal images were acquired using PerkinElmer Operetta High-content imaging system (Biological Optical Microscopy Platform, University of Melbourne) and analysed using Harmony software (PerkinElmer). The roundness describes how closely the shape of an object approaches that of a mathematically perfect circle. Cell roundness was calculated by Harmony software to identify changes in cell morphology.

3.2.5 Determination of gene expression

Serum-starved BEAS-2B cells were treated with TGF-β1 (100-21C, PeproTech) for 24 h and Dexamethasone (Dex, D1756, Sigma) for 4 h. Supernatants were collected for ELISA analysis, as described in Section 2.4.2. Cells were lysed to perform RNA isolation, as described in Section 2.4.1. Specifically, the lysis buffer used for cells in 2D soft settings was 200 µL. The expression of glucocorticoid-inducible and TGF-β1 induced genes were measured by RT-qPCR as described in Section 2.4.1.

3.2.6 Detection of IL-11 and PAI-1 in supernatants by ELISA

Following TGF-β1 and steroid treatment, the supernatants were collected and assayed for IL-11 and PAI-1 levels, using DuoSet ELISA kit, according to manufacturer's instructions (Section 2.4.2).

3.2.7 Detection of IL-6, IL-8, and GM-CSF in supernatants by ELISA

Serum-starved BEAS-2B cells were treated with Dex for 30 min prior 24 h incubation with tumour necrosis factor alpha (TNF-α, 554618, BD Biosciences). Supernatants were collected

and assayed for IL-6, IL-8, and GM-CSF levels, using OptEIA ELISA kit, according to manufacturer's instructions (Section 2.4.2).

3.3 Results

3.3.1 Comparison of airway epithelial cell morphology under different stiffness microenvironment

Airway epithelial cell morphology was first examined in a variety of models to find appropriate approaches to investigate the influence of stiffness on cell functions. In two dimensions, gelatin coating, collagen-hydrogel coating (2D soft), and *Cytosoft*® plates were used, and the resulting cell morphology compared to conventional culture plastic (2D stiff). The same number of cells were seeded in each setting. Differences in confluency may influence cell shape. Thus, the morphology of cells in the confluent area only were compared in this study. BEAS-2B cells exhibited typical epithelial-like polygonal shape in 2D stiff environment (**Figure 3.1 A**). The cells displayed similar spindle shape when cultured in gelatin coating environment (**Figure 3.1 B**). However, in the 2D soft environment, the cells assumed a cuboidal shape (**Figure 3.1 C**). The *Cytosoft*® plates possess various rigidities ranging from 0.2 to 64 kPa. However, no morphology change was observed across the whole range of stiffness compared to the reference 2D stiff environment (**Figure 3.2**).

Scaffold-free 3D spheroids were generated. Previous experience from the lab indicated that epithelial cells along could only generate a loose cell cluster, rather than form a cohesive spheroid. Here we introduced fibroblast cells into the model to stabilise the spheroid. The fibroblast cell line MRC-5 and the alveolar cell line A549 were mixed at ratios of 1:20, 1:10, and 1:5 with three densities of A549 cells (**Figure 3.3 A**). Spheroids with MRC-5 cells alone were also generated as a reference and a positive control. At Day 0, cell mixtures aggregated into a loose cell cluster with an irregular border. After 24 h, cell clusters condensed into a tight spheroid and single cell morphology could no longer be observed. None of the cell seeding combinations formed spheroids with a smoother border than the MRC-5 cell spheroids. The diameter of the spheroid was dependent on the number of epithelial cells and kept constant after three days (**Figure 3.3 B**). The spheroid diameter was significantly influenced by the number of A549 cells, whereas the ratio of fibroblast cells in the cell type combination had no statistical influence. The spheroids with 10,000 and 30,000 A549 cells showed a round shape. With 100,000 A549 cells, the spheroids assumed an oval shape. The cell viability was detected by measuring released LDH levels. After 4 days, the LDH level was low in all the A549 and MRC-5 spheroids, whereas LDH increased to over 50% in MRC-5 spheroids (**Figure 3.3 C**).

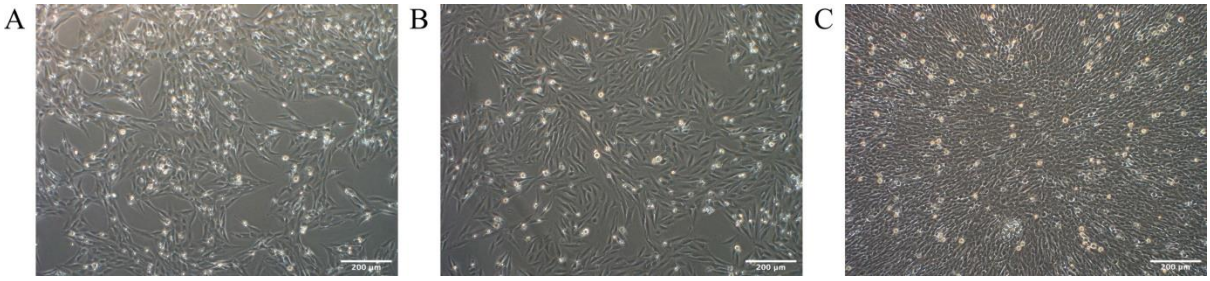

Figure 3.1 BEAS-2B cell morphology under 2D stiff, 2D soft, and gelatin-coated environments

Representative brightfield images (10x objective) of BEAS-2B cells cultured in 2D stiff (A), gelatin coating (B), and 2D soft (C) environment.

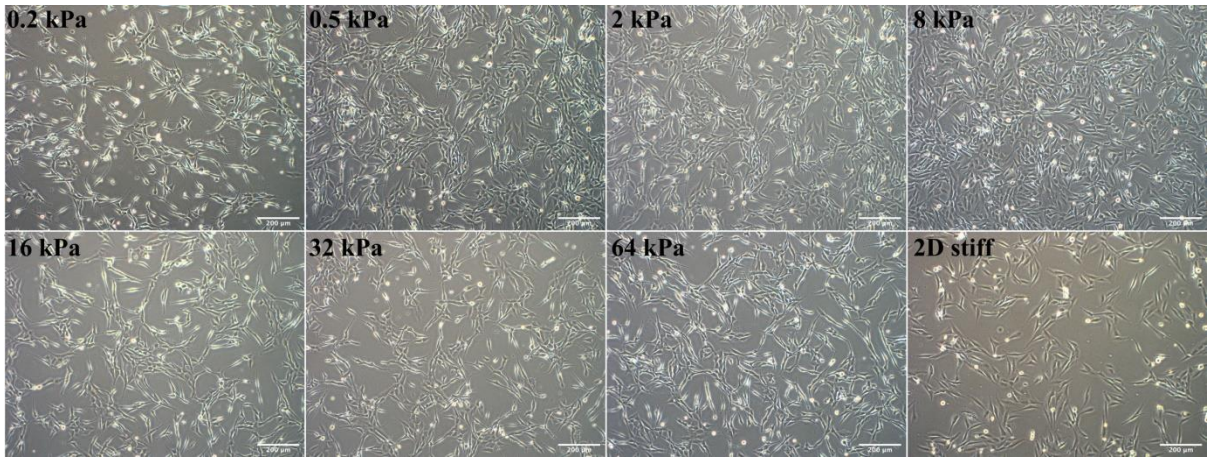

Figure 3.2 Morphology of BEAS-2B cells in environments of increasing stiffness.

BEAS-2B cells were cultured on *Cytosoft*® plates, ranging from 0.2 kPa to 64 kPa, and 2D stiff environment. Images were captured using brightfield microscopy (10x objective).

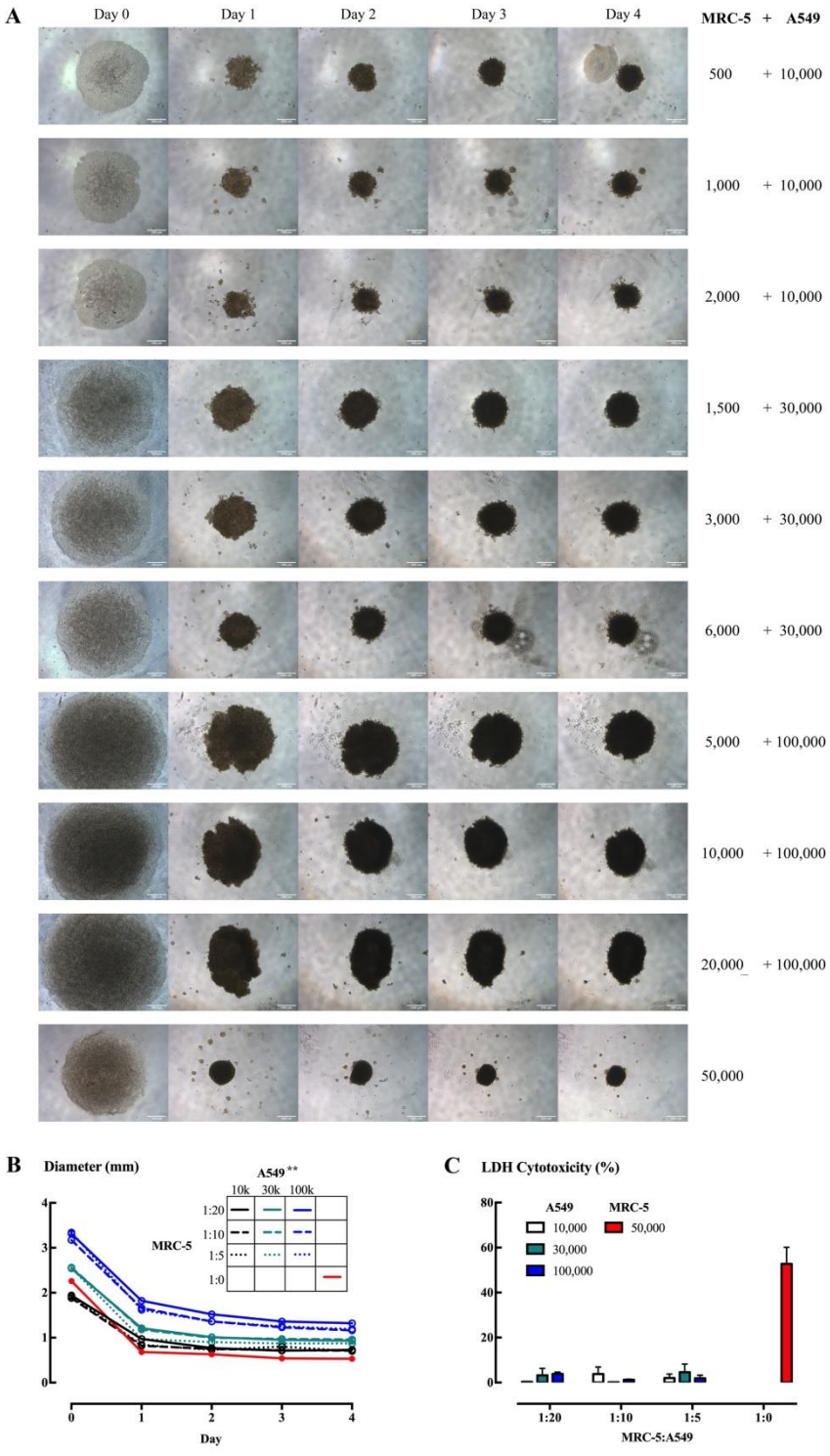

Figure 3.3 3D spheroid of A549 and MRC-5 cells growth curve

MRC-5 and A549 cells were mixed at ratios of 1:20, 1:10, and 1:5, with three densities of A549 cells. MRC-5 cells alone were used as control. (A) 3D spheroid was recorded everyday using brightfield microscopy. (B) The diameter of 3D spheroid was measured by Image J. Two-way ANOVA, **: P<0.01. (C) LDH release was analysed after 4 days of culture. Data are presented as means and SD for n=3 (technical repeat).

As the morphology change was only observed in 2D soft environment compared to 2D stiff environment, the actin distribution was measured in cells in these environmental conditions. Gelatin coating was included to control for the collagen. Monomeric globular G-actin and polymeric filamentous F-actin were stained in BEAS-2B cell under 2D stiff, gelatin coating, and 2D soft environment (**Figure 3.4 A, B, C**). The F-actin filaments were more obvious in cells under 2D stiff and gelatin coating compared to 2D soft. The F/G actin ratio was calculated from the fluorescence intensity of F-actin and G-actin. Data showed that the average F/G actin ratio in 2D stiff environment was similar to gelatin coating, and near two times higher than in the 2D soft condition (**Figure 3.4 D**). The roundness describes how closely the shape of an object approaches that of a mathematically perfect circle. The cells in 2D stiff and gelatin-coated environments had an average roundness at 0.54 (**Figure 3.4 E**). In 2D soft, the cells had a significantly higher average roundness at 0.64, which was consistent with the morphological changes observed under brightfield microscopy. The 2D stiff and 2D soft environments were then used in the following work to illustrate the influence of stiffness on epithelial cell function.

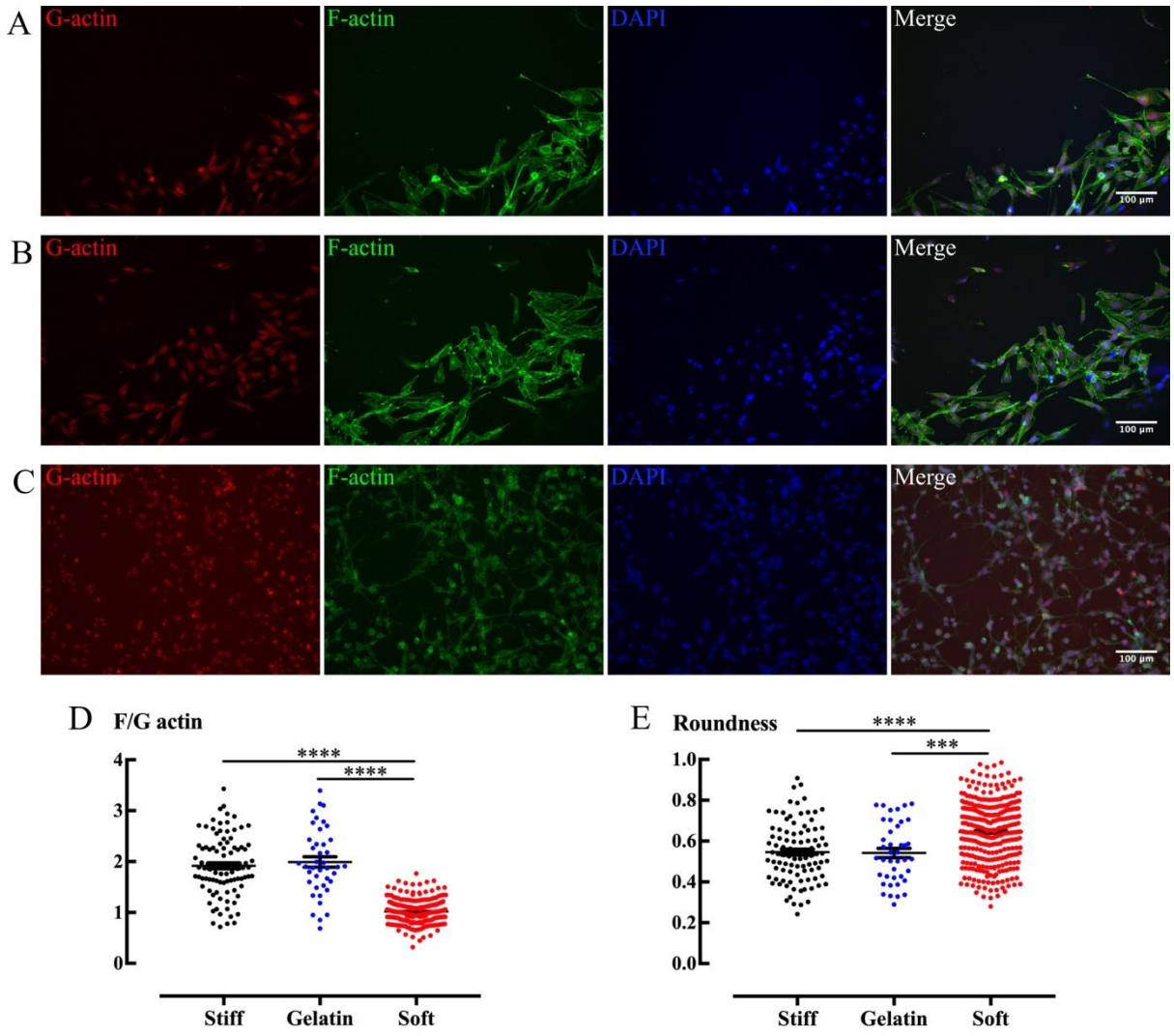

Figure 3.4 F-G actin distribution in BEAS-2B cells under 2D stiff, gelatin coating, and 2D soft environment

BEAS-2B cells were cultured under 2D stiff (A), gelatin coating (B), and 2D soft (C) environment. F actin (green), G actin (red), and nucleus (blue) were stained. Images were captured using Operetta high-content microscopy. Quantitative results (2D stiff, n=96; gelatin, n=41; 2D soft, n=301) of the F/G actin ratio (D) and cell roundness (E) were analysed using Harmony software. Data are presented as means and SEM. One-Way ANOVA, Dunnett's post hoc tests, ***: P<0.001, ****: P<0.0001.

3.3.2 Airway epithelial cell gene expression in 2D stiff and 2D soft environments

First, the expression of a variety of genes was measured to obtain a general view of the potential influence of stiffness on airway epithelial cells. The native human primary bronchial epithelial brushing cells (HBEB) were first analysed as a benchmark. Native HBEB cells

were established into submerged culture in conventional culture plastic and propagated until passage 2. Native cells were regarded as from soft environment, whereas submerged cells are cultured on a stiff substrate. In genes we have measured, the gene expression of CFTR was significantly decreased after submerged culture (**Figure 3.5 A**). TGF-β associated genes parathyroid hormone like hormone (PTHLH) and plasminogen activator inhibitor-1 (PAI-1) gene expression, on the other hand, increased after submerged culture (**Figure 3.5 C, D**). The ENaCα gene expression stayed at the same level after propagation (**Figure 3.5 B**).

Next, bronchial epithelial cell line BEAS-2B, alveolar epithelial cell line A549, and immortalized primary basal cell line BCi NS1.1 were analysed. In BEAS-2B cells, the gene expression of ENaCα and EMT marker E-Cadherin (E-Cad) were increased by soft environment, whereas PTHLH and PAI-1 were reduced (**Figure 3.6**). In A549 cells, the influence of soft environment on these genes showed the same trend as observed in BEAS-2B cells (**Figure 3.7**). Again, similar trends were seen in BCi NS1.1 cells (**Figure 3.8**). Across all the three cell lines, ENaCα showed an interestingly consistent increase in expression in the soft environment, which was not seen in HBEB cells.

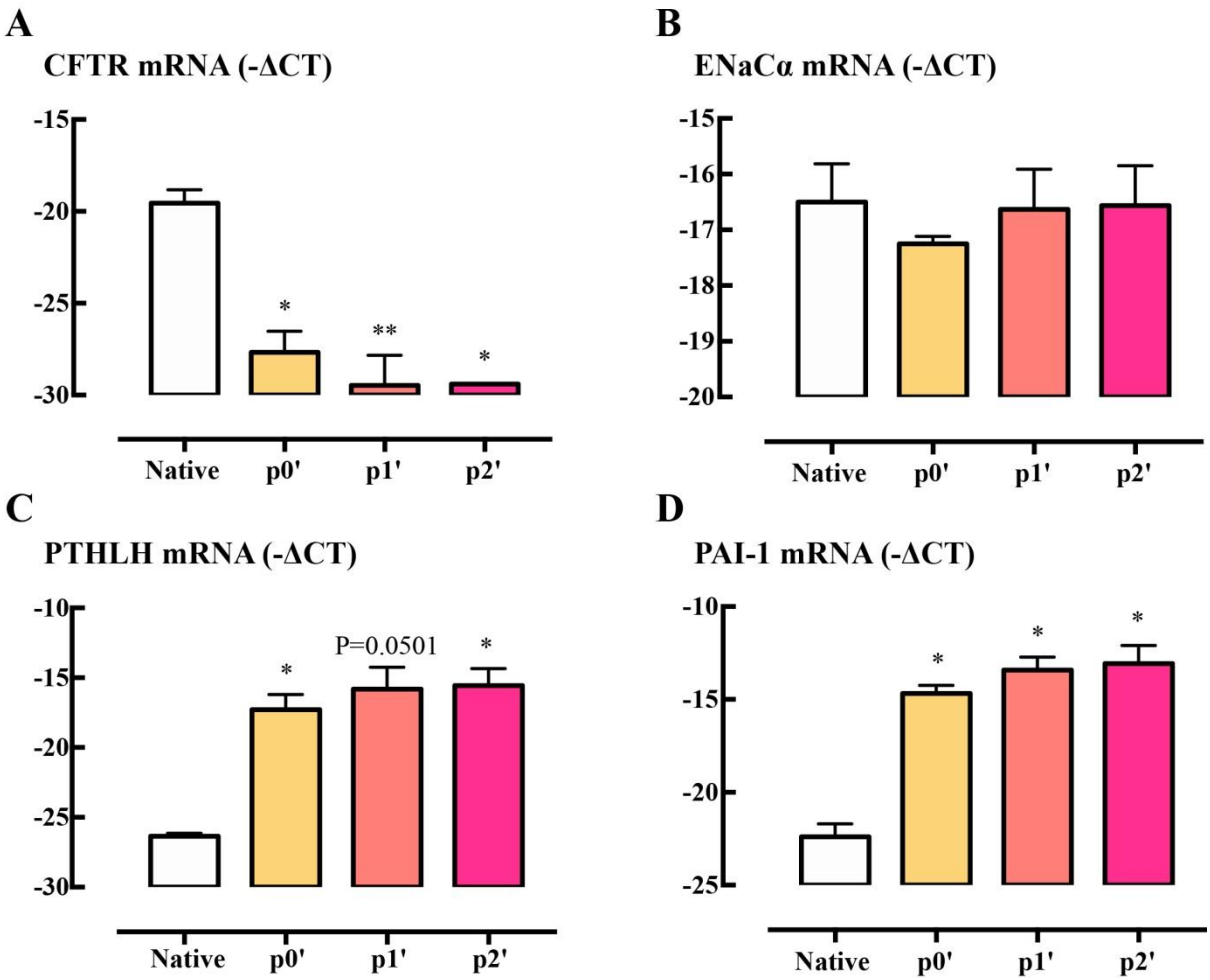

Figure 3.5 The gene expression in native human primary bronchial epithelial brushing cells

HBEB cell were collected from native samples, and the three passages (0-2) were from submerged culture. Total RNA was extracted and gene expression of CFTR (A), ENaCα (B), PTHLH (C), and PAI-1 (D) were measured by RT-qPCR. Gene expression is expressed as -ΔCT (Log2). Data are presented as mean and SEM for n=3 independent cultures, *: $P<0.05$, **: $P<0.01$.

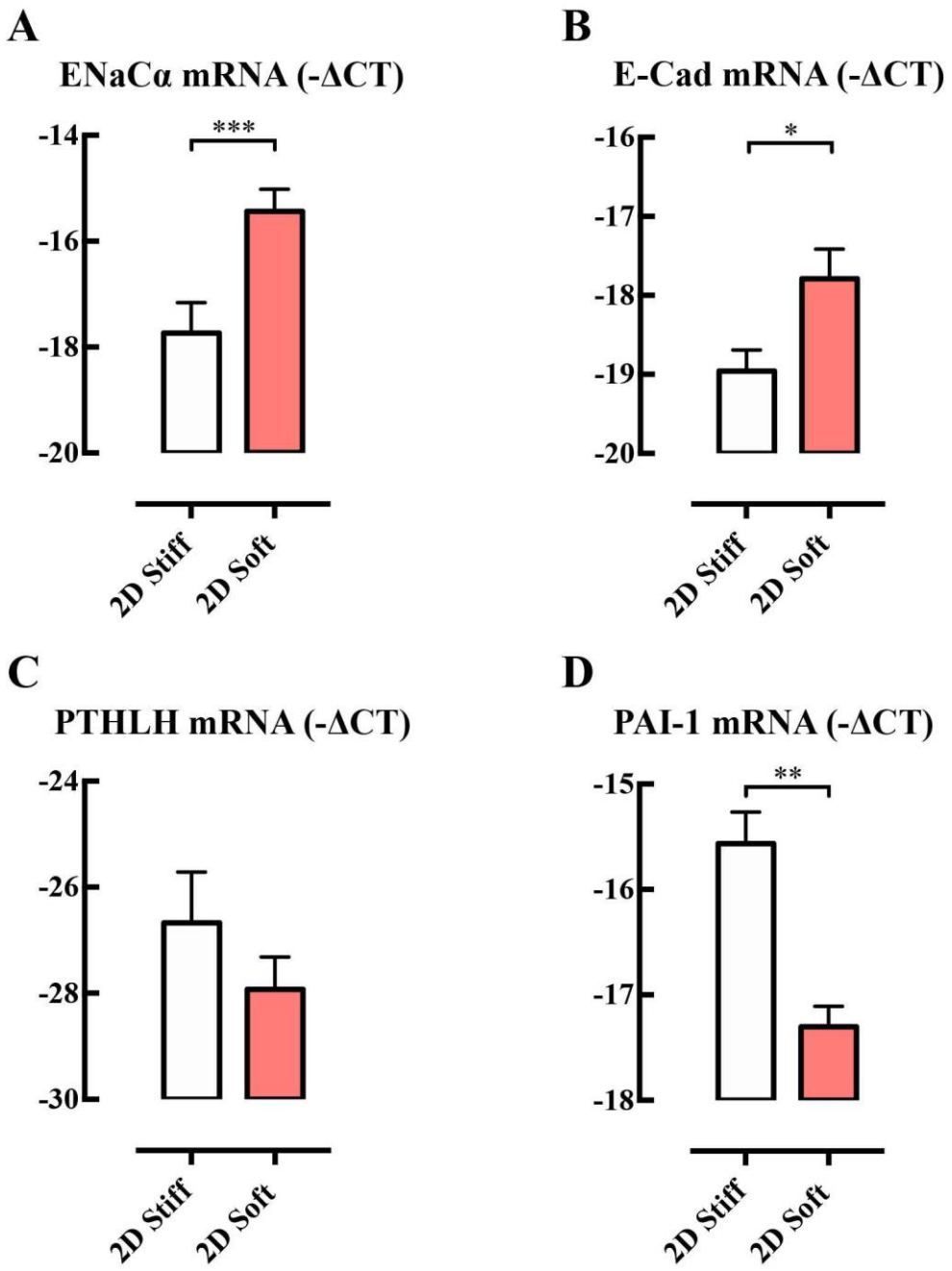

Figure 3.6 The gene expression in BEAS-2B cells on 2D Stiff and 2D Soft environment

BEAS-2B cells were in contact with the 2D Stiff and 2D Soft environment for 72 h. Total RNA was extracted and gene expression of ENaCα (A), E-Cad (B), PTHLH (C), and PAI-1 (D) were measured by RT-qPCR. Gene expression is expressed as -ΔCT (Log2). Data are presented as mean and SEM for n=5 independent experiments. A paired-samples t-test was used for analysis, *: $P<0.05$, **: $P<0.01$, ***: $P<0.001$.

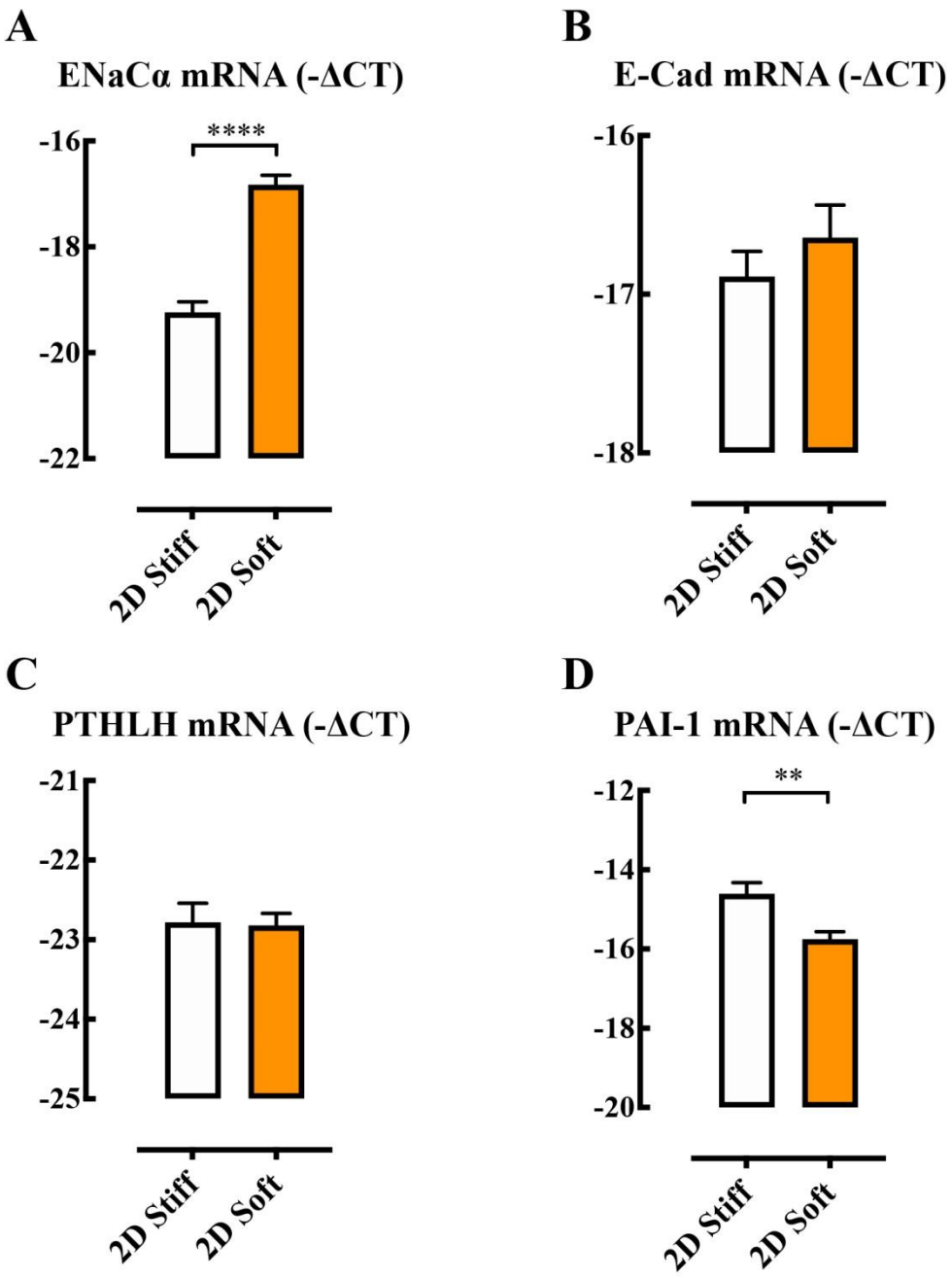

Figure 3.7 The gene expression in A549 cells on 2D Stiff and 2D Soft environment

A549 cells were in contact with the 2D Stiff and 2D Soft environment for 72 h. Total RNA was extracted and gene expression of ENaCα (A), E-Cad (B), PTHLH (C), and PAI-1 (D) were measured by RT-qPCR. Gene expression is expressed as -ΔCT (Log2). Data are presented as mean and SEM for n=5 independent experiments. A paired-samples t-test was used for analysis, **: P<0.01, ****: P<0.0001.

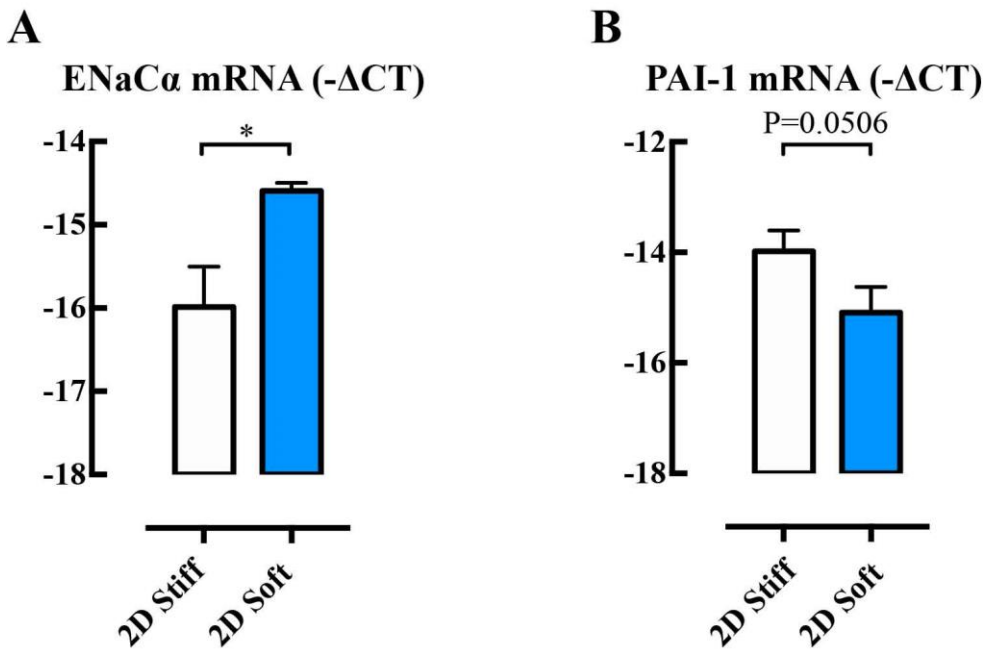

Figure 3.8 The gene expression in BCi-NS1.1 cells on 2D Stiff and 2D Soft environment

BCi NS1.1 cells were in contact with the 2D Stiff and 2D Soft environment for 72 h. Total RNA was extracted and gene expression of ENaCα (A) and PAI-1 (B) were measured by RT-qPCR. Gene expression is expressed as -ΔCT (Log2). Data are presented as mean and SEM for n=4 independent experiments. A paired-samples t-test was used for analysis, *: P<0.05.

3.3.3 TGF-β induction of IL-11 was inhibited by culture on a soft environment

The high expression of PTHLH and PAI-1 in airway epithelial cells in stiff environment addresses the question as to whether the matrix stiffness has an influence on TGF-β activity. BEAS-2B cells were incubated with different concentrations of TGF-β ranging from 4 to 400 pM to ascertain the influence of stiffness on its pro-fibrotic activity. The expression of PAI-1, IL-11, and PTHLH genes was increased by TGF-β in a concentration-dependent manner (**Figure 3.9 A, B, D**), whereas E-Cad was decreased by TGF-β (**Figure 3.9 C**). The IL-11 expression was significantly down regulated by soft environment. Although the PAI-1 expression was low in 2D soft environment at the baseline, TGF-β increased it to levels higher than in 2D stiff environment at concentrations greater than 40 pM. For PTHLH, TGF-β (4 pM) the expression level in 2D soft was slightly elevated over 2D stiff environment. In 2D soft environment, 400 pM TGF-β reduced the E-Cad gene expression to the level 100 pM TGF-β did in 2D stiff environment. At protein level, PAI-1 production was significantly induced by TGF-β with the levels in 2D soft being lower than in 2D stiff when TGF-β

concentration exceeded 40pM (**Figure 3.10 A**). Surprisingly, the induction of IL-11 by TGF-β was diminished by soft environment (**Figure 3.10 B**).

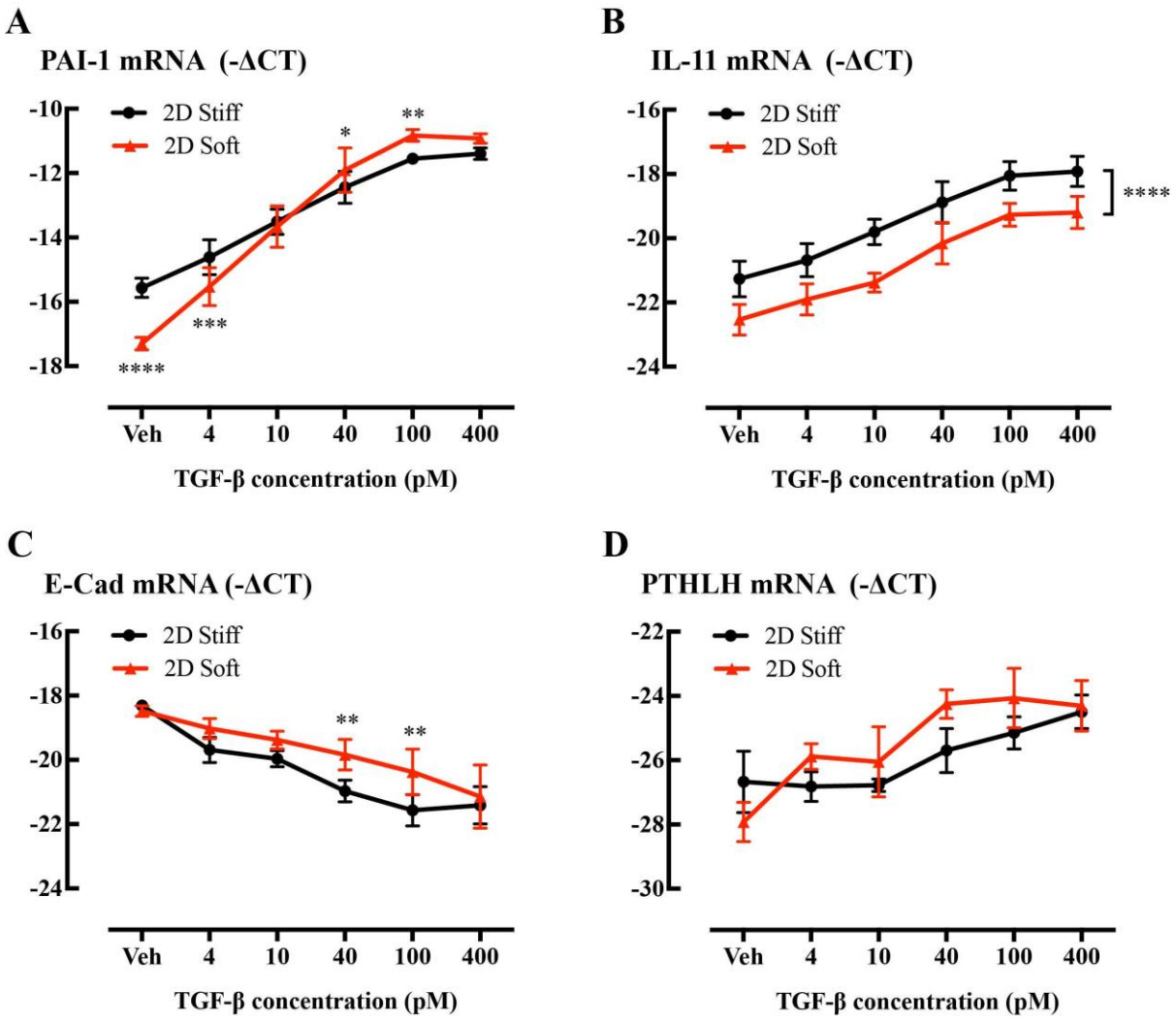

Figure 3.9 The regulation of TGF-β on fibrogenic gene expression in BEAS-2B cells under 2D Stiff and 2D Soft environment

BEAS-2B cells cultured in 2D Stiff and 2D soft environment were incubated with TGF-β (0, 4, 10, 40, 100, 400 nM) for 24 h. Total RNA was extracted and gene expression of PAI-1 (A), IL-11 (B), E-Cad (C), and PTHLH (D) were measured by RT-qPCR. Gene expression is expressed as -ΔCT (Log2). Data are presented as mean and SEM for n=5 independent experiments. Two-way ANOVA with Bonferroni *post-hoc* test was performed to compare the response between 2D stiff and 2D soft, *: P<0.05, **: P<0.01, ***: P<0.001, ****: P<0.0001.

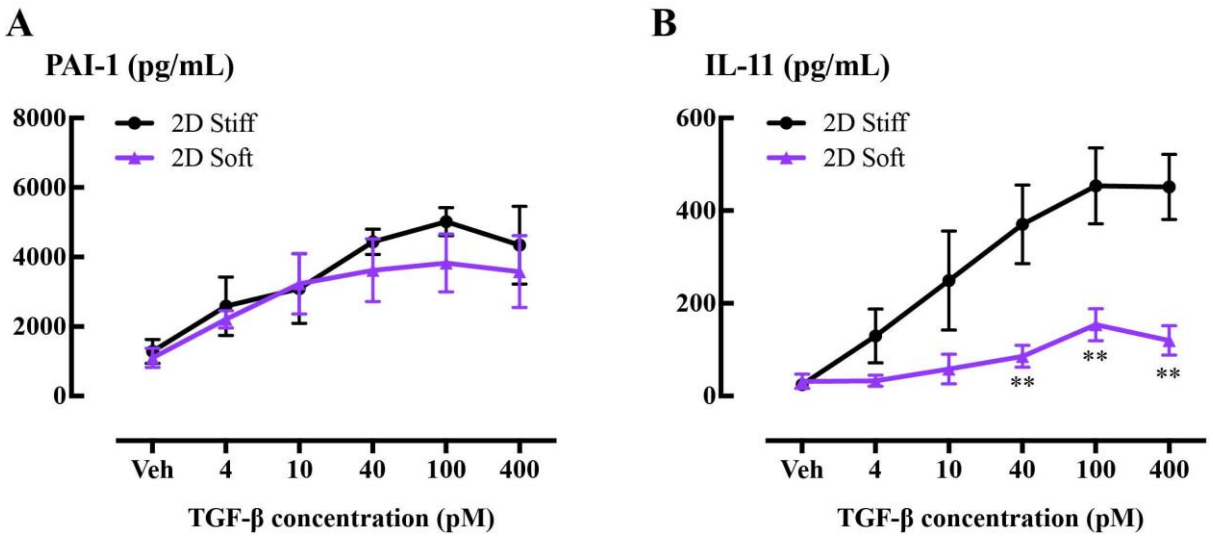

Figure 3.10 The regulation of TGF-β on fibrogenic cytokines production in BEAS-2B cells under 2D Stiff and 2D Soft environment

BEAS-2B cells cultured in 2D Stiff and 2D soft environment were incubated with TGF-β (0, 4, 10, 40, 100, 400 nM) for 24 h. Supernatants were collected and analysed for fibrogenic cytokines PAI-1 (A) and IL-11 (B) levels by ELISA. Data are presented as means and SEM for n=5 independent experiments. Two-way ANOVA with Bonferroni *post-hoc* test was performed to compare the response between 2D stiff and 2D soft, **: P<0.01.

A549 cells incubated with TGF-β were examined to further ascertain the pro-fibrotic effect of TGF-β. In addition to fibrogenic genes, N-Cadherin (N-Cad) and collagen type I alpha (COL1A) gene expression was measured as markers of EMT. Similarly, TGF-β elevated PAI-1 and PTHLH expression level in 2D soft over 2D stiff environment once certain concentrations were reached (**Figure 3.11 A, E**). The baseline difference of IL-11 gene expression between 2D stiff and 2D soft environment was reduced by increasing concentration of TGF-β (**Figure 3.11 B**). The expression of N-Cad showed a similar trend to that of IL-11 (**Figure 3.11 D**). E-Cad expression was more decreased by TGF-β in 2D stiff compared to in 2D soft environment (**Figure 3.11 C**). The induction of COL1A gene expression, however, was not influenced by stiffness (**Figure 3.11 F**). At protein level, PAI-1 and IL-11 baseline production level were lowered in the soft environment (**Figure 3.12 A, B**). More importantly, the induction of IL-11 by TGF-β was also diminished by soft environment as in BEAS-2B cells.

To investigate whether the low level of IL-11 in 2D soft environment was caused by binding of IL-11 to collagen, IL-11 was added to plain 2D stiff and 2D soft settings and incubated the same time as previous experiments. The IL-11 level was near the detection limitation in

control group, regardless of whether in 2D stiff or 2D soft environments (**Table 3.1**). In the IL-11 incubated uncoated plastic and collagen hydrogel, IL-11 remained at similar levels, but the concentration was less than the nominal concentration in each case. This could be explained by the affinity of binding antibody in ELISA assay to the IL-11 protein used for incubation. As limited by COVID-19, this provisional conclusion needs further repeats of the experiment to confirm that the IL-11 reduction by soft environment is not caused by binding to collagen.

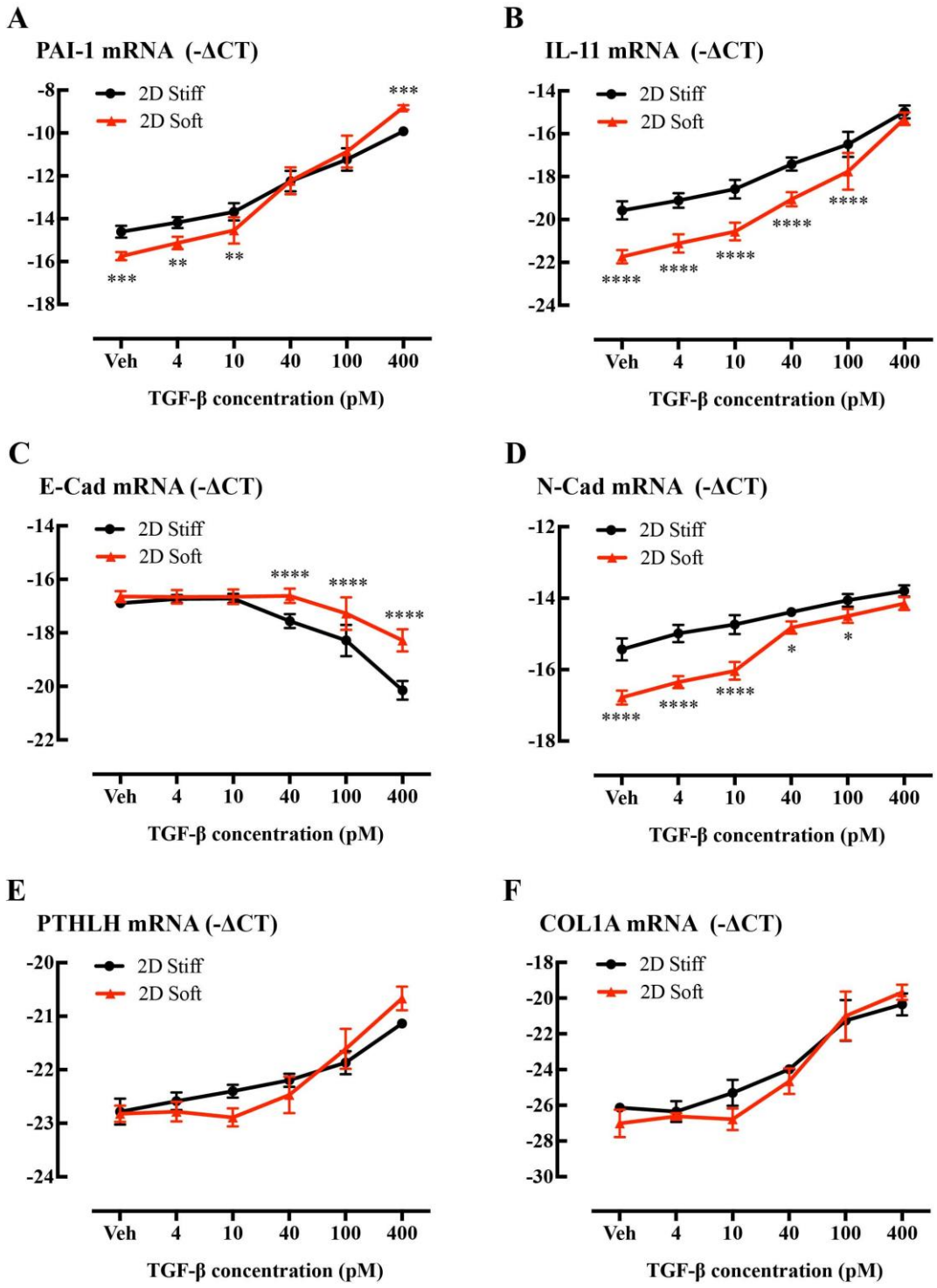

Figure 3.11 The regulation of TGF-β on fibrogenic gene expression in A549 cells under 2D Stiff and 2D Soft environment

A549 cells cultured in 2D Stiff and 2D soft environment were incubated with TGF-β (0, 4, 10, 40, 100, 400 nM) for 24 h. Total RNA was extracted and gene expression of PAI-1 (A), IL-11 (B), E-Cad (C), N-Cad (D), PTHLH (E), and COL1A (F) were measured by RT-qPCR. Gene expression is expressed as -ΔCT (Log2). Data are presented as mean and SEM for n=5 independent experiments. Two-way ANOVA with Bonferroni *post-hoc* test was performed to compare the response between 2D stiff and 2D soft, *: P<0.05, **: P<0.01, ***: P<0.001, ****: P<0.0001.

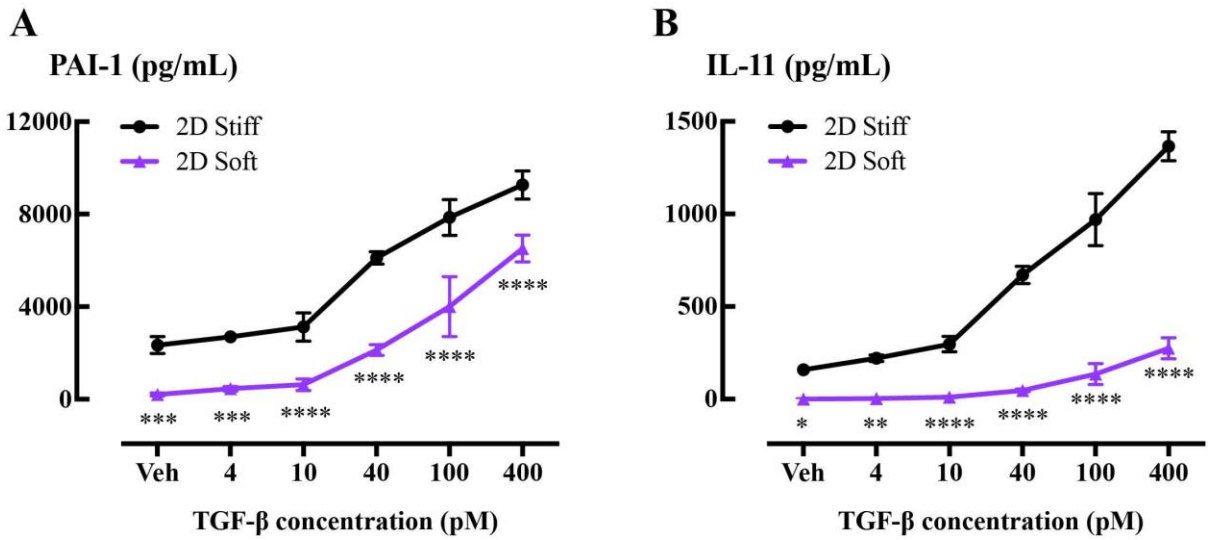

Figure 3.12 The regulation of TGF-β on fibrogenic cytokines production in A549 cells under 2D Stiff and 2D Soft environment

A549 cells cultured in 2D stiff and 2D soft environment were incubated with TGF-β (0, 4, 10, 40, 100, 400 nM) for 24 h. Supernatants were collected and analysed for fibrogenic cytokines PAI-1 (A) and IL-11 (B) levels by ELISA. Data are presented as means and SEM for n=5 independent experiments. Two-way ANOVA with Bonferroni *post-hoc* test was performed to compare the response between 2D stiff and 2D soft, *: P<0.05, **: P<0.01, ***: P<0.001, ****: P<0.0001.

Table 3.1 The IL-11 binding levels in 2D Stiff and 2D Soft environment

The 2D stiff and 2D soft settings were prepared without cells and the medium was removed, replenished and IL-11 (nominal concentration of 500 pg/ml) was incubated for 24 h. Supernatants were collected and analysed for IL-11 levels by ELISA. Data are presented as means for n=2 (technical repeats).

IL-11 level (pg/mL)	**Control**	**500 pg/mL IL-11**
2D Stiff	Undetectable	308.2
2D Soft	1.1	257.1

3.3.4 Glucocorticoid responses were not altered by matrix stiffness

In 2D stiff environment, the GC inducible genes GILZ, ENaCα, IκBα, and MKP-1 were induced by Dex in a concentration dependent manner (**Figure 3.13 A, B, C, D**). The GC response curves were markedly suppressed by soft environment, especially at higher concentration of Dex. However, there was no difference when comparing the absolute ΔCT

value, except for ENaCα (**Figure 3.13 E, F, G, H**). In 2D soft environment, the baseline expression of these genes was higher than in 2D stiff, consistent with previous observations (Section 3.3.2). The high baseline expression of ENaCα in soft environment might preclude the GC induction and explain the huge difference compared to stiff environment.

Next, the anti-inflammatory activity of GC was assessed by measuring cytokine production induced by TNF-α in BEAS-2B cells pre-treated with different concentration of Dex ranging from 1 to 100 nM. As anticipated, cytokine IL-6, IL-8, and GM-CSF levels were significantly induced by TNF-α (control levels were below the limit of detection) and inhibited by addition of Dex (**Figure 3.14**). However, Dex regulation of these cytokines was similar in stiff and soft environments. To further ascertain the effect of stiffness on GC anti-inflammatory activity, different concentrations of TNF-α ranging from 0.1 to 10 ng/mL were added to BEAS-2B cells after Dex pre-treatment. GC effectively inhibited the cytokines induced by TNF-α at all concentrations in both stiff and soft environment (**Figure 3.15**). Again, no difference was found between stiff and soft environments.

To investigate the effect of stiffness on TGF-β dependent glucocorticoid resistance, BEAS-2B cells were incubated with 40 pM TGF-β for 24 h, followed by 4 h Dexamethasone. The induction of glucocorticoid inducible genes GILZ and ENaCα by Dex was impaired by TGF-β in both 2D stiff and 2D soft environment (**Figure 3.16 A, B**). For cyclin-dependent kinase inhibitor 1C (CDKN1C) and MKP-1, soft environment also tended decrease their induction by Dex, albeit not as significant as in the stiff environment (**Figure 3.16 C, D**). Similarly, TGF-β reduced E-Cad and increased N-Cad in both stiff and soft environment with no difference (**Figure 3.16 E, F**).

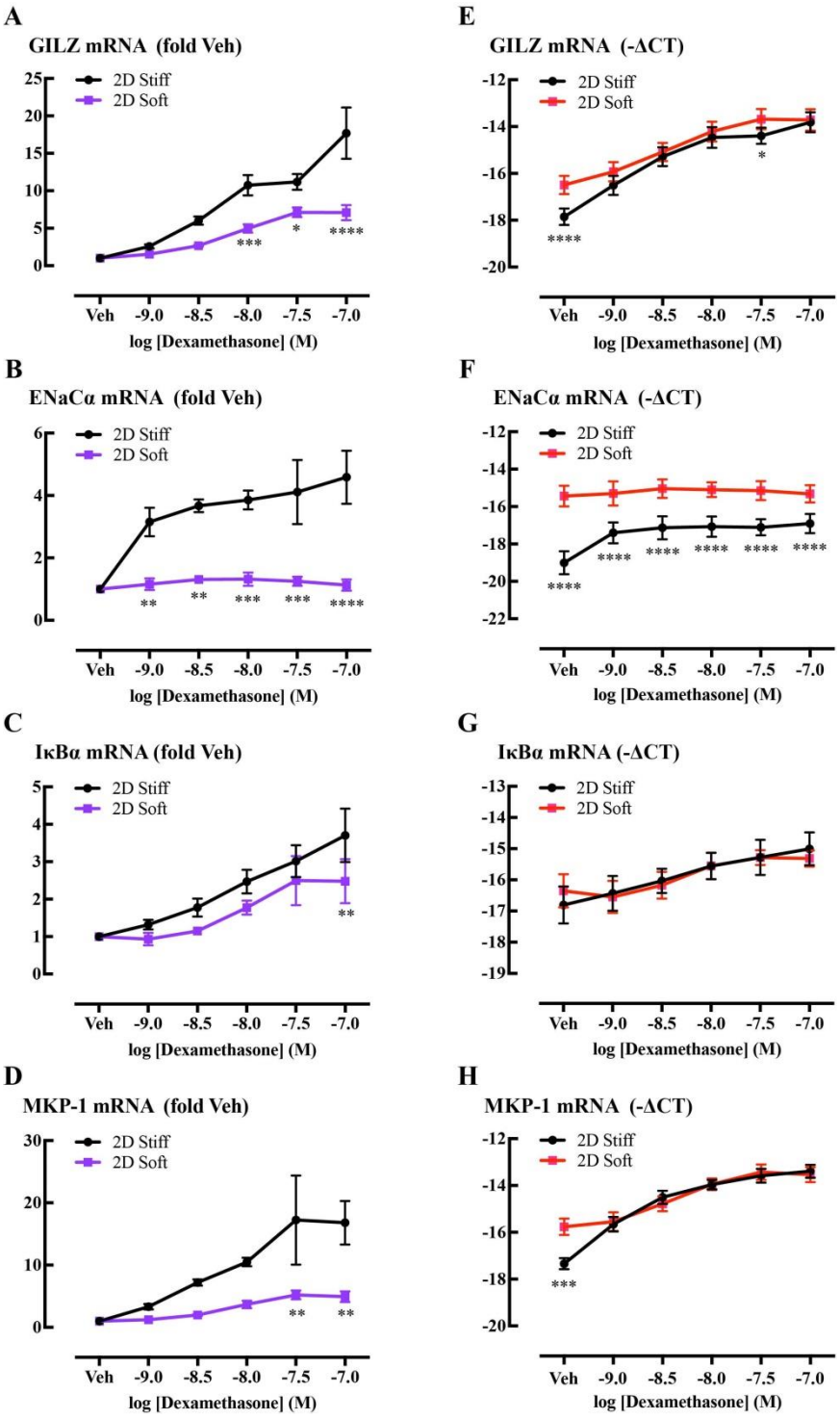

Figure 3.13 The effect of Dexamethasone on the expression of glucocorticoid inducible genes in BEAS-2B cells under 2D Stiff and 2D Soft environment

BEAS-2B cells cultured in 2D Stiff and 2D soft environment were treated with Dex (0, 1, 3, 10, 30, 100 nM) for 4 h. After which, total RNA was extracted and gene expression of GILZ (A, E), ENaCα (B, F), IκBα (C, G), and MKP-1 (D, H) were measured by RT-qPCR. Gene expression is expressed as fold change to Veh and -ΔCT (Log2). Data are presented as mean and SEM for n=5 independent experiments. Two-way ANOVA with Bonferroni *post-hoc* test was performed to compare the response between 2D stiff and 2D soft, *: P<0.05, **: P<0.01, ***: P<0.001, ****: P<0.0001.

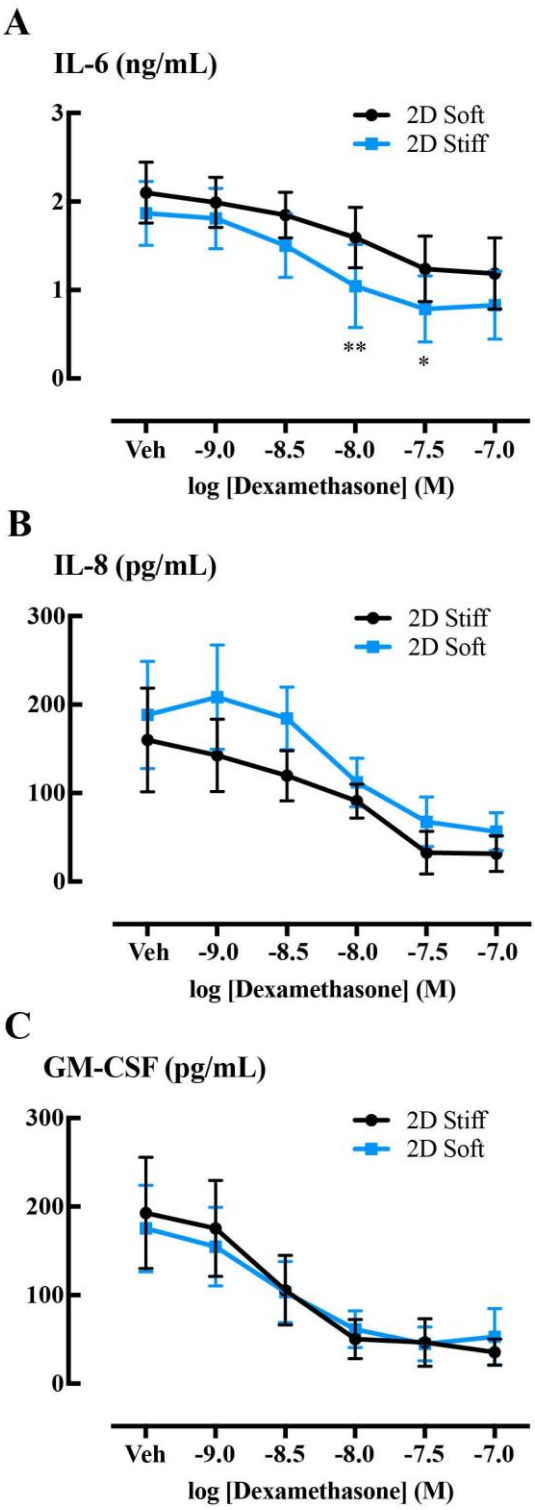

Figure 3.14 The anti-inflammatory activity of Dexamethasone against TNF-α in BEAS-2B cells under 2D Stiff and 2D Soft environment

BEAS-2B cells cultured in 2D Stiff and 2D Soft environment were pre-treated with Dex (1, 3, 10, 30, 100 nM) for 30 min and then stimulated with TNF-α (10 ng/mL) for 24 h. Supernatants were collected and analysed for pro-inflammatory cytokines IL-6 (A), IL-8 (B), and GM-CSF (C) levels by ELISA. Data are presented as means and SEM for n=5 independent experiments. Two-way ANOVA with Bonferroni *post-hoc* test was performed to compare the response between 2D stiff and 2D soft, *: $P<0.05$, **: $P<0.01$.

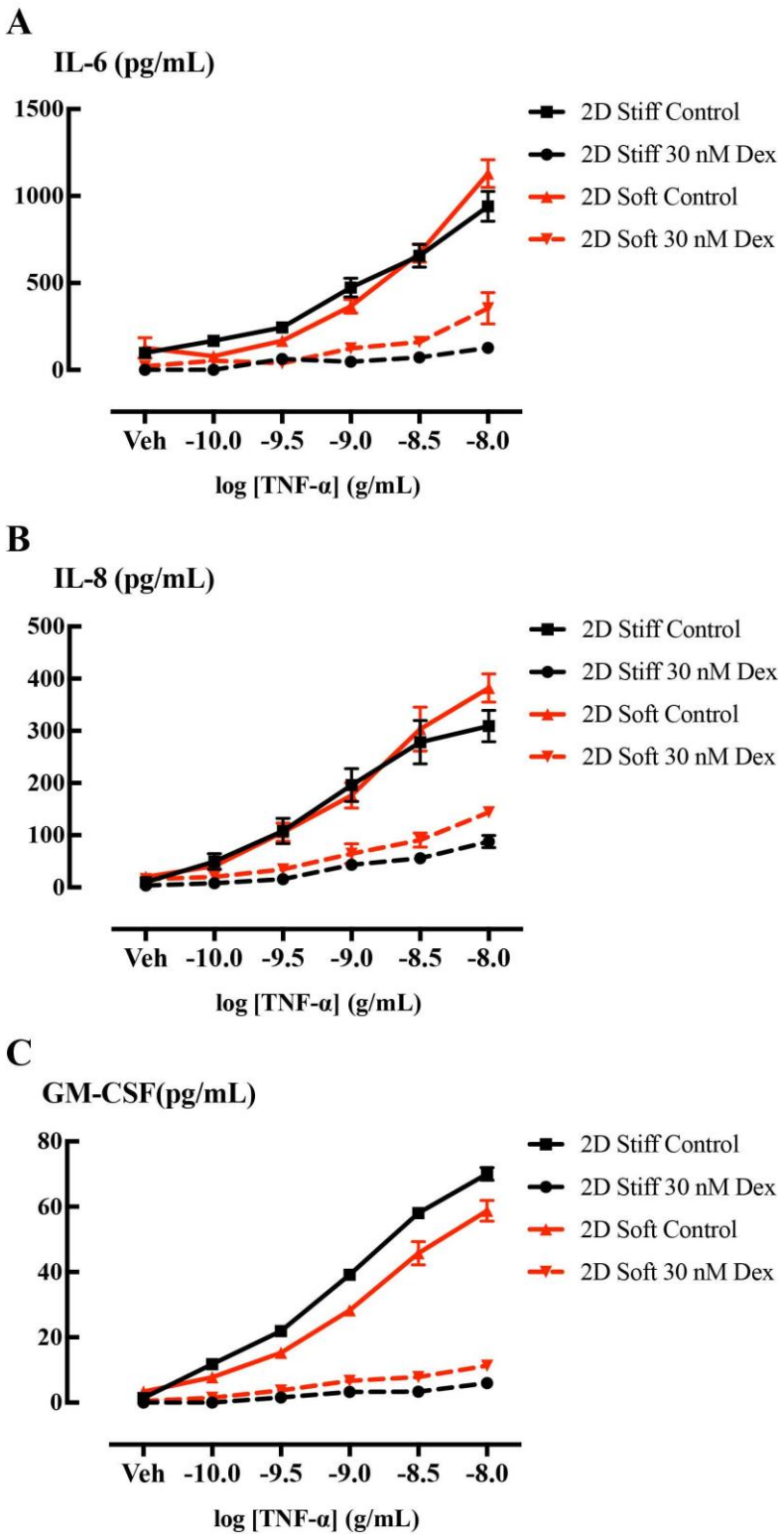

Figure 3.15 The pro-inflammatory activity of TNF-α in the presence and absence of Dexamethasone in BEAS-2B cells under 2D Stiff and 2D Soft environment

BEAS-2B cells cultured in 2D Stiff and 2D Soft environment were pre-treated with Dex (30 nM) for 30 min and then stimulated with TNF-α (0, 0.1, 0.3, 1, 3, 10 ng/mL) for 24 h. Supernatants were collected and analysed for pro-inflammatory cytokines IL-6 (A), IL-8 (B), and GM-CSF (C) levels by ELISA. Data are presented as means and SEM for n=5 independent experiments.

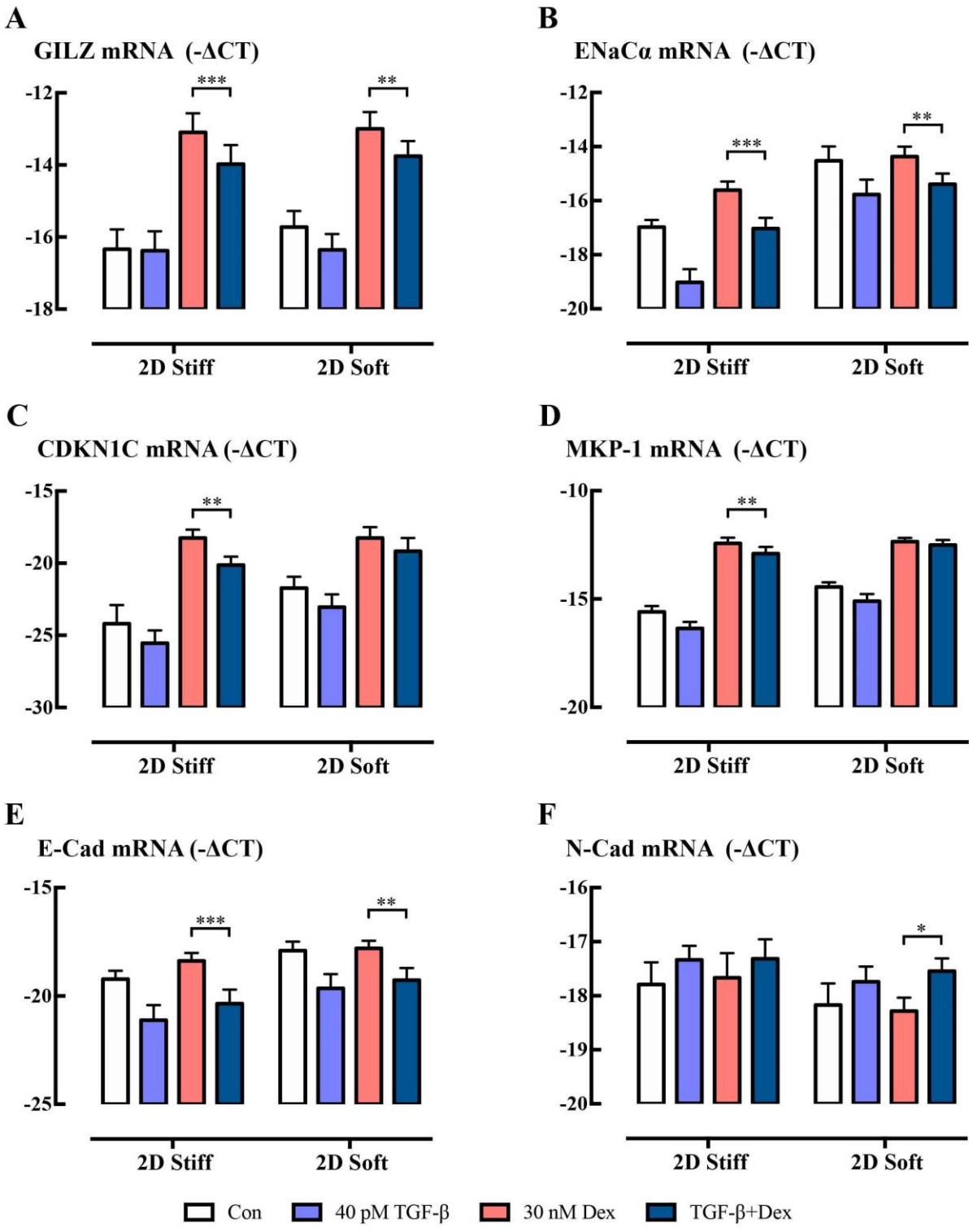

Figure 3.16 The effect of TGF-β on glucocorticoid transactivation in BEAS-2B cells under 2D Stiff and 2D Soft environment

BEAS-2B cells were incubated with TGF-β (40 pM) for 24 h before Dex (30 nM) for 4 h. Total RNA was extracted and gene expression of GILZ (A), ENaCα (B), CDKN1C (C), MKP-1 (D), E-Cad (E), and N-Cad (F) were measured by RT-qPCR. Gene expression is expressed as -ΔCT (Log2). Data are presented as mean and SEM for n=5 independent experiments. Two-way ANOVA with Bonferroni *post-hoc* test was performed, *: P<0.05, **: P<0.01, ***: P<0.001.

3.4 Discussion

In this chapter, we employed collagen-hydrogel to represent soft environment compared to conventional stiff culture plastic to study airway epithelial cell biology. The gene expression in airway epithelial cells cultured on 2D soft environment was much closer to levels of native primary epithelial cells. The soft environment diminished TGF-β induced fibrogenic protein IL-11 and partially protected the cells from TGF-β induced EMT. However, the glucocorticoid transactivation and anti-inflammatory effect were not influenced by matrix stiffness, nor did TGF-β induce profound GC-resistance. These observations emphasize that matrix stiffness does play a role in TGF-β related actions in airway epithelial cells, suggesting that matrix stiffness might influence cellular response to drugs targeting TGF-β signalling.

The morphology of epithelial cells changed from cuboidal shape and less F-actin on collagen hydrogel to spindle shape and stress fibre like F-actin, indicating cells could sense the different force/strain/load created by culture in 2D soft and 2D stiff setting. Airway epithelial cells attach to their neighbouring cells and surrounding ECM through focal adhesions. They adhere to the substrate via actin-myosin cytoskeleton and sense the forces, which in turn respond to the forces through the cytoskeleton (Wells, 2008). Cells on stiffer substrates have more organized cytoskeletons and stable focal adhesions, albeit there is cell type variability (Discher et al., 2005a). Human mesenchymal stem cell on a stiff 62-68 kPa ECM displayed a polygonal morphology, accompanied by smaller and shorter F-actin (Sun et al., 2018). Fibroblasts on soft substrate exhibited less or even no stress fibres compared to fibroblasts on stiff substrate that have articulated stress fibres (Huang et al., 2012b; Liu et al., 2015; Liu et al., 2010; Mih et al., 2011; Yeung et al., 2005). Primary alveolar type II cells became elongated with decreased circularity, displayed aligned and thick F-actin filaments, and expressed less E-Cadherin protein on stiff substrate and glass (Brown et al., 2013). It was surprising that cells showed no morphology change in *Cytosoft*® plates. According to the manufacturer, these plates are made of silicone (polydimethylsiloxane) and required an activation by collagen solution prior seeding cells. Insufficient activation might result in reduced cell attachment, which was observed in the practice. Previously, our lab has used 3D spheroids as a soft setting, revealing the regulation of prostaglandin E_2 (PGE_2) production and signalling pathway in fibroblasts by matrix stiffness (Berhan et al., 2020). However, epithelial cells could barely generate a 3D spheroid, requiring assistance from stromal cells. Interestingly, epithelial cells appeared to preserve fibroblast viability in 3D spheroids,

suggesting epithelial cells might produce anti-apoptosis products or consume toxic substances. Further investigation using cross transfer of epithelial cell and fibroblast conditioned medium and metabolomics analyses might help to explain the "protective' effect.

Airway epithelial cells expressed higher level of fibrogenic genes PTHLH and PAI-1 in stiff environment, suggesting a potential relationship between matrix stiffness and TGF-β. Parathyroid hormone-related protein (PTHrP) encoded by PTHLH gene, is the primary cause of humoral hypercalcemia of malignancy (Mirrakhimov, 2015; Rosol and Capen, 1992). In lung, PTHrP level was sensitive to gravity caused stretch (Torday, 2003). Overdistension of alveolar type II cells downregulated PTHrP expression, resulting in lipofibroblast differentiation to myofibroblasts (Torday et al., 2003). PTHrP increased procollagen I and fibronectin gene expression in primary and immortalized pancreatic stellate cells (Bhatia et al., 2012). Although not fully illustrated, PTHrP has been reported to be associated with TGF-β. Breast cancer cells expressed more PTHrP after treatment of TGF-β, which was reversed by dominant–negative signalling blockade of TGF-β type I receptor (Yin et al., 1999). PTHrP increased alpha smooth muscle actin (α-SMA) and decreased E-cadherin protein level in renal tubuloepithelial cells, which could be inhibited by blockage of TGF-β and inhibition of ERK1/2 (Ardura et al., 2008; Ardura et al., 2010). PAI-1 inhibits the plasminogen activation and urokinase, and hence fibrinolysis. The role of PAI-1 in lung fibrosis has been firmly established (Eitzman et al., 1996; Ghosh and Vaughan, 2012; Olman et al., 1995). Overexpression of PAI-1 enhanced bleomycin induced lung fibrosis, whereas deletion of PAI-1 protected mice from fibrosis (Eitzman et al., 1996). It has also been proved that TGF-β can induce PAI-1 expression in a variety of cell types (Albo et al., 1994; Dennler et al., 1998; Samarakoon et al., 2005). Inhibition of PAI-1 could ease the degree of lung fibrosis induced by TGF-β and protected mouse lung epithelial cells from TGF-β induced EMT (Huang et al., 2012a; Senoo et al., 2010). Native cells expressed more of these fibrogenic genes after established into submerged culture, confirming the observations seen in 2D stiff and 2D soft setting. However, interpretation of this finding was limited by the fact that ciliated and secretory cells were not presented in submerge cultured native cells. Advanced organotypic cultures with tuneable stiffness would be useful to reinforce or refute our conclusion.

The soft culture environment inhibited TGF-β induced IL-11 production at protein level compared to stiff environment, which may mean that "softness" protects lung from fibrosis. Interleukin 11 was first identified in 1990 and subsequently identified as a member of IL-6

family, as they share the ubiquitously expressed co-receptor gp130 (Barton et al., 2000; Boulanger et al., 2003; Paul et al., 1990). Initially, IL-11 was characterized as a hematopoietic cytokine and developed as a recombinant biological treatment for thrombocytopenia in chemotherapy patients (Isaacs et al., 1997). Most recent studies have shown that IL-11 gene is upregulated the most in TGF-β1 stimulated human atrial fibroblasts and it in turn activates a post-transcriptional fibrogenic response, suggesting IL-11 to be a novel therapeutic target for fibrosis (Schafer et al., 2017). In the lung, IL-11 expression was upregulated in asthma and patients and correlated with lung function in disease (Lindahl et al., 2013; Minshall et al., 2000; Strikoudis et al., 2019). Respiratory syncytial virus (RSV) infection and TGF-β stimulation both induced IL-11 gene and protein expression in A549 cells (Elias et al., 1994), which could be inhibited by dexamethasone (Wang et al., 1999). IL-11 neutralizing antibody reduced collagen levels in fibrotic mice lung through inhibiting ERK and Smad activation (Ng et al., 2019). In A549 cells, TGF-β induced IL-11 gene transcription might be through AP-1 dependent pathway (Tang et al., 1998). Consistently, we have also observed that TGF-β induced IL-11 gene expression in BEAS-2B and A549 cells but at different extents between 2D stiff and 2D soft environments. Thus, the inhibition of soft environment on IL-11 protein levels might be through regulation of transcription or post-transcription. It might be questioned that there was baseline gene expression difference between stiff and soft environment in IL-11 expression. However, the baseline protein expression was the same. Longer exposure of cells to soft environment might answer the question. Another potential explanation is that IL-11 is trapped in the “basolateral” hydrogel pores (Howat et al., 2002; Howat et al., 2001), thereby not appearing in the supernatant. It would be interesting to further investigate how cells respond to exogenous IL-11 on 2D stiff and 2D soft environment.

Matrix stiffness had no influence on glucocorticoid actions. Although we have seen the influence of matrix stiffness on TGF-β related targets, TGF-β induced GC resistance was not altered by matrix stiffness. This finding was unexpected, as TGF-β regulates GC actions through a non-canonical pathway involving LIM domain kinase 2 (LIMK2), cofilin 1, Phospholipase Ds (PLDs) (Li et al., 2019). Rho kinase (ROCK) induced LIMK inhibition of cofilin 1 is involved in both MRTF-SRF and YAP/TAZ induced mechanotransduction (Aragona et al., 2013; Olson and Nordheim, 2010; Panciera et al., 2017). Hence, airway epithelial cells might sense the matrix stiffness through other mechanosensory mechanisms, which requires further investigation.

To conclude, our findings suggest that the matrix stiffness does have an influence on airway epithelial cell morphology and TGF-β related fibrogenic genes and proteins. Although no evidence suggested matrix stiffness regulates glucocorticoid responses, the possibility of its regulation by other therapies, especially those targeting the cytoskeleton or TGF-β related, cannot be excluded. To continue the study, ECM substrates within the physiological to pathological stiffness range and organotypic cultures with multiple cell phenotypes should be applied. TGF-β induced IL-11 signalling is also worth further investigation, as it may provide new therapeutic targets for fibrosis.

CHAPTER 4

ENAC EXPRESSION AND ACTIVITY IN AIRWAY EPITHELIAL CELLS

4.1 Introduction

Degenerin/epithelial Na^+ channels (DEG/ENaC) are a family of proteins forming non-voltage gated, amiloride-sensitive cation channels (Garty and Palmer, 1997). The channels have been convincingly implicated in many different physiological functions, acting as ionotropic receptors for diverse extracellular stimuli (Ben-Shahar, 2011). The amiloride-sensitive epithelial sodium channel (ENaC) is a member of the DEG/ENaC family. The mammalian ENaC channels are located at the apical membrane of epithelial cells. They play essential roles in regulating sodium gradients in lung (Matalon et al., 2015), kidney (Nesterov et al., 2012; Schafer, 2002), and colon (Malsure et al., 2014). In the early 1990s, the mature ENaC was demonstrated to comprise three highly related, but independent subunits (Lingueglia et al., 1993a; Lingueglia et al., 1993b), ENaCα, ENaCβ, and ENaCγ (Canessa et al., 1994). In addition to these three subunits, the fourth ENaC subunit, ENaCδ was isolated from a human kidney cDNA library with transcriptional expression in brain, pancreas, testis, and ovary (Waldmann et al., 1995). Initially, little was known about ENaCδ as it was expressed at much lower levels compared to other subunits. Recently, more studies have been focusing on ENaCδ, indicating its distinct biophysical and channel regulatory properties (Giraldez et al., 2012).

The airway surface liquid (ASL) is composed of the periciliary layer (PCL) and mucus layer. To maintain effective mucociliary clearance, the PCL is maintained at approximately 7 µm in height in normal airways, whereas the mucus layer varies from 7 to 70 µm (Jayaraman et al., 2001). The ENaC, cystic fibrosis transmembrane conductance regulator (CFTR), and Ca^{2+}-activated Cl^- channels work collaboratively to regulate PCL height, viscosity, and pH (Matalon et al., 2015). Airway epithelial cells absorb Na^+ through ENaC and facilitate the secretion of Cl^- via the basolateral membranes through Na^+ -K^+ -$2Cl^-$ transporters, following an electrochemical gradient generated by Na^+ -K^+ -ATPase (Matalon and O'Brodovich, 1999). Apical Cl^- exits through CFTR and transmembrane protein 16a. Mature ENaC channel is required for airway epithelium to function properly, as evidenced by αENaC-deficient mice dying shortly after birth due to failure of lung liquid clearance (Hummler et al., 1996). Furthermore, overexpression of ENaCβ caused ASL volume depletion, increased mucus concentration, delayed mucus transport, and mucus adhesion to airway surfaces, sharing features with cystic fibrosis (Mall et al., 2004).

In the gas exchange zone alveolar epithelial cells transport of Na^+ from alveolar lining fluid to the interstitium (Matalon and O'Brodovich, 1999). Cl^- ions passively move across cell junctions or transcellularly (Matthay et al., 1996). Together, the alveolar fluid passively moves from the air space to the interstitium. This process is crucial for the reabsorption of alveolar fluid, when alveolar permeability to fluid and plasma proteins is increased, resulting in compromised gas exchange (Matalon et al., 2015). ENaC regulated Na^+ transport is also essential in this process. Under diseases associated with pulmonary edema, such as high-altitude pulmonary edema, ENaC channel is inhibited by a variety of factors (Scherrer et al., 2010). The decreased channel activity leads to decreased water reabsorption and fluid accumulation in the air space, which made the edema more problematic. Moreover, the inhibition of ENaCα by specific small interfering RNA (siRNA) in the rat lung decreases baseline fluid clearance (Li and Folkesson, 2006), further evidencing the physiological importance of this channel to preserve efficiency of alveolar gas exchange.

The ENaC channel expression/synthesis, intracellular channel trafficking, and single-channel properties are regulated by a variety of factors (Bhalla and Hallows, 2008; Garty and Palmer, 1997). Induction of serum and glucocorticoid-regulated kinase by aldosterone resulted in fourfold increase in the ENaC channel activity (Shigaev et al., 2000). The high GILZ expression induced by aldosterone, in turn, stimulated ENaC activity by inhibiting extracellular signal-regulated kinase (ERK) signalling (Soundararajan et al., 2005). ENaC is potentially controlled by the circadian clock. Disruption of Period 1 (*Per 1*) gene in renal medulla of mice attenuated ENaCα mRNA expression and caused urinary sodium excretion (Gumz et al., 2010; Gumz et al., 2009). Inhibition of casein kinases 1 delta and epsilon (CK1δ/ε), which phosphorylate *Per 1* to enter nucleus, reduced ENaCα mRNA and activity (Richards et al., 2012). Lung injury causes increased level of cytokines, which lead to accumulation of alveolar fluid, edema, and acute respiratory distress syndrome. Cytokine-induced inflammation can thereby alter alveolar ENaC expression and activity (Wynne et al., 2017). For example, TGF-β1 reduced ENaCα gene and protein expression through ERK1/2 activity, promoting alveolar edema (Frank et al., 2003). TGF-β also drives internalization of ENaCβ, the subunit that stabilizes the cell-surface ENaC-αβγ complex (Peters et al., 2014).

Among all the above-described factors, growing evidence is suggesting that ENaC is a mechanosensitive channel. It is not surprising, as the DEG family has been implicated in mechano-sensation transduction pathways (Ben-Shahar, 2011; Drummond et al., 2004). Fluid flow is one of the major factors. Fluid flow increased laminar shear stress activates ENaC

(Satlin et al., 2001) by increasing ion channel open probability without affecting active channel numbers (Althaus et al., 2007). Airway epithelium is exposed to shear forces from inspiratory and expiratory airflows (Tarran et al., 2006). Although there is no direct experimental evidence, one could speculate that higher shear forces at the airway epithelial cell surface could increase ENaC activity. Growing evidence are now suggesting cytoskeleton can modulate activity of ion transport proteins, including ENaC. Since 1990s, studies have shown that ENaC can directly or through actin-binding proteins interact with actin (Morachevskaya and Sudarikova, 2021; Sasaki et al., 2014; Sudarikova et al., 2015). The finding that F-actin specifically binds to the carboxyl terminus of α-ENaC suggested the participation of actin in ENaC function (Mazzochi et al., 2006). Actin filament disrupter cytochalasin D and short actin filaments can induce Na+ channel activity (Berdiev et al., 1996; Cantiello et al., 1991).

ENaC is regarded as therapeutic target in multiple pathological conditions, such as acute respiratory distress syndrome, cystic fibrosis, hypertension, and pulmonary infection (Qadri et al., 2012). Among these, cystic fibrosis (CF) is in our focus of interest. CF is a genetic disorder caused by mutations in CFTR, with signs of salty-tasting skin, poor weight gain and accumulated mucus. Dehydrated airway surface liquid and viscus mucus result in the failure of mucociliary escalator (Birket et al., 2014). Although the relationship between CFTR and ENaC remains controversial (Chen et al., 2010; Collawn et al., 2012; Hobbs et al., 2013; Itani et al., 2011), it is commonly accepted that CFTR mediated Cl^- secretion and ENaC mediated Na^+ absorption together maintain the ASL homeostasis. ENaC-targeted therapy for CF is particularly appealing, as it is independent of CFTR (Farinha and Matos, 2016), which could also be applicable to those who have rare mutations for whom no channel correctors are available (Harutyunyan et al., 2018). However, small molecules inhibiting ENaC, like amiloride, benzamil, and GS-9411 failed in clinical trials, mostly due to off-target effects, short half-life, or adverse effects (Graham et al., 1993; Hirsh et al., 2004; Knowles et al., 1990; O'Riordan et al., 2014). Nevertheless, a new generation of small molecule inhibitors, channel-activating protease inhibitors and siRNA are currently in development, and some have been undergoing clinical trials (De Boeck and Amaral, 2016; Shei et al., 2018).

Currently, there are several assays for measuring ENaC channel activity. The Ussing chamber, invented by Hans Ussing in 1950s (Ussing and Zerahn, 1951), is a simple but powerful tool to investigate ion transport. It has helped understand the mechanisms of cystic fibrosis by monitoring Cl^- secretion (Itani et al., 2011). The Ussing chamber has also been

applied in measuring ENaC channel activity (Bangel-Ruland et al., 2010; Myerburg et al., 2010). An updated Ussing chamber design can accommodate multiple chambers and offers measurement of permeability using fluorescent probes as well as electrophysiological measurements (Thomson et al., 2019). Patch-clamp technique is another common tool to study ion currents. Variations of the basic techniques, such as cell-attached patch, whole-cell patch, inside-out patch, have fulfilled different research requirements. Patch clamp also has a long history in studying ENaC activity (Cook et al., 2002; Nesterov et al., 2008; Nesterov et al., 2016; Palmer and Frindt, 1986; Yu et al., 2008). However, both the Ussing chamber and the patch-clamp technique are only suitable for epithelial tissues or monolayer cells on transwell membranes. Therefore, they are not ideal for large scale drug screening. Recently, more high-throughput screening technologies have been developed for ion channels, including ligand binding assay, flux-based assay, fluorescence-based assay, and automated electrophysiological assay (Yu et al., 2016). For voltage-gated sodium channel, fluorescence-based membrane potential dye assay is more often used. New dyes have been developed intending to improve the assay accuracy (Du et al., 2015; Felix et al., 2004). The FLIPR® membrane potential assay is designed to enhance signal windows and yield acceptable Z-scores. It has been shown to have great applicability in evaluating voltage-gated sodium channels (Na_vs), CFTR, and ENaC activities (Ahmadi et al., 2017; Chen et al., 2015; Huang et al., 2020b; Maitra et al., 2013; Tay et al., 2019).

In Chapter 3 of this thesis, we observed consistent high expression of ENaCα gene in a 2D soft environment and TGF-β reduced ENaCα gene expression in both 2D stiff and 2D soft environments. Considering its role in maintaining ASL homeostasis and mechanosensation transduction, it is of interest to investigate whether ENaC is mechanosensitive to matrix stiffness. As described in Section 1.3.1, thickening of basement membrane is a feature of airway remodelling in asthma. Airway distensibility negatively correlated with basement membrane thickness in asthmatic patients compared to healthy subjects, indicating a stiffer airway (Brackel et al., 2000b; Brown et al., 2007; Wilson et al., 1993b). Thus, in this chapter, we first measured the ENaC protein expression in biopsies from a community cohort of asthmatic and non-asthmatic subjects representing *in situ* stiffness range. ENaC channel activity was then measured across cell lines and primary epithelial cells from normal donors and CF patients, using high-throughput FLIPR® membrane potential assay under 2D stiff and 2D soft environment.

4.2 Methods

4.2.1 Determination of ENaCα expression in epithelial cells of the large human airway biopsies from the MESCA study

4.2.1.1 Melbourne Epidemiological Study of Childhood Asthma (MESCA)

The airway biopsies used in this study were obtained from subjects recruited from the Melbourne Epidemiological Study of Childhood Asthma (MESCA) cohort. Details are described as in Section 2.4.4. Characteristics of all MESCA subjects that were used in this chapter are shown in **Table 4.1**.

Table 4.1 Characteristics of the MESCA subjects used for ENaCα staining using Immunohistochemistry

SID	Status	Sex	Smoking	ICS	β_2-agonist	Oral CS	Atopic status	FEV_1% predict
MM9928401	Non-A	Female	Y	N	N	N	N	104
MW0003101	Non-A	Female	Y	N	N	N	N	98
JS9926301	Non-A	Female	Y	N	N	N	Y	112
MM9914401	Non-A	Male	N	N	N	N	N	115
NM0002701	Non-A	Male	Y	N	N	N	N	132
KR9918201	Non-A	Male	N	N	N	N	Y	115
SJ9933601	Non-A	Male	Y	N	N	N	Y	100
FR9933602	MILD	Female	N	Y	Y	N	N	108
JF9920701	MILD	Male	N	N	N	N	Y	93
JK0006601	MILD	Male	N	Y	Y	N	Y	103
PJ0005501	MILD	Male	N	N	Y	N	Y	83
CA9915401	MOD	Female	N	Y	Y	N	Y	58
PA9927701	MOD	Male	N	Y	Y	N	Y	60

TR0004801	MOD	Male	N	Y	Y	N	Y	68
MP9933301	MOD	Male	N	Y	Y	N	Y	50
PP9933302	MOD	Male	N	Y	Y	N	Y	55
PL9931202	MOD	Male	Y	Y	Y	N	Y	66
WU9927902	MOD	Male	Y	Y	Y	Y	Y	67
HH0020601	SSA	Female	N	Y	Y	Y	N	58
HI0025101	SSA	Female	N	Y	Y	Y	N	61
JM0025501	SSA	Female	N	Y	Y	Y	N	57
FG0021601	SSA	Female	N	Y	Y	Y	Y	101
KF0019201	SSA	Female	N	Y	Y	Y	Y	56
MM0023401	SSA	Female	N	Y	Y	Y	Y	99
SM0024401	SSA	Female	N	Y	Y	Y	Y	67
ET0024101	SSA	Male	N	Y	Y	Y	N	80
FV0028601	SSA	Male	N	Y	Y	Y	Y	57

Non-A: non-asthmatic control (n=7); MILD: mild asthma (n=4); MOD: moderate asthma (n=7); SSA: severe asthma (n=9); N: no; Y: yes. CS: corticosteroids. Post bronchodilator FEV_1: forced expiratory volume in one second.

4.2.1.2 Immunohistochemistry staining of ENaCα

The expression of ENaCα in the epithelial cells of MESCA biopsies was measured by the three-layer immunoperoxidase staining of paraffin-embedded tissue sections, as described in Section 2.4.4.3. Briefly, non-specific binding sites were blocked in 1.5% normal goat serum for 20 min after antigen retrieval. Sections were incubated with rabbit polyclonal alpha-ENaC antibody at 4°C for overnight. Matched concentration of normal rabbit IgG isotype control was used as negatived control and pan-actin antibody was used as positive control. Following 30 min incubation of Vectastain® biotinylated goat anti-rabbit secondary antibody, sections were further incubated with ABC reagent and subsequent specific visualization of staining

with stable peroxidase substrate buffer DAB. Images were taken using Olympus BX51. The ENaCα expression in epithelial cells was determined by a semi-quantitative IHC scoring method.

4.2.2 ENaC channel activity measurement using FLIPR® Membrane Potential Assay

4.2.2.1 Cell culture

BEAS-2B, A549, and primary epithelial cells were established in 2D stiff and 2D soft settings as described in Section 2.2. Cells were seeded at 20,000 cells/well in 96-well plate, as described in Section 2.1. On the second day, cells were serum-starved in incomplete DMEM medium or 1x minimal medium, supplemented as described in Section 2.1.1.2 and 2.1.2.2.

4.2.2.2 Cell and drug preparation for FLIPR assay

Following 24 h starvation, cells and drugs were prepared as described in Section 2.4.6. Briefly, the culture medium was replaced by Tyrode's buffer. The assay dye was added and incubated at room temperature for 40 min. Meanwhile, a drug plate was prepared by adding serial concentrations of Amiloride or 5-(*N*-Ethyl-*N*-isopropyl) amiloride (EIPA) into a 96-well plate. The volume of each reagent and drug concentrations are as shown in **Table 4.2**.

Table 4.2 Volume of reagents and drug concentration used in FLIPR assay

Injection ratio	Tyrode's buffer (µL)	Assay dye (µL)	Drug concentration (multiple of final)	Injection volume
1:20	95	95	20x	10
1:10	90	90	10x	20
1:5	80	80	5x	40

4.2.2.3 FLIPR assay

Following the dye incubation, both cell plate and drug plate were placed into FlexStation® 3 Benchtop Multi-Mode Microplate Reader and balanced at 37°C for 10 min. The assay was then carried out as following settings (**Table 4.3**).

Table 4.3 FlexStation® 3 settings for measuring ENaC activity using FLIPR® Membrane Potential Assay

	Content	Value
Reading settings	Excitation wavelength (nm)	530
	Emission wavelength (nm)	565
	Emission cut-off (nm)	550
Timing settings	Run time (sec)	600
	Interval (sec)	5
Compound transfer	Initial volume (µL)	190/180/160
	Pipette Height (µL)	195/190/180
	Volume (µL)	10/20/40
	Rate (µL/sec)	1
	Time point (sec)	180

4.2.3 Determination of ENaC α, β, γ gene expression

BEAS-2B cells and HBEB cells were lysed to perform RNA isolation, as described in Section 2.4.1. Specifically, the lysis buffer used for cells in 2D soft settings was 200 µL. The expression of ENaC α, β, γ genes was measured by RT-qPCR as described in Section 2.4.1.

4.3 Results

4.3.1 ENaCα expression in airway epithelial cells has no correlation with asthma severity

To ascertain whether the differential ENaCα gene expression in cells under 2D stiff and 2D soft environment was related to *in situ* stiffness change, the ENaCα expression was measured in biopsies from Melbourne Epidemiological Study of Childhood Asthma (MESCA) by immunohistochemistry. Firstly, the ENaCα antibody titration was performed to determine the optimal concentration with minimum background. Non-asthmatic control and severe asthma subjects were used to test three concentrations of the antibody (**Figure 4.1A**). Normal rabbit IgG isotype control was used as a negative control to avoid non-specific binding of the antibody (**Figure 4.1A**). Additionally, antibody against pan-actin and no primary antibody were included as positive and negative controls for the IHC staining (**Figure 4.1 B**). The antibody at 0.125 µg/mL gave low intensity staining in both samples. Antibody at 0.5 µg/mL gave definitive staining, but the isotype control in non-asthmatic control showed some non-specific binding. Thus, antibody at 0.25 µg/mL was chosen for the subsequent IHC staining, as clear signal was achieved at minimal non-specific reactivity.

The ENaCα expression was compared in the airway epithelial cells of non-asthmatic control, mild, moderate, and severe asthmatic patients from MESCA study using semi-quantitative IHC scoring method (**Figure 4.2; Figure 4.3**). In severe asthmatics, the basement membrane was thicker than other subjects (**Figure 4.2D**) (Wilson and Li, 1997), indicating airway remodelling. Regardless of the disease status, the ENaCα appeared to be expressed in ciliated and basal cells. The quantitative results showed that the expression of ENaCα was not altered by the disease status (**Figure 4.3A**) nor was there a clear relationship between ENaCα expression and smoking status (**Figure 4.3B**) or FEV_1% level (**Figure 4.3D**). However, ENaCα appeared to be expressed at lower levels in male compared to female subjects (**Figure 4.3C**) (P=0.0598).

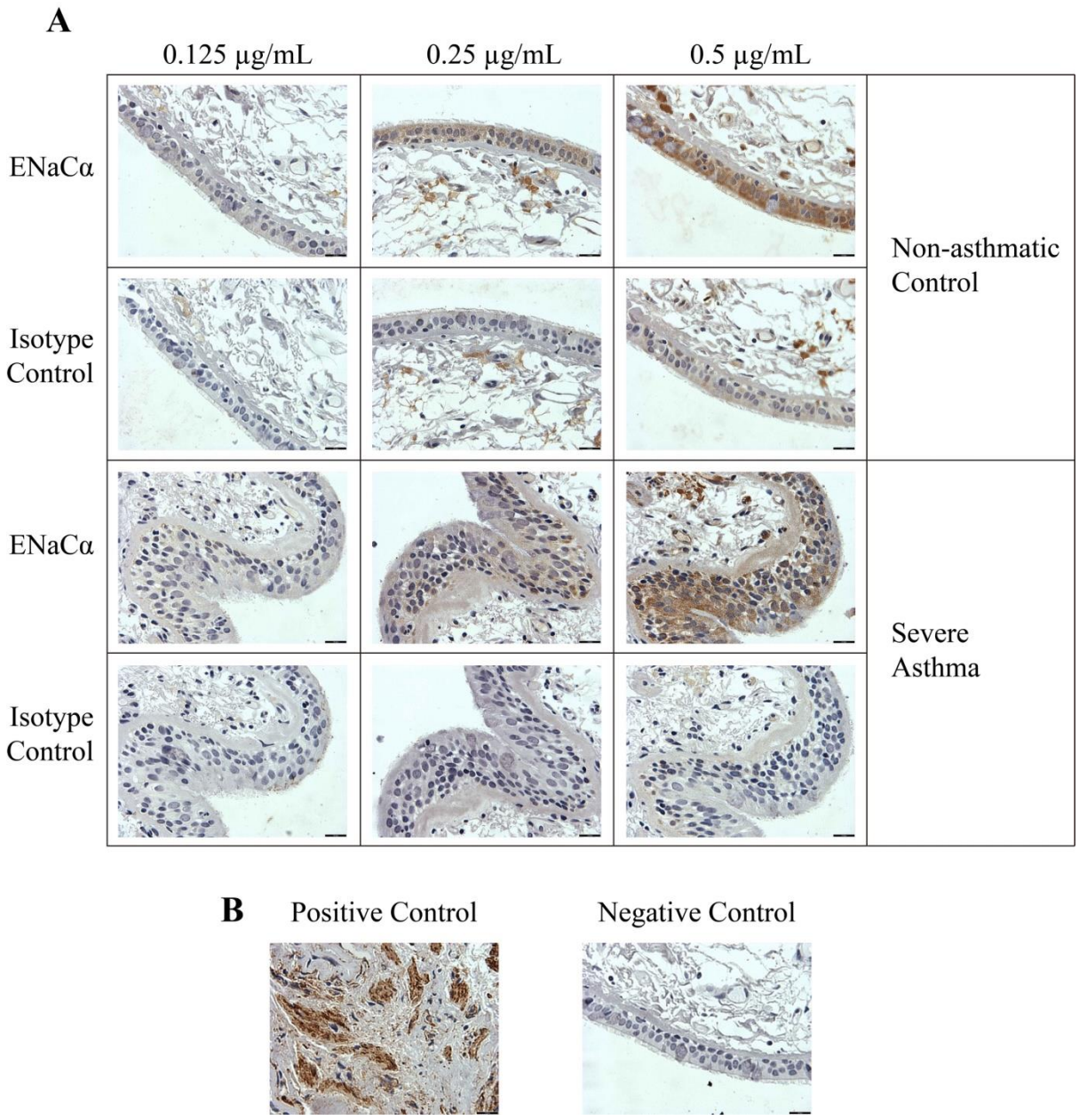

Figure 4.1 ENaCα antibody titration in the large airway biopsies from the Melbourne Epidemiological Study of Childhood Asthma study

Paraffin-embedded sections of human airways from non-asthmatic control and severe asthma patients were stained using three-layer immunoperoxidase method. (A) The expression of ENaCα was detected with three concentrations of the antibody, 0.125 µg/mL, 0.25 µg/mL, and 0.5 µg/mL. Matched concentration of normal rabbit IgG isotype control were used. (B) Pan-actin antibody was used as a positive control and incubation with the secondary antibody only was used as a negative control. Images were taken using Olympus IX51 with 60x objective. Scale bar = 18 µm.

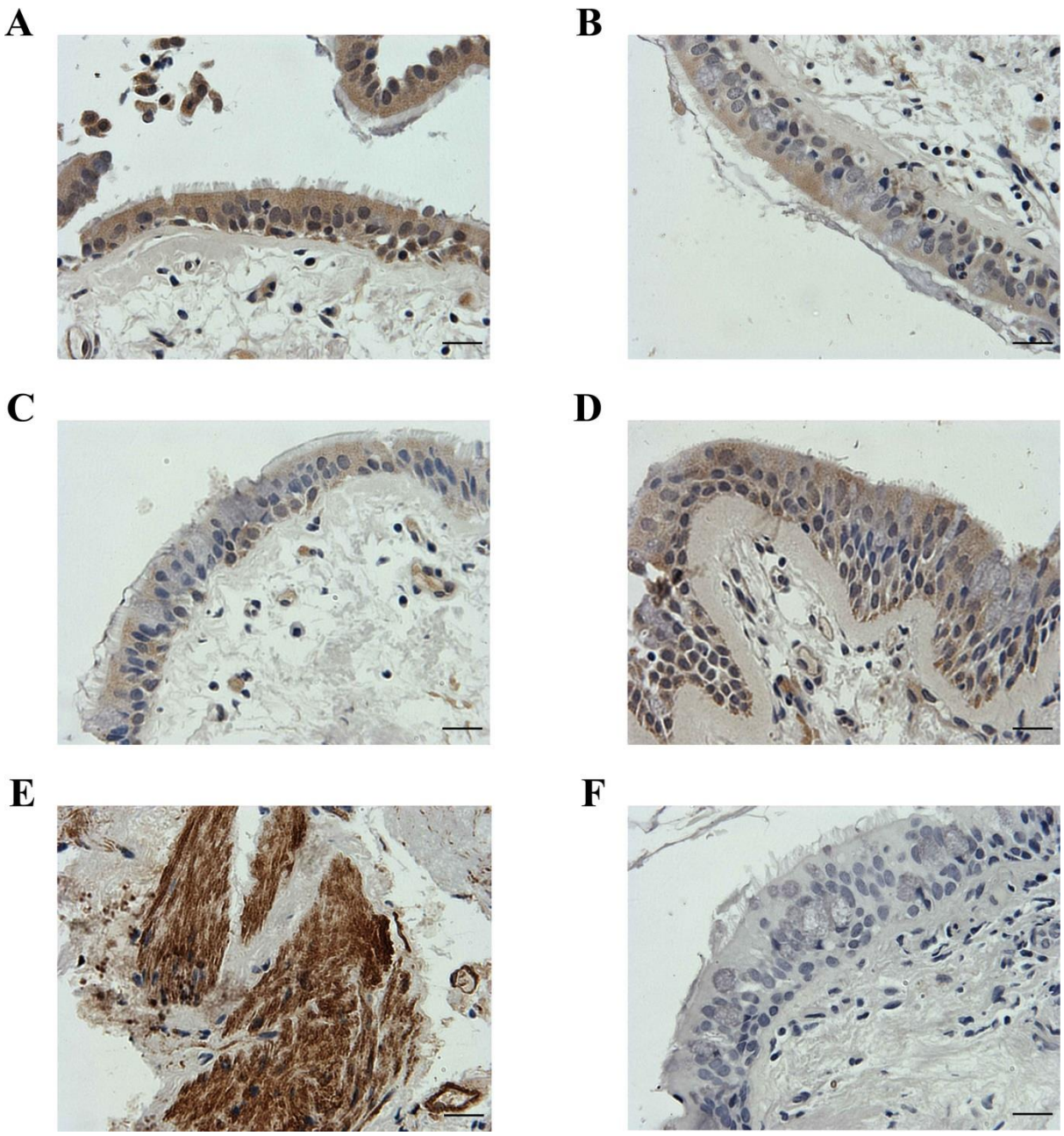

Figure 4.2 The expression of ENaCα in biopsies of large airways from the Melbourne Epidemiological Study of Childhood Asthma study cohort

Paraffin-embedded sections of human airways from non-asthmatic control (A), mild asthma (B), moderate asthma (C), and severe asthma (D) patients were stained using three-layer immunoperoxidase method. The expression of ENaCα was detected with specific ENaCα antibody at 0.25 µg/mL. Specific pan-actin antibody was used as a positive control (E). Matched concentration of normal rabbit IgG isotype control were used as a negative control (F). Representative images were taken using Olympus IX51 with 60 x objective. Scale bar = 18 µm.

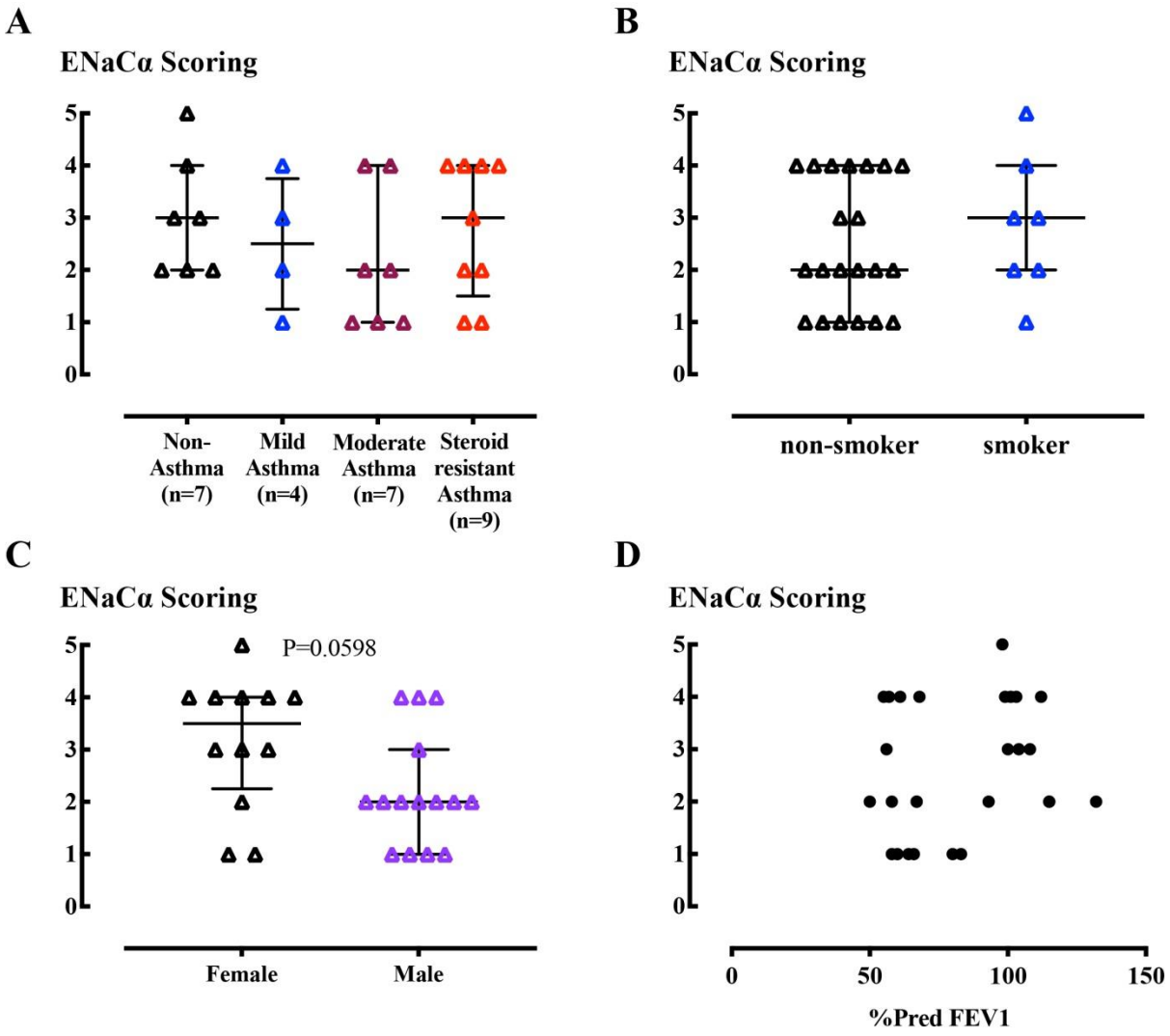

Figure 4.3 Detection of ENaCα expression in biopsies of large airways from the Melbourne Epidemiological Study of Childhood Asthma study cohort

(A) Comparison of the ENaCα expression in the non-asthmatic control, mild, moderate, and severe asthmatic patients using semi-quantitative IHC scoring method, in which the negative controls were scored with 0, and the positive controls with 5. Data are presented as median with interquartile range. Non-parametric Kruskal-Wallis test was used for analysis. Comparison of the ENaCα expression in the epithelial cells between smoking status (B), sex (C), and %Pred FEV_1 (D) using semi-quantitative IHC scoring method. Data are presented as median with interquartile range. Non-parametric Mann-Whitney test was used for analysis.

4.3.2 ENaC channel activity under 2D stiff and 2D soft environment

To further investigate the consequence of higher ENaCα gene expression in the 2D soft environment, the channel activity was determined using the FLIPR® membrane potential assay. Increased fluorescence intensity indicates cell depolarization, whereas decreased fluorescence intensity refers to cell hyperpolarization. The A549 cells were used to measure

the channel activity, but not the BEAS-2B cells because of the low fluorescence signal changes observed in the latter cell type. The potent derivative of amiloride, 5-(N-Ethyl-N-isopropyl) amiloride (EIPA), known to inhibit ENaC (Kong et al., 2009; Mattes et al., 2014), was used to measure ENaC activity. However, the concentration-response relationship was not obvious. For the rest of the study, amiloride was used to measure ENaC activity. In the assay, the amiloride was injected at a ratio of 1:20, 1:10, and 1:5. No significant difference was observed between these ratios. For the rest of the study, 1:10 was used in the assay. The baseline fluorescence intensity in A549 cells was first recorded for 5 min (**Figure 4.4A**). Interestingly, the cells in 2D stiff exhibited a strong baseline fluorescence signal compared to cells in 2D soft environment. Next, increasing concentrations of amiloride, ranging from 30 nM to 10 µM, were added to block the epithelial sodium channel, resulting in cell hyperpolarization. In the 2D stiff environment, A549 cells rapidly responded to the addition of amiloride and stabilized within 10 min (**Figure 4.4B**). However, in the 2D soft environment, the fluorescence signal increased after rapid and transient decreasing (**Figure 4.4C**). The initial peak after addition of amiloride (**Figure 4.5A**) was measured to generate the concentration-response curve. Amiloride 3 and 10 µM elicited a change in fluorescence that consistently exceeded that of the vehicle. ENaC response to 10 µM amiloride was arithmetically greater in 2D stiff environment, although not statistically significant (**Figure 4.5B**).

The primary epithelial cells were then be assayed in the same manner. Here, we used primary epithelial cells from normal human donor (NHBE), chronical respiratory disease patient (HBEC), cystic fibrosis infants (HBEB-CF), and non-CF infant (HBEB-non CF) (**Figure 4.5C**). Contrary to A549 cells, the channel activity in NHBE cells and HBEB-non CF cells was apparently elevated in 2D soft environment compared to conventional 2D stiff culture substrate. Although the ENaC response was modest in HBEC and CF cells, there was a trend that soft environment increased the channel activity.

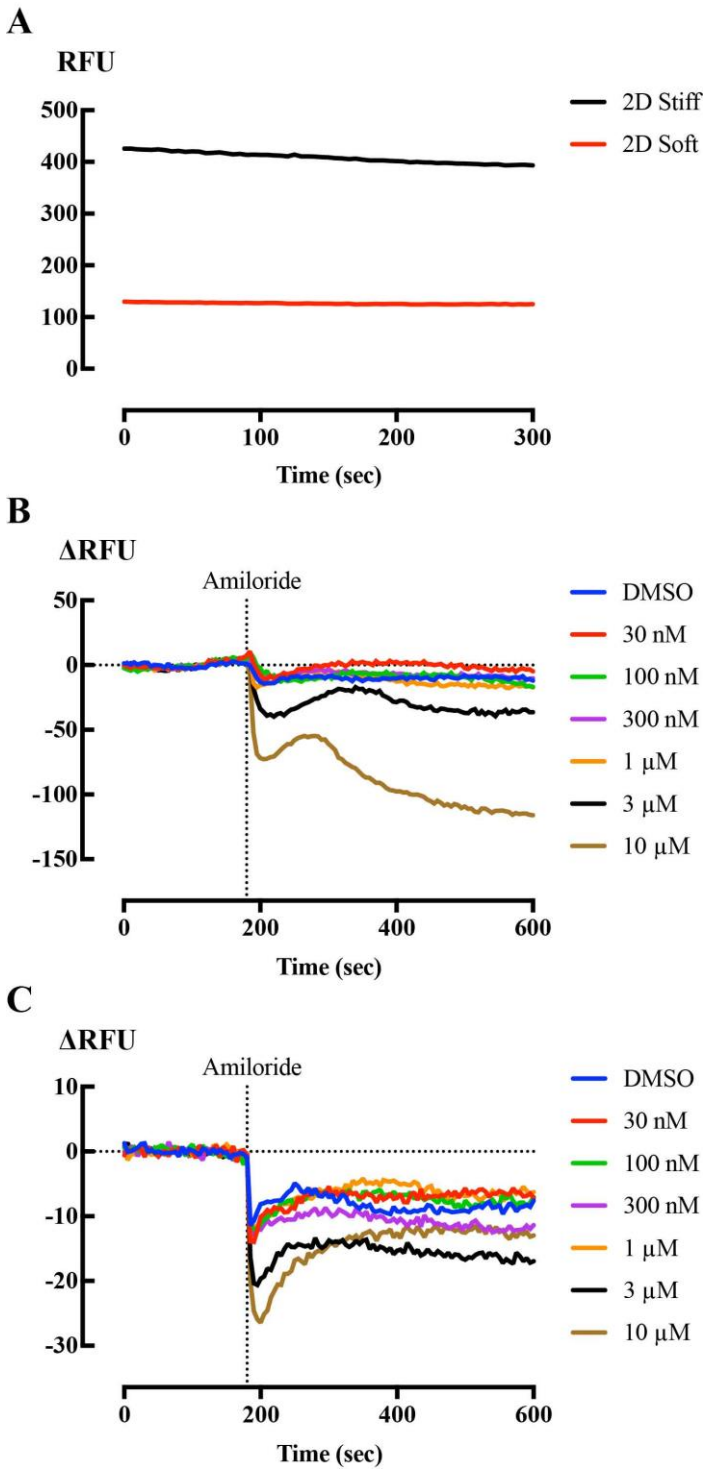

Figure 4.4 ENaC activity in A549 cells under 2D Stiff and 2D Soft environment

After 24 h of serum-starvation, culture media of A549 cells was replaced with Tyrode's buffer. Cells were incubated with FLIPR assay dye at room temperature for 40 min and then equilibrated in FlexStation® at 37°C for 10 min. The amiloride or DMSO was injected at 180 sec. The baseline fluorescence readings were recorded over 5 min (n=3) (A). Time course of concentration-dependent amiloride-evoked fluorescence intensity changes in A549 cells under 2D Stiff (B) and 2D Soft (C) environment (n=3). Fluorescence is presented as the reading in time t minus the average baseline reading in 0-180 sec before drug injection. RFU = relative fluorescence units.

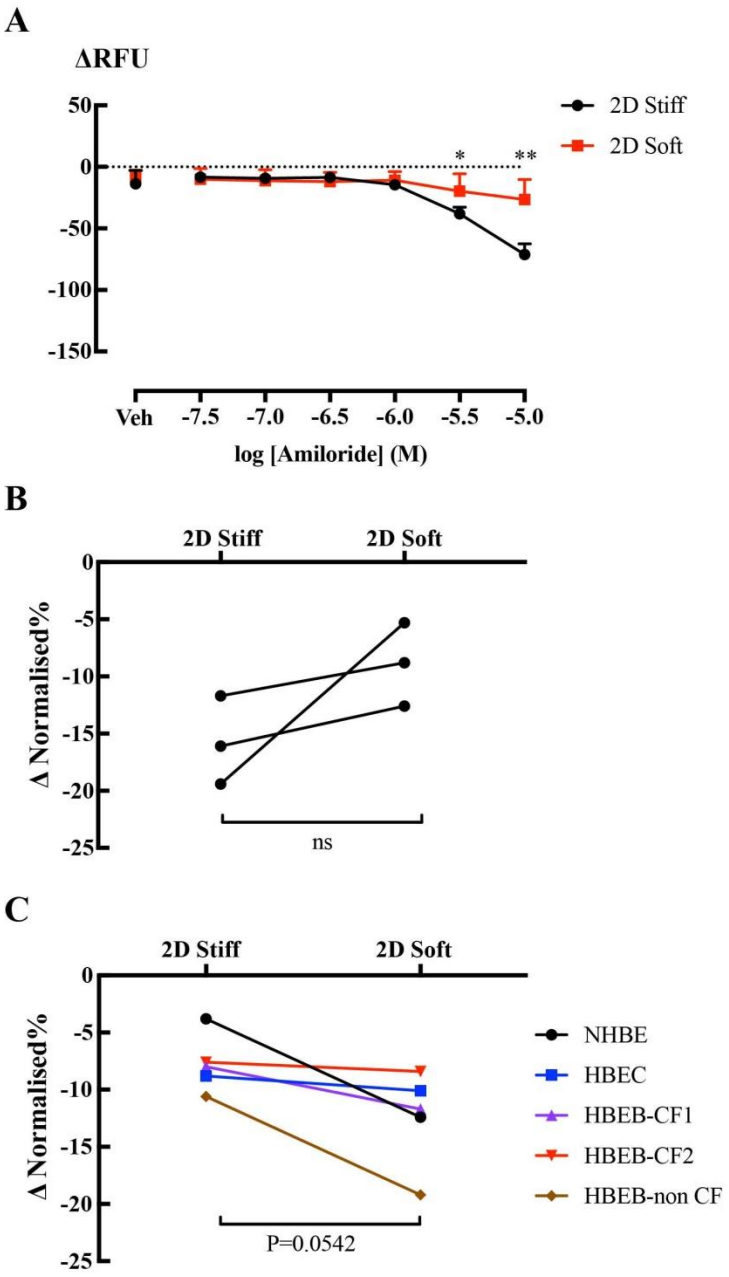

Figure 4.5 ENaC activity in A549 cells and primary epithelial cells under 2D Stiff and 2D Soft environment

After 24 h of serum-starvation, culture medium was replaced with Tyrode's buffer. Cells were incubated with FLIPR assay dye at room temperature for 40 min and then equilibrated in the FlexStation® at 37°C for 10 min. The amiloride or DMSO was added at 180 sec. (A) Amiloride-evoked fluorescence intensity changes in A549 cells under 2D Stiff and 2D Soft environment (n=3). Data are presented as the initial peak reading minus the average baseline reading in the 0-180 sec before drug injection. (B) Fluorescence intensity changes in A549 cells under 2D stiff and 2D soft environment in respond to 10 μM Amiloride (n=3). Values were subtracted from DMSO and then normalized to average baseline readings. (C) Normalized fluorescence intensity changes in primary epithelial cells under 2D Stiff and 2D Soft environment. In the assay, 10 μM Amiloride was added to the cells and DMSO was added as vehicle. Two-way ANOVA with Bonferroni *post-hoc* test (A) and a paired-samples t-test (B, C) were used for analysis. *: $P<0.05$, **: $P<0.01$, ns: not significant.

4.3.3 ENaC β and γ subunits loss in submerged cultures

The contrasting observations of ENaC channel activity in A549 cells and primary epithelial cells and the similar expression of ENaCα in MESCA cohorts drew our attention to the other two subunits of ENaC, namely the β and γ subunits. The gene expression of ENaCα, β, γ subunits was measured in HBEB cells first (**Figure 4.6A**). In native cells, all the three subunit genes were expressed at a high level. After being established in submerged culture, the β and γ subunit gene expression levels were significantly reduced, especially that of γ subunit. In BEAS-2B cells, the α subunit was highly expressed in the 2D stiff environment, whereas β and γ subunits were reduced in expression level compared to native HBEB cells (**Figure 4.6B**). The soft culture environment only increased the expression of the α subunit, but not the β and γ subunits. In A549 cells, β subunit expression level was higher than in BEAS-2B cells, albeit lower than in native HBEB cells (**Figure 4.6C**). The soft environment elevated both α and β subunits, whereas γ was decreased.

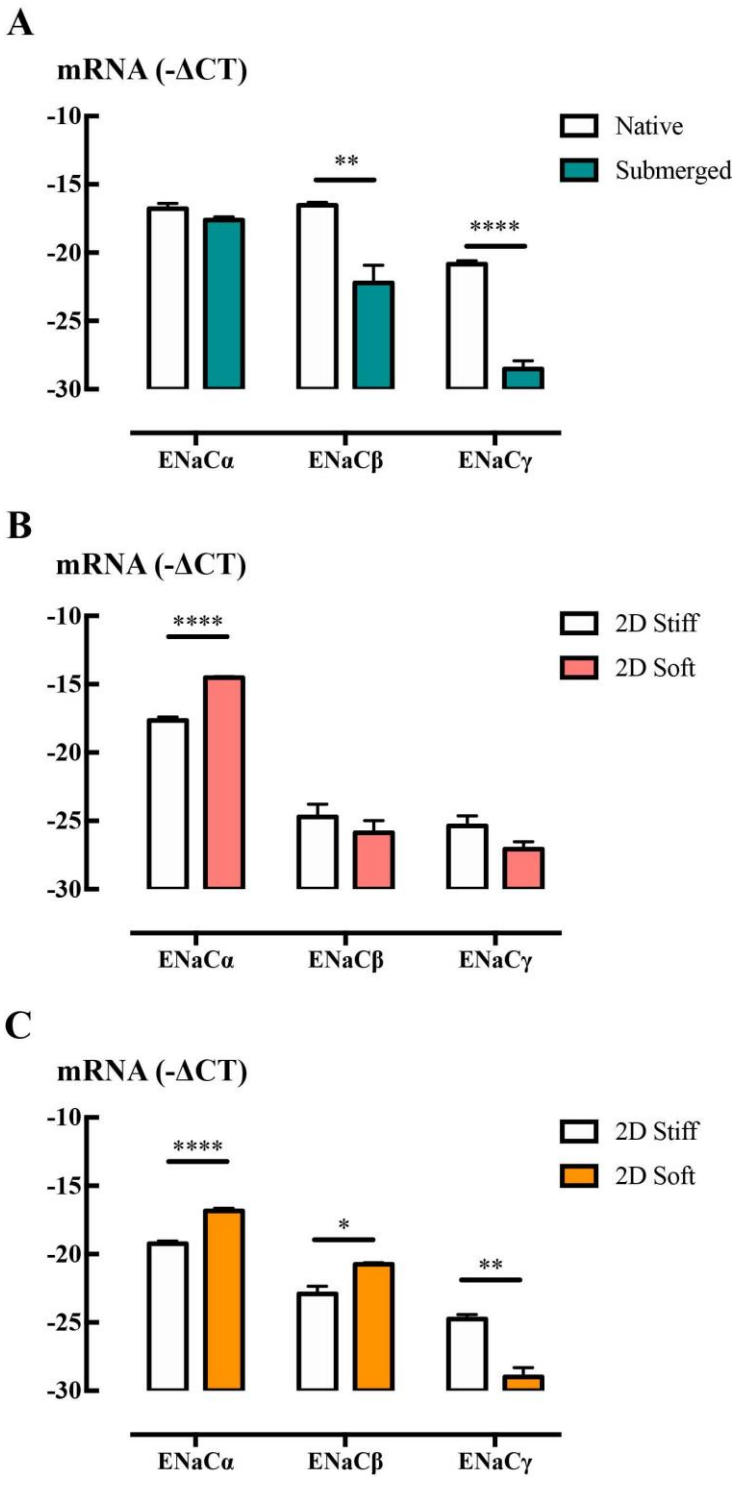

Figure 4.6 The gene expression of ENaCα, β, γ in BEAS-2B, A549, and primary epithelial cells

Total RNA was extracted and the expression of genes encoding ENaCα, ENaCβ, and ENaCγ were measured by RT-qPCR. Gene expression is expressed as -ΔCT (Log2). Data are presented as mean and SEM for n=6 independent HBEB cultures (A), n=5 independent experiments from BEAS-2B cells (B), and n=5 independent experiments from A549 cells (C). A paired-samples t-test was used for analysis, *: P<0.05, **: P<0.01, ****: P<0.0001.

4.4 Discussion

In this chapter, we showed that the ENaC expression in the MESCA cohort subset of airway biopsies was not associated with severity of asthma, smoking or sex. We have applied a high-throughput indirect assay to measure ENaC channel activity. The influence of stiffness on ENaC channel activity seemed to be opposite between primary epithelial cells and cell lines. The low expression or even loss of ENaC β and γ subunits in cell lines may explain the contrary results and the low signal detected. Collectively, these findings suggest that 2D submerged cultures are not adequate to evaluate ENaC channel activities or expression. Genetic modified cell cultures or organotypic cultures, with native levels of the β and γ subunits, may be required in pre-clinical research to provide better prediction in drug development.

Normal human parenchymal lung tissue possesses a mean Young's modulus of 2 kPa, whereas the mean stiffness of idiopathic pulmonary fibrosis (IPF) tissue increases to 16 kPa (Booth et al., 2012). Stiffness measured by magnetic resonance elastography at total lung capacity increased from 0.8 kPa in healthy control to 1.3 kPa in patients with fibrotic interstitial lung disease (Marinelli et al., 2017). Strikingly, most of the stiffness measurements were carried out in lung parenchyma, containing mostly type I and III collagen (Suki et al., 2005). In MESCA samples, the epithelial cells presented were in direct contact with basement membrane, who was thickened in severe asthma. Asthmatic airway is stiffer than healthy airway but there has no report measuring the Young's modulus of basement membrane. Despite that, tissue culture plastic coated by polystyrene is extremely stiff ranging from 2 to 4 GPa (Butcher et al., 2009). In our 2D soft setting, the collagen hydrogel only has a stiffness around 0.2 to 0.8 kPa (Berhan et al., 2020). Thus, the expression of ENaC might not be altered in tissues having a narrower range of stiffness. This observation also emphasized the importance of considering mechanics in pre-clinical research.

Fluorescence-based assays for ion channels in general produce a robust and homogeneous cell population measurement (Yu et al., 2016). Various choices of instruments and fluorescent dyes make them easy to be optimized to achieve high throughput. However, any event that changes the membrane potential could modulate the signal resulting in false-positive and/or false-negative readouts. Firstly, we noticed the baseline difference of cells in 2D stiff and 2D soft environment. In our 2D soft setting, the collagen hydrogel has a downward meniscus caused by surface tension, which was more obvious in the small surface

area setting. Consequently, cells were more distributed in unevenly coated centre area of the well. In future investigations, "well-in-a-well" technology (Ibidi) preventing gel meniscus and providing a planar surface could be considered (Lazarovici et al., 2018). Secondly, the buffer matters. The pH change of the buffer was inevitable when moving the cells out of the incubator gassed with 5% CO_2, albeit cells were placed into Tyrode's solution to help maintaining the pH and osmotic balance. Hence, whether Tyrode's buffer is suitable for highly pH-sensitive ENaC (Konstas et al., 2000) needs to be further investigated. Ion-free buffer is another option as it is suggested by the manufacturer and used in measuring CFTR function (Ahmadi et al., 2017). Using FLIPR® membrane potential assay, cells exhibited an amiloride-evoked reduction in fluorescence signal when switching from sodium-containing Tyrode's solution to sodium-free solution (Chen et al., 2015). Thirdly, ENaC is regulated by shear stress. In the assay, amiloride was injected by the instrument into the medium. By adjusting the injection volume, the shear stress was altered. Although there was no difference found between the volume injection ratios we have tested, it might be due to the low injection speed we have used. Therefore, the FLIPR® membrane potential assay condition needs to be further optimized to rule out the possibility of the low fluorescence signal changes observed in this study being false-negative. To improve, more care should be taken in fluorescence-based assays and electrophysiological techniques might be applied for validation.

The ENaC heterotrimers assemble in a counterclockwise α-β-γ orientation with a ratio of 1:1:1 (**Figure 4.7**) (Staruschenko et al., 2005; Stewart et al., 2011; Wichmann and Althaus, 2020). The channel transmembrane domain contains two transmembrane helices (TM1 and TM2) of each subunit, connecting the extracellular loop and NH_2 and COOH termini into cytosol (Noreng et al., 2018). The cysteine-rich extracellular domain of each subunit is a highly organized structure, resembling a hand with the palm, knuckle, finger, and thumb domains clenching a 'ball' of β strands (Noreng et al., 2018; Wichmann and Althaus, 2020). Among these subdomains, gating relief of inhibition by proteolysis (GRIP) domain harbours autoinhibitory peptides, which support the channel activation by proteolytic cleavage (Kashlan et al., 2011). Molecular control of channel activity by proteolytic cleavage is specific to ENaCs as they are the only DEG/ENaC member containing GRIP domain (Jasti et al., 2007; Noreng et al., 2018). Various studies have demonstrated proteolytic cleavage of α and γ subunit can regulate ENaC activity and may play an important role in CF (Bruns et al., 2007; Hughey et al., 2004; Masilamani et al., 1999; Passero et al., 2008). However, the β subunit lacks protease cleavage sites (Kleyman et al., 2009). Although under debate, post-

translation process of the channel, including furin-dependent cleavage, requires expression of all three subunits (Hughey et al., 2004). Gene knockout mice without either one of α, β, or γ subunits die soon after birth with respiratory insufficiency or kidney dysfunction, indicating all three subunits are essential for survival (Barker et al., 1998; Bonny and Hummler, 2000; Hummler et al., 1996). Incomplete ENaC structure in *Xenopus oocytes* resulted in minimal or no detectable channel activity (Canessa et al., 1994; Edelheit et al., 2011). Low expression of β subunit impairs baseline of alveolar fluid clearance and decreases the sensitivity to amiloride (Randrianarison et al., 2008). Cells expressing either βγ or α subunit alone didn't response to amiloride in FLIPR assay, whereas genetically modified cells expressing the α subunit and mutant βγ subunits yielded significantly higher fluorescence signal (Chen et al., 2015). Thus, the low expression of β and γ subunits in BEAS-2B and A549 cells are most likely to limit activity of the ENaC channel.

Taken together, our findings suggest the ENaC α subunit expression in airway epithelial cells might not be altered in physiological to pathological stiffness range, but rather be changed when stiffness increases to that of stiff plastic culture plates. All three ENaC subunits may be required to assess the influence of stiffness on channel activity. To continue the investigation, a versatile *in vitro* model containing complete ENaC channels needs to be developed.

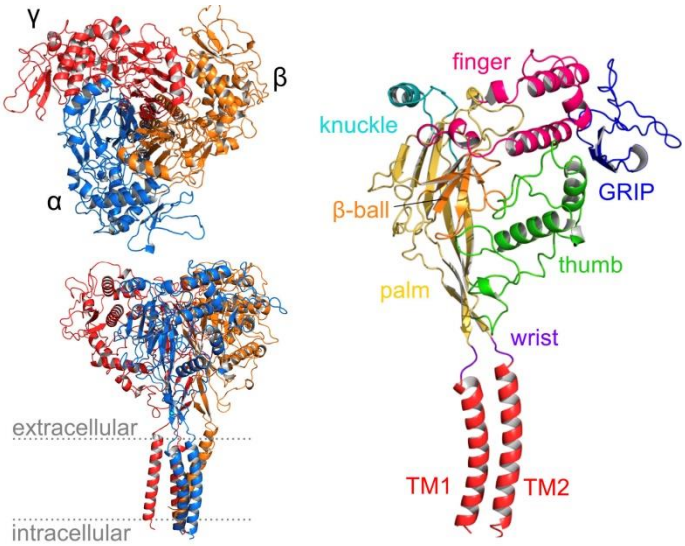

Figure 4.7 Structure of ENaC

Left: top and side views of a *Xenopus laevis* αβγ-ENaC homology model. Right: *Xenopus* ENaC α subunit structure showing the topological organization of individual subdomains.

Reproduced from (Wichmann and Althaus, 2020) with permission of the American Physiological Society.

CHAPTER 5

AIRWAY ORGANOTYPIC CULTURES

5.1 Introduction

To gain access to mammalian tissues and organs for experimental manipulation and observation, Harrison and other researchers isolated embryonic tissue from a living frog and grew it outside the body in 1907 (Harrison et al., 1907), marking the beginning of two-dimensional (2D) culture. In the past century, 2D culture enabled researchers to develop deep understanding of mammalian biology and to promote novel medical treatments. As time goes by, the need for reconstituting organ function *ex vivo* drove the development of three-dimensional (3D) organ-like (organotypic) culture. For lung, organotypic cultures include lung slice, embryonic whole organ, primary cells, air-liquid interface (ALI) culture, and organoids (Shamir and Ewald, 2014). Specific to airway, the approaches usually involve primary cell culture to generate ALI, and airway organoid culture. Uncultured primary cells are highly valuable, but limited in utility by *ex vivo* lifespan, and will not be our focus.

Organotypic ALI airway cell cultures were first developed in the 1980s (Pruniéras et al., 1983; Whitcutt et al., 1988). The culture environment in ALI is divided into apical and basolateral compartment by a permeable membrane. The cells grown on apical chamber are exposed to the air and are simultaneously in contact with basolateral culture medium. Primary epithelial cells under ALI culture differentiate into heterogeneous cell populations with a polarized mucociliary phenotype resembling their origin tissue (Cao et al., 2021). Human epithelial cells from nasal, large, and small airway have all been successfully differentiated in ALI culture (Fuchs et al., 2003; Fulcher et al., 2005; Rayner et al., 2019; Schogler et al., 2017). Currently, ALI culture has been widely employed for elucidating the mechanisms of respiratory diseases, such as asthma, COPD, pathogen-host interaction (Bai et al., 2015; Comer et al., 2013; Gindele et al., 2020; Kılıç et al., 2020; Xia et al., 2017; Zhu et al., 2020). Nanomaterials and volatile chemicals have also been tested in ALI culture with aerosol/vapor delivery system, mimicking *in vivo* inhalation (Geiser et al., 2017; McGraw et al., 2020; Tilly et al., 2020).

In ALI culture, the cells are seeded onto the semi-permeable microporous membrane coated with extracellular matrix (ECM) proteins, such as collagen, fibronectin, or gelatin (Aufderheide et al., 2016; Keenan et al., 2014; Kim et al., 2005). Type-I collagen coating has become a standard method since 1990s, as it can promote mucocilliary differentiation compared to uncoated membranes (Davenport and Nettesheim, 1996; Gray et al., 1996). In the first couple days of ALI culture, the culture medium is normally the same as in culture

flask to support cell proliferation. Once confluent, the medium is changed to differentiation medium. At the early stage, the medium is composed of bronchial epithelial growth medium and Dulbecco's modified Eagle's medium (BEGM: DMEM) at a ratio of 50:50 (Fulcher et al., 2005; Gray et al., 1996). Commercial ALI medium kits, like Clonetics™ B-ALI™ medium (Lonza), PneumaCult™ ALI medium (STEMCELL Technologies), MucilAir™ medium (Epithelix), are then developed and helped standardization of the ALI culture. After three to four weeks of culturing, mature culture containing differentiated cells is ready to use in physiology, pathology, and pharmacology studies. Tissue responses can be evaluated by measuring gene and protein expression, cell morphology, barrier function, cilia beating frequency and pattern, and ion transport (Gianotti et al., 2018; Keenan et al., 2014; Kuek et al., 2018; Prodanovic et al., 2017; Schögler et al., 2017; Srinivasan et al., 2015; Stewart et al., 2012a; Zhu et al., 2020).

Airway organoid culture was first described in 1993 (Benali et al., 1993) and refocused after intestinal organoids had been reported (Barker et al., 2007; Sato et al., 2009). Generally, the airway organoid culture is composed of ECM and medium. Primary epithelial cells are embedded in ECM and nourished from differentiation medium. A 3D self-organizing sphere-like structure will be generated after two to three weeks of culturing. To date, primary epithelial cells and induced pluripotent stem cell (iPSCs) are mostly used to generate airway organoids (Chen et al., 2017; Konishi et al., 2016; Sachs et al., 2019; Zhou et al., 2018). Like ALI culture, airway organoid culture has also shown advantages in recapitulating *in vivo* structure and function, suggesting its utility in studying airway physiology and pathology. However, there were not as many reports as expected until a long-term-expanding culture protocol been published (Sachs et al., 2019). In the COVID-19 pandemic, airway organoids are now extensively employed to study SARS-COV-2 infection (Han et al., 2021; Huang et al., 2020a; Lamers et al., 2020; Salahudeen et al., 2020).

From 2009, various culture methods have been reported (**Table 5.1**) (human pluripotent stem cells (hPSCs) derived airway organoids not included). Tracheospheres were generated from mouse tracheal epithelial cells and human basal cells, indicating the potential of basal cells to be differentiated in the sphere-forming setting (Rock et al., 2009). Normal human bronchial epithelial cells grown on Matrigel® were reported to differentiate into 3D glandular acini expressing mucous and serous cell markers, but not ciliated cell markers (Wu et al., 2011). Airway organoids from NHBE cells grown in a 384-well plate provided a high-throughput screening assay (Danahay et al., 2015; Hild and Jaffe, 2016). Human lung organoids

developed from hPSCs comprised epithelial and mesenchymal compartments similar to those seen in human fetal lung (Dye et al., 2015). Further study applying an artificial biomimicking scaffold niche improved human lung organoid long-term survival and maturation of epithelium (Dye et al., 2016). Addition of DAPT, Notch pathway inhibitor, promoted induction of multi-ciliated airway cells with motile cilia in hPSCs derived proximal airway epithelial cell spheroids (Konishi et al., 2016). Low Wnt condition directed iPSC-derived lung progenitor cells and enabled generation of cystic fibrosis patient-specific airway organoids (McCauley et al., 2017). NHBE cells, human microvascular lung endothelial cells, and human lung fibroblasts were mixed to form airway organoids, which were capable to exhibit multicellular responses to TGF-β (Tan et al., 2017). Adult stem cell derived airway organoids changed to 1:1 AO media and PneumaCult^{TM} ALI medium supplemented with DAPT had increased ciliated cell number (Zhou et al., 2018).

In Chapter 3 and 4 of this thesis, we have shown that certain *in vivo* functions relating to ENaC activity could not be reflected in airway epithelial cells in 2D submerge culture. The influence of stiffness on epithelial cells also needs further confirmation by ruling out the loss of specific cell phenotypes. Thus, we aim to evaluate ALI culture and airway organoid culture to answer these questions. Previously the lab has published on the pharmacology and infectivity of ALI cultures (Keenan et al., 2014; Prodanovic et al., 2017; Xia et al., 2017). In this chapter, we explored culture formats reported in the literature to generate airway organoids. Airway organoids were then characterized in parallel with ALI culture. Last, gene expression of ENaC subunits was measured to evaluate the potential of these two organotypic airway cultures in studying ion channel activity.

Table 5.1 Summary of airway organoid culture method

Cell	ECM	Medium	Format	Duration	Reference
Human basal cells	50% GFR Matrigel® in ALI medium	ALI medium	Embed	25 days	(Rock et al., 2009)
NHBE cells	100% Matrigel®	ALI medium	Overlay	22 days	(Wu et al., 2011)
NHBE cells	25% GFR Matrigel® in ALI medium	5% GFR Matrigel® in ALI medium	Overlay	14 days	(Danahay et al., 2015; Hild and Jaffe, 2016)
NHBE cells + endothelial cells + fibroblasts	40% Matrigel® in PneumaCult™ ALI medium	5% Matrigel® in PneumaCult™ ALI medium	Overlay	14 days	(Tan et al., 2017)
Adult stem cells isolated from lung tissue	60% GFR Matrigel® in AO media	1:1 AO media and PneumaCult™ ALI medium + DAPT	Embed	16 days	(Zhou et al., 2018)
Lung cell isolated from solid lung tissue	100% GFR Matrigel®	AO media	Embed	18 days	(Sachs et al., 2019)

5.2 Method

5.2.1 Two-layer Matrigel® organoid culture

The primary epithelial cells were cultured in BEGM as described in Section 2.1. Pre-chilled 40% (w/w) Matrigel® in BEGM was added to 96-well plate and incubated at 37°C for 20 min. Cells were dissociated from the culture flask. Cell pellet was resuspended in BEGM medium containing 5% (w/w) Matrigel® and added to the top of solidified 40% Matrigel®. The cells then were incubated at 37°C in a humidified atmosphere containing 5% CO_2 and the medium was replaced three times a week for 3 to 4 weeks. Brightfield images were obtained using an Olympus IX51 microscope.

5.2.2 Airway organoid culture in droplet

The airway organoid culture was generated in a droplet format as described in Section 2.3.2. Briefly, the silicone mask was adhered to the culture plate and centre area was coated with 1% BSA at 37°C for 45 min. Primary epithelial cells were dissociated and collected by centrifugation. Cell pellet was resuspended in same volume of AO media and pre-cold Matrigel® to form a 50% (w/w) Matrigel® mixture. A 40 µL or 25 µL drop of the cell mixture was then seeded into pre-warmed culture plate with silicone mask. Following solidification of the droplet by incubating at 37°C for 20 min, AO media was added to cover the droplet. The cells were incubated at 37°C in a humidified atmosphere containing 5% CO_2 and the medium was replaced three times a week for 3 to 4 weeks. Differentiation of the cells was confirmed through visualisation of the beating cilia under Olympus IX53 microscope equipped with QImaging optiMOS high speed camera at 100 frames/sec.

5.2.3 Air-liquid interface culture

The primary epithelial cells were seeded to generate air-liquid interface culture as described in Section 2.3.1. Briefly, cells were seeded at 75,000 cell/well in collagen-coated transwell inserts. PneumaCult™ Ex Plus medium was added to both apical and basal chamber. Cells were incubated at 37°C in a humidified atmosphere containing 5% CO_2. The medium was replaced for both apical and basal chamber for 3 days. At Day 4, the apical medium was removed, and basal medium was replaced to PneumaCult™ ALI medium (P-ALI). Cells

were then re-fed three times a week over a period of 4 weeks by aspirating medium from basal chamber and refilling with fresh medium. From Day 14, excess mucus was removed from apical surface once a week. Differentiation of the cells was confirmed through visualisation of the beating cilia under Olympus IX53 microscope equipped with QImaging optiMOS high speed camera at 100 frames/sec.

5.2.4 Determination of gene expression in airway organoid culture

After removal of supernatant, the airway organoids in Matrigel® were washed twice with PBS at room temperature. Organoids were lysed to perform RNA isolation, as described in Section 2.4.1. The expression of cell marker and ENaC subunit genes were measured by RT-qPCR as described in Section 2.4.1.

5.2.5 Determination of gene expression in ALI culture

After removal of basal medium, both apical and basal chamber were washed twice with PBS. Cell were lysed in 150 µL lysis buffer to perform RNA isolation, as described in Section 2.4.1. The expression of ENaC subunit genes were measured by RT-qPCR as described in Section 2.4.1.

5.2.6 Immunofluorescence staining of airway organoids

The fixation and immunofluorescence staining steps were adapted from previous reported protocols (Broutier et al., 2016; Dekkers et al., 2019).

5.2.6.1 Fixation of airway organoids

For fixing airway organoids, all the pipette tips were pre-coated with the solution by pipetting the solution up and down for 1 min. After removal of the supernatant, 1 mL of cold 0.1% BSA in PBS to each well. The Matrigel® droplet was gently suspended using coated tips, after which the organoid suspension was carefully transferred into a 1.7 mL Eppendorf tube (pre-coated with 1% BSA in PBS at 4°C for overnight). The tube was vertically left in the ice for 10 min to allow organoids settle down under gravity. The solution was carefully removed

to not aspirate the organoids. Pre-cold PBS was added, and the tube was inverted five times to wash off the Matrigel®. After 30 min incubation on ice, PBS was carefully removed. The PBS washing step was repeated two to three times. The organoids were then incubated in 1 mL 10% NBF on ice for 30 min, followed by two times of PBS wash. The fixed organoids were then stored at 4°C prior immunofluorescence staining.

5.2.6.2 Preparation of fructose-glycerol clearing solution

To prepare 33 mL of clearing solution, 16.5 mL glycerol (242-2.5 L, Thermo Scientific), 3.5 mL MilliQ water, and 14.86 g fructose (F0127, Sigma) was mixed on a magnetic stirrer. The clearing solution was stored at 4°C in dark.

5.2.6.3 Immunofluorescence staining of airway organoids

The organoids were collected by centrifugation at 70 g for 5 min at 4°C and resuspended in 0.1% Triton X-100 in 0.5% BSA/PBS blocking buffer. The organoid suspension was carefully transferred into Poly (2-hydroxyethyl methacrylate) (Poly-HEMA) coated 96-well round bottom plate, 200 µL/well. After 1 h blocking, organoids were incubated with primary antibodies (2x concentration) diluted in blocking buffer at 4°C for overnight. Specifically, 100 µL blocking buffer was removed and 100 µL primary antibodies were added. At the second day, organoids were washed three time of PBS for 5 min, followed by incubation of secondary antibodies (2x concentration) diluted in blocking buffer at room temperature for 1 h. Nucleus was stained by DAPI for 10 min. After washing in PBS, the remaining liquid was removed as much as possible. Fructose-glycerol clearing solution was added using a 200 µL tip with the end cut off. The organoids were incubated in clearing solution at room temperature for 20 min. A 1 cm square was drawn on a glass slide using PAP pen, bordered by double-side sticky tape (Scotch 3M). The organoids in clearing solution were then transferred into the square by a 200 µL tip with the end cut off. For each layer of the double-side sticky tape, 20 µL organoids was applied. The coverslip was slowly placed on top and attached to the double-side sticky tape by gently applying pressure. Confocal images were acquired using Zeiss LSM880 Airyscan Fast confocal microscope.

5.2.7 Immunofluorescence staining of ALI cultures

5.2.7.1 Fixation of ALI cultures

After removal of basal supernatant, both apical and basal chamber was washed twice with PBS. The cells were then fixed for 30 min by adding 150 µL 10% (w/w) NBF to apical chamber and 350 µL 10% NBF to basal chamber, followed by two times of PBS wash. Fixed transwells were stored at 4°C prior immunofluorescence staining.

5.2.7.2 Paraffin embedding

A 3% Agarose solution was dissolved by microwave for 2 min and kept at 65°C. The transwell membrane was excised using a no. 23 scalpel blade and transferred in a petri dish containing PBS. The membrane was then cut into 2 pieces with straight pointed surgical scissors. The back side of the membrane pieces were sticked to each other and vertically embedded in an agarose droplet on a disposable base mold. Additional agarose solution was added to cover the membrane, if needed. After solidification, the agarose droplet was moved into a cassette and then placed in 70% ethanol overnight. The paraffin processing was carried out by Melbourne Histology Platform (University of Melbourne).

5.2.7.3 Whole mount immunofluorescence staining of ALI

The transwell membrane was excised using a no. 23 scalpel blade and cut into 4 pieces with straight pointed surgical scissors. The membrane pieces were transferred into 1.7 mL Eppendorf tubes. The membrane pieces were then stained as described in Section 2.4.5. Briefly, following 1 h blocking in 5% goat serum, primary antibodies diluted in 0.1% Triton X-100 in 1% BSA in PBS was incubated overnight at 4°C. At the second day, secondary antibodies diluted in 1% BSA in PBS were incubated at room temperature for 1 h. Cells were then stained with Alexa Fluor® 488 Phalloidin for 20 min and DAPI for 10 min to stain nuclei. The membrane was then mounted on a glass slide bordered by double-sided sticky tape. Confocal images were acquired using Zeiss LSM880 Airyscan Fast confocal microscope.

5.2.7.4 Immunofluorescence staining of paraffin embedded ALI sections

Paraffin-embedded ALI blocks were cut into 2 µm or 4 µm sections. The sections were dewaxed in histolene, rehydrated through gradient ethanol, and washed in PBS as described in Section 2.4.4.3. Immunofluorescence staining was then finished as described in Section 5.2.7.4. The double-sided sticky tape was not required.

5.2.8 Haematoxylin and Eosin (H&E) staining of paraffin embedded ALI

Paraffin-embedded ALI blocks were cut into 3 µm sections. The sections were dewaxed in histolene, rehydrated through gradient ethanol, and washed in water as described in Section 2.4.4.3. Sections were stained in following orders: Mayer's Haematoxylin for 5 min, running tap water to clear, 1% Acid Alcohol for 1 dip, running tap water to clear, Schott's Water (Amber Scientific) for 20 sec, running tap water for 30 sec, Eosin (Amber Scientific) for 3 min, running tap water for 2 dips. The sections were then dehydrated through 70%, 100%, and 100% ethanol for 5 dips in each, followed by 30 dips in histolene twice. Finally, the sections were coverslipped with DPX Mountant for Histology and imaged by Olympus BX51.

5.3 Results

5.3.1 Optimization of airway organoid culture format

The airway organoid culture was started from a two-layer of Matrigel® format, based on protocols from STEMCELL Technologies and Aron Jaffe group (Hild and Jaffe, 2016; STEMCELL, 2015). The cells were layered on top of the 40% Matrigel® and gradually invaded into the Matrigel® (**Figure 5.1A**). The top layer medium containing 5% Matrigel® was refreshed continuously during the whole culture period to support cell proliferation and differentiation. The bottom layer Matrigel® had a concave meniscus instead of the flat surface, which increased the chance to break the Matrigel® when doing medium changing. Here, we used NHBE and BCi NS1.1 cells to generate airway organoids (**Figure 5.1C**). After 7 days, the cells grown into small cell clusters. After 14 days, the organoid-like structure was formed. Organoids from BCi NS1.1 cells had a smoother border compared to NHBE cells. The size of the organoids from NHBE cells was more variable. Under higher powered objective, lumen structure was found in BCi NS1.1 cells (**Figure 5.1D**). Intriguingly, we found the cells also grew into monolayer cells within the Matrigel® (**Figure 5.1B**).

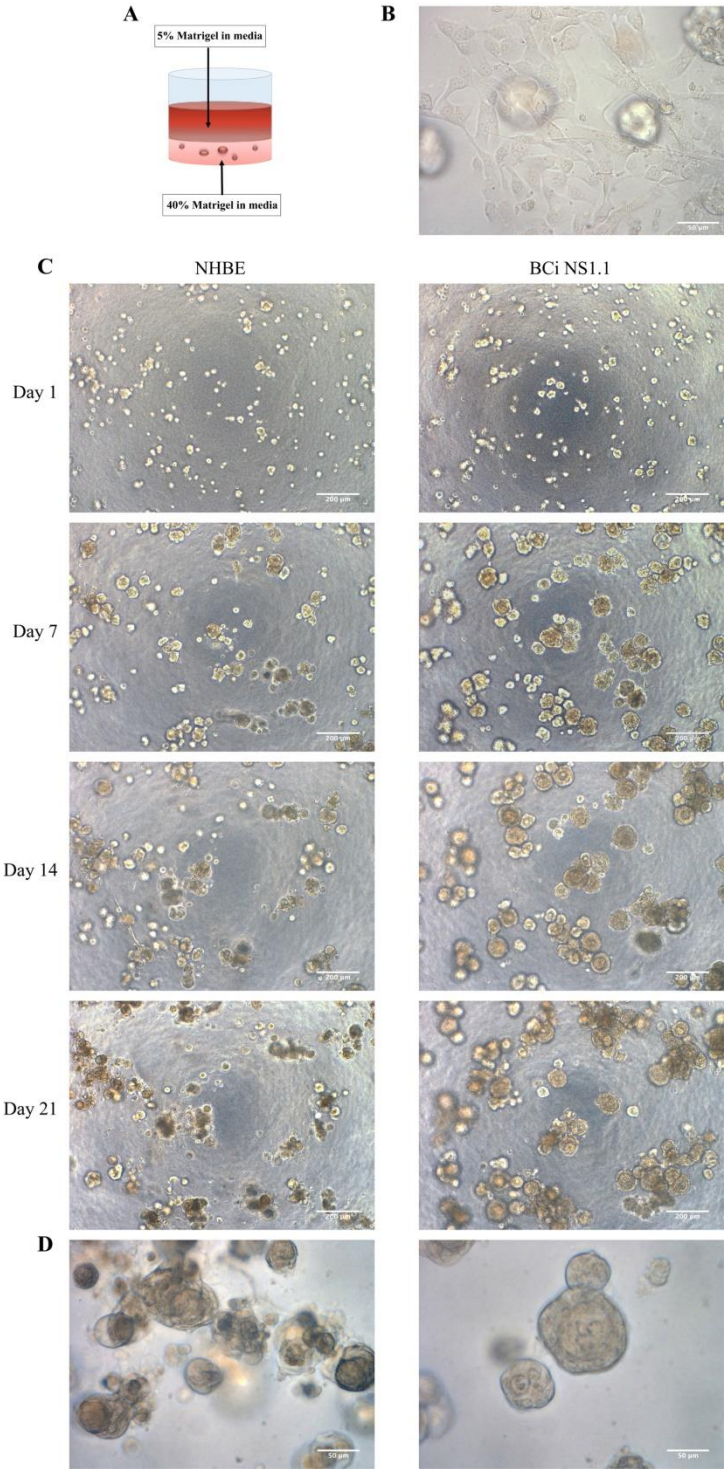

Figure 5.1 Airway organoids generated from NHBE and BCi NS1.1 cells under two-layer Matrigel® culture format

The cells were embedded in 40% Matrigel®. After solidification of the Matrigel®, medium contained 5% Matrigel® were added to the top layer and refreshed every two to three days for four weeks. (A) Schematic diagram of the two-layer Matrigel® culture format. (B) Monolayer epithelial cells in airway organoid culture found at Day 7. (C) Representative brightfield images (10x objective) of NHBE and BCi NS1.1 cells derived airway organoids at Day 1, 7, 14, and 21. (D) Representative brightfield images (40x objective) of NHBE and BCi NS1.1 cells derived airway organoids at Day 21.

Next, we adapted the liver and intestine organoid culture format into airway organoid culture (Boj et al., 2017; Broutier et al., 2016). The cells were mixed with 50% Matrigel® and added into the centre of the culture plate well to generate a droplet (**Figure 5.2A**). After solidified, media was added to cover the droplet. However, the droplet could be easily disrupted by small vibrations. To shape the droplet, an elastomeric stencil mask was introduced to help constrain the droplet (**Figure 5.2A**). The hydrophobicity of the mask helped to shape the Matrigel® and cell mixture into a hemispherical droplet, confined inside the centre aperture. The diameter of outer and inner well of the silicone make were optimized to 10 mm/8 mm and 6 mm/5 mm for 24/48-well plate. Moreover, porous silicone mask can be manufactured to control the size and shape of the droplet (**Figure 5.2B, C**). BCi cells were then cultured into airway organoids in droplet format (**Figure 5.3A**). Organoids with and without lumen were observed under microscope and they kept growing as time went by. Unexpectedly, monolayer cells were generated and organoids with irregular border cells were observed after 21 days (**Figure 5.3B**). As the monolayer cells were mainly found attaching to the plate bottom, surface coating was then considered. Poly-HEMA was tested to prevent cell adhesion. But it also prevented the attachment of Matrigel®. BSA was then be tested for its activity in "triggering" the attachment of cells to low levels of adhesion molecules (Koblinski et al., 2005). Even though BSA could not prevent the cell adhesion around the silicone border, we did see a remarkable reduction of the number monolayer cells. Thus, BSA coating was applied to subsequent airway organoid cultures, together with the silicone mask.

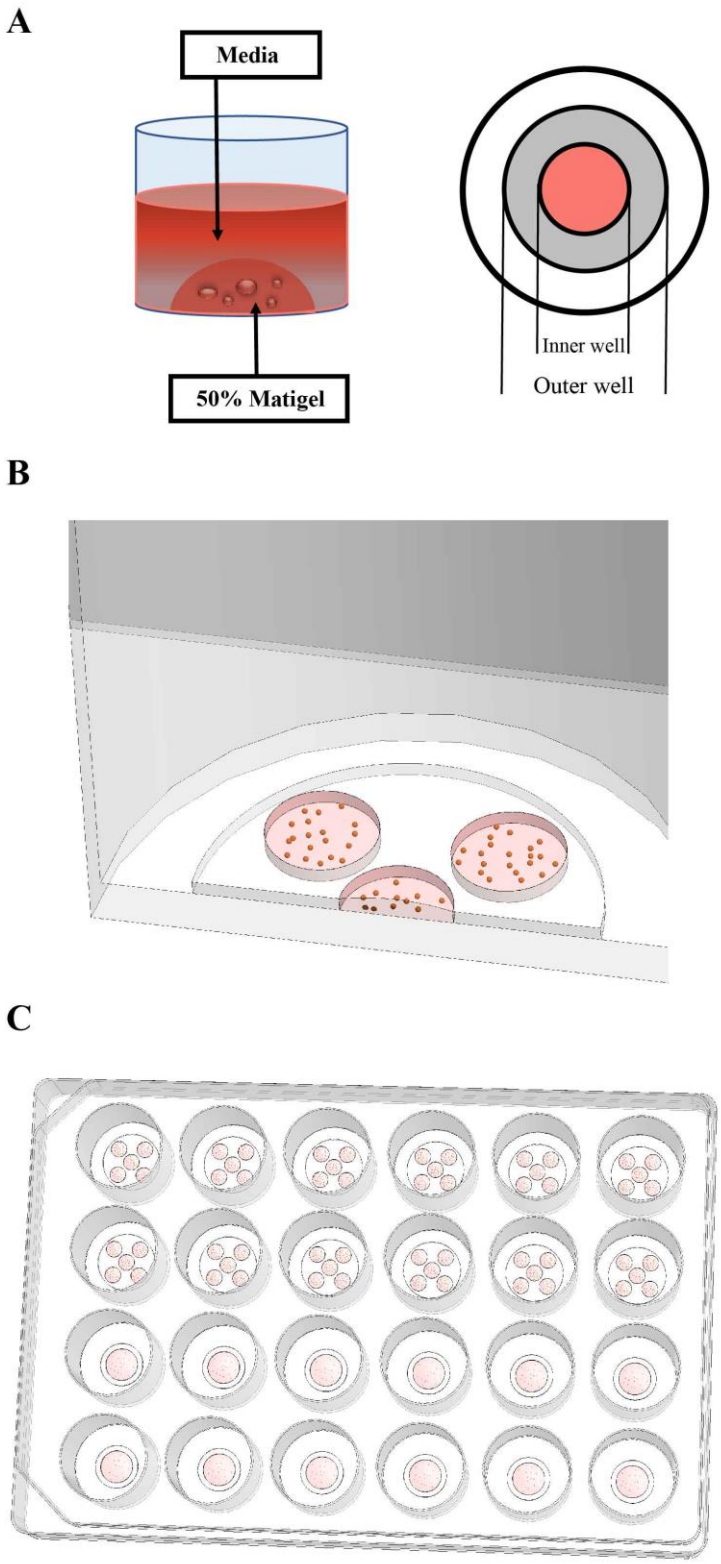

Figure 5.2 Airway organoid culture in droplet format

(A) Schematic diagram of airway organoid culture in droplet format and top view of silicone mask. The diameter of inner well is 5 mm (48-well plate) or 6 mm (24-well plate), outer well is 8 mm (48-well plate) or 10 mm (24-well plate). (B) Silicone mask with multiple holes. Red balls represent cells and pink represent Matrigel®. (C) Top view of silicone masks in culture plate. The mask can be made with single hole or multiple holes.

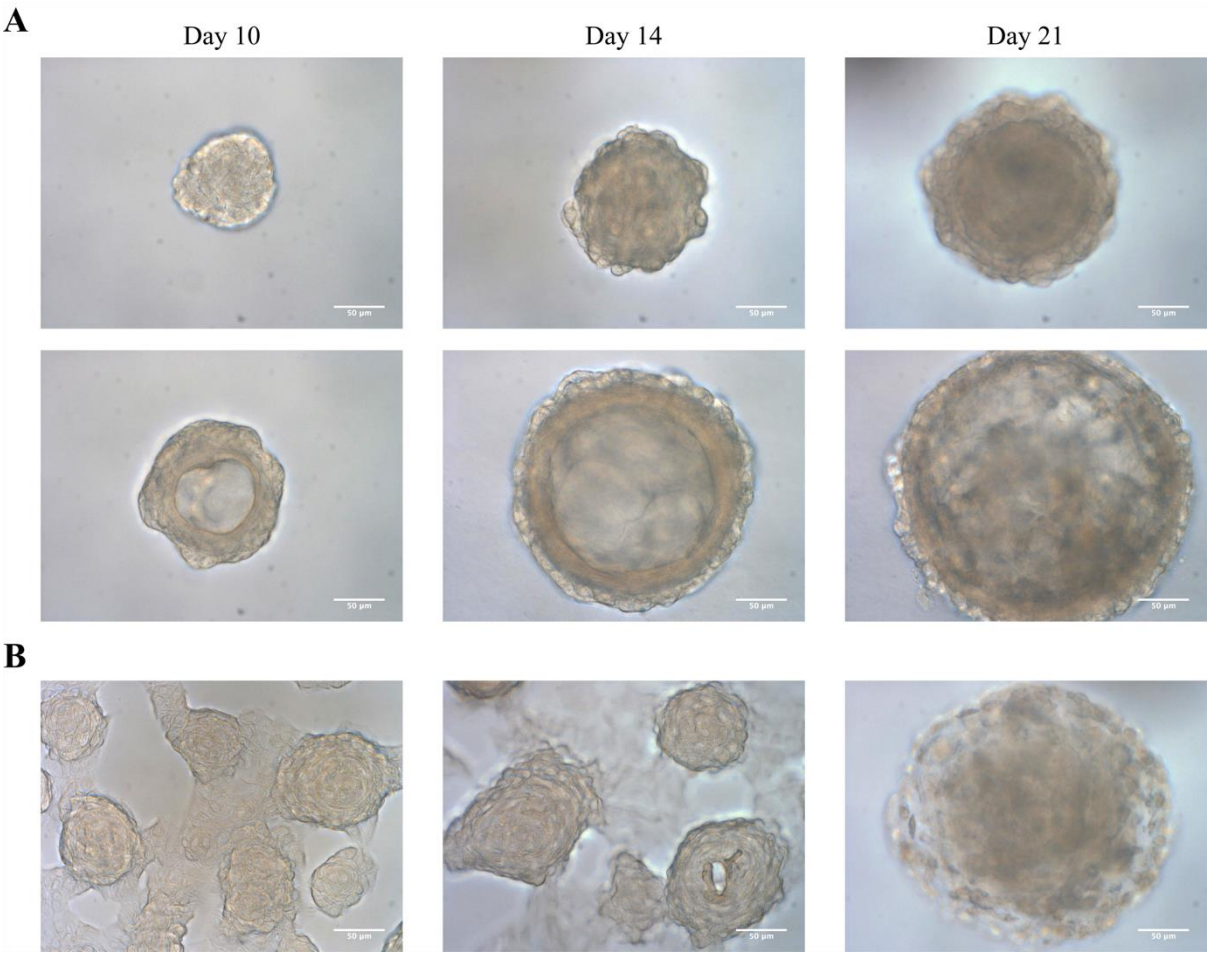

Figure 5.3 Airway organoids generated from BCi cells in Matrigel® droplet within silicone mask

BCi cells were mixed with Matrigel® and dropped into the inner well of silicone mask. After solidification, medium was added to cover the droplet and refreshed every two to three days for four weeks. (A) Representative brightfield images (40x objective) of airway organoids at Day 10, 14, and 21. (B) Abnormal airway organoids: connected organoids at Day 19 (left), Day 21 (middle), and "dying" organoid at Day 21.

5.3.2 Investigation of cell density and cell passage in airway organoid culture

After further standardizing the culture method, we then investigated the influence of cell density and cell passage on airway organoid culture. Firstly, NHBE cells were seeded at 1,000 cells/well, 2,000 cells/well, 5,000 cells/well, 8,000 cells/well, and 10,000 cells/well. The organoid morphology changes were recorded for four weeks (**Figure 5.4**). After two weeks, the organoids initiated from 1,000 cells and 2,000 cells were sparse. Organoids initiated from 5,000 cells and 8,000 cells were similar in size and quantity, whereas organoids

initiated from 10,000 cells showed less confluency. The mRNA of organoids was extracted weekly to monitor the cell growth (**Table 5.2**). Concentration above 50 ng/µL was regarded as a feasible mRNA concentration according to the laboratory protocol. Organoids started from 1,000 cells/well and 2,000 cells/well were all below 50 ng/µL. All the other three densities gave a relatively high yield. They reached the peak after two weeks and dropped afterwards. Taking the morphology change and mRNA concentration into consideration, 5,000 cells/well in 24-well plate was used as the seeding density in the subsequent airway organoid cultures.

The experience from ALI cultures taught us that the progenitor cells lose the differentiation potential at later passages. To assess the influence of cell passage in airway organoid culture, HBEB cells were used. HBEB cells were established into submerged culture from native primary bronchial epithelial cells and call as “P1” cells. Once they reached confluency, “P1” cells were seeded into airway organoid culture and passaged into “P2”. Three HBEB cultures were used to generate airway organoids in this order (**Figure 5.5**). The organoids from “P1” cells were all in a regular shape and contained visible lumen structure. Organoids from “P2” cells started to look irregular in size and shape. Organoids from “P3” cells lost the shape as “P1” and reduced in numbers, especially for culture M1C130 and M1C154. Therefore, early passage cells were preferred in airway organoid cultures.

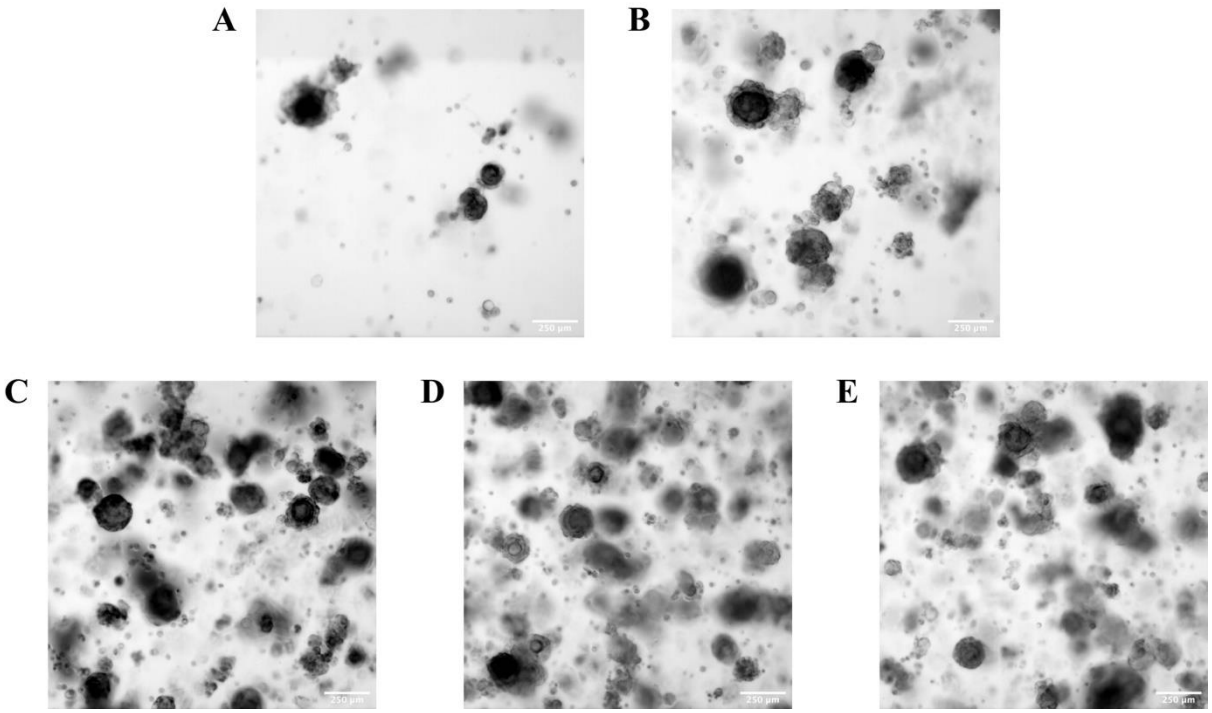

Figure 5.4 Cell density investigation of airway organoid culture

NHBE cells were seeded at 1,000 cells (A), 2,000 cells (B), 5,000 cells (C), 8,000 cells (D), and 10,000 cells (E) per well to generate airway organoids. Representative brightfield images (4x objective) were taken at Day 18.

Table 5.2 The mRNA concentration of NHBE derived airway organoids

NHBE cells were seeded at 1,000 cells, 2,000 cells, 5,000 cells, 8,000 cells, and 10,000 cells per well to generate airway organoids. Total mRNA was extract at Day 7, 14, 21, and 28 and the concentration was measured by Nano Drop 1000.

mRNA concentration (ng/µL)	**1,000 cells/well**	**2,000 cells/well**	**5,000 cells/well**	**8,000 cells/well**	**10,000 cells/well**
Day 7	11	36	75	85	94
Day 14	9	39	107	110	104
Day 21	7	43	75	92	83
Day 28	1	10	52	45	41

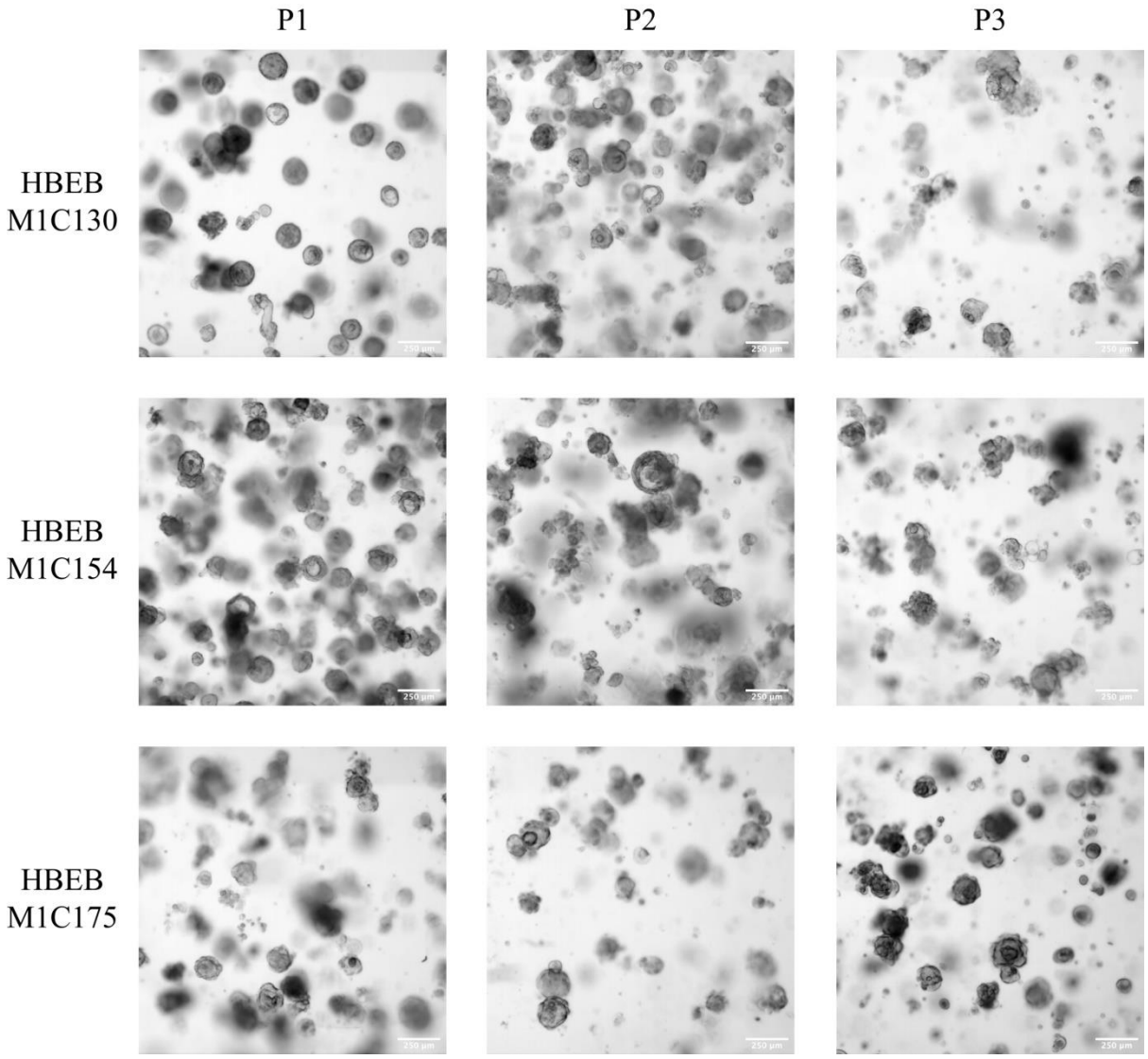

Figure 5.5 Airway organoids generated from HBEB cells at different passages.

HBEB cells at passage 1, 2, and 3 were seeded to generate airway organoids. Representative brightfield images (4x objective) were taken at Day 21

5.3.3 Investigation of culture media in airway organoid culture

With all the modifications illustrated above, we then tried to achieve a successful airway organoid culture with cell differentiation. Primary cells from normal donors, asthmatic patients, and COPD patients were used to generate airway organoids. All these cells have been previously confirmed to be differentiable in ALI cultures (Prodanovic et al., 2017). After three weeks, there was not much difference in morphology among NHBE, asthmatic-HBE, and COPD-HBE cells (**Figure 5.6A, B, C**), except that asthmatic-HBE organoid culture had fewer small cell clumps or single cells. The mRNA was extracted weekly and cell

marker genes expression was measured to monitor the cell differentiation: basal cell markers, integrin alpha-6 (ITGA6), p63, and keratin 5 (KRT5) (**Figure 5.6D**); ciliated cell markers, dynein heavy chain 1, 5 (DNAH1, DNAH5), and forkhead box protein J1 (FOXJ1) (**Figure 5.6E**); and secretory cell markers, mucin 5AC (MUC5AC), mucin 5B (MUC5B), and trefoil factor 3 (TFF3) (**Figure 5.6F**). MUC5B was not shown, as it was below the limit of detection. As expected, the levels of basal cell markers ITGA6 and KRT5 were decreased over time. Ciliated cell marker DNAH1 increased, whereas DNAH5 and FOXJ1 stayed at the same level. Likewise, secretory cell markers didn't change. Overall, the relative levels of ciliated and secretory cell markers remained close to the limit of detection.

We further reviewed our culture method and noticed that the culture media might be the key factor in this apparently limited differentiation response. We started organoid culture from 2017 when there was no standard protocol available. Hence, the BEGM medium was used to support ALI cultures as one report suggested it can support airway organoid culture (Hild and Jaffe, 2016). We used BEGM in airway organoid cultures as well. With more and more airway organoid reports published, we turned to the airway organoid media (AO media) recipe from Han Clevers group (Sachs et al., 2019) (**Table 5.3**) in 2019. From the recipe, we selected A83-01 and Y-27632 supplemented into BEGM. We also supplemented BEGM with the Notch inhibitor DAPT (Zhou et al., 2018). However, none of these combinations supported the cell differentiation in airway organoid culture. Then, we replaced the BEGM with AO media in airway organoid culture. Three NHBE cultures were tested in AO media (**Figure 5.7A, B, C**). As expected, gene expression of basal cell markers, secretory cell markers, and ciliated cell markers suggested the cell differentiation (**Figure 5.7D**). MUC5AC, MUC5B, and TEKTIN gene expression was profoundly increased. The beating cilia captured under microscope reinforced the evidence of cell differentiation (**Video S1, S2, S3**). Notably, inverted cilia were found across all the cultures.

Furthermore, we did a cross combination of media to investigate the best condition for airway organoid culture. The STEMCELL PneumaCult™ medium system were included as a promising ALI medium over BEGM medium. Submerged NHBE and BCi cells were cultured in BEGM or PneumaCult™ Ex Plus medium and changed to AO media or PneumaCult™ ALI (P-ALI) medium for airway organoid culture as illustrated in **Table 5.4**. Only NHBE cells from BEGM medium to AO media successfully differentiated (**Figure 5.8A; Video S4**). NHBE cells from Ex Plus medium generated nice shape of organoids in AO media, but no evidence showed cell differentiation (**Figure 5.8B**). NHBE cells died in PneumaCult™ Ex

Plus medium to P-ALI medium (**Figure 5.8C**). For BCi cells, none of the combinations of media supplements supported the cell differentiation (**Figure 5.8D, E, F**). Cells from Ex Plus medium to P-ALI medium didn't support the generation of organoid-like structure and massively expanded the monolayer cell numbers.

Table 5.3 Airway organoid media recipe

From reported protocol(Sachs et al., 2019).

Media component	**Signalling pathway**	
	Activation	**Block**
R-Spondin 1	Wnt/β-catenin signalling	
FGF 7	FGFR2b signalling	
FGF 10	FGFR2b signalling	
Noggin		TGF-β signalling
A83-01		TGF-β signalling
Y-27632		ROCK signalling
SB202190		p38 MAPK signalling
B27 supplement	a.o. insulin signalling	
N-Acetylcysteine	Antioxidant	
Nicotinamide	Co-enzyme precursor	
GlutaMax 100x	Nutrient	
HEPES	Buffer	
Penicillin / Streptomycin	Antibiotics	
Primocin	Antibiotic/antimycotic	
Advanced DMEM/F12	Base medium	

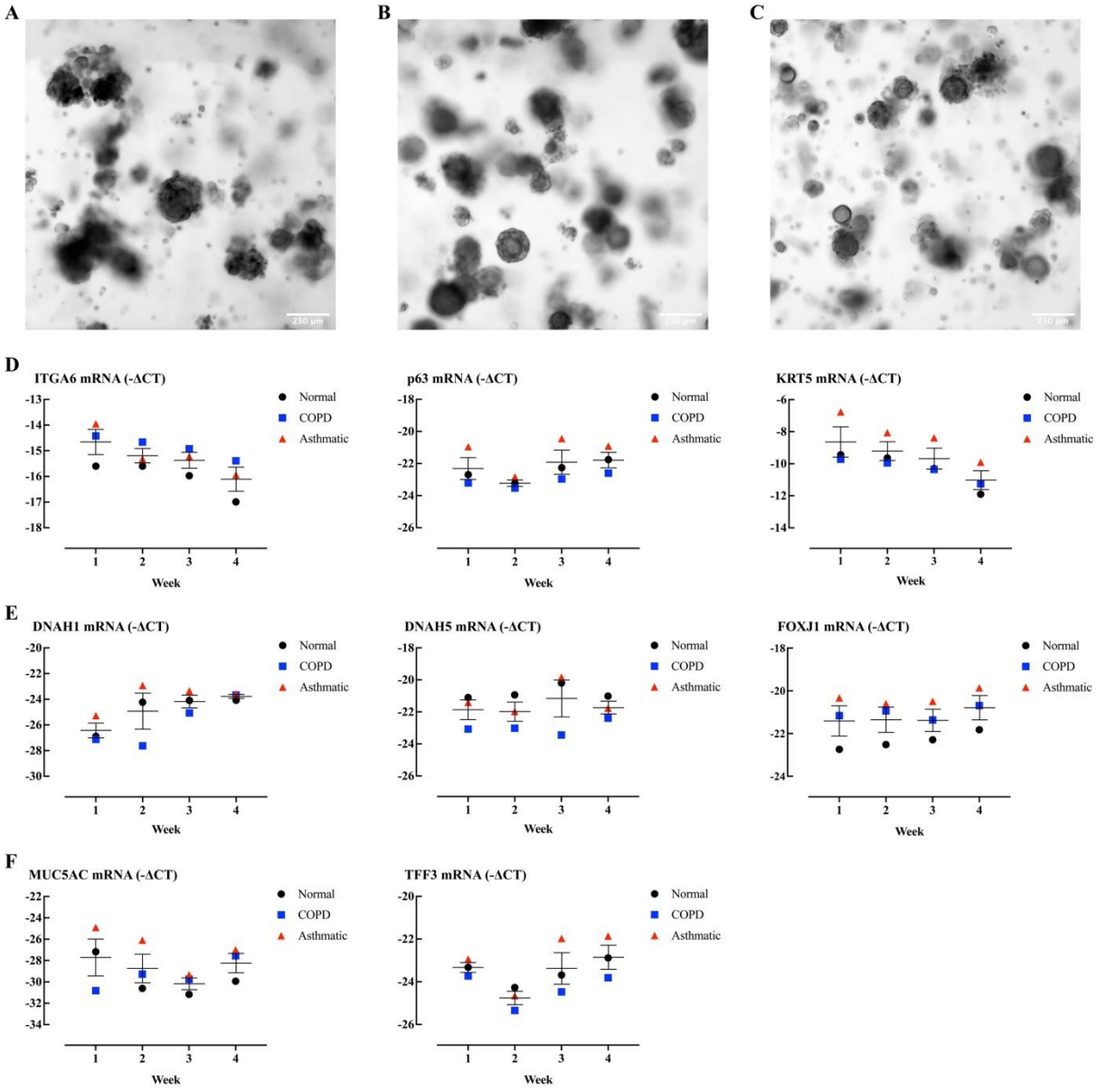

Figure 5.6 Airway organoids generated from NHBE, Asthmatic-HBE, and COPD-HBE cells in BEGM medium

NHBE, Asthmatic-HBE, and COPD-HBE cells were seeded to generate airway organoids using BEGM medium. Representative brightfield images (4x objective) of NHBE (A), Asthmatic-HBE (B), COPD-HBE (C) cells derived airway organoids were taken at Day 21. Total RNA was extracted and gene expression of basal cell markers (A), ciliated cell markers (B), and secretory cell markers (C) were measured by RT-qPCR. Gene expression is expressed as -ΔCT (Log2). Data are presented as mean and SEM for n=3 independent cultures.

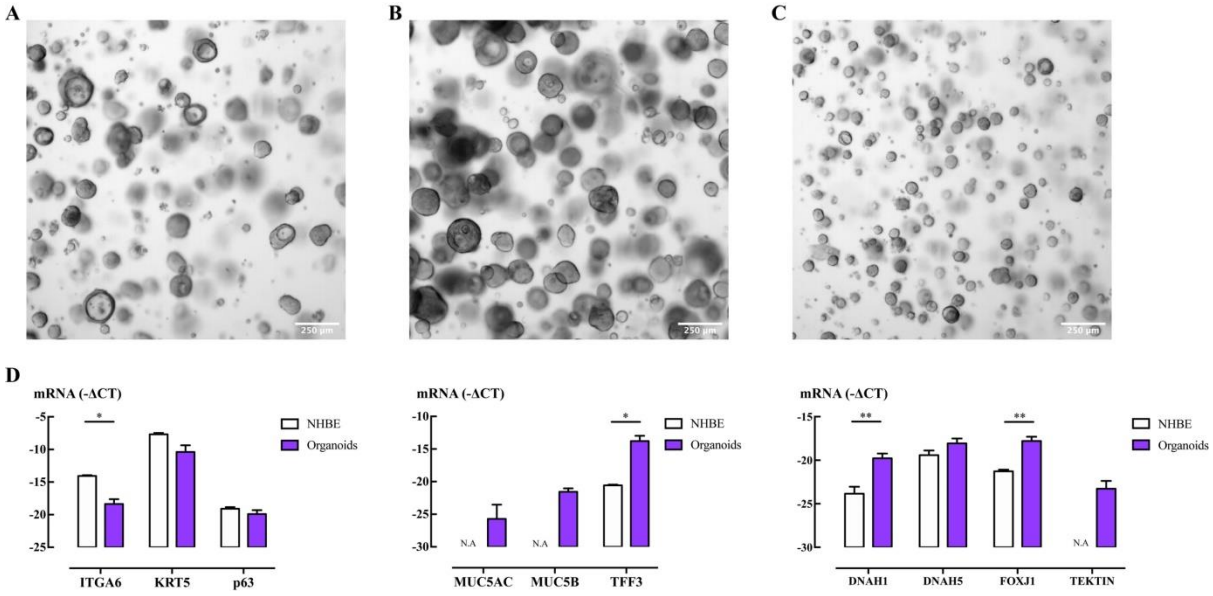

Figure 5.7 Airway organoids generated from NHBE cells in Airway Organoid medium

NHBE cells were seeded to generate airway organoids using Airway Organoid medium. Representative brightfield images (4x objective) of three independent NHBE cell cultures (A, B, C) derived airway organoids were taken at Day 21. (D) Total RNA was extracted and gene expression of basal cell markers (left), secretory cell markers (middle), and ciliated cell markers (right) were measured by RT-qPCR. Gene expression is expressed as -ΔCT (Log2). Data are presented as mean and SEM for n=3 independent cultures. A paired-samples t-test was used for analysis, *: $P<0.05$, **: $P<0.01$.

Table 5.4 Cross combination of media in airway organoid culture

Submerge culture	Airway organoid culture
BEGM	AO media
PneumaCult™ Ex Plus	AO media
	PneumaCult™ ALI (P-ALI)

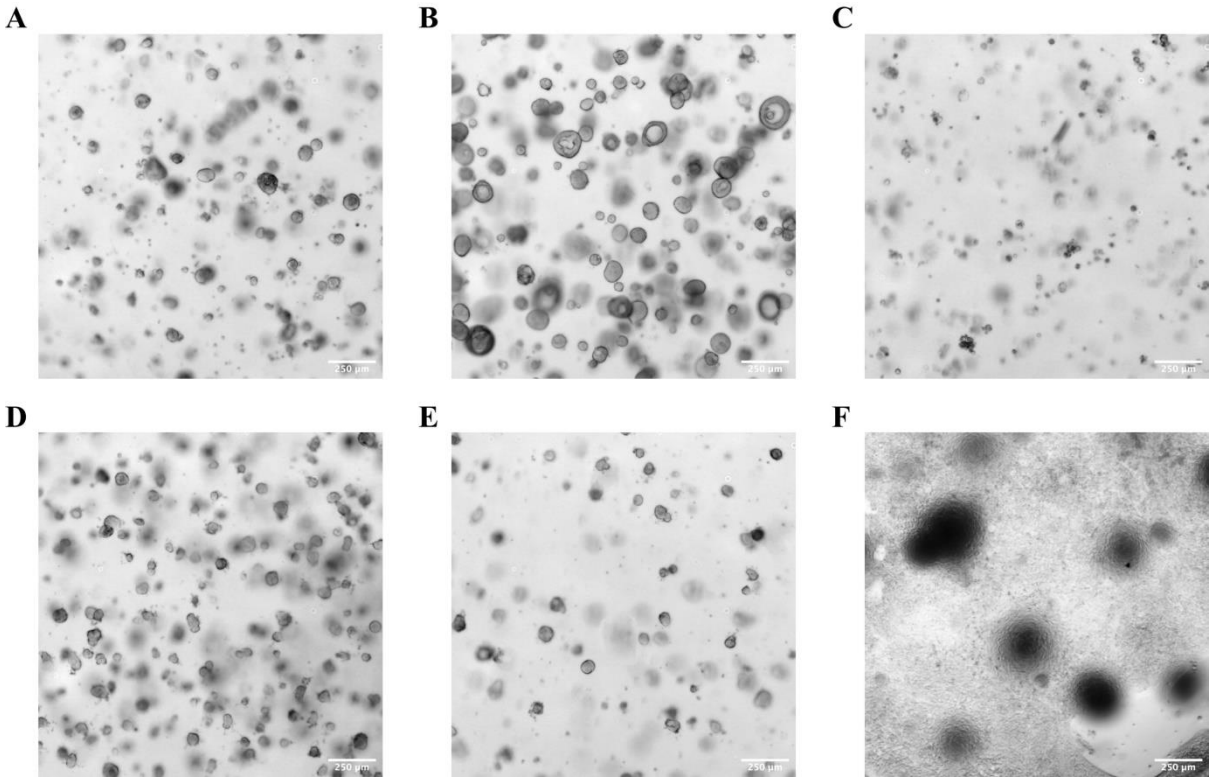

Figure 5.8 Airway organoids generated from NHBE and BCi cells in different combination of culture media

Submerged NHBE cells in BEGM medium seeded in AO medium (A), submerged NHBE cells in PneumaCult™ Ex Plus medium seeded in AO medium (B) or P-ALI medium (C) to generate airway organoids. Submerged BCi cells in BEGM medium seeded in AO medium (D), submerged BCi cells in PneumaCult™ Ex Plus medium seeded in AO medium (E) or P-ALI medium (F) to generate airway organoids. Representative brightfield images (4x objective) were obtained at Day 21.

5.3.4 Characterization of airway organoids

To gain a detail view of the structure, airway organoids were fixed and stained with cell marker antibodies and junction proteins. In comparison, whole mount staining and staining of paraffin sections was performed in ALI cultures as a reference. For airway organoids, we only performed whole mount staining, whereas paraffin-embedding was difficult to achieve for the size and number of organoids. In airway organoids, the basal cells marker KRT5 was highly expressed in cells at the border of the organoid (**Figure 5.9A**). F-actin was distributed at the cell membrane and highlighted the lumen structure inside the organoid. MUC5AC were positively stained in the lumen, suggesting the goblet cells secreted mucin into the lumen. In ALI cultures, H&E staining showed pseudostratified columnar epithelial cells (**Figure 5.9B**). IF staining indicated that the basal cells were localized underneath the ciliated and secretory cells (**Figure 5.9C**). In whole mount staining, E-Cad were evenly distributed at the cell membrane, further demonstrated the columnar structure.

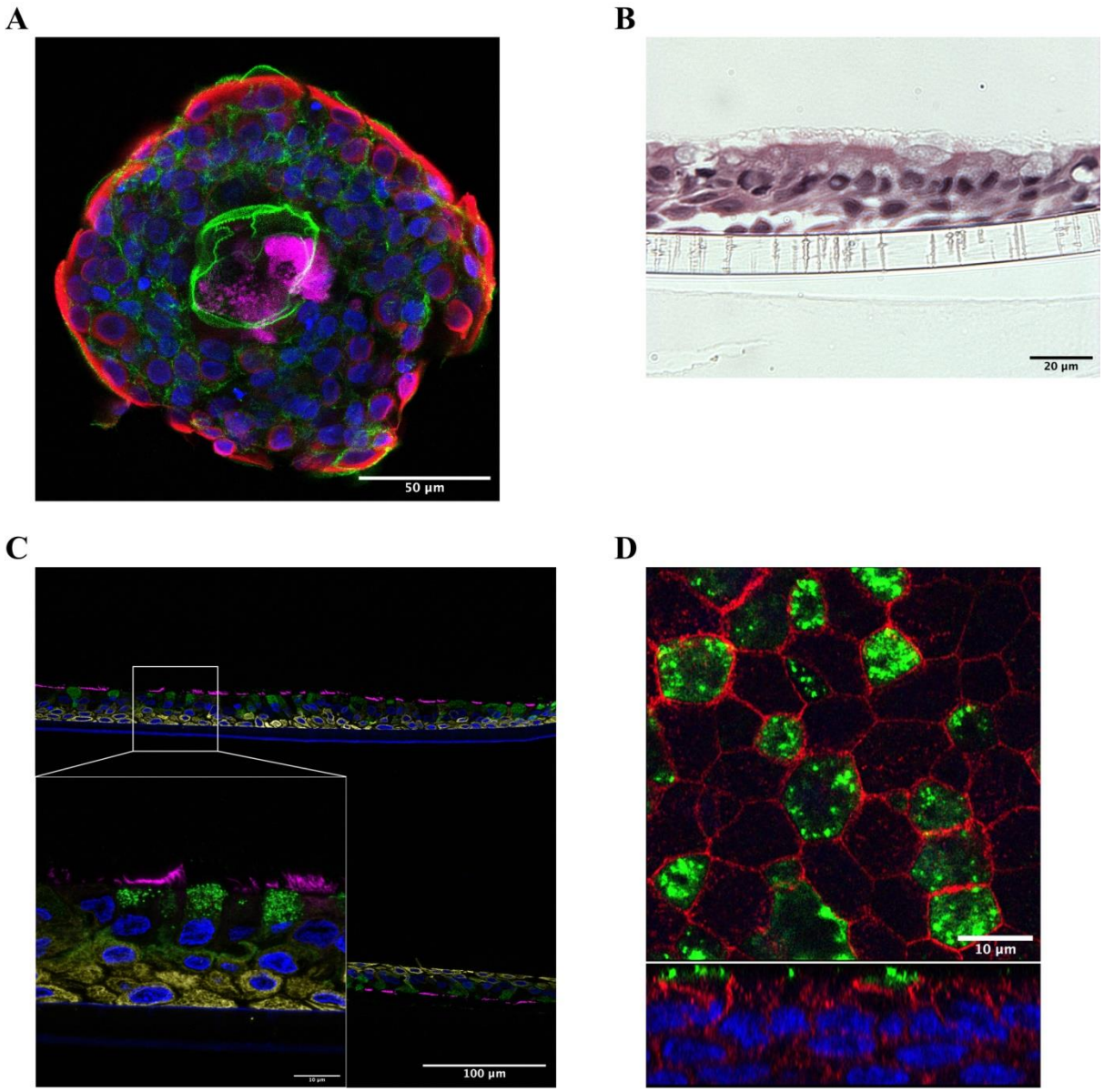

Figure 5.9 Characterization of air-liquid interface culture and airway organoids

NHBE cells were differentiated in airway organoid culture and air-liquid interface culture. Airway organoids were fixed after 21 days of culture. Air-liquid interface culture was fixed after 28 days. (A) Immunofluorescence staining of basal cell marker KRT5 (red), goblet cell marker MUC5AC (magenta), F-actin (green), and nucleus (blue) in NHBE cells derived airway organoid. (B) H&E staining on NHBE cells derived ALI paraffin section. (C) Immunofluorescence staining of basal cell marker KRT5 (yellow), ciliated cell marker acetylated tubulin (magenta), club cell marker CC10 (green), and nucleus (blue) on NHBE cells derived ALI paraffin section. Images were taken with 20x and 60x objective. (D) Whole mount staining of E-cad (red), club cell marker CC10 (green), and nucleus (blue) on NHBE cells derived ALI.

5.3.5 ENaCα, β, γ subunits gene expression was restored by airway organoid culture and ALI culture.

Hence the airway organoid culture been finalized, the gene expression of ENaCα, β, γ subunits was measured to identify whether they are suitable for assessing channel activity. The mRNA from submerged NHBE cells, NHBE derived organoids, and NHBE derived ALI were collected and measured (**Figure 5.10**). The comparison was made within the same NHBE culture to exclude donor variation. The ENaCα gene expression was not altered by either airway organoid culture or ALI culture, same as native and submerged HBEB cells (**Figure 4.6B**). Interestingly, both airway organoid and ALI culture increased the ENaC β and γ subunits gene expression to levels close to in native HBEB cells (**Table 5.5**).

Table 5.5 The comparison of ENaCα, β, γ subunits gene expression in HBEB cells, NHBE cells, airway organoids, and ALI

Airway organoid cultures were collected after 21 days of culture. Air-liquid interface culture was collected after 28 days. Total RNA extracted and gene expression of ENaCα, ENaCβ, and ENaCγ were measured by RT-qPCR. Gene expression is expressed as -ΔCT (Log2). Data are presented as mean and SEM for n=6 independent HBEB cultures, n=4 independent experiments from NHBE cells and airway organoid cultures, n=10 ALI cultures.

ΔCT (Log2)	**Native HBEB**	**HBEB Submerged**	**NHBE Submerged**	**NHBE-Organoids**	**NHBE-ALI**
ENaCα	-16.8±0.4	-17.6±0.2	-15.1±0.2	-14.5±0.4	-15.9±0.1
ENaCβ	-16.5±0.2	-22.2±1.3	-22.5±1.0	-17.6±0.7	-17.3±0.2
ENaCγ	-20.8±0.3	-28.5±0.6	-26.9±0.8	-23.8±0.8	-25.2±0.2

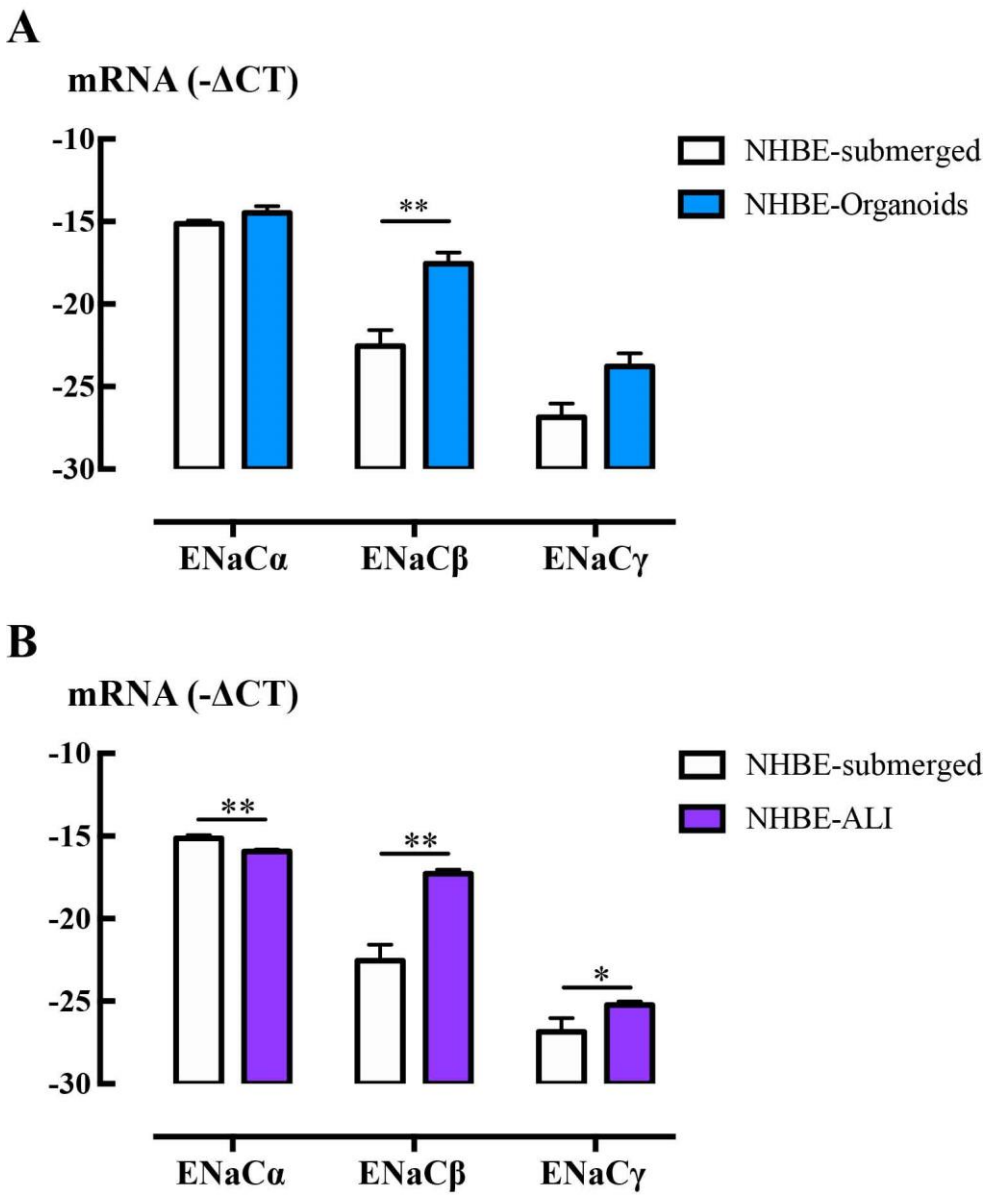

Figure 5.10 The gene expression of ENaCα, β, γ in submerged NHBE cells, airway organoid cultures, and ALI culture

NHBE cells were differentiated in airway organoid culture and air-liquid interface culture. Airway organoid cultures were collected after 21 days of culture. Air-liquid interface culture was collected after 28 days. Total RNA extracted and gene expression of ENaCα, ENaCβ, and ENaCγ were measured by RT-qPCR. Gene expression is expressed as -ΔCT (Log2). Data are presented as mean and SEM for n=4 independent experiments from NHBE cells and airway organoid cultures (A), n=10 ALI culture (B). A paired-samples t-test (A) and unpaired t-test (B) were used for analysis, *: $P<0.05$, **: $P<0.01$.

5.4 Discussions

In this chapter, we successfully generated airway organoids using protocols modified from the culture formats reported in the literatures. The silicone mask made the droplet uniform in size and shape to reduce the variance of organoids between wells of culture plate, increasing the reproducibility. The cell differentiation in airway organoid culture requires specific culture media. Both airway organoid culture and air-liquid interface culture supported cell differentiation and recapitulated *in vivo* architecture. They restored the ENaC subunits expression to levels in native human epithelial cells, suggesting they have the potential to be used in evaluating ENaC channel activity.

Overlaying cells on Matrigel® bed could lead to insufficient cell migration, increasing the culture complexity. Initially, some studies chose to overlay the cells on top of the Matrigel® bed (Hild and Jaffe, 2016; Tan et al., 2017; Wu et al., 2011). Overlaying NHBE cells on Matrigel® showed more efficiency than embedding cells either in 100% Matrigel® or 1:1 diluted Matrigel® to generate 3D glandular acini (Wu et al., 2011). It is understandable considering the characteristic of Matrigel®. Basement membrane is mainly composed of type IV collagen, laminin, nidogen/entactin, and perlecan (LeBleu et al., 2007). Matrigel®, extracted from the Engelbreth-Holm-Swarm (EHS) tumour, contains collagen IV (~30%), laminin (~60%), entactin (~8%), and perlecan (~2-3%) (Corning, 2019; Kleinman et al., 1986; Kleinman et al., 1982). It also contains a wide range of growth factors, including TGF-β, fibroblast growth factors (FGFs), epidermal growth factor (EGF), platelet-derived growth factor (PDGF), vascular endothelial growth factor (VEGF), and insulin-like growth factor (IGF) (Corning, 2019). The gelation of Matrigel® happens at 22-37°C, during which entactin crosslinks collagen and laminin to create a water-swollen, crosslinked network (Aisenbrey and Murphy, 2020). It is extremely important to handle the Matrigel® in chilled/ice-cold environment to avoid pre-gelling. In airway organoid culture, overlaying cells on gelled Matrigel® might protect cells from a “temperature shock”. Temperature reduction might regulate cell cycle, metabolism, transcription, translation, and cell cytoskeleton (Al-Fageeh et al., 2006). But mammalian cells can survive under 4°C at a reduced growth rate (Fujita, 1999; Hunt et al., 2005). Therefore, it is probably acceptable to mix the cells with cold Matrigel® in airway organoid culture. We have seen cells remain on top of the Matrigel® layer instead of moving into the Matrigel®. Using a model containing both monolayer cells and sphere-like cells has the potential to make the results confusing, especially in mechanopharmacology. It was well established that membrane-anchored matrix metalloproteinases (MT-MMPs)

regulate cell migration through ECM and affect cell self-organization (Hotary et al., 2000; Quaranta, 2000). Insufficient expression of MT-MMPs could be responsible for the formation of monolayer cells.

Hydrophobic polydimethylsiloxane is the most familiar silicone polymer (Owen, 2017). Although the initial purpose of introducing it into airway organoid culture was to use as a mask to assist Matrigel® gelation, the outcome indicated its potential for standardization and industrialization of airway organoid culture. Moreover, the size of the silicone mask determines the droplet curvature. Tissue shape and growth can be regulated by surface tension, which is related to local curvature (Beltrán-Heredia et al., 2017; Ehrig et al., 2019; Fischer-Friedrich et al., 2014). Therefore, the response of organoids to surface tension can be investigated by controlling silicone mask.

The cell condition used in organotypic cultures might be one of the key factors. It is well accepted that the primary cells have limited lifespan and numbers of time cells can divide. Most of the studies use cells at passage one or two to guarantee their differentiation potential. In ALI cultures, it is now possible to use cells beyond passage four in presence of Rho kinase (ROCK) inhibitor or in PneumaCult™ Ex Plus medium (Rayner et al., 2019). ROCK inhibitor, Y-27632, allowed extension of airway basal cells (Horani et al., 2013; Wolf et al., 2017). Cells treated with Y-27632 expressed more intermediate filament and desmosomal genes and less protease gene expression with implications for ECM remodelling (Reynolds et al., 2016). The use of the ROCK inhibitor can also maintain iPSCs phenotype and enhance the recovery of iPSCs by phosphorylating and activating the myosin II pathway (Claassen et al., 2009; Vernardis et al., 2017; Watanabe et al., 2007). Although confidential, one could speculate that PneumaCult™ Ex Plus medium contains ROCK inhibitor. However, cells submerged in PneumaCult™ Ex Plus medium only differentiated in ALI culture, not in airway organoid culture. It is an interesting contrast, considering that the ROCK inhibitor is one of the components of the airway organoid media. This is suggesting that airway organoid culture might have different requirements for cell conditions than those supporting ALI culture. In airway organoid cultures, stem cells isolated from lung tissue and hPSCs are more often used (Chen et al., 2017; McCauley et al., 2017; Sachs et al., 2019; Song et al., 2021; Zhou et al., 2018). Freshly isolated cells keep the most *in vivo* features as well as having the best maintained differentiation potential. However, these cells are short supply and low in number and with limited range of sources. Lack of maturity, phenotypic heterogeneity, and

genetic instability limit the use of iPSCs (Doss and Sachinidis, 2019). Further study on generating airway organoids from BCi cells would benefit large scale screening.

Media component is another key factor. For ALI culture, retinoic acid (RA) is believed to be the essential component for promoting mucociliary differentiation (Cao et al., 2021; Luengen et al., 2020). Lack of RA resulted in decreased mucin secretion and mucin genes expression in ALI culture (Yoon et al., 1997). Binding of RA to receptors activate the transcription of primary target genes, induce epigenetic changes, and induce genes encoding transcription factors and signalling proteins which further alter the gene expression (Gudas and Wagner, 2011). The activation of retinoic acid receptor α led to c-FOX/c-JUN dependent claudin 1 promoter activation and increased tight junction permeability (Lochbaum et al., 2020). However, neither BEGM with RA, nor PneumaCult^{TM} ALI medium support mucociliary differentiation in airway organoid culture. The AO media from Hans Clevers group was developed from medium for intestine, liver, pancreas (Broutier et al., 2016). These organoid cultures share most of the components, whereas airway organoids do not require exogenous WNT3A (Sachs et al., 2019). For iPSCs, low Wnt conditions promoted lung progenitors to airway progenitors to grow airway organoids, whereas high Wnt drove to differentiation of alveolar progenitors (McCauley et al., 2017). Addition of A83-01 or Y-27632 into BEGM could not support cell differentiation, suggesting that all the AO media components might be indispensable. Nevertheless, it would be interesting to investigate the key components in airway organoid culture so that other growth factors could be reduced/replaced in pharmacology and pathophysiology studies. For instance, A83-01 (IC_{50}=12 nM) is more potent in inhibiting TGF-β receptor ALK5 than SB431542 (IC_{50}=94 nM), a selective inhibitor of ALK5 (Inman et al., 2002; Tojo et al., 2005). The existence of such a potent TGF-β inhibitor would compromise the predictive value of airway organoid culture in investigating the influence of matrix stiffness on TGF-β actions.

Controlling mucociliary differentiation direction in organotypic cultures could provide models for disease associated with goblet cell hyperplasia. IL-6 addition in ALI cultures resulted in increased ciliated cells and fewer secretory cells, which was through activation of STAT3 to regulate Notch1, Mcidas, and FOXJ1 genes (Tadokoro et al., 2014). Interleukin-13 and interleukin-4 have been shown to increase goblet cell formation (Kuperman et al., 2002; Laoukili et al., 2001; Munitz et al., 2008). IL-13 increased mucin genes expression in airway organoids was inhibited by Notch2 inhibitor, suggesting Notch2 might be required for goblet cell metaplasia (Danahay et al., 2015). The Notch signalling inhibitor, DAPT promoted

ciliated cells over secretory cell differentiation (Konishi et al., 2016; Zhou et al., 2018). In ALI cultures, Notch signalling also regulated the balance of ciliated and secretory cell (Gomi et al., 2015; Rock et al., 2011) However, we didn't see any evidence suggesting cell differentiation in airway organoids cultured in BEGM supplemented with DAPT. It might not be surprising, considering that the BEGM medium might not be suitable.

Airway organoid culture and ALI culture both brought ENaC β and γ subunits to levels close to native cells. Ussing chamber and single-clamp patch assay have been used in ALI culture to measure ENaC and CFTR activity (Den Beste et al., 2013; Gentzsch et al., 2016; Gianotti et al., 2018; Rayner et al., 2019). These conventional methods to measure ENaC channel activity, as described in Chapter 4, are either single-use or tissue based. The membrane in the transwell could be cut to fit into the Ussing chamber, but this would be too difficult for airway organoids. Forskolin-induced swelling assay (FIS assay) is applicable to airway organoids (Boj et al., 2017; Dekkers et al., 2013). Forskolin activates CFTR by increasing intracellular cyclic adenosine monophosphate (cAMP) levels (Collawn and Matalon, 2014). Organoids exposed to forskolin swell as a result of ion and water transport. In the assay, the organoids swelling is recorded by fluorescent cell-permeable dye, calcein green. ENaC channel works co-ordinately with CFTR. Therefore, the FIS assay might also be suitable to measure ENaC channel activity. Compared to FLIPR® membrane potential assay used in Chapter 4, FIS assay visualizes the functional consequences of the channel current change but might not be extendable to high-throughput and has not been validated in airway organoids.

In summary, organotypic culture can restore the ciliated and secretory cell populations. The culture medium and cell conditions in organotypic culture are critical for mucociliary differentiation. Controllable organotypic cultures could be beneficial for physiology, pathology, and pharmacology research.

CHAPTER 6

ORGANOTYPIC AIRWAY EPITHELIAL CULTURES FOR SARS-COV-2 RESEARCH

6.1 Introduction

Coronavirus disease 2019 (COVID-19) caused by severe acute respiratory syndrome coronavirus 2 (SARS-CoV-2) has rapidly spread globally since December 2019. The World Health Organization (WHO) declared the COVID-19 outbreak a pandemic in March 2020 (WHO, 2020). As of June 2021, more than 175 million people have been confirmed infected with more than 3.8 million deaths announced. The symptoms of COVID-19 when present are highly varied, but may include fever, dry cough, and shortness of breath. Severe cases of COVID-19 can lead to hypoxia, respiratory failure, and death. Currently, the US Food and Drug Administration (FDA) has approved the anti-viral agent remdesivir for hospitalized patients who require supplemental oxygen (FDA, 2020) and monoclonal anti-spike protein antibodies bamlanivimab and etesevimab in combination for the treatment of mild to moderate COVID-19 in adults and paediatric patients (FDA, 2021). Dexamethasone, alone or in combination with remdesivir, is approved for hospitalized patients. Baricitinib in combination with remdesivir is also approved for hospitalized patients requiring supplemental oxygen or extracorporeal membrane oxygenation. Pfizer-BioNTech, Moderna, Oxford-AstraZeneca, and Sinopharm vaccines have been approved for use in several countries. The progress of vaccination and emerging data suggests that the burden of infection in many countries is reduced but not eliminated. Control of COVID-19 is complicated by the emergence of variant viruses that are more transmissible (e.g., the delta variant) or against which current vaccines show reduced effectiveness (beta variant). Vaccine hesitancy, an inevitable fraction of the population who fail to mount an adequate immune response and the potential development of new virus strains resistant to vaccines further emphasize the necessity to continue to understand and develop additional rational treatment approaches for COVID-19, including repurposed drugs and perhaps even novel agents.

Case studies of hospitalized COVID-19 patients suggest older age, hypertension, diabetes, cardiovascular disease, and higher number of comorbidities are associated with disease severity (Li et al., 2020; Wu and McGoogan, 2020; Zhang et al., 2020b). Surprisingly, asthma, chronic obstructive pulmonary disease (COPD), and allergic disease have not been identified as risk factors for COVID-19 severity (Chhiba et al., 2020; Li et al., 2020; Lovinsky-Desir et al., 2020; Zhang et al., 2020b). This lack of susceptibility of patients with lung diseases contrasts with observations with other respiratory viruses, such as rhinovirus (RV), respiratory syncytial virus (RSV), or influenza virus, which are known to exacerbate the inflamed airways in these prevalent airway/lung diseases (Tan et al., 2020). Additionally,

patients with cystic fibrosis (CF) were also underrepresented in COVID-19 cohort (Colombo et al., 2020). The hallmark of pulmonary manifestations of cystic fibrosis is infection by bacterial and viral pathogens(De Boeck and Amaral, 2016). The unexpectedly low proportion of patients with chronic respiratory disease in COVID-19 cohorts led us to question whether the underlying inflammatory features and/or therapeutics for chronic respiratory disease could provide any insights into determinants of COVID-19 severity.

A range of airway cellular models have been developed for investigation of respiratory infections. Freshly isolated and uncultured primary cells provide the closest model to the native condition but are limited in utility by a short *ex vivo* lifespan, access to donors, and cell numbers that can be obtained. The A549 type II alveolar epithelial carcinoma cell line and BEAS-2B simian virus 40 (SV40)-transformed bronchial epithelial cell lines have been commonly used in respiratory research. The data from these cell lines may sometimes be extrapolated to primary epithelial cells (Hillyer et al., 2018; Keenan et al., 2014). Notwithstanding their widespread usage, these cell lines lack *in vivo* architecture and phenotypic diversity, and their transformed proliferative pathways distort cellular pharmacology. One of the difficulties noted in studying SARS-CoV-2 is that most of the human cell lines were not infectible, except for CaCo2 and Calu3 cells (Chu et al., 2020). Therefore, more (patho)physiologically relevant cellular models are needed for COVID-19.

Since development in 1980s, the air-liquid interface (ALI) culture has become a routine approach to differentiate epithelial cells (Chen and Schoen, 2019) for a variety of viral infection studies, including influenza (Pharo et al., 2020; Wu et al., 2016), RSV (Xia et al., 2017), coronaviruses (Dijkman et al., 2013; Jia et al., 2005; Jonsdottir and Dijkman, 2016), and SARS-CoV-2 (Abo et al., 2020; Marsh et al., 2021; Pizzorno et al., 2020; Vanderheiden et al., 2020; Zhu et al., 2020). In the last decade, self-renewing organoid models have rapidly advanced understanding of stem cell biology, organogenesis, and human pathologies (Dutta et al., 2017). The use of organoids in studying influenza virus (Zhou et al., 2018) and adeno-associated virus (Meyer-Berg et al., 2020) promised researchers versatile models to cover the gaps between *in vitro* and *in vivo* infection models. In recent work, liver organoids (Yang et al., 2020) and lung bud tip organoids (Lamers et al., 2020) both showed susceptibility to SARS-CoV-2 infection.

We have systematically compared airway cell lines, ALI, and airway organoid culture to freshly isolated human bronchial epithelial cells to benchmark the expression and distribution of angiotensin converting enzyme 2 (ACE2), the main or primary receptor for SARS-CoV-2.

Biopsies from a cohort of asthmatic and non-asthmatic subjects (Keenan et al., 2018; Li et al., 2019) were also evaluated for the distribution and abundance of ACE2. The level and cellular distribution of the ACE2 in biopsies provided a further benchmark for comparison with ALI and airway epithelial cultures. Cytokine levels and morphogenic changes in ALI cultures after SARS-CoV-2 infection confirmed their utility in investigations of COVID-19.

6.2 Methods

6.2.1 Study participants

Twelve paediatric cystic fibrosis (CF) patients and four non-CF participants at the Royal Children's Hospital Melbourne were recruited. The clinical characteristics of the subjects with CF are shown in **Table 6.1**. The research ethics committees of the Royal Children's Hospital Melbourne (approval no. HREC 25054) and the University of Melbourne (approval no. HREC 2056658) approved the study. Written consent was obtained from the parents of the children enrolled into the study.

Table 6.1 Characteristics of donors of primary human bronchial epithelial brushing cell cultures

ID	CF/ Non-CF	Age	Sex	CFTR mutation 1	CFTR mutation 2	Modulator use
M1C130	CF	4.9	Male	deltaF508	G551D	Ivacaftor
M1C154	CF	3.2	Male	deltaF508	deltaF508	No
M1C175	CF	1.0	Female	c.1521_1523 (delCTT)	c.1521_1523 (delCTT)	No
M1C134	CF	5.0	Male	delta F508	delta F508	No
M1C172	CF	2.0	Male	delta F508	delta F508	No
M1C151	CF	4.0	Male	delta F508	delta F508	No
M1C123	CF	6.0	Female	delta F508	delta F508	Lumacaftor -ivacaftor
M1C126	CF	5.9	Female	p.F508del	p.F508del	No
M1C129	CF	5.9	Male	delta F508	p.G551D	Yes
M1C158	CF	3.9	Female	p.Arg1158Ter	p.Arg1158Ter	No
M1C176	CF	1.9	Male	p.Phe508del	p.Phe508del	No
M1C184	CF	0.5	Female	p.1507del	p.F508del	No

M1N050	Non-CF	8.4	Female	N/A	N/A	N/A
M1N055	Non-CF	1.1	Male	N/A	N/A	N/A
M1N056	Non-CF	5.9	Female	N/A	N/A	N/A
M1N057	Non-CF	3.7	Male	N/A	N/A	N/A

CFTR: cystic fibrosis transmembrane conductance regulator.

6.2.2 Primary human bronchial epithelial cell brushings

The establishment of primary human bronchial epithelial brushing cells (HBEB) were described as in Section 2.1.3.3. Briefly, the bronchial epithelial brushing cells obtained during flexible bronchoscopy using cytology brushes were dislodged by agitation, then seeded onto collagen-coated 25 cm^2 cell culture flasks in Bronchial Epithelial Growth Medium supplemented with Single Quots and Amphotericin B at 37°C in air containing 5% CO_2. The native cells were sedimented onto cytocentrifuge slides (Cytospin 2, Shandon, 350 rpm, 10 min) left to dry overnight and fixed in pre-chilled methanol for 5 min and then washed with PBS, prior to storage or staining.

6.2.3 Primary human bronchial epithelial cell (HBEC)

Primary human bronchial epithelial cells were established from bronchi of lung resection specimens derived from donors without chronic respiratory disease as previously describe (Schuliga et al., 2009). Samples were obtained with approval from the University of Melbourne (approval no. HREC 1750014) and Alfred Hospital (approval no. 336/13; Alfred Hospital, Melbourne, VIC, Australia). The establishment of primary human bronchial epithelial cells (HBEC) were described as in Section 2.1.3.4. Briefly, the bronchial epithelial cells were obtained by scraping the inner surface of airway with a no. 23 scalpel blade. The cells were resuspended in BEGM medium and seeded on collagen-coated 25 cm^2 cell culture flasks. Cells were cultured at 37°C in a humidified atmosphere containing 5% CO_2.

6.2.4 Primary human bronchial epithelial cell cultures

Primary human bronchial epithelial cell cultures, purchased from Lonza or prepared as described in Section 6.2.2 and 6.2.3. Briefly, cells were cultured in BEGM at 37°C in air containing 5% CO_2. Once cell cultures reached 80% confluency, the cells were dissociated using trypsin/EDTA and trypsin neutralizing solution.

6.2.5 Cell culture

The well-characterized immortalized BCi cell line (Walters et al., 2013) was provided by Drs. Mathew Walters and Ronald Crystal (Weill Cornell Medical College, NY) and cultured as described in Section 2.1.2 and 2.1.3.

African green monkey kidney epithelial cells Vero cells (#CCL-81, ATCC) were cultured at 37°C, 5% CO_2 in Minimum Essential Media (MEM) (Media Preparation Unit, Peter Doherty Institute) supplemented with 5% Fetal Bovine Serum (Sigma), 1X penicillin/streptomycin (Gibco), 1X GlutaMAX (Gibco), and 15 mM HEPES (Gibco). Vero/hSLAM cells (European Collection of Authenticated Cell Cultures [ECACC], #04091501) were grown at 37°C, 5% CO_2 in MEM with 7% FBS (Sigma), 1X penicillin/streptomycin (Gibco), 1X GlutaMAX (Gibco), and 15 mM HEPES (Gibco) and 0.4 mg/ml geneticin (Gibco).

6.2.6 Air-liquid interface

The primary epithelial cells were seeded to generate air-liquid interface culture as described in Section 2.3.1. Briefly, cells used for ALI culture were originally passaged in submerged culture in BEGM prior to medium change to PneumaCult™ Ex Plus medium (STEMCELL Technologies), supplemented with hydrocortisone (STEMCELL Technologies). Upon reaching 80% confluency, the cells were dissociated using an animal component-free cell dissociation kit (STEMCELL Technologies), then seeded on fibrillar collagen (0.03 mg/mL rat tail collagen)-coated 24-well Corning® Transwell® (surface area: 0.33 cm^2) with 0.4 µm pore polyester membrane inserts (Corning). The cells were cultured in PneumaCult™ Ex Plus for 4 days until 100% confluency was reached. Upon confluency, the cells were "air-lifted" by removing the growth medium from the apical surface and replacing the basal medium with PneumaCult™ ALI Medium (STEMCELL Technologies), supplemented with hydrocortisone and heparin (STEMCELL Technologies) according to manufacturer's

instructions. The PneumaCult™ ALI medium was changed every second day and apical surfaces were washed with PBS (no Ca^{+}, Mg^{2+}) every week, from one week after air lifting. One day before viral infection or drug treatment, if not otherwise specified, the hydrocortisone concentration in the medium was reduced to 100nM according to previous protocol (Prodanovic et al., 2017; Xia et al., 2017). Bright-field microscopy detectable cilia beating was captured using Olympus IX53 microscope equipped with QImaging optiMOS high speed camera (100 frames/sec). The cells were fixed in 10% neutral buffered formalin (NBF, Grale Scientific) for 10 min. The membrane was excised from the transwell and cut into 4 pieces (Levardon et al., 2018) for whole-mount staining or embedded in paraffin and sectioned for staining.

6.2.7 Airway organoids

The airway organoid culture was generated in a droplet format as described in Section 2.3.2. Briefly, the elastomeric stencil silicone mask was used to standardize the size and shape of the Matrigel® droplet (**Figure 6.1**). The diameter of the mask can be adjusted to fit different culture plates or bio-printing settings. Briefly, an elastomeric stencil silicone mask was placed in the 48-well plate (diameter: 11 mm). The outer diameter and inner diameter of the silicone mask are 8mm and 5mm. The inner surface bounded by the mask was then coated with 25 µL of 1% BSA for 1h at 37°C. The residue was removed and washed once with PBS. The plate was left to dry and pre-warmed in the incubator. The NHBE cells cultured in BEGM were dissociated as descried above and resuspended in 50% growth factor reduced (GFR) Matrigel® (Corning) at a density of 3,000 cells/well. A 25 µL droplet was added onto the inner surface of the silicone mask. After solidification of the droplet, 250 µL of the airway organoid medium (**Table 2.6**) was added into the plate. The medium was changed every second day. All the organoids were cultured for 3 weeks. The development of airway organoids was recorded using the same microscope, camera and methodology as for ALI. The organoids were fixed in 10% NBF for 30 min as described previously (Broutier et al., 2016; Dekkers et al., 2019). All the tips and tubes in contact with organoids were coated with 1% BSA to minimise cell adherence.

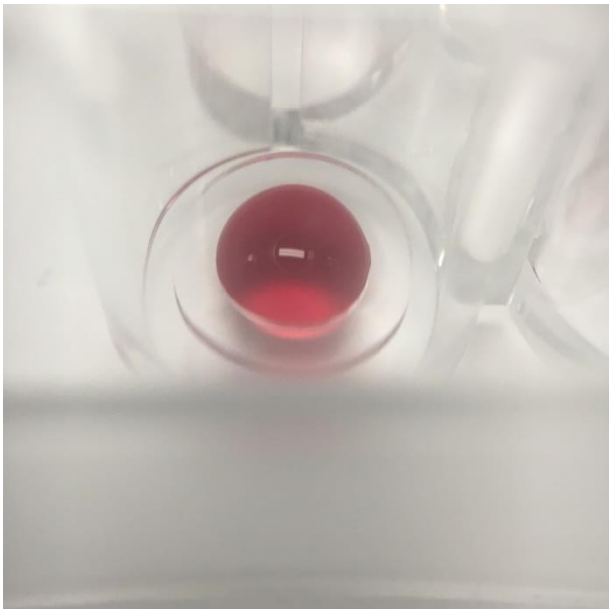

Figure 6.1 Airway organoid culture with silicone mask

6.2.8 Immunofluorescence staining

In general, samples were blocked in 5% goat serum/0.1% Triton X-100 in PBS for 1 h at room temperature. The samples were incubated with primary antibodies (**Table 2.8**) diluted in 1% BSA/0.1% Triton X-100 in PBS overnight at 4°C, followed by incubation of secondary antibodies (**Table 2.8**) for 1 h at room temperature. Nuclei and actin filaments were stained with DAPI (Santa Cruz) and Alexa Fluor® 488 Phalloidin (Cell Signaling). DAKO fluorescent mounting medium (DAKO) was used for mounting. Airway organoids were stained, cleared, and mounted as described previously (Dekkers et al., 2019). Specifically, Poly (2-hydroxyethyl methacrylate) (Poly-HEMA, Sigma) coated plates were used for immunofluorescence staining. For ALI samples, all the staining steps were carried out in Eppendorf tubes. The membrane piece was transferred into the mounting media dropped onto a microscope slide bordered by double-sided sticky tape (Scotch 3M) to avoid disruption of the 3D organoid structure. The confocal images were acquired using a Zeiss LSM880 Airyscan Fast confocal microscope (Biological Optical Microscopy Platform, University of Melbourne) and analysed using Imaris 9.2 and FIJI Image J software.

6.2.9 Immunohistochemistry staining

The airway biopsies used in this study were obtained from subjects recruited from the Melbourne Epidemiological Study of Childhood Asthma (MESCA) cohort. Details are described as in Section 2.4.4. The demographic data are provided in **Table 6.2**.

Paraffin-embedded sections of human airway and ALI derived from NHBE cells were stained with ACE2 or IgG isotype control using three-layer immunoperoxidase protocol, as described in Section 2.4.4.3. ACE2 expression level was determined by a semi-quantitative IHC scoring method.

Table 6.2 Demographic data for subjects from the MESCA cohort from whom biopsies were obtained for ACE staining using Immunohistochemistry

	Non-Asthma	**Mild Asthma [1]**	**Moderate Asthma [1]**	**Severe Asthma [1]**
Subject n (M/F)	12 (7/5)	17 (3/12 [2])	9 (7/2)	9 (2/7)
FEV_1 %pred	114 (98-141)	102 (83-115)	66 (50-73)	64 (56-101)
Atopic (%)	50	94	100	56
Current smokers (%)	0	53	56	50 [3]
β_2-adrenoceptor agonists (%)	0	65	100	N/A
Inhaled steroids (%)	0	41	100	100
Oral steroids (%)	0	88	22	0

Data presented as median (interquartile range) or %. M: male; F: female; FEV_1: forced expiratory volume in one second; %pred: % predicted. [1]: classified using Global Initiative for Asthma guidelines; [2]: 2 unknowns; [3]: 5 unknowns.

6.2.10 SARS-CoV-2 preparation

Briefly, a SARS-CoV-2 isolate (BetaCoV/Australia/VIC01/2020), provided by the Victorian Infectious Diseases Reference Laboratory (VIDRL) was passaged in Vero hSLAM cells and stored at -80°C. Virus stocks were quantified by virus titration as the median tissue culture

infectious dose ($TCID_{50}$) in Vero cells as previously described (Mills et al., 2021). All work with infectious virus was performed inside a biosafety II cabinet, in a biosafety containment level 3 facility, and personnel wore powered air-purifying respirators (3M TR-315A VERSAFLO) or P2 masks.

6.2.11 SARS-CoV-2 infection

Primary normal human bronchial epithelial cell (NHBE)-ALI and BCi-ALI cultures were inoculated at a multiplicity of infection (MOI) of 0.1 and 1 (10^4 and 10^5 $TCID_{50}$) of SARS-CoV-2 via the apical surface for 1 hour at 37°C at University of Melbourne. The inoculum was removed, and the apical surface washed twice with PBS (second wash is the D0 sample). Up to day six, daily apical samples were obtained by PBS washing for 30 minutes at 37°C and stored at -80°C. Infectious virus titre was quantified as $TCID_{50}$/ml as previously described (Mills et al., 2021). For immunofluorescence analysis, cells were fixed using 10% formalin. NHBE ALI cultures inoculated with SARS-CoV-2 at a MOI of 0.05 for 1 h at 37°C at Australian Centre for Disease Preparedness (Marsh et al., 2021). The inoculum was removed, and the apical surface washed with PBS. Cells were cultured at 37°C for 48 h. Cells were lysed for RT-qPCR analysis. Basolateral supernatants were collected and gamma-irradiated before cytokine analyses. All work with infectious virus was performed in a biosafety containment level 4 facility.

6.2.12 Rhinovirus infection and Poly I:C treatment

Human rhinovirus (RV), RV16 strain (ATCC VR-283) was prepared as previously described (Xia et al., 2017). NHBE ALI cultures was inoculated with rhinovirus at a MOI of 1 for 1 h at 37°C. The inoculum was removed, and the apical surface washed with PBS. Cells were cultured at 37°C for 48 h. NHBE ALI cultures treated with 10 µg/mL Polyinosinic:polycytidylic acid (Poly I:C) were cultured at 37°C for 24 h. Basolateral supernatants were collected for cytokine/chemokine analysis.

6.2.13 Isolation of total RNA and RT-qPCR

Total mRNA extraction and RT-qPCR were carried out as described in Section 2.4.1. Briefly, total RNA from SARS-CoV-2 infected cells was extracted using MagMAX™-96 Total RNA Isolation Kit (Invitrogen) or TRIzol (Invitrogen). Total RNA from all the other experiments was extracted using illustra RNAspin Mini RNA Isolation Kit (GE Healthcare). RNA extracts were reverse transcribed using a High Capacity RNA-to-cDNA Kit (Applied Biosystem). Real-time PCR was performed on QuantStudio 6 Flex Real-Time PCR System using iTaq™ Universal SYBR® Green Supermix (Bio-Rad). 18S ribosomal RNA was used as reference. Primer sequences documented in **Table 2.7**.

6.2.14 Quantification of cytokine levels in supernatant

Supernatants were collected for measurement of IL-6, IL-8, GM-CSF by ELISA, as described in Section 2.4.2.1. High throughput cytokine/chemokine measurement was done by using Bio-Plex Pro™ Human Cytokine Grp I Panel 27-Plex, as described in Section 2.4.2.

6.2.15 Statistical analysis

All data were statistically analysed by GraphPad Prism 7.0 (GraphPad, San Diego, CA, USA) and presented as the mean ± standard error of mean (SEM) for n individual experiments in cell lines, n individual donors of primary epithelial cell culture. For one independent variable, one-way analysis of variance (ANOVA) with the Dunnett's *post-hoc* test or unpaired *t* test were used. Two-way ANOVA with Bonferroni post-hoc tests were used for two independent variables. $P<0.05$ was considered to be statistically significant.

6.3 Results

6.3.1 Air-liquid interface culture and bronchial organoid culture can recapitulate in vivo bronchial epithelial structures

In cells derived from bronchial brushing and subsequently fixed prior to any *ex vivo* culture, the ciliated cells, goblet cells, club cells, and basal cells were stained by the respective cell type specific markers: acetylated tubulin, MUC5AC, CC10, p63, and KRT5 (**Figure 6.2**). Following isolation, the native epithelial cells were cultured in tissue culture flask to generate submerged primary epithelial cell culture. Increased basal cell marker gene expression and decreased ciliated and secretory cell marker gene expression is consistent with the inability of the ciliated and secretory cells to propagate in conventional two-dimensional culture (**Figure 6.3**). To assess the possibility of maintaining ciliated and secretory cells, native bronchial epithelial cells were seeded into 24-well plate. After 72 h, the cilia beating was captured by microscopy (**Video S5**). Additionally, the native human bronchial epithelial cells were embedded in Matrigel®. From the second day of Matrigel® culture, the cell clusters started to generate spheroid-like structures. The cilia kept beating for 14 days (**Video S6**) and maintained their outward orientation in the spheroid. However, there was no enlargement of the spheroids during this period, consistent with a lack of cell proliferation under these conditions.

We used normal human bronchial epithelial cells (NHBE) or immortalized human airway basal epithelial cell line BCi (Walters et al., 2013) to generate ALI cultures. Each cell preparation differentiated into ciliated and secretory cells under ALI culture conditions (**Figure 6.4A, B**), consistent with previous observations (Keenan et al., 2014; Prodanovic et al., 2017; Xia et al., 2017).

Advanced DMEM/F12 supplemented with FGF7, FGF10, R-Spondin 1, Noggin, A83-01, Y-27632, and SB202190 supported the differentiation of NHBE, but not BCi cells. The size of the organoids not only varied within each culture, but also varied between cultures derived from different donors (**Figure 6.5**). Moreover, a lumen structure was not consistently obtained. Beating cilia were identified after two weeks of culture. Notably, the cilia were oriented toward both the outer surface of the organoid and inside of the lumen (**Video S1, S7**). This phenomenon was observed across four different NHBE cultures, with most of the cilia facing outwards. The immunofluorescence staining clearly showed that the mucin was also secreted to both the outside and inside of the organoid (**Figure 6.4C**). These “bipolar”

organoid structures have rarely been reported (Zhou et al., 2018), whereas "unipolar" organoid structures are commonly reported (Danahay et al., 2015; Sachs et al., 2019).

Although the primary human epithelial cells can differentiate under both ALI and organoid culture conditions, the proportion of ciliated and secretory cells differed. The expression of genetic markers of ciliated cells was higher in ALI whereas secretory cell marker expression was higher in organoids (**Figure 6.6**). The IF staining of ALI showed that the majority of cells are ciliated (**Figure 6.7**), whereas fewer than 10% of epithelial cells in the organoids were ciliated.

The transwell membrane creates a stiff microenvironment for ALI culture which is partially shielded by the layer of collagen hydrogel coated on the polystyrene base, whereas organoids develop in soft Matrigel®. F-actin was evident as abundant filaments throughout cells at bottom layer in ALI culture; more limited amounts of F-actin appeared to be restricted to the cell membrane in organoids (**Figure 6.8**). Mechanical influences on organotypic culture differentiation require further investigations.

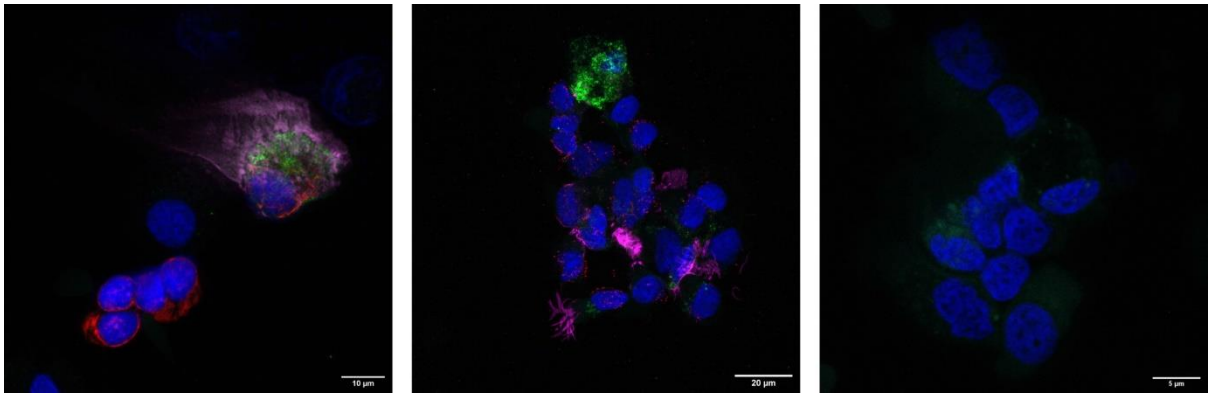

Figure 6.2 Detection of differentiated cells in native human bronchial brushing epithelial cells

Immunofluorescence staining for ciliated cells (acetylated tubulin, magenta), club cells (CC10, green), basal cells (p63 and KRT5, red), and nucleus (DAPI, blue).

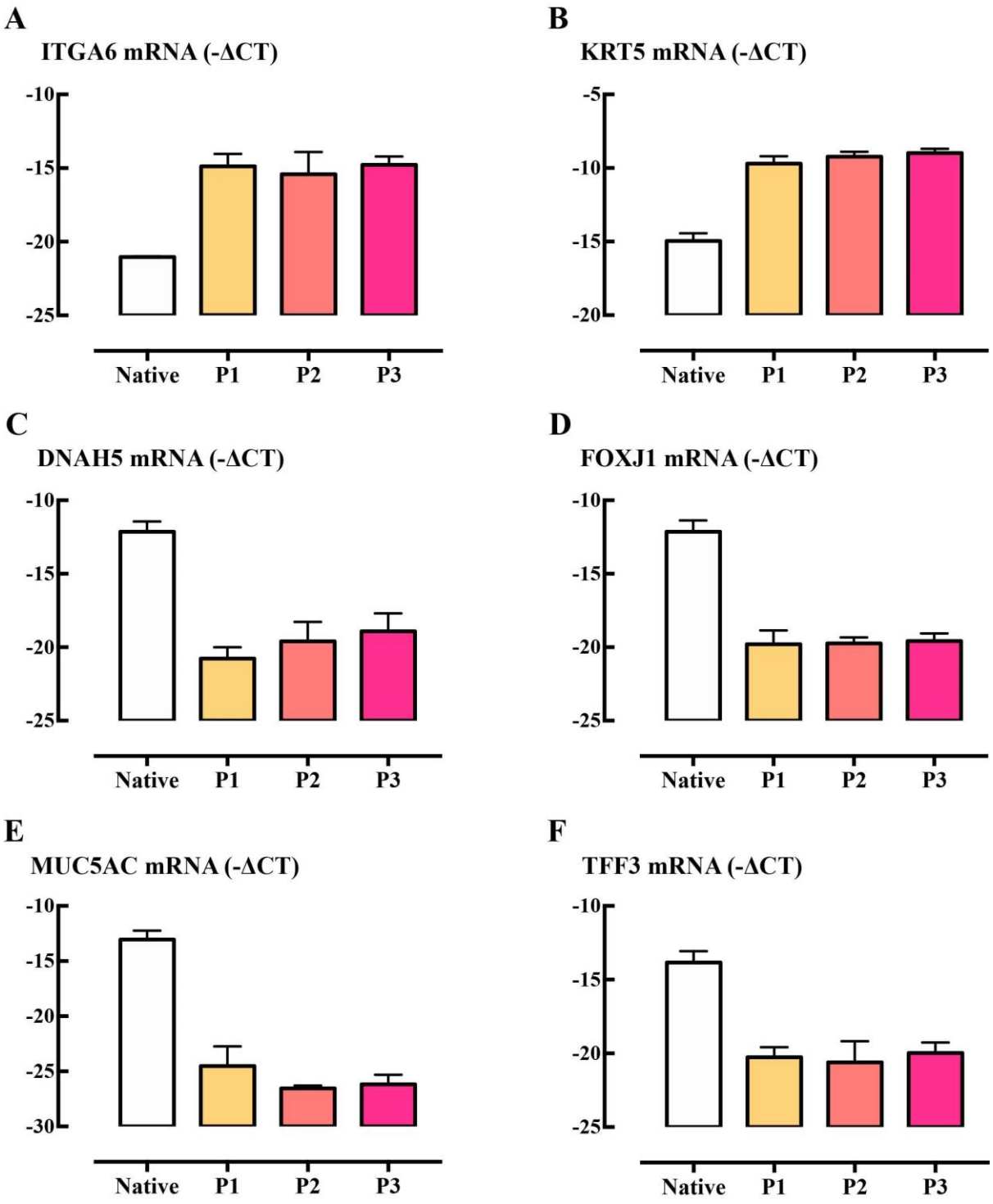

Figure 6.3 The gene expression in native human primary bronchial epithelial brushing cells

HBEB cells were collected from native samples, three passages from submerged culture. Total RNA was extracted and gene expression of basal cell marker ITGA6 (A) and KRT5 (B), ciliated cell marker DNAH5 (C) and FOXJ1 (D), secretory cell marker MUC5AC (E) and TFF3 (F) were measured by RT-qPCR. Gene expression is expressed as -ΔCT (Log2). Data are presented as mean and SEM for n=3 independent cultures analysed without culture (native) or at stated passage numbers (P1-3).

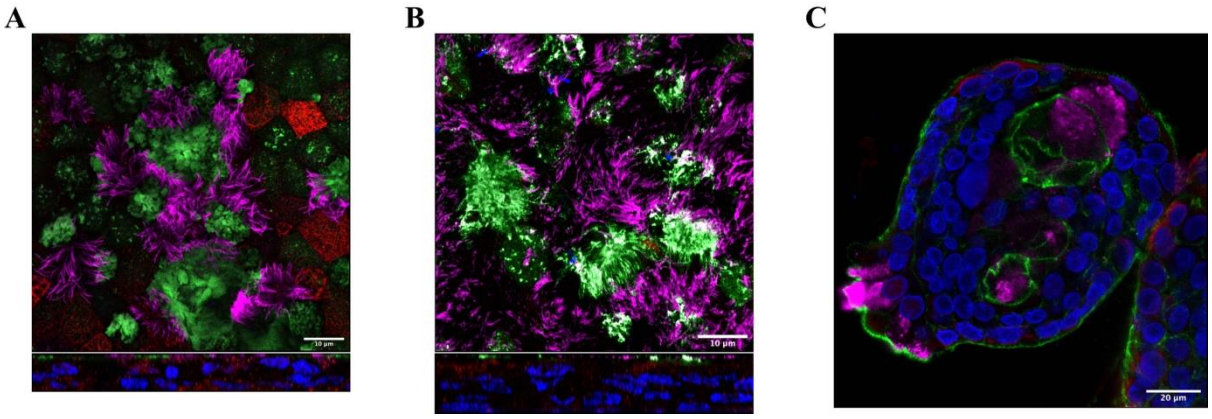

Figure 6.4 Characterization of air-liquid interface culture and airway organoids

NHBE cells were differentiated in airway organoid culture and air-liquid interface culture. BCi cells were differentiated in ALI culture. Immunofluorescence staining of acetylated tubulin (magenta), CC10 (green), KRT5 (red), and nucleus (blue) in BCi (A) and NHBE (B) cell derived ALI. Immunofluorescence staining of MUC5AC (magenta), F-actin (green), KRT5 (red), and nucleus (blue) in NHBE cell derived bronchial organoid (C).

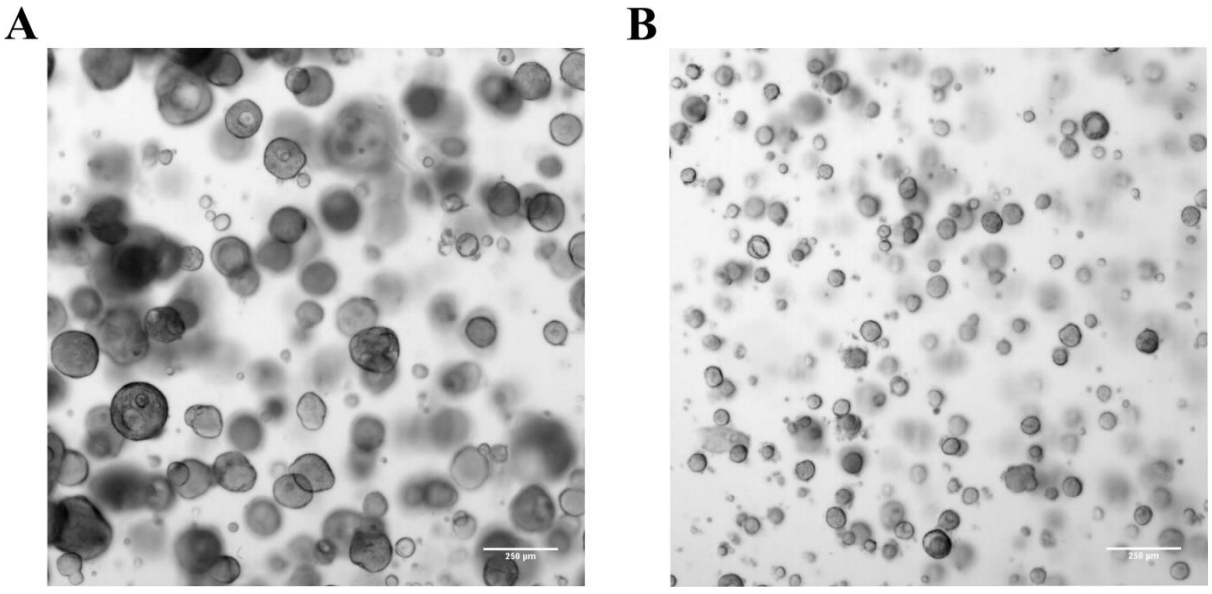

Figure 6.5 Airway organoids generated from NHBE cells

NHBE cells were seeded to generate airway organoids using Airway Organoid medium. Representative brightfield images (4x objective) of two independent NHBE cell cultures (A, B) derived airway organoids were taken at Day 21.

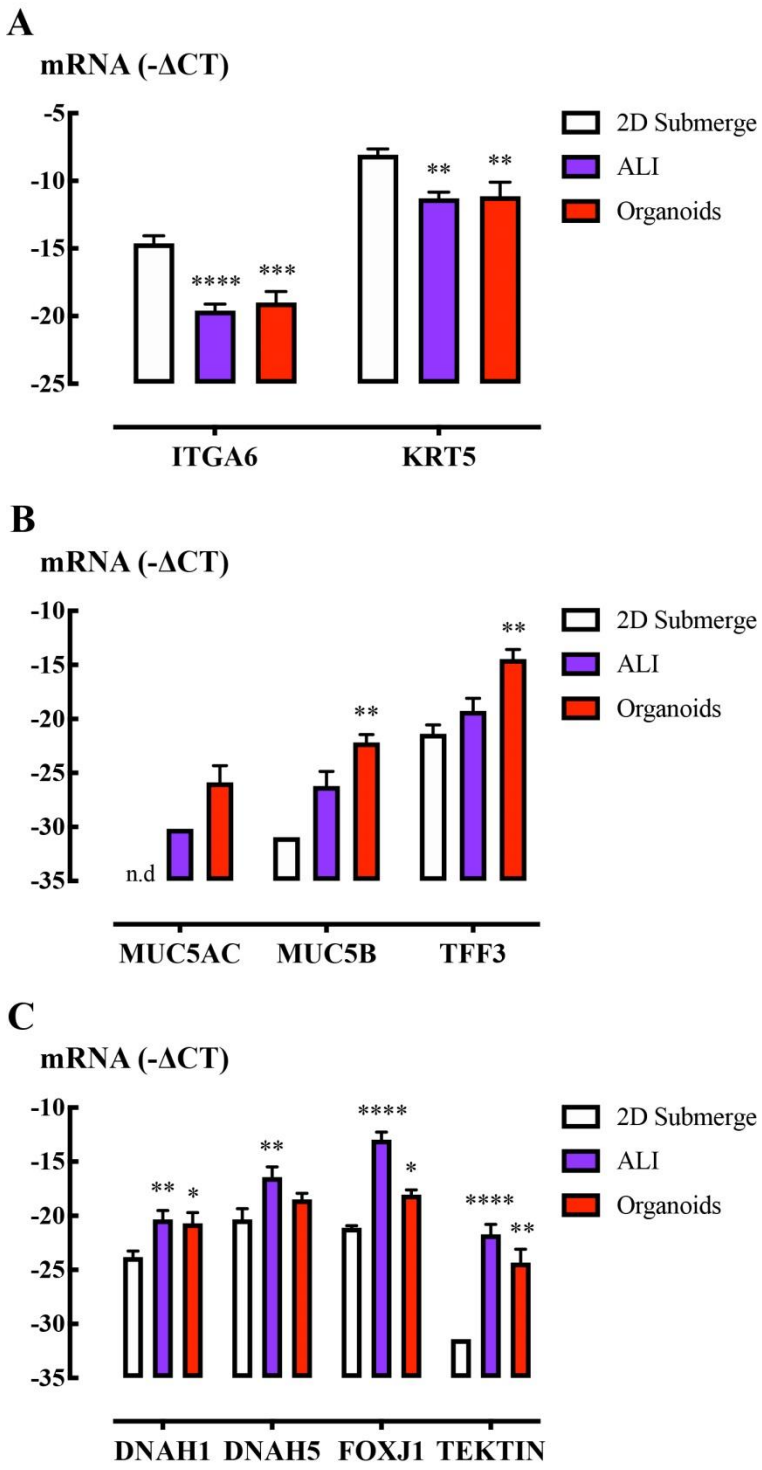

Figure 6.6 The gene expression in airway organoids and ALI generated from NHBE cells

NHBE cells were differentiated in airway organoid culture and air-liquid interface culture. Total RNA was extracted and gene expression of basal cell markers (A), secretory cell markers (B), and ciliated cell markers (C) were measured by RT-qPCR. Gene expression is expressed as -ΔCT (Log2). Data are presented as mean and SEM for n=4 independent experiments from 2D submerged NHBE cells and airway organoid cultures, n=5 ALI culture. Two-way ANOVA was performed to compare the gene expression in ALI and organoid culture to 2D submerge, *: P<0.05, **: P<0.01, ***: P<0.001, ****: P<0.0001.

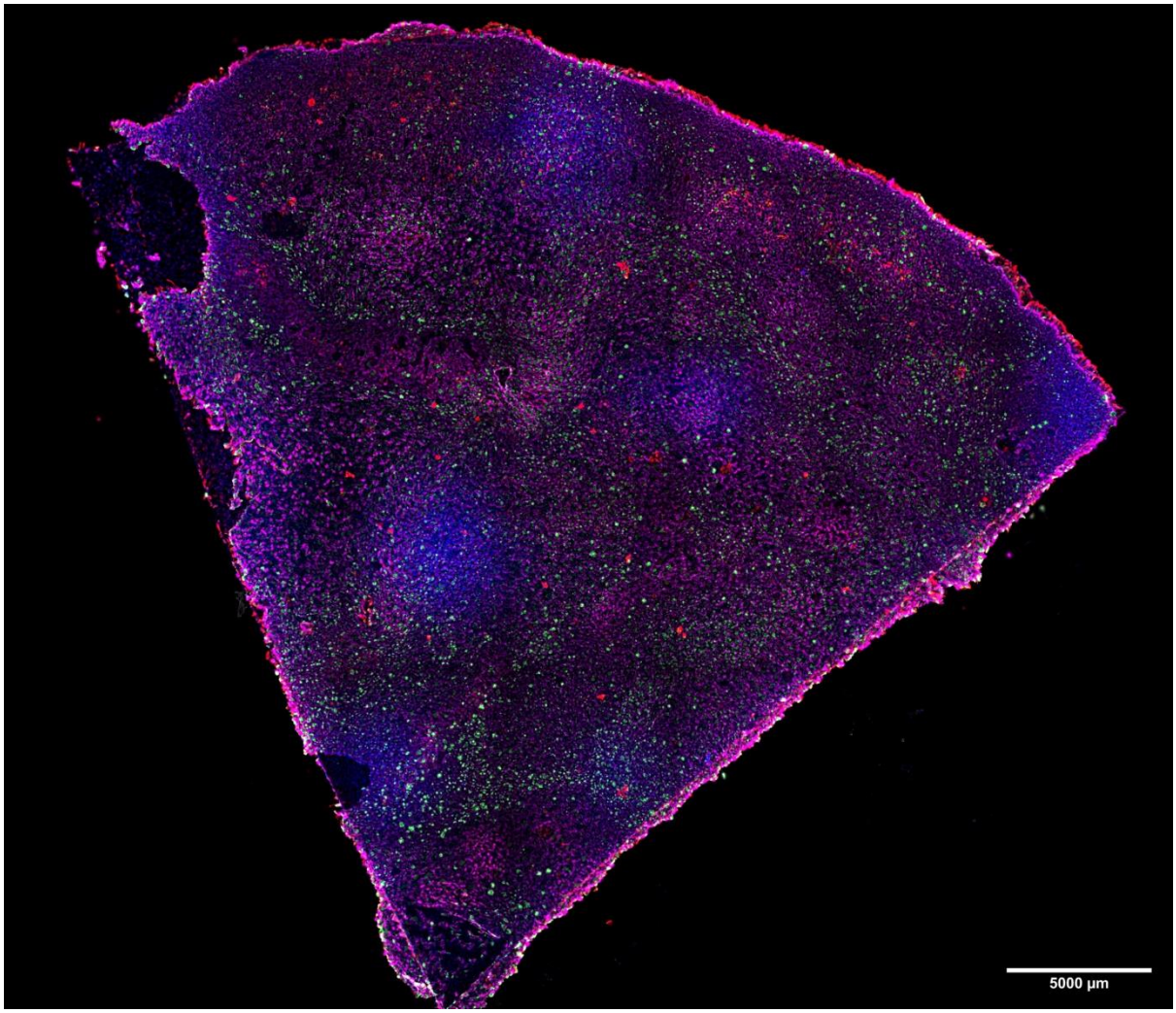

Figure 6.7 Whole mount staining of NHBE cell derived ALI

Immunofluorescence staining of acetylated tubulin (magenta), CC10 (green), KRT5 (red), and nucleus (blue) in NHBE cell derived ALI. Confocal fluorescence images were acquired using Leica Confocal microscope with THUNDER Analysis (Leica).

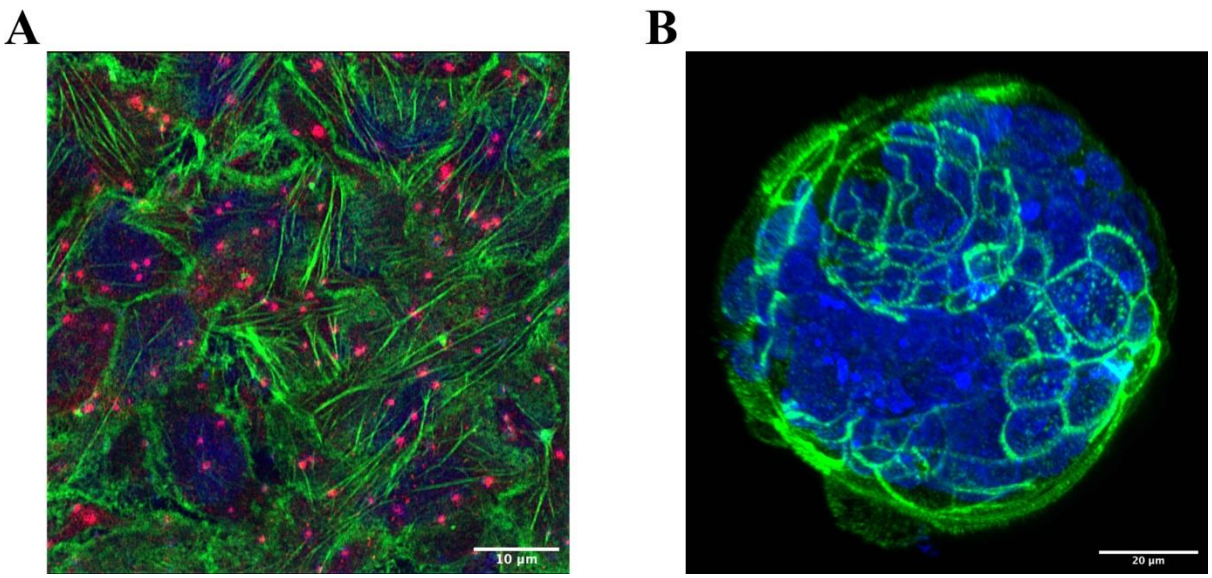

Figure 6.8 F-actin distribution in ALI and airway organoids

Immunofluorescence staining of F-actin (green), KRT5 (red), and nucleus (blue) in NHBE cell derived ALI (left) and organoid (right) cultures.

6.3.2 ACE2 and TMPRSS2 are restored by air-liquid interface culture and bronchial organoids culture

To evaluate the utility of airway epithelial *in vitro* models in viral infection studies, the expression of toll-like receptor (TLR) genes was assessed in comparison to levels expressed in native human epithelial cells. The TLRs were divided into four groups based on the expression pattern among native epithelial cells, submerged NHBE cells, submerged BEAS-2B cells, ALI, and organoids. TLR3 was similarly expressed in each of the five models (**Figure 6.9A**). In BEAS-2B cells, ALI, and organoids but not in NHBE cells, TLR4 and TLR6 expression levels were similar to those measured in native cells. The expression of TLR1, TLR2, TLR5, and TLR7 in ALI and organoids were lower than those in native cells, but higher than in submerged epithelial cells (**Figure 6.9B**). TLR8 and TLR9 were 8-fold more highly expressed in organoids compared to ALI (**Figure 6.9C**). TLR10 was expressed to similar levels in BEAS-2B, NHBE, and ALI, but was almost undetectable in organoids (**Figure 6.9D**). In general, the aberrant TLR expression in submerged cells was restored to near native cell expression levels by culture in ALI and organoid formats.

To further differentiate the utility of these models in studying SARS-CoV-2 infection, SARS-CoV-2 receptor ACE2 and priming protein transmembrane serine protease 2 (TMPRSS2) gene expression levels were evaluated. ACE2 and TMPRSS2 genes were expressed to similar levels in native epithelial cells derived from adult and infant donors (**Figure 6.10A; Figure 6.11A**). There was also no obvious difference between non-CF and CF infants, albeit the study was not statistically powered for this question. ACE2 and TMPRSS2 gene expression levels markedly declined upon subjecting primary cells to submerged cell culture conditions (**Figure 6.10B; Figure 6.11B**). BEAS-2B and A549 cells expressed significantly lower levels of ACE2 and TMPRSS2 than native cells (**Figure 6.10C; Figure 6.11C**). BCi and NHBE cultured at ALI showed restoration of ACE2 and TMPRSS2 expression levels compared to submerged culture, albeit the levels remained somewhat lower than those in native cells (**Figure 6.10D; Figure 6.11D**). As the BCi cells did not form differentiated organoids, only ALI from BCi cells were evaluated in this study. Organoids cultured from NHBE cells also showed a restoration of the ACE2 and TMPRSS2 to near-native expression levels. The primary epithelial cell cultures derived from COPD and asthma patients were differentiated under ALI; ACE2 and TMPRSS2 gene expression in these cultures did not appear to be different in this limited set of samples from COPD and asthma donors, but the study was not powered to address this question (**Figure 6.10E; Figure 6.11E**).

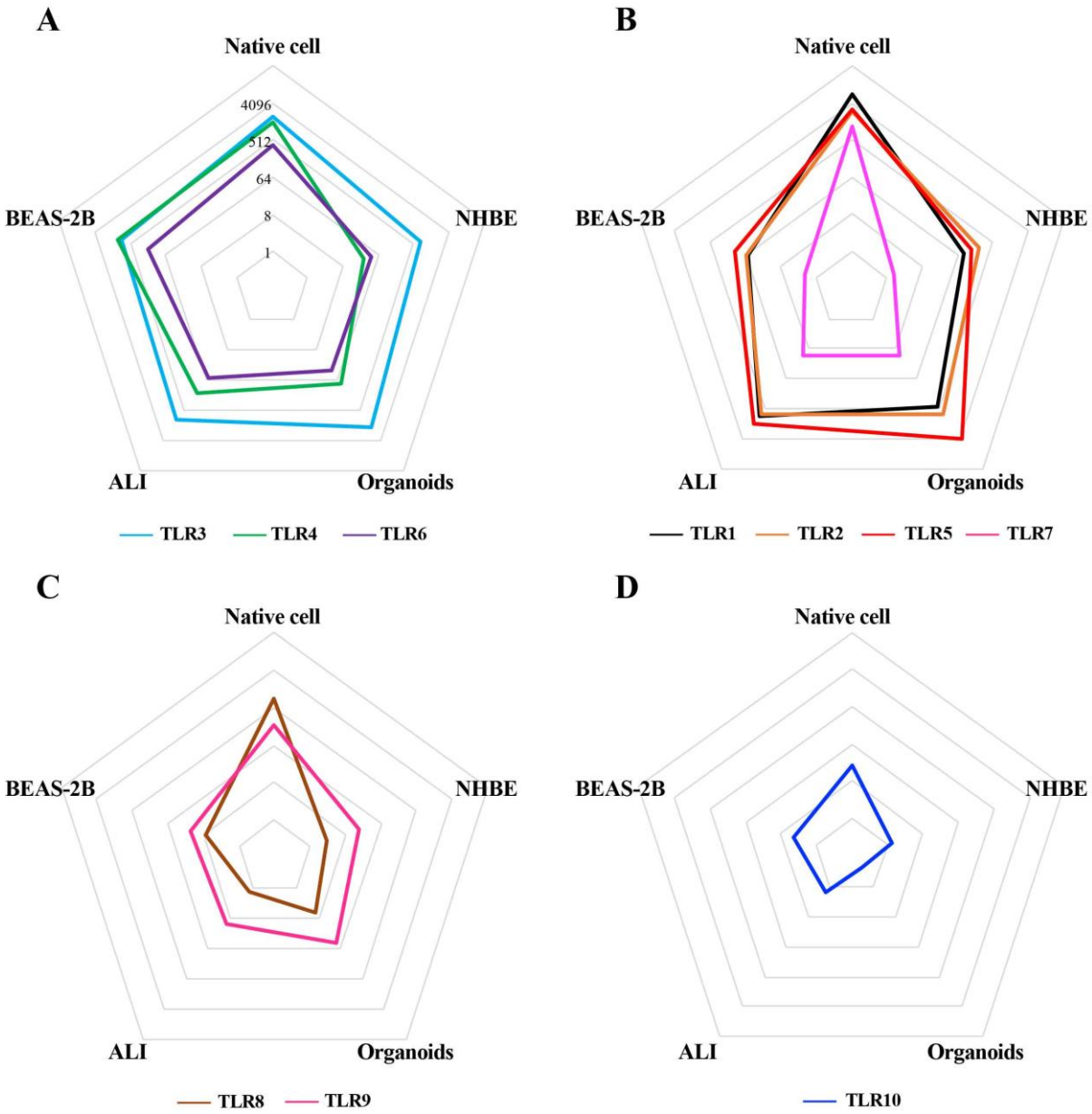

Figure 6.9 The gene expression of TLRs in airway epithelial cells

Total RNA was extracted and gene expression of TLR 1-10 were measured by RT-qPCR. Gene expression is expressed as -ΔCT (Log2). Interval equals to 8-fold difference. Data are presented as mean and SEM n=4 for native HBEC, n=5 for BEAS-2B, n=5 for A549, n=4 for NHBE, n=5 for NHBE-ALI, n=4 for NHBE-organoids.

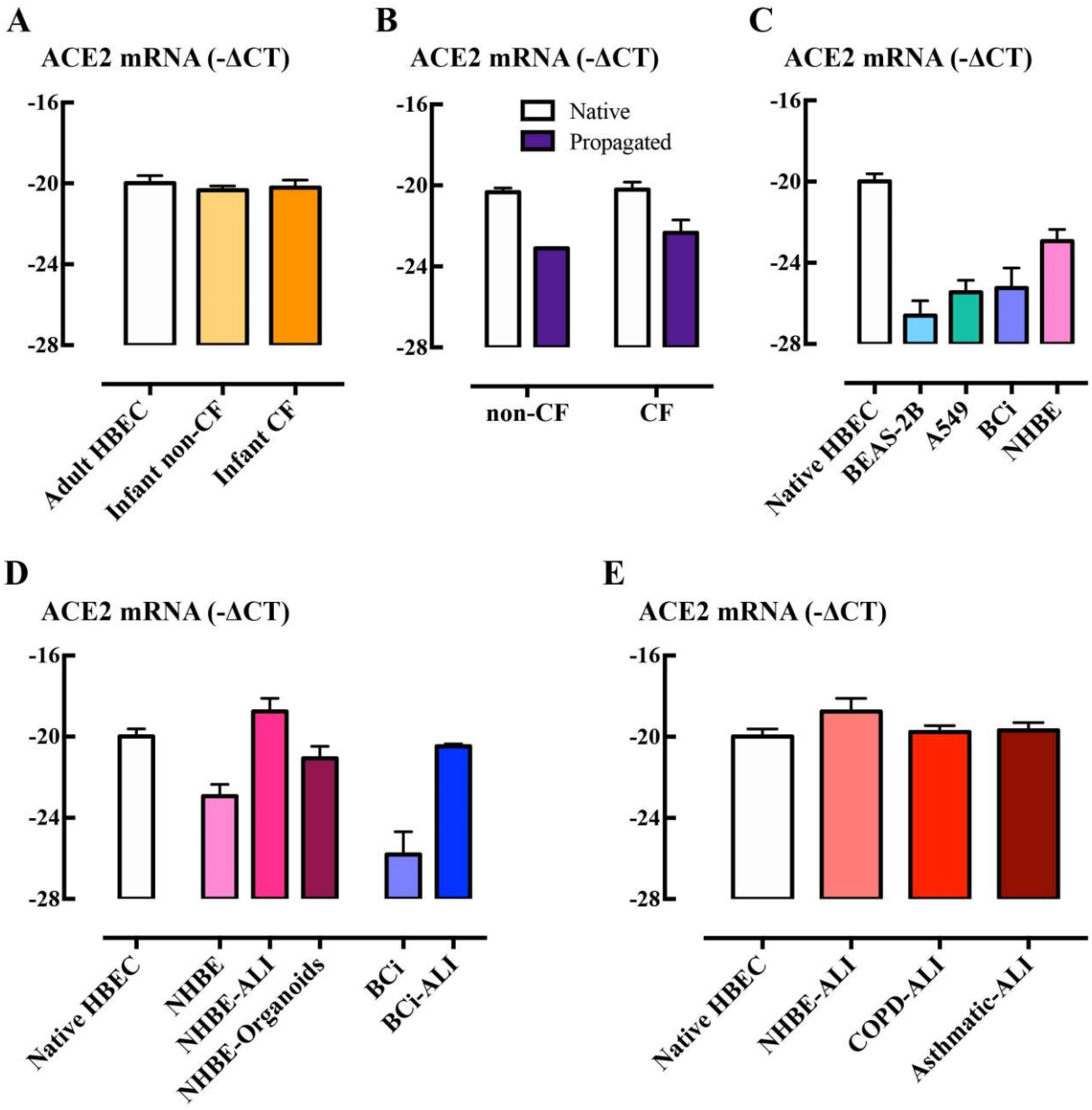

Figure 6.10 The gene expression of ACE2 in airway epithelial cells

Total RNA was extracted and gene expression of ACE2 were measured by RT-qPCR. Gene expression is expressed as -ΔCT (Log2). Data are presented as mean and SEM n=4 for native adult HBEC, n=4 for native infant non-CF, n=8 for native infant CF, n=1 propagated infant non-CF, n=3 for propagated infant CF, n=5 for BEAS-2B, n=5 for A549, n=5 for BCi, n=4 for NHBE, n=5 for NHBE-ALI, n=4 for NHBE-organoids, n=3 for BCi-ALI, n=3 for COPD-ALI, n=4 for asthmatic-ALI.

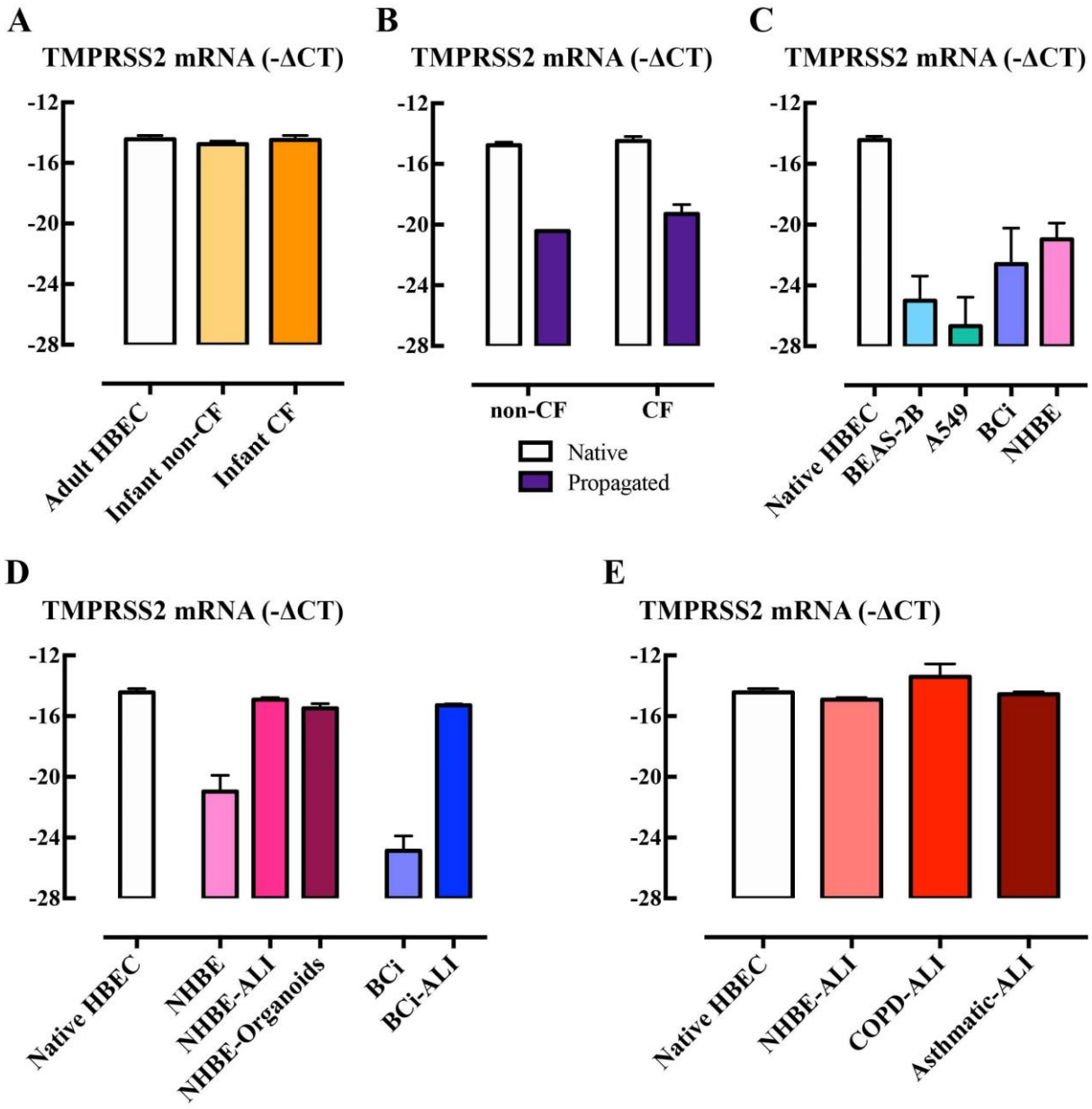

Figure 6.11 The gene expression of TMPRSS2 in airway epithelial cells

Total RNA was extracted and gene expression of TMPRSS2 were measured by RT-qPCR. Gene expression is expressed as -ΔCT (Log2). Data are presented as mean and SEM n=4 for native adult HBEC, n=4 for native infant non-CF, n=8 for native infant CF, n=1 propagated infant non-CF, n=3 for propagated infant CF, n=5 for BEAS-2B, n=5 for A549, n=5 for BCi, n=4 for NHBE, n=5 for NHBE-ALI, n=4 for NHBE-organoids, n=3 for BCi-ALI, n=3 for COPD-ALI, n=4 for asthmatic-ALI.

6.3.3 ACE2 is highly expressed in ciliated and basal epithelial cells

ACE2 protein expression levels were measured immunohistochemically in biopsies from non-asthmatic subjects, patients with mild, moderate, and severe (steroid-resistant) asthma (**Figure 6.12**). Mild asthma subjects showed slightly lower levels of ACE2 compared to non-asthma control subjects (**Figure 6.13**). The ACE2 expression appeared to be uninfluenced by sex or atopic status, nor usage of inhaled corticosteroids (ICS) or long acting β_2-agonist (LABA) (data not shown), whereas smokers showed reduced ACE2 expression compared to non-smokers. Interestingly, in BCi cell derived ALI cultures, ACE2 gene expression was not altered by budesonide (ICS), alone or in combination with formoterol (LABA), and dexamethasone (**Figure 6.14A**). However, pilot data showed that Dexamethasone tended to increase ACE2 gene expression when hydrocortisone concentration in the medium was reduced from 1 to 0 µM (**Figure 6.14B**), suggesting that the medium composition has a potentially confounding effect when considering effects of synthetic ICS, as we have observed previously (Prodanovic et al., 2017).

Goblet cell and submucosal gland enlargement are the typical structural changes in COPD airway remodelling (Bergeron et al., 2009; Wadsworth et al., 2012). The reduced ACE2 in smokers may be explained by changes in cellularity as ACE2 expression in the airway epithelium proved to be cell type dependent in ALI and organoid cultures (see below). The paraffin blocks of biopsies were cut into 2 µm sections. Sequential 2 µm sections were stained with cell markers: acetylated tubulin for ciliated cells, CC10 for club cells, MUC5AC for goblet cells, and KRT5 for basal cells. High magnification images (63x objective) were taken from the same area to target the similar/overlapping cells. The 2 µm biopsy sections from both non-smoking non-asthma subject (**Figure 6.15A**) and smoking mild-asthma subject (**Figure 6.15B**) showed that ACE2 was present in cells expressing ciliated and basal cell markers. Regions of goblet cell hyperplasia in smoking mild asthma were devoid of ACE2 expression, potentially explaining the lower level of receptor expression in this group.

In ALI sections, ACE2 was readily identified but was differentially distributed within the cell populations present (**Figure 6.16**). Whole mount staining images suggested that ACE2 is expressed in both NHBE cell derived ALI (**Figure 6.17A**) and BCi cell derived ALI (**Figure 6.17B**). ACE2 immunoreactivity was attenuated at the cell membrane. ACE2 was also expressed at cell membrane in both inside-out (**Figure 6.18A**) and inside-in organoids (**Figure 6.18B**). In 2 µm ALI sections, ACE2 was expressed in basal cells and ciliated cells, with especially high expression in the cilia (**Figure 6.19**) but appeared to be undetectable in

secretory club and goblet cells. In airway organoids, ACE2 was localised in cells with cilia, but not in secretory cells expressing CC10 (**Video S8**). Thus, ACE2 distribution observed in airway biopsies was recapitulated in the ALI and airway organoids.

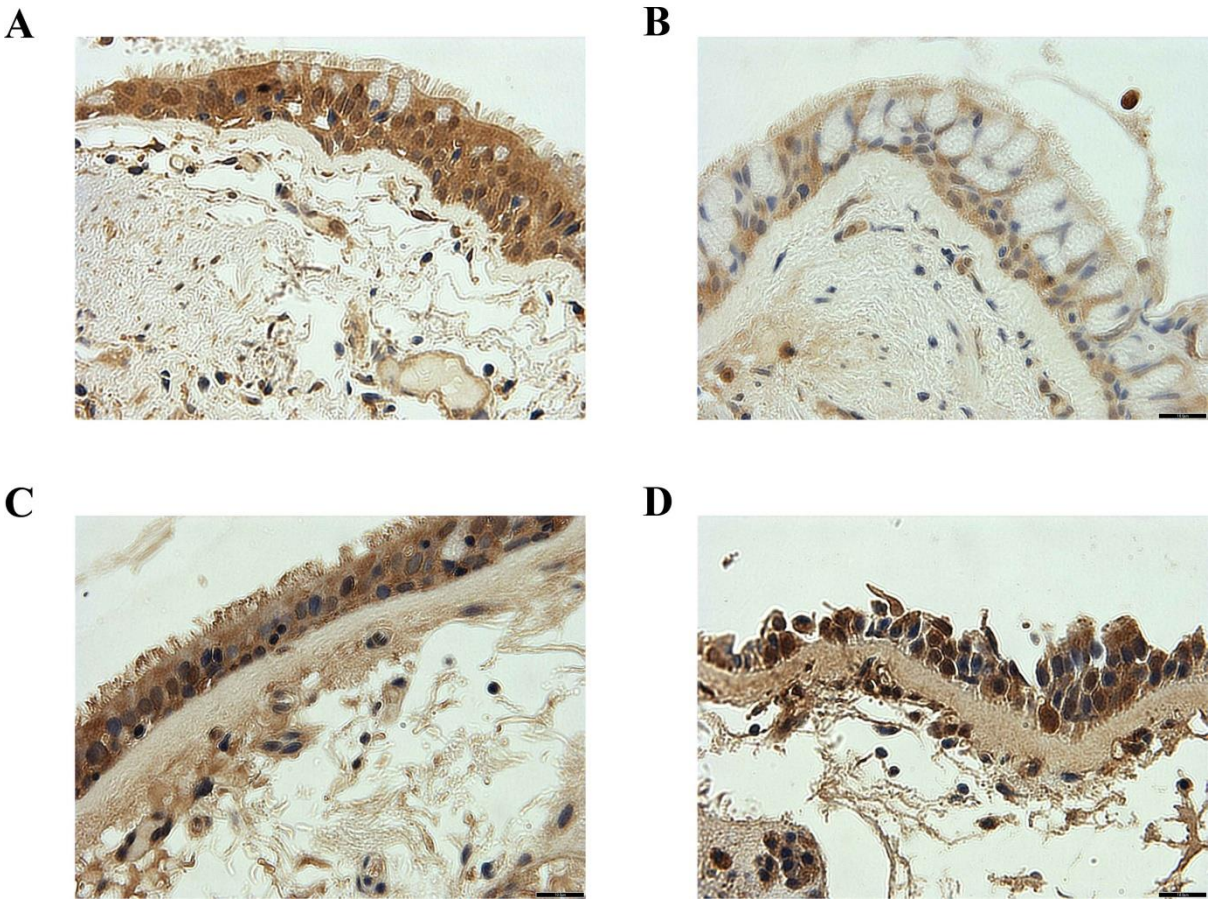

Figure 6.12 The expression of ACE2 in the large airway biopsies from the Melbourne Epidemiological Study of Childhood Asthma study

Paraffin-embedded sections of human airways from non-asthmatic control (A), mild asthma (B), moderate asthma (C), and steroid resistant asthma (D) patients were stained using three-layer immunoperoxidase method. The expression of ACE2 was detected with specific ACE2 antibody. Representative images were taken using Olympus IX51 with 60x objective. Scale bar = 18 µm.

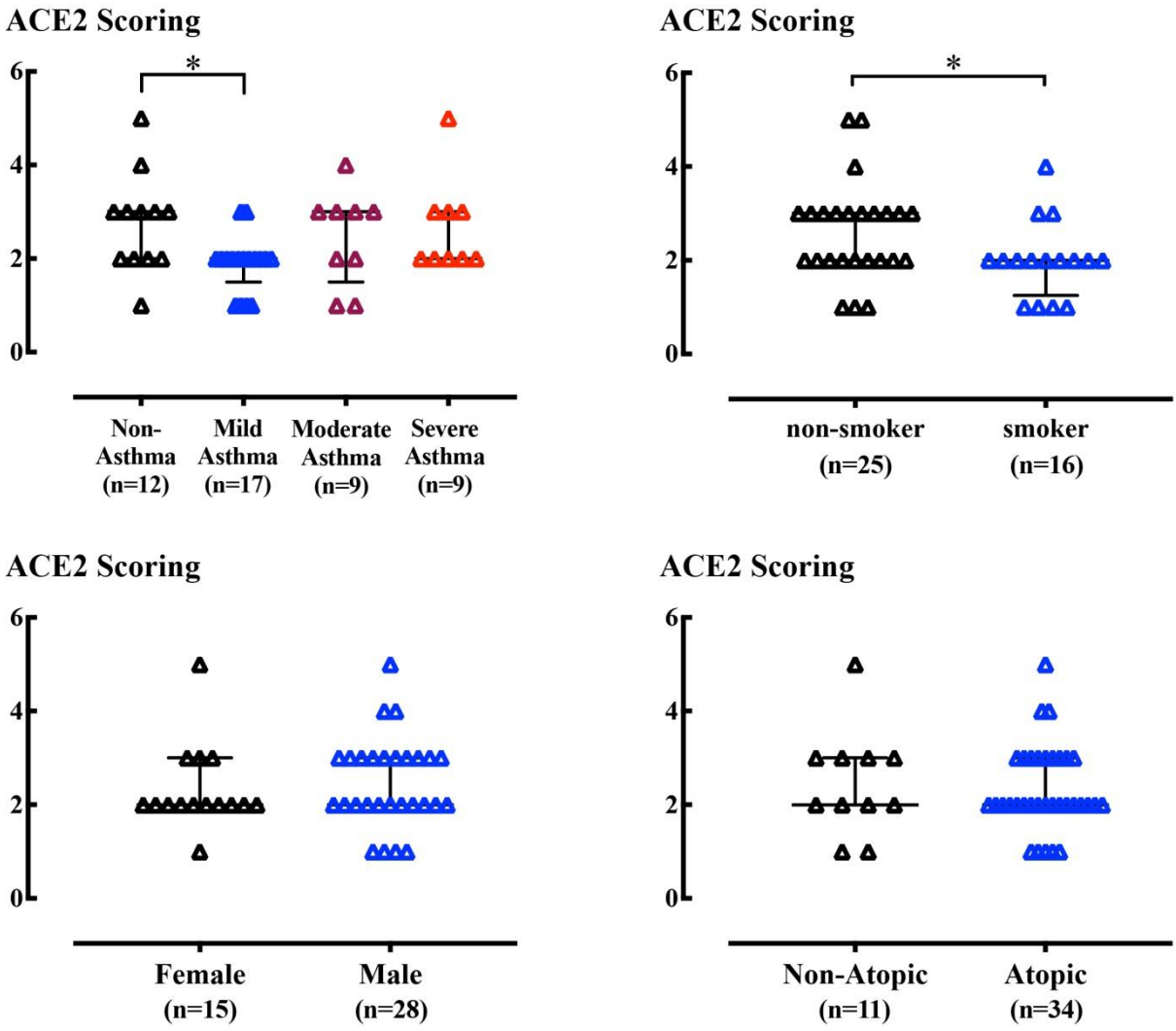

Figure 6.13 Detection of ACE2 expression in the epithelial cells of the large airways from the Melbourne Epidemiological Study of Childhood Asthma study

(A) Comparison of the ACE2 expression in the non-asthmatic control, mild, moderate, and severe asthmatic patients using semi-quantitative IHC scoring method, in which the negative controls were scored with 0, and the positive controls with 5. Data are presented as median with interquartile range. Non-parametric Kruskal-Wallis test was used for analysis. Comparison of the ACE2 expression in the epithelial cells between smoking status (B), sex (C), and atopic status (D) using semi-quantitative IHC scoring method. Data are presented as median with interquartile range. Non-parametric Mann-Whitney test was used for analysis. *: $P<0.05$.

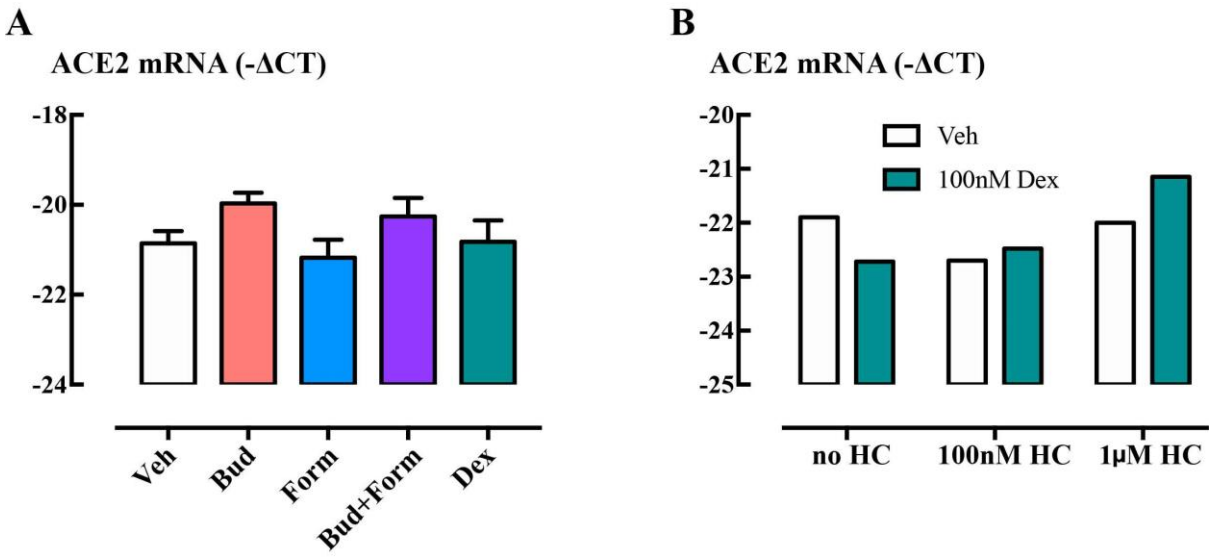

Figure 6.14 The influence of ICS, LABA, and hydrocortisone on ACE2 gene expression in ALI culture

(A) BCi-ALI culture medium was changed to medium containing 100nM hydrocortisone 24h prior treatment of Budesonide (Bud) and/or formoterol (Form) and Dexamethasone (Dex). Gene expression of ACE2 is expressed as -ΔCT (Log2) for n=3. (B) BCi-ALI culture medium was changed to medium containing 0, 100 nM, and 1 μM hydrocortisone 24 h prior Dexamethasone treatment. Gene expression of ACE2 is expressed as -ΔCT (Log2). Data are presented as mean and SEM.

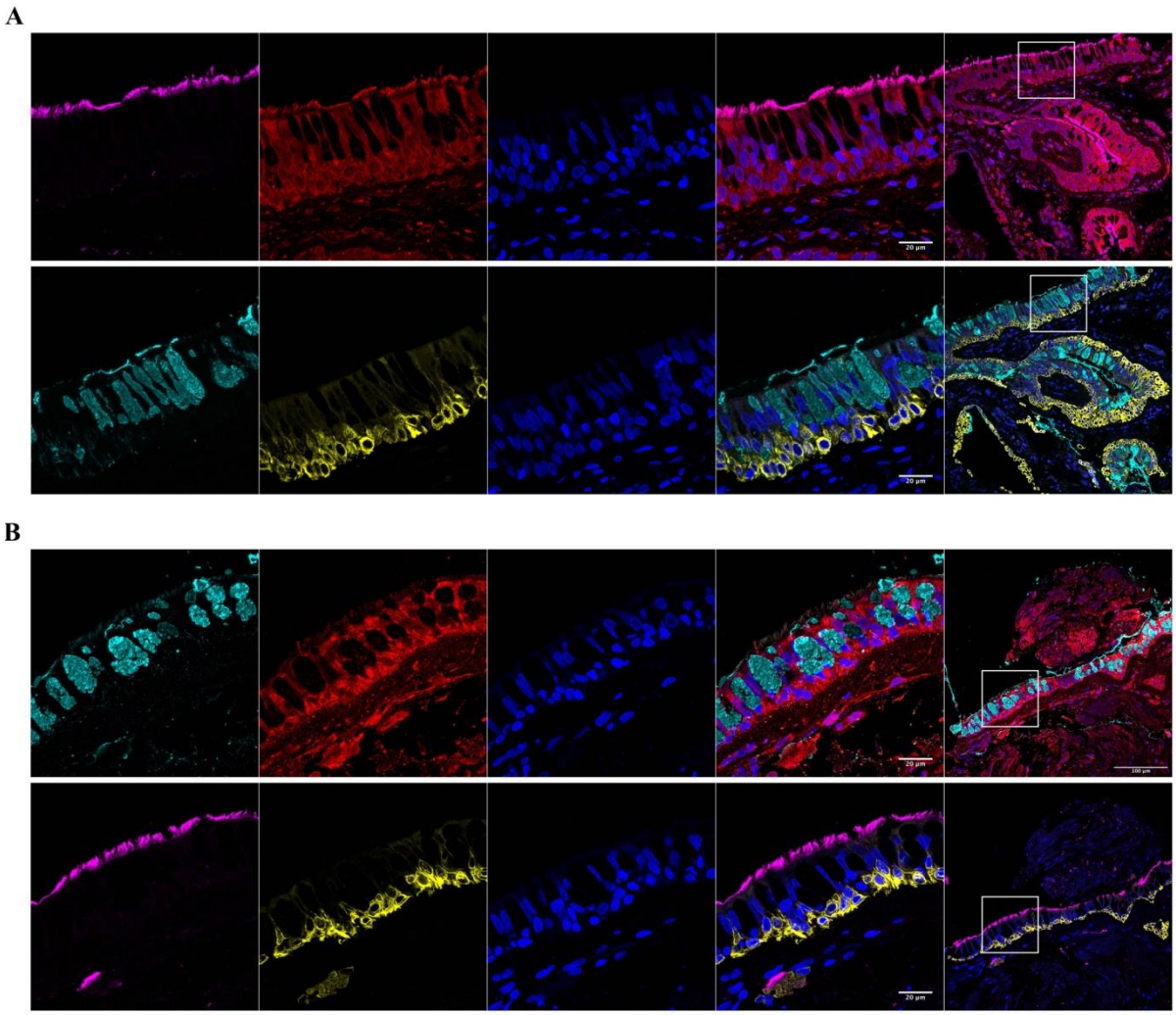

Figure 6.15 ACE2 localization in 2 µm human airway biopsy sections

Immunofluorescence staining of acetylated tubulin (magenta), CC10 (green), MUC5AC (cyan), KRT5 (yellow), ACE2 (red), and nucleus (blue) in 2 µm NHBE cell derived non-smoking, non-asthma subject (A) and smoking, mild-asthma subject (B) paraffin sections. The left panel images were obtained using 63x objective and were taken from the highlighted area in the corresponding right-hand side panel (20x objective).

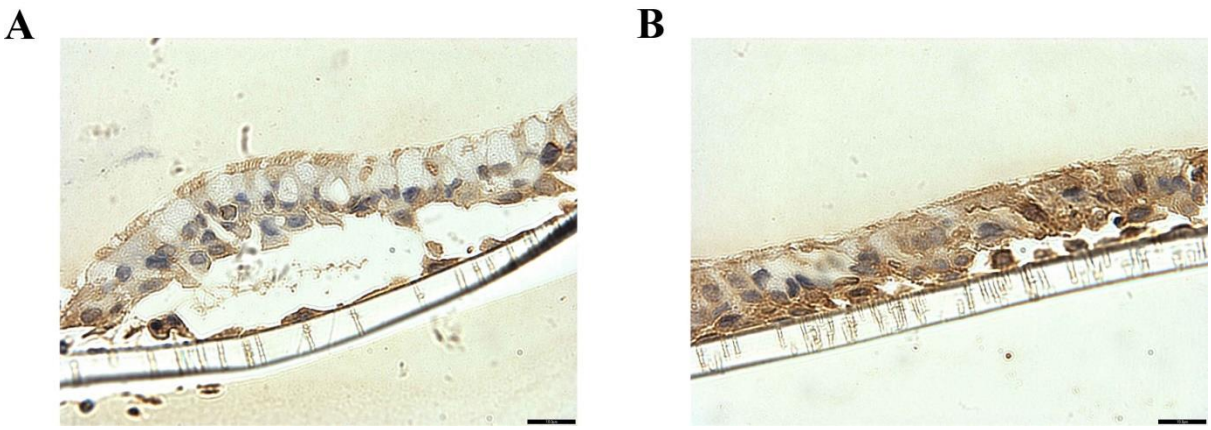

Figure 6.16 The expression of ACE2 in the air-liquid interface culture

ACE2 immunoreactivity in NHBE cells derived ALI cultures. Images from same section. Scale bar = 180 µm.

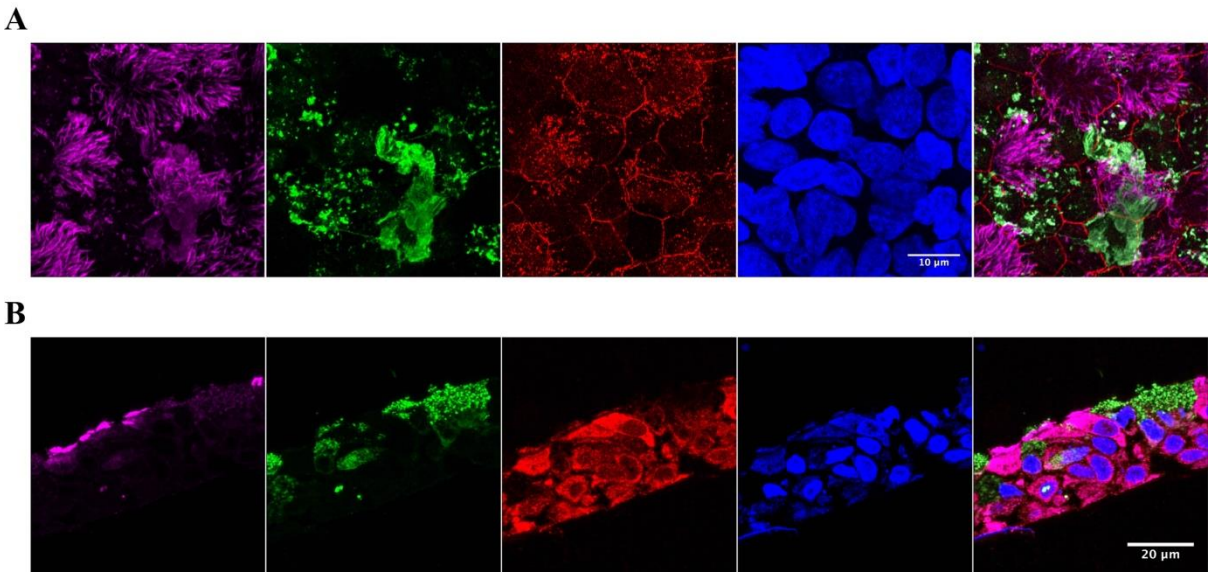

Figure 6.17 The expression of ACE2 in NHBE and BCi cells derived air-liquid interface culture

Immunofluorescence staining of acetylated tubulin (magenta), CC10 (green), ACE2 (red), and nucleus (blue) in NHBE cells derived ALI (A), BCi cells derived ALI (B).

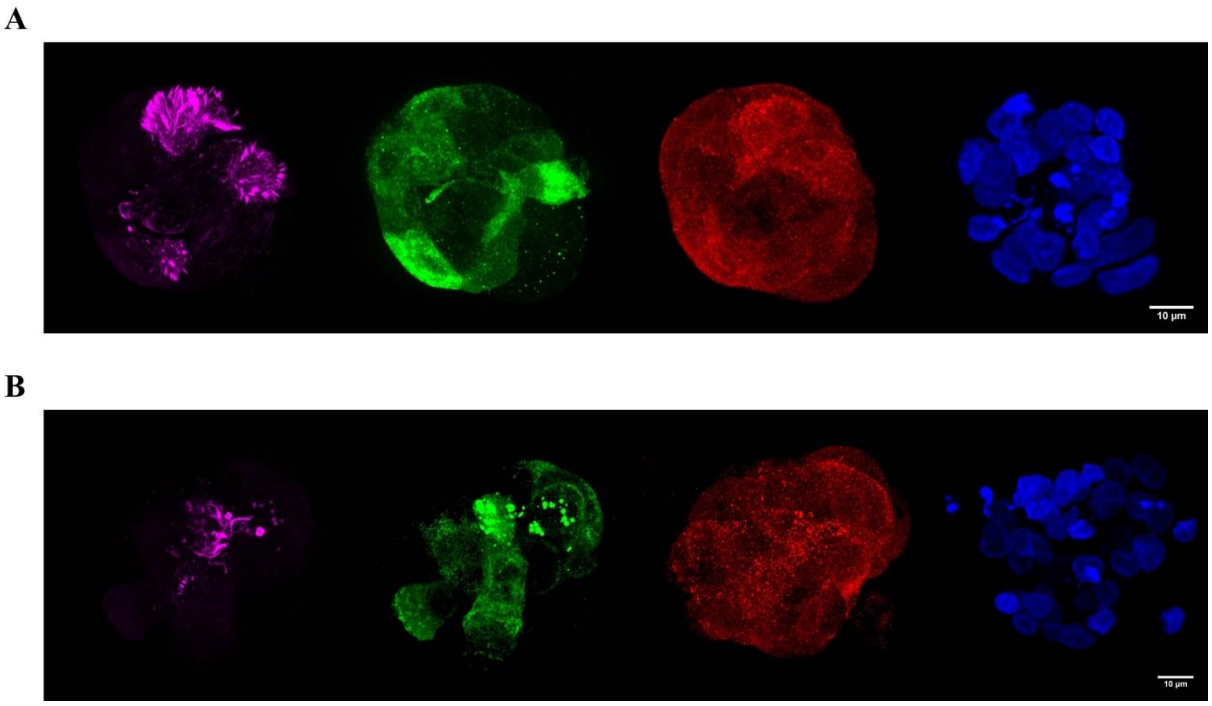

Figure 6.18 The expression of ACE2 in NHBE cells derived airway organoids

Immunofluorescence staining of acetylated tubulin (magenta), CC10 (green), ACE2 (red), and nucleus (blue) in NHBE cells derived airway organoids with cilia towards outside (A) and inside (B).

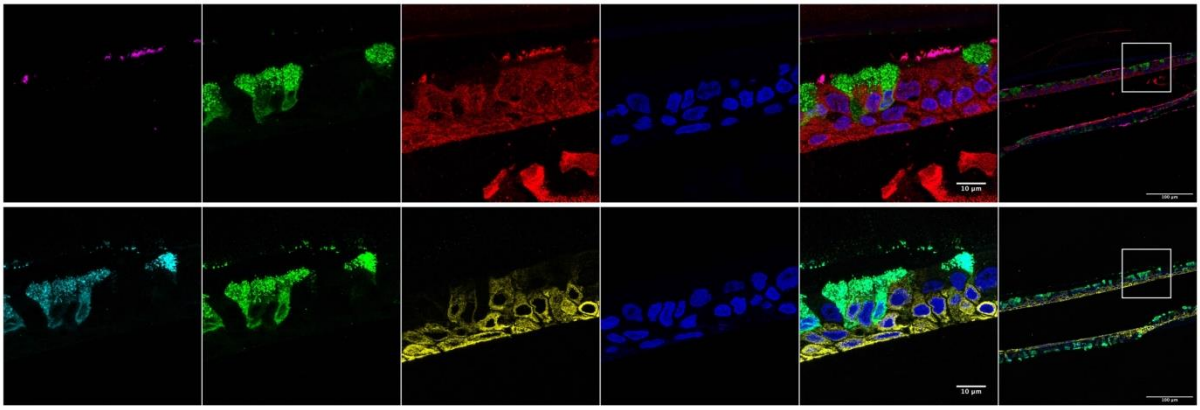

Figure 6.19 ACE2 localization in 2µm ALI sections

Immunofluorescence staining of acetylated tubulin (magenta), CC10 (green), MUC5AC (cyan), KRT5 (yellow), ACE2 (red), and nucleus (blue) in 2 µm NHBE cell derived ALI paraffin sections. The left panel images were obtained using 63x objective and were taken from the highlighted area in the corresponding right-hand side panel (20x objective).

6.3.4 SARS-CoV-2 can infect NHBE and BCi ALI

To evaluate the infectivity of SARS-CoV-2, NHBE and BCi ALI cultures and submerged NHBE and BCi cells were inoculated with SARS-CoV-2. At the outset, airway organoids were deemed unsuitable, based on challenges in their use in biosafety level 3 (and higher) facilities. As expected, based on ACE2 expression levels, submerged NHBE and BCi cells were not susceptible to SARS-CoV-2 (data not shown). In contrast, both NHBE (**Figure 6.20A**) and BCi (**Figure 6.20B**) ALI cultures were susceptible to SARS-CoV-2 infection, with peak virus shedding in the apical wash at 48-96 h post infection remaining detectable up to 6 days. Additionally, SARS-CoV-2 viral RNA (vRNA) was readily detectable in cells at 48h (**Figure 6.20C**) and 5-6 days post infection (**Figure 6.20D, E**). However, there was no induction of interferons by SARS-CoV-2 in either NHBE or BCi ALI at 48 h or 6 days post-infection (**Figure 6.21A, B, C**). Although IL-6 was reported to be elevated in serum in severe COVID-19 (Cummings et al., 2020), there was no significant inflammatory cytokine induction by SARS-CoV-2 (**Figure 6.22A**), whereas in separate experiments increased cytokine levels were induced by rhinovirus (**Figure 6.22B**) or Poly I:C (**Figure 6.22C**). Mean IL-6 concentrations remained at 2pg/mL after SARS-CoV-2 infection, whereas IL-6 was increased 100-fold by Poly I:C.

To confirm viral tropism, SARS-CoV-2 (dsRNA, magenta) was co-stained with the viral receptor ACE2 (red) and club cell marker CC10 (green) (**Figure 6.23A, B**). At 5 days post infection, viral dsRNA was found in cells infected with both doses of virus. There appeared to be more mucus secreted after viral infection. Surprisingly, the virus seemed to be mostly colocalized with secretory cells, but not other cell phenotypes. ACE2 expression was diminished compared to mock-infected cells, especially at cell membranes (**Figure 6.23B**). The peptide sequence used to generate ACE2 antibody is from the C-terminus and is part of the ectodomain that is subject to ADAM17 cleavage (Jia et al., 2009). The corollary of this observation is that the residual intracellular product of cleaved ACE2 will not be detected by this antibody. These findings raise the possibility that SARS-CoV-2 infection triggers ACE2 cleavage, which is suggested to be protective of further infection (Taglauer et al., 2021), but carries the strong potential for host damage (Wang et al., 2022). In addition, ACE2 shedding may explain discordance between single cell mRNA expression and IHC findings. This further suggested that SARS-CoV-2 infected ALI cultures through ACE2. Furthermore, the disruption of the tight junction protein ZO-1 (**Figure 6.24**) suggested a loss of cell integrity following infection with SARS-CoV-2.

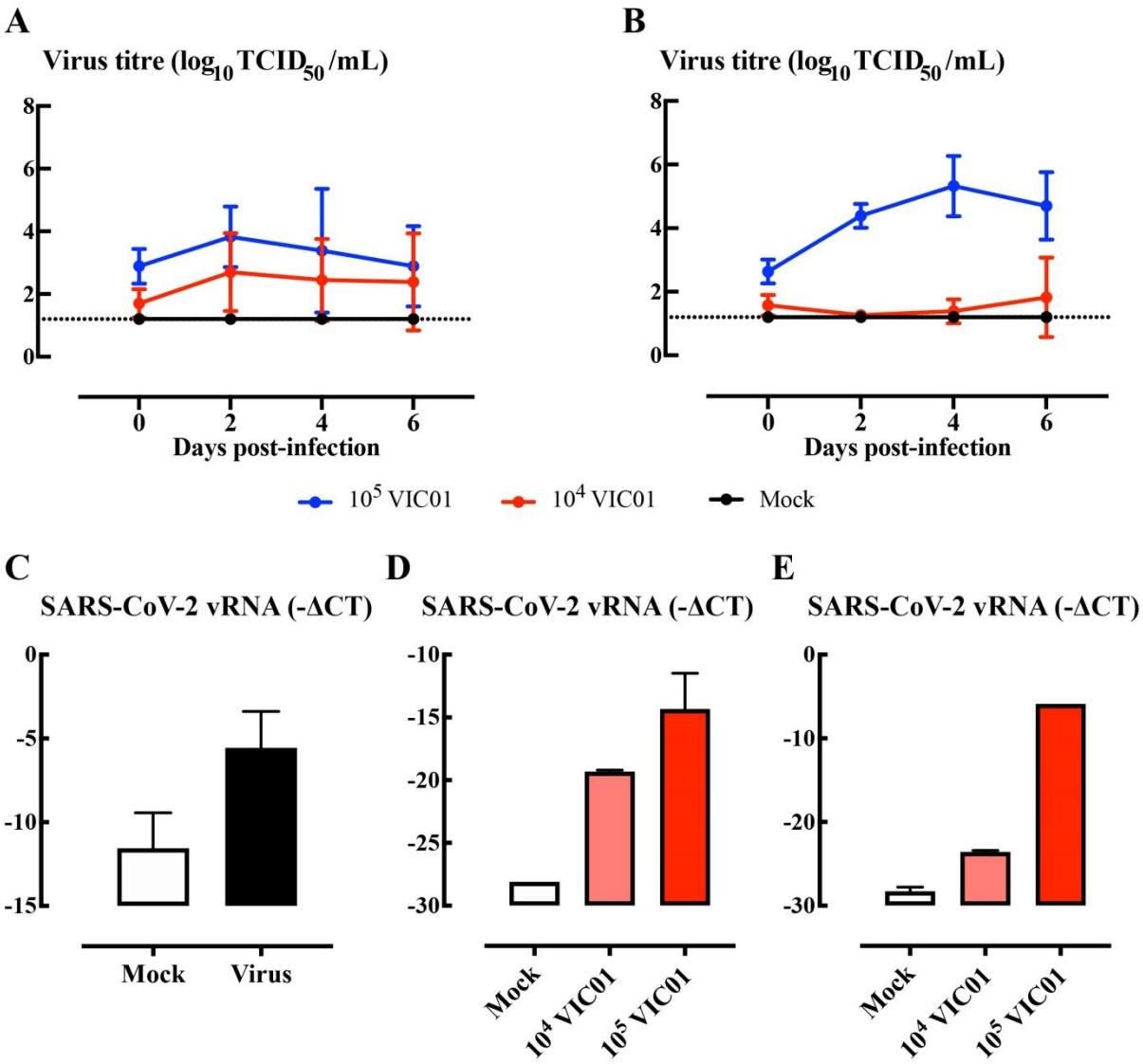

Figure 6.20 ALI cultures infected with SARS-CoV-2

ALI cultures were infected with SARS-CoV-2 for 1h. SARS-CoV-2 replication kinetics in NHBE cell derived ALI (A) and BCi cell derived ALI (B) were detected from apical washes. Gene expression of SARS-CoV-2 in NHBE-ALI was measured 48 h (C) and 6 days (D) post-infection, in BCi-ALI was measured 5 days (E) post-infection. Gene expression is expressed as -ΔCT (Log2). Data are presented as mean and SEM for n=1 independent culture with 3-4 technical repeats. NHBE cells used for (C) and (A)(D) were from 2 independent donors.

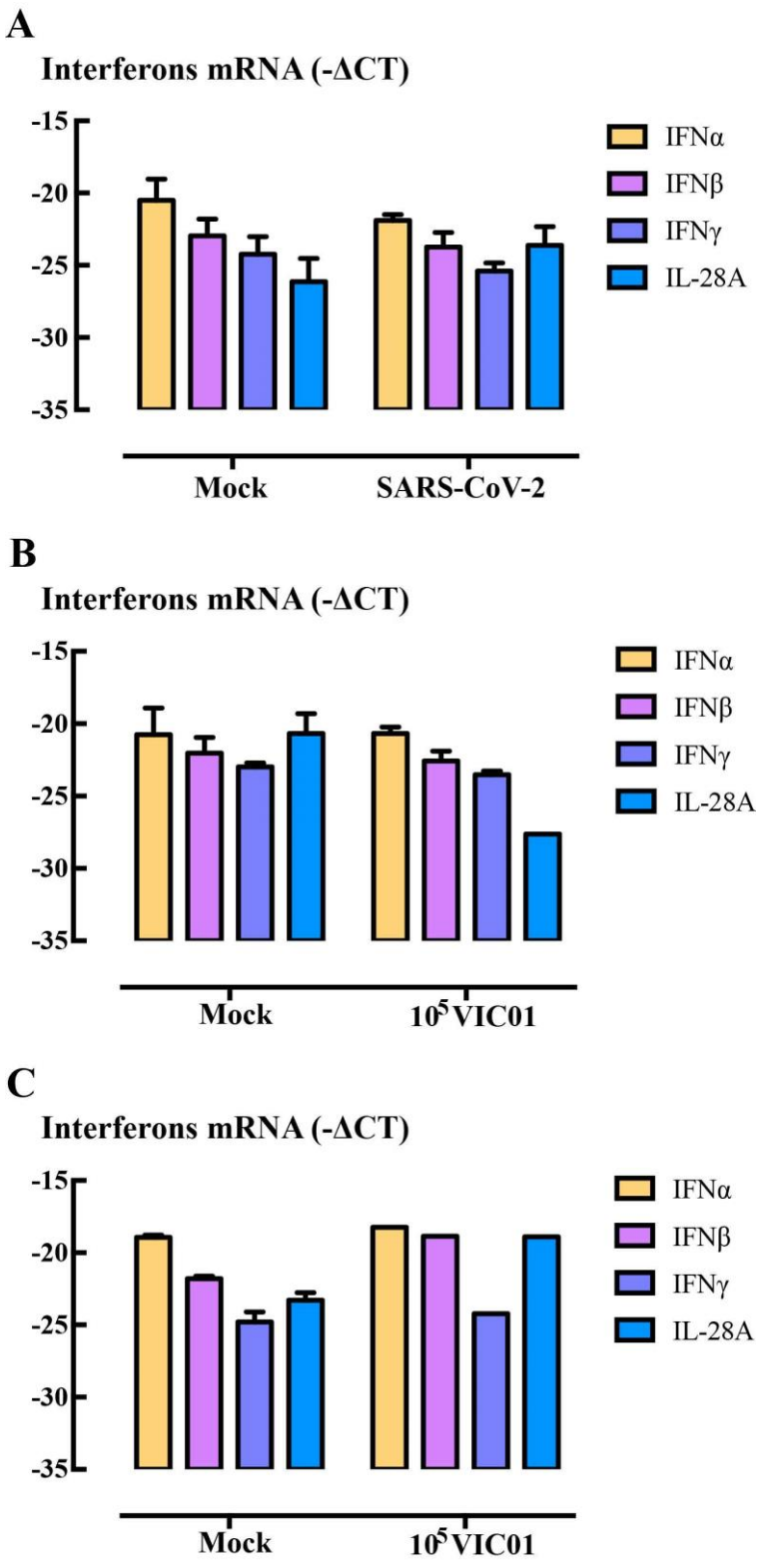

Figure 6.21 Interferons gene expression in SARS-CoV-2 infected ALI cultures

ALI cultures were infected with SARS-CoV-2 for 1 h. Gene expression of interferons in NHBE cell derived ALI was measured 48 h (A) and 6 days (B) post-infection, in BCi cell derived ALI was measured 5 days post-infection (C). Gene expression is expressed as -ΔCT (Log2) for n=1 independent culture with 3-4 technical repeats. NHBE cells used for (A) and (B) were from 2 independent donors.

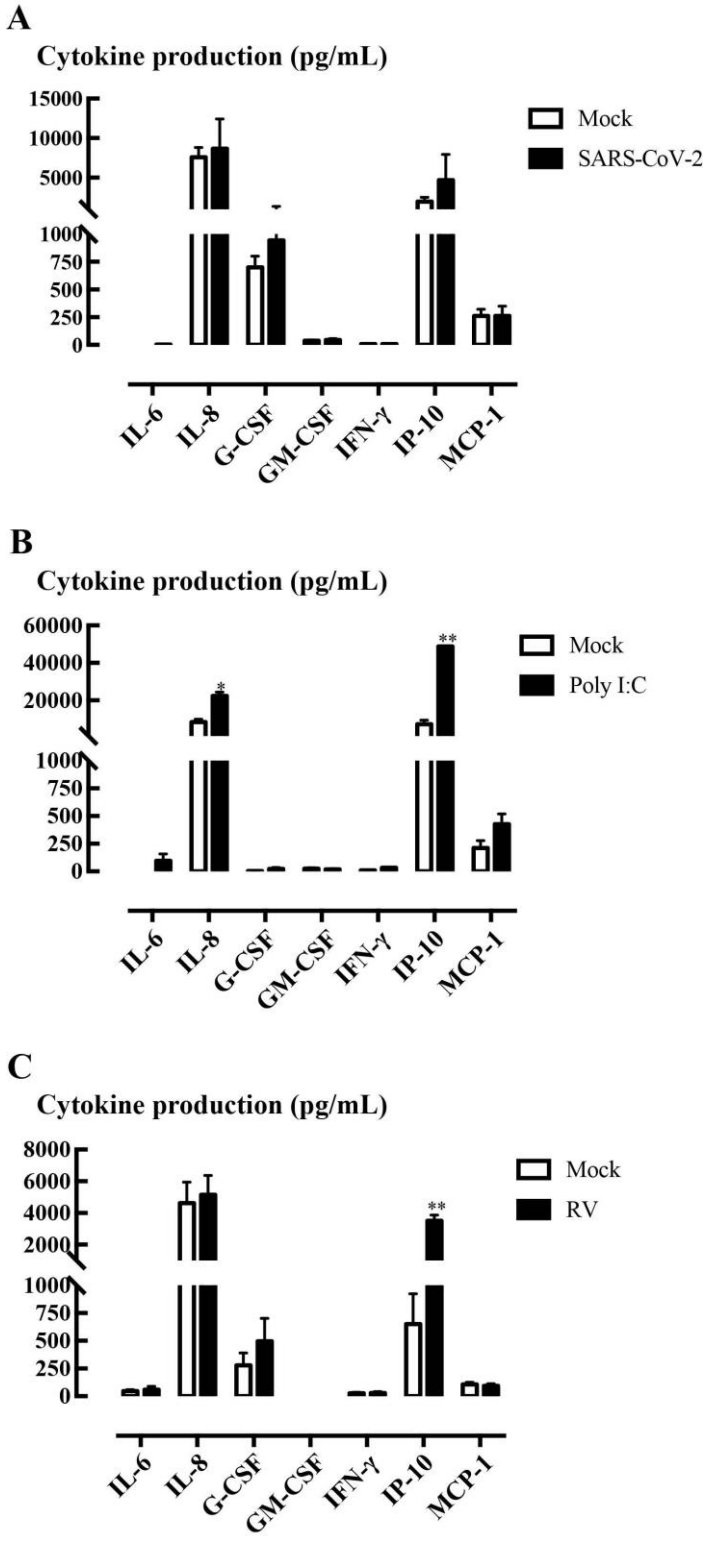

Figure 6.22 Cytokine production in SARS-CoV-2, Poly I:C, and Rhinovirus infected ALI cultures

Cytokines in supernatants were measured in ALI cultures 48 h post-infected with SARS-CoV-2 (A, n=1 independent culture with 3-4 technical repeats) and Rhinovirus (RV, C, n=4 independent culture), and 24 h post-stimulated with 10µg/mL Poly I:C (B, n=3 independent culture). Data are presented as mean and SEM. A paired-samples t-test was used for analysis, *: P<0.05, **: P<0.01. NHBE cells used for ALI cultures were from 8 independent donors.

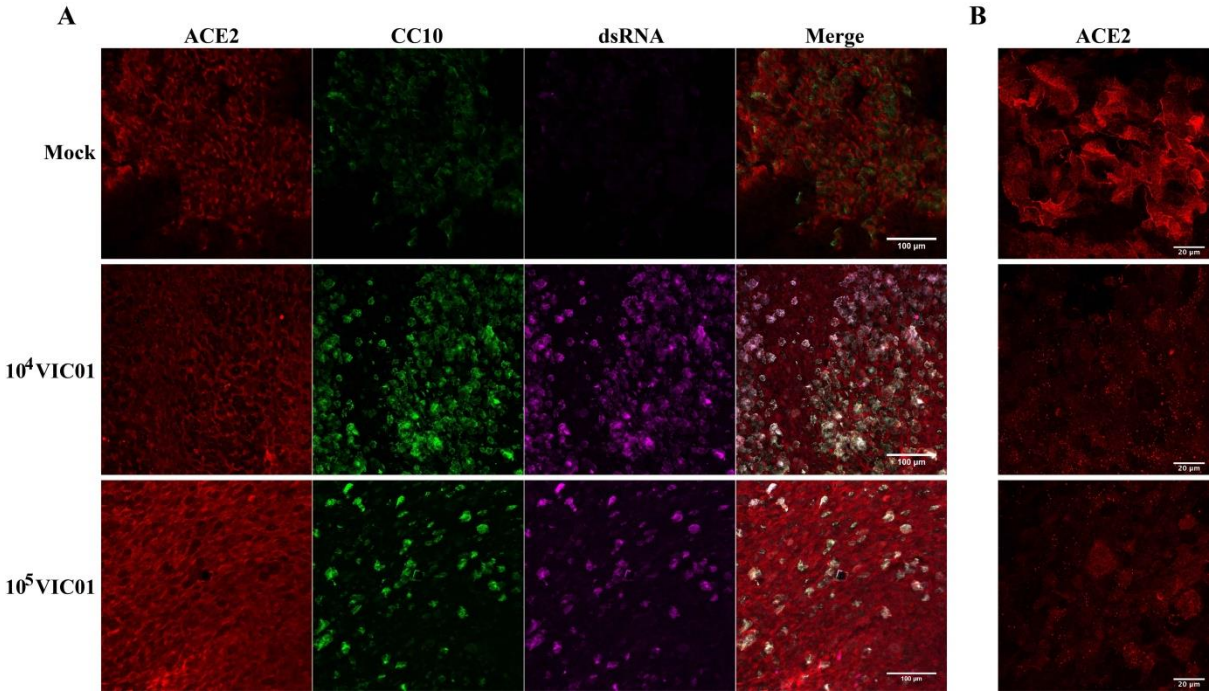

Figure 6.23 Immunofluorescence staining of SARS-CoV-2 dsRNA in ALI cultures

SARS-CoV-2 infected BCi-ALI cultures were stained for ACE2 (red), CC10 (green), and dsRNA (magenta) at 6 days post-infection. Images were obtained using 20x objective (A) and 63x objective (B).

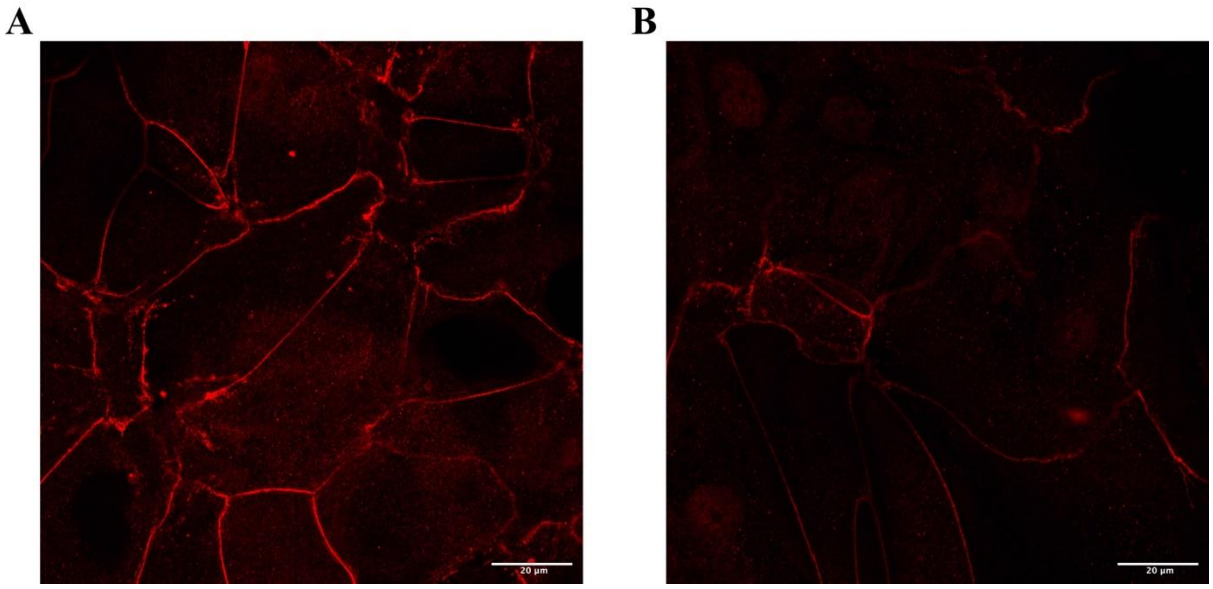

Figure 6.24 SARS-CoV-2 disturbed tight junction of ALI culture

NHBE-ALI cultures were infected with SARS-CoV-2 for 1 h and stained with ZO-1 (red) at 6 days post-infection. (A) Mock; (B) NHBE-ALI infected with 10^4 SARS-CoV-2 (n=1).

6.4 Discussion

Following evaluation of the potential utility of a range of airway cellular models for the study of viral infections, ALI organotypic cultures proved the most promising of airway cellular models for studies of SARS-CoV-2 infection. Both ALI and airway organoid organotypic culture recapitulate ACE2 and TMPRSS2 gene expression, that was suppressed in primary epithelial cells under submerged culture conditions lacking ciliated, secretory or goblet cell phenotypes. Moreover, benchmarking against ACE2 distribution patterns in non-asthmatic and asthmatic subject biopsies, it was clearly evident that ALI and airway organoid culture could faithfully replicate the heterogeneous distribution of ACE2 in different cell populations. Based on current techniques, the reproducibility and easy-handling properties of ALI prioritize it over airway organoid culture in studying infectious diseases, especially in the context of biosafety level 3 and higher facilities. After SARS-CoV-2 infection of ALI, cytokine levels were not elevated; a finding that is perhaps to have been expected, given the majority of the population under 80 years of age with COVID-19 suffer few or no symptoms (Oran and Topol, 2020). However, we note a disparity between the typical age and health status of donors of available airway epithelial cultures and those needed to represent the most affected demographic.

Native epithelial cells could be considered to be ideal tools for short-term *in vitro* studies. However, drug screening usually requires large numbers of cells, limiting their direct use in drug screening. Therefore, attention has been directed to the three-dimensional models: air-liquid interface and airway organoid. ALI and airway organoid organotypic cultures share the capacity to recapitulate the *in vivo* structure and the functionally differentiated airway epithelium of conducting airways. The differentiation of basal cells at ALI restored the complete loss of ciliated and secretory cells during submerged culture, thereby restoring the elements of the mucociliary clearance mechanisms. Donor or patient pluripotent stem cells (PSC) are also used following further differentiation to make ALI and organoid cultures (Chen et al., 2017; Dye et al., 2016; Huang et al., 2020a; Konishi et al., 2016). Although the latter approaches enable personalized assessment of therapy, these types of organotypic cultures require three to four weeks of time consuming and costly manual preparation. In the context of earlier discussion about age-appropriate sources of culture material it is generally held that induced PSC (iPSC)-derived cells show a more fetal phenotype (Doss and Sachinidis, 2019; Volpato and Webber, 2020).

ALI and airway organoid cultures differ in several aspects (**Table 6.3**). The ALI culture method has been optimized during the last 30 years (Pruniéras et al., 1983; Rayner et al., 2019). Although the organoid culture technology in general has rapidly developed in the last 10 years, airway organoid culture has not been as widely published as other mature organoid cultures, such as intestine organoids. The variability of organoid morphology and function renders these structures prone to reproducibility issues (Fustin et al., 2019). Some of the requirements for innovative engineering approaches for the production, control, and analysis of organoids and microenvironment have been fulfilled by "organoids-on-a-chip" (Park et al., 2019). For studying infectious diseases, the microbes can be simply added to the apical surface of ALI, whereas for organoid culture, inoculation has to be done by microinjection (Meyer-Berg et al., 2020) or mechanical disruption and re-embedding (Zhou et al., 2018). Therefore, further technical improvements are required for organoids to have the potential to displace ALI as the preferred format for higher-throughput pre-clinical research.

Table 6.3 Comparison of ALI and airway organoid culture

	ALI	**Airway organoid**
Mature protocol	+++	+
Easy handling	+++	+
Reproducibility	+++	+
Physiological mechanical environment	+	+++
In vivo architecture	++	+++
Patient specific	+++	+++
Time consuming	+++	+++
Confounding from media components	+++	+++

The collagen-coated transwell membrane in ALI cultures and the Matrigel® in organoid cultures can be regarded as extracellular matrix (ECM), with the transwell being the stiffer substrate. The ECM in organoid culture may be tuneable (Gjorevski et al., 2016). The cytoskeletal components function as mechanosensitive elements to sense the external

mechanical inputs and transduce these into intracellular signals (Jansen et al., 2017). As a result, the cytoskeleton distribution in different ECM may lead to different drug responses between ALI and organoid culture. The epithelial cells are uni-polar in ALI culture, but bi-polar in organoid culture, an unexpected phenomenon that requires further investigation to potentially reveal differential mechanical cues for development in these two settings. The bidirectionality of organoids certainly creates more unwanted and unphysiological heterogeneity. Everted organoids have been reported (Zhou et al., 2018), but the mechanism behind this morphogenesis is not known. In prostate epithelial cells, the E-cadherin and the spindle positioning interacts with cell polarity protein SCRIB and forms a ternary protein complex to bridge cell polarity and cell division orientation (Huang et al., 2014). Whether E-cadherin and SCRIB or other factors are involved in mediating the airway organoid orientation is worthy of further investigation, especially if controllable everted organoid morphologies could be developed to facilitate infection studies.

The immortalized basal cell line (BCi) was generated from a healthy donor and has been well characterized for its unique multipotent differentiation capacity over long-term culture (Walters et al., 2013). The expression of ACE2 and TMPRSS2 in BCi-derived ALI reinforce its potential in studying SARS-CoV-2 infection. However, we did notice dyskinetic motile cilia in BCi-derived ALI, which has been described previously (Kuek et al., 2018). Regardless, BCi cells offer a robust and strategically important model for genetic manipulation and drug screening.

Pulmonary epithelial cells express pattern recognition receptors (PRRs) for pathogen-associated molecular patterns (PAMPs) from viruses, bacteria, fungi, and multicellular parasites (Lloyd and Marsland, 2017). Toll-like receptors expressed in respiratory epithelial cells can mediate the innate host defence responses (Ioannidis et al., 2013). TLR 1, 2, 4, 5, and 6 bind to components of microbial cell walls and membranes allowing innate response to pathogens. TLR3, 7, 8, and 9 bind to microbial nucleic acids, including double and single-stranded RNA from RNA viruses and DNA from most organisms (Christmas, 2010). The similar TLR expression levels in submerged cell cultures and native cells make the cell lines potentially useful for studying TLR-mediated inflammatory cytokine production. Whilst certain phenomena, such as the impairment of glucocorticoid activity by RSV infection in BEAS-2B cells is also observed in NHBE-derived ALI (Xia et al., 2017), responses requiring communication between diverse of cell phenotypes are unlikely to be faithfully modelled in cell lines such as BEAS-2B and A549.

ACE2 has been identified as the primary receptor of SARS-CoV-2, as it is for both SARS-COV and HCoV-NL63 (Hoffmann et al., 2020b; Hofmann et al., 2005; Kuhn et al., 2004). The receptor binding domain (RBD) within the S1 region of the spike (S) protein binds to the ACE2 receptor in host cell (Cannalire et al., 2020). Following binding to ACE2, the S protein is proteolytically cleaved by TMPRSS2 to promote viral access to host cellular cytosol (Hoffmann et al., 2020b). Targeting both the viral and host factors for SARS-CoV-2 entry may be a promising strategy for controlling viral infections. The TMPRSS2 inhibitor, camostat mesylate suppresses SARS-CoV-2 infection (Hoffmann et al., 2021). Although clinical trial of camostat mesylate 200 mg t.i.d was not associated with increased adverse events during hospitalization of COVID-19 (Gunst et al., 2021), there was no beneficial effect. The possibility of benefit with other TMPRSS2 inhibitors and higher doses of camostat mesylate cannot be excluded. Moreover, TLR4 may have a crucial role in SARS-CoV-2 induced inflammation (Choudhury and Mukherjee, 2020). TLR adaptor signalling may contribute to a protective innate immune response to SARS-COV infection (Totura et al., 2015). Thus, organotypic cultures with a more globally faithful phenotype are strategically favoured over the use of submerged cultures in evaluating these anti-viral approaches.

There was no apparent relationship between ACE2 and TMPRSS2 gene expression and asthma, cystic fibrosis or COPD status of native cells or ALI cultures. In our well-powered investigation of ACE2 expression in airway epithelium, ACE2 levels did not consistently change in asthma of different severities (Li et al., 2019; Qiao et al., 2017; Ward et al., 2008). Consistent with our findings, ACE2 and TMPRSS2 mRNA expression in bronchial brush samples and sputum cells have also been reported to be unaffected by asthma status and shows no correlation with sex or age (Bradding et al., 2020; Peters et al., 2020). SARS-CoV-2 transmits by droplets and aerosols and has been detected in sputum (Wolfel et al., 2020). COPD patients on ICS had a reduced sputum cell expression of ACE2 gene (Finney et al., 2021). However, our findings do not show an effect of ICS on ACE2 *in vitro*, which may have been due to cortisol in the differentiation media. The medium for both ALI and airway organoid cultures are highly bioactive and include growth factors, cortisol, potent TGF-β inhibitors, antioxidant reagents, and ROCK inhibitors. These components are necessary for cell proliferation and differentiation but compromise the predictive pharmacology. For example, cortisol concentration used in ALI culture limits gene transactivation by synthetic ICS (Prodanovic et al., 2017).

ACE2 is highly expressed in ciliated and basal epithelial cells in patient biopsies, allowing comparison with organotypic ALI culture which indeed show similar cellular distributions of ACE2. Single-cell transcriptomics data indicated high expression of ACE2 in ciliated cells (Hikmet et al., 2020). Immunohistochemical staining in bronchial tissues from donors aged between 45-75 years further confirmed the high expression of ACE2 in ciliated cells compared goblet cells (Hikmet et al., 2020). The ACE2 is also evident in transient secretory cells (Lukassen et al., 2020), displaying a phenotype between goblet and ciliated cells. Airway remodelling in asthma (and COPD) includes goblet cell metaplasia and submucosal gland enlargement. Thus, the increased proportion of ciliated cells or secretory cells might lead to differences in ACE2 abundance, resulting in different SARS-CoV-2 infectivity or COVID-19 severity in remodelled airways. However, data contrasting with our findings has indicated elevated ACE2 gene expression by smoking (Zhang et al., 2020a). Notably, this was only observed in small airway epithelium and the proportion of ciliated and secretory cells was not analysed. ACE2 protein expression in the small airway epithelium from a smoker with COPD has been contrasted with non-smokers who showed no detectable ACE2 immunoreactivity (Brake et al., 2020). However, the study was limited to a single biopsy, the epithelial layer in the control sample was incomplete and the ACE2 immunoreactivity in COPD-smoker sample was identified in basal and ciliated cells.

Early in the COVID-19 pandemic, severe respiratory illness was ascribed to a cytokine storm with blood IL-6 levels correlated to mortality (Hojyo et al., 2020; Zhou et al., 2020). However, asymptomatic persons now seem to account for approximately 40% to 45% of SARS-CoV-2 infections, able to transmit the virus for an extended period (Oran and Topol, 2020). Asymptomatic individuals exhibited lower levels of pro- and anti-inflammatory cytokines, suggesting a weaker innate response to SARS-CoV-2 infection (Long et al., 2020). Compared to patients with cytokine release syndromes unrelated to COVID-19, the mean serum concentration of IL-6 in severe COVID-19 was as low as one hundredth (Leisman et al., 2020). Interferons (IFN) mediate cellular anti-viral defences, with Interferon beta therapy undergoing clinical trial, as interferon beta-1b in combination with lopinavir and ritonavir reduced viral load and accelerated recovery (Hung et al., 2020). The logic of such an approach is further emphasized by the observation by us and others that SARS-CoV-2 infection only induces low or no IFN-I and IFN-III (Blanco-Melo et al., 2020; Vanderheiden et al., 2020). Understanding the limited interferon induction may support therapeutic augmentation. The preponderance of severe cases occurs in subjects of advanced age for

which we lack biobanks of specimens or culture material to ascertain age-related differential ACE2 expression and interferon responses.

Taken together, our comparison of the utility of different cell lines and cultures suggests that ALI cultures provide the greatest utility to model SARS-CoV-2 infection. ALI culture could reflect the pathological changes after SARS-CoV-2 infection, including morphogenic changes and inflammatory responses.

CHAPTER 7

GENERAL DISCUSSION AND CONCLUSIONS

7.1 Key findings and their significance

7.1.1 Matrix stiffness influences airway epithelial cell biology

Airway epithelium acts as a physical barrier and plays critical roles in respiratory diseases. These cells sit on a basement membrane that becomes thicker in remodelled airway. Transforming growth factor beta (TGF-β) has been identified to be involved in airway remodelling, epithelial mesenchymal transition, and fibrosis (Aschner and Downey, 2016; Halwani et al., 2011; Stewart et al., 2018; Willis and Borok, 2007). Glucocorticoids (GC) are one of the major therapeutic treatments for respiratory diseases, such as asthma, COPD, and COVID-19 (GINA, 2020; GOLD, 2020; Group et al., 2021). This thesis provided the evidence that conventional stiff culture plastic promotes airway epithelial cells to exhibit fibre-like cytoskeleton morphology and be high responsiveness to TGF-β compared to cells cultured on soft environment. However, GC actions and TGF-β induced GC resistance appeared to be uninfluenced by matrix stiffness.

These findings are significant in several aspects. Firstly, gene expression levels in cells cultured on soft environment are closer to those in native epithelial cells, compared to extreme stiff culture plastic. In such circumstances, drugs developed in conventional culture plastic, targeting these differentially expressed genes, are more likely to fail in efficacy or have adverse effect in clinical trial. Secondly, fibrogenic genes and proteins, especially IL-11, are highly expressed and produced in response to TGF-β in airway epithelial cells cultured on stiff environment. This is indicating a potential feedback loop in pulmonary fibrogenesis. Fibroblasts and airway smooth muscle cells contribute to the deposition of extracellular matrix (ECM), which thickens the basement membrane. Oval-shaped pores are found in basement membrane at a density of 863 pores/mm^2 and have a diameter ranging from 0.75 to 3.85 μm (Howat et al., 2002; Howat et al., 2001). These pores traverse the full depth of the basement membrane, providing a conduit for immune cells. Therefore, fibrogenic proteins, secreted by airway epithelial cells on stiffened basement membrane, might travel through basement membrane and in turn further activate fibrogenic response in fibroblasts. This suggestion may explain the finding that epithelial cell derived IL-11 level after incubation on collagen hydrogel is considerably reduced, possibly by its polar release into the “basolateral” hydrogel rather than the supernatant. Thirdly, GC transactivation on inflammatory factors and inhibition on TNF-α-induced cytokines are not influenced by matrix stiffness, further providing evidence showing the effectiveness of GC in inflammation. Taken together, these

results demonstrated the importance of mechanics in pre-clinical research and provided airway epithelial cells to be a potential therapeutic target for fibrosis.

7.1.2 Versatile *in vitro* model is required in studying epithelial sodium channels

Epithelial sodium channels (ENaC) play critical role in regulating airway surface liquid to maintain mucociliary clearance. This thesis showed that ENaC α subunit gene is highly expressed in soft environments. However, ENaCα protein expression is not associated with severity of asthma, indicating culture plastic cannot accurately represent pathological stiffness. ENaC channel activity in cell lines is not regulated by matrix stiffness, whereas ENaC channel is more active in primary epithelial cells cultured on soft environment. These controversial results led us to the finding that submerged cultured airway epithelial cells lack of ENaC β and γ subunit, when all three subunits are essential in an active channel (Chen et al., 2015; Hughey et al., 2004; Randrianarison et al., 2008). In contrast, native cells from the "soft" human body and containing ciliated and secretory cells have all three subunits highly expressed. Hence, our data further illustrated the importance of mechanics in pre-clinical research and raised the requirement for versatile *in vitro* models to facilitate ENaC channel studies and perhaps other ion channels.

Additionally, this thesis applied a high-throughput assay to measure ENaC channel activity. Despite the fact that this assay needs further optimization, this assay enables us to achieve quick and high-content screening in early stage of drug development. Furthermore, real-time monitoring of channel activity might also be achieved, as it is a fluorescence-based assay.

7.1.3 Organotypic cultures utility in infection and inflammation

In an effort to fulfil the requirement of versatile *in vitro* models, this thesis applied airway organotypic cultures, air-liquid interface culture (ALI) and airway organoid culture, to systematically compare the utility of these models for the study of viral infection and inflammation. Firstly, data obtained in this thesis showed that ALI and airway organoid culture can recapitulate *in vivo* architecture. The most distinct difference between submerged culture and *in vivo* is the cell diversity. The lack of ENaC β and γ subunit in submerged cultured cells is due to lack of ciliated and secretory cells, which are restored by organotypic

culture. Secondly, this thesis presented the differences between ALI and airway organoid cultures, which should be considered in choosing them for specific applications. ALI culture is a mature protocol, enabling direct infection and drug treatment. Uniform transwells ensure high reproducibility of ALI cultures, whereas airway organoids have huge inter- and intra-donor variation. Transwells in ALI culture are relatively stiff compared to soft Matrigel® in airway organoid culture, albeit not as stiff as culture plastic, given the thin collagen hydrogel coating. The distribution of F-actin filaments further proved the different stiffness environment in these two models. Lastly, ALI and airway organoids are both time consuming and may have confounding effects on pharmacological and physiological responses from the bioactive media components required for their differentiation. Although cell differentiation starts at 10-14 days, it generally takes 3 to 4 weeks to fully mature. Culture media is the most important factor in cell differentiation, especially for airway organoids. However, the complex compositions in the media may compromise the predictive value of these models in pharmacological and pathophysiological research. Nevertheless, our work has demonstrated organotypic airway cultures have the potential to be applied in a variety of studies, but extra consideration should be taken to provide better predictive value.

7.1.4 ACE2 expression is restored in organotypic cultures and cell phenotype dependent

Therapeutic strategies for severe acute respiratory syndrome coronavirus 2 (SARS-CoV-2) infection caused coronavirus disease 2019 (COVID-19) are urgently needed, regardless of the increasingly successful vaccination outcomes. However, most of the human cell lines are not susceptible to SARS-CoV-2, except for CaCo2 and Calu3 cells (Chu et al., 2020). This thesis provided evidence that expression of SARS-CoV-2 receptor angiotensin converting enzyme 2 (ACE2) and priming protein transmembrane serine protease 2 (TMPRSS2) in organotypic cultures is at similar level as that of native epithelial cells, whereas submerged cultures only express low levels of ACE2 and TMPRSS2. ACE2 is highly expressed at the cell membrane and in ciliated and basal epithelial cells, further demonstrating the potential of organotypic cultures in studying SARS-CoV-2 infection. Given the considerations elucidated above, ALI culture is prioritized in SARS-CoV-2 infection. Our initial data that ALI cultures are susceptible to SARS-CoV-2 and viral RNA remains detectable up to 6 days. Moreover, the lack of cytokine production and interferon (IFN) expression correlates with the weaker innate response in asymptomatic individuals (Oran and Topol, 2020). These findings provide

evidence that ALI cultures can recapitulate the pathological changes after SARS-CoV-2 infection.

The proportion of patients with chronic respiratory disease, including asthma, chronic obstructive pulmonary disease (COPD), and cystic fibrosis (CF) (Chhiba et al., 2020; Colombo et al., 2020; Lovinsky-Desir et al., 2020) is unexpectedly low in COVID-19 cohorts. Our initial findings showed that ACE2 expression is not related to severity of asthma, compatible with the lack of increased susceptibility of asthmatics to SARS-CoV-2 infection over and above that of non-asthmatics.

7.2 Future directions

7.2.1 Is the difference between 2D stiff and 2D soft due to collagen?

This thesis has utilized conventional culture plastic as a2D stiff environment and collagen hydrogel as a 2D soft environment, demonstrating the influence of matrix stiffness on airway epithelial cells. Collagen type I is most widely used in preparing collagen hydrogels for bioengineered tissue microenvironment and can be easily extracted (Antoine et al., 2014), despite the fact that epithelial cells predominantly interact with basement membrane components collagen IV and laminin *in vivo* (LeBleu et al., 2007). Matrigel® provides high concentration of collagen IV but also contains a variety of growth factors. Thus, collagen type I hydrogel was initially selected as our 2D soft setting, albeit that it is more abundant in pathological conditions. Epithelial cells bind to basement membrane through Arg-Gly-Asp (RGD)-based integrin ligands. There are about 24 human integrin heterodimers binding to the RGD-recognition sequence (Plow et al., 2000; Takada et al., 2007). Collagen and heat denatured collagen (gelatin) binds to α_v integrins through RGD sites (Davis, 1992). Culture plastic is made of polystyrene, a long carbon chain polymer. Polystyrene surface is normally treated using corona discharge or gas-plasma to turn it from hydrophobic to hydrophilic (Ramsey et al., 1984). Modified polystyrene generates high surface density of hydroxyl groups, which is important in cell adhesion (Curtis et al., 1983). Therefore, in our experimental settings, cells bind to collagen via integrins but to polystyrene through vitronectin and fibronectin (Curtis et al., 1983; Ramsey et al., 1984), raising the question as to whether different binding sites might initiate different mechanotransduction signalling. Moreover, the collagen hydrogel might increase the dimensionality. Although the cells appeared to be in 2D when cultured on the collagen hydrogel, this would be better evidenced with 3D reconstruction using confocal microscopy. Denatured gelatin-coated culture plastic can preserve the RGD binding site of collagen and maintain the cells in 2D. This was in our initial plan but paused by COVID-19. Further investigations on well-controlled stiff and soft settings are needed to rule out the influence of substrate differences.

Additionally, other substrates with tuneable stiffness are also preferred to verify our findings. The most commonly used substrates include synthetic hydrogels, like polyacrylamide (PA) gel (Liu et al., 2010; Shkumatov et al., 2015) and polyethylene glycol (PEG) gel (Lin and Anseth, 2009), and hybrid hydrogels, combining two or more components to amplify the advantages of each component and potentially create new properties (Visser et al., 2015).

7.2.2 Applying shear stress and compression force into further investigation

In this thesis, we have focused on the influence of matrix stiffness on airway epithelial cells, which is more related to fibrotic rather than immune pathology. As summarized in Chapter 1, airway epithelial cells are in a complex mechanical environment, including stiffness from basement membrane, shear stress from mucociliary transport, and compression from neighbour cells. Moreover, airway epithelial cells can also feel compression from bronchoconstriction. It would also be interesting to learn how cells respond to these mechanical forces.

To study compression, an *in vitro* compressive system might be preferable (Park et al., 2012; Park and Tschumperlin, 2009; Tschumperlin et al., 2004). In this system, a transwell supplied with a silicone plug forms pressurized chamber. By controlling the pressure ranging from 3 cm H_2O of pressure as in normal breathing to 30 cm H_2O as in asthmatic airway, goblet cell hyperplasia and MUC5AC high expression was observed in ALI cultures (Park and Tschumperlin, 2009). Combining this compressive system with different stiffness settings might provide new insights into drug therapies for asthma and COPD, as they together mimic the remodelled airway.

Lung-on-a-chip technique has advanced the capability of conventional cellular models (Huh et al., 2007; Huh et al., 2010). In this microfluidic device, the airway epithelial cells and endothelial cells are cultured on each side of the membrane. The medium perfused through the channels gives cells shear stress. Additionally, stretchable membrane also can mimic the contractile forces or strains. Although it provides a superb model, the foreseeable challenge is how to apply organotypic cultures in these “small” and multi-tubing devices. As presented in this thesis, ALI culture and airway organoid culture both need long-term culture and most importantly medium renewal. Organoids-on-a-chip seems to be able to fulfil the need for controlling organoids and their microenvironment (Park et al., 2019). Nevertheless, combining multidisciplinary technologies will enable us to gain better understanding of airway epithelium and other tissues.

7.3 General conclusions

This thesis has provided evidence that matrix stiffness has an influence on airway epithelial cells biology, particularly on TGF-β-induced fibrogenesis. This thesis also illustrated that diverse epithelial cell phenotypes are needed in assessing epithelial sodium channel (ENaC) activity. To fulfil the requirement for cell diversity and mechanically relevant microenvironment, organotypic cultures are applied in this thesis and systematically characterized to better identify their potential utility. In response to COVID-19, this thesis further demonstrates that air-liquid interface cultures (ALI) provide the greatest utility in modelling SARS-CoV-2 infection. The findings within this thesis have emphasised the importance of mechanics and cell diversity in pre-clinical research, and ultimately may provide insights into new therapeutic targets for fibrosis. Organotypic airway epithelial cultures, especially ALI cultures, are superior to submerged cultures in drug screening and disease mechanisms, enabling evaluation of clinical potential therapeutics for COVID-19.

REFERENCES

Abo KM, Ma L, Matte T, Huang J, Alysandratos KD, Werder RB, Mithal A, Beermann ML, Lindstrom-Vautrin J, Mostoslavsky G, Ikonomou L, Kotton DN, Hawkins F, Wilson A and Villacorta-Martin C (2020) Human iPSC-derived alveolar and airway epithelial cells can be cultured at air-liquid interface and express SARS-CoV-2 host factors. *bioRxiv*.

Agusti A, Fabbri LM, Singh D, Vestbo J, Celli B, Franssen FME, Rabe KF and Papi A (2018) Inhaled corticosteroids in COPD: friend or foe? *Eur Respir J* **52**.

Ahmadi S, Bozoky Z, Di Paola M, Xia S, Li C, Wong AP, Wellhauser L, Molinski SV, Ip W, Ouyang H, Avolio J, Forman-Kay JD, Ratjen F, Hirota JA, Rommens J, Rossant J, Gonska T, Moraes TJ and Bear CE (2017) Phenotypic profiling of CFTR modulators in patient-derived respiratory epithelia. *npj Genomic Medicine* **2**:12.

Aisenbrey EA and Murphy WL (2020) Synthetic alternatives to Matrigel. *Nat Rev Mater* **5**:539-551.

Akram KM, Lomas NJ, Spiteri MA and Forsyth NR (2013) Club cells inhibit alveolar epithelial wound repair via TRAIL-dependent apoptosis. *European Respiratory Journal* **41**:683.

Al-Fageeh MB, Marchant RJ, Carden MJ and Smales CM (2006) The cold-shock response in cultured mammalian cells: harnessing the response for the improvement of recombinant protein production. *Biotechnol Bioeng* **93**:829-835.

Alberts B, Bray D, Hopkin K, Johnson AD, Lewis J, Raff M, Roberts K and Walter P (2015) *Essential cell biology*, Garland Science.

Alberts B JA, Lewis J, et al. (2002) *Molecular Biology of the Cell. 4th edition. Fibroblasts and Their Transformations: The Connective-Tissue Cell Family.* , New York: Garland Science.

Albo D, Arnoletti J, Castiglioni A, Granick M, Solomon M, Rothman V and Tuszynski G (1994) Thrombospondin (TSP) and Transforming Growth Factor β 1 (TGF-β) Promote Human A549 Lung Carcinoma Cell Plasminogen Activator Inhibitor Type 1 (Pal-1) Production and Stimulate Tumor Cell Attachment in Vitro. *Biochemical and biophysical research communications* **203**:857-865.

Ali MH and Schumacker PT (2002) Endothelial responses to mechanical stress: where is the mechanosensor? *Critical care medicine* **30**:S198-S206.

Allingham JS, Klenchin VA and Rayment I (2006) Actin-targeting natural products: structures, properties and mechanisms of action. *Cellular and molecular life sciences : CMLS* **63**:2119-2134.

Althaus M, Bogdan R, Clauss WG and Fronius M (2007) Mechano-sensitivity of epithelial sodium channels (ENaCs): laminar shear stress increases ion channel open probability. *FASEB journal : official publication of the Federation of American Societies for Experimental Biology* **21**:2389-2399.

Amin K, Ekberg-Jansson A, Löfdahl C-G and Venge P (2003) Relationship between inflammatory cells and structural changes in the lungs of asymptomatic and never smokers: a biopsy study. *Thorax* **58**:135-142.

Amin K, Janson C, Boman G and Venge P (2005) The extracellular deposition of mast cell products is increased in hypertrophic airways smooth muscles in allergic asthma but not in nonallergic asthma. *Allergy* **60**:1241-1247.

An SS, Kim J, Ahn K, Trepat X, Drake KJ, Kumar S, Ling G, Purington C, Rangasamy T, Kensler TW, Mitzner W, Fredberg JJ and Biswal S (2009) Cell stiffness, contractile stress and the role of extracellular matrix. *Biochemical and biophysical research communications* **382**:697-703.

Antoine EE, Vlachos PP and Rylander MN (2014) Review of collagen I hydrogels for bioengineered tissue microenvironments: characterization of mechanics, structure, and transport. *Tissue Eng Part B Rev* **20**:683-696.

Aragona M, Panciera T, Manfrin A, Giulitti S, Michielin F, Elvassore N, Dupont S and Piccolo S (2013) A mechanical checkpoint controls multicellular growth through YAP/TAZ regulation by actin-processing factors. *Cell* **154**:1047-1059.

Ardura JA, Berruguete R, Rámila D, Alvarez-Arroyo MV and Esbrit P (2008) Parathyroid hormone-related protein interacts with vascular endothelial growth factor to promote fibrogenesis in the obstructed mouse kidney. *American Journal of Physiology-Renal Physiology* **295**:F415-F425.

Ardura JA, Rayego-Mateos S, Rámila D, Ruiz-Ortega M and Esbrit P (2010) Parathyroid hormone-related protein promotes epithelial-mesenchymal transition. *Journal of the American Society of Nephrology : JASN* **21**:237-248.

Arrowsmith J (2011) Trial watch: phase III and submission failures: 2007-2010. *Nature reviews Drug discovery* **10**:87.

Asano S, Ito S, Takahashi K, Furuya K, Kondo M, Sokabe M and Hasegawa Y (2017) Matrix stiffness regulates migration of human lung fibroblasts. *Physiol Rep* **5**.

Aschner Y and Downey GP (2016) Transforming Growth Factor-beta: Master Regulator of the Respiratory System in Health and Disease. *Am J Respir Cell Mol Biol* **54**:647-655.

Athirasala A, Hirsch N and Buxboim A (2017) Nuclear mechanotransduction: sensing the force from within. *Curr Opin Cell Biol* **46**:119-127.

Au SH, Chamberlain MD, Mahesh S, Sefton MV and Wheeler AR (2014) Hepatic organoids for microfluidic drug screening. *Lab on a chip* **14**:3290-3299.

Aufderheide M, Förster C, Beshay M, Branscheid D and Emura M (2016) A new computer-controlled air–liquid interface cultivation system for the generation of differentiated cell cultures of the airway epithelium. *Experimental and Toxicologic Pathology* **68**:77-87.

Aulthouse AL, Beck M, Griffey E, Sanford J, Arden K, Machado MA and Horton WA (1989) Expression of the Human Chondrocyte Phenotype in vitro. *In Vitro Cellular & Developmental Biology* **25**:659-668.

Bai J, Smock SL, Jackson GR, Jr., MacIsaac KD, Huang Y, Mankus C, Oldach J, Roberts B, Ma YL, Klappenbach JA, Crackower MA, Alves SE and Hayden PJ (2015) Phenotypic responses of differentiated asthmatic human airway epithelial cultures to rhinovirus. *PLoS One* **10**:e0118286.

Baldi S, Dellacà R, Govoni L, Torchio R, Aliverti A, Pompilio P, Corda L, Tantucci C, Gulotta C and Brusasco V (2010) Airway distensibility and volume recruitment with lung inflation in COPD. *Journal of Applied Physiology* **109**:1019-1026.

Ball M, Hossain M and Padalia D (2020) Anatomy, Airway, in *StatPearls*, StatPearls Publishing

StatPearls Publishing LLC., Treasure Island (FL).

Bangel-Ruland N, Sobczak K, Christmann T, Kentrup D, Langhorst H, Kusche-Vihrog K and Weber WM (2010) Characterization of the epithelial sodium channel delta-subunit in human nasal epithelium. *Am J Respir Cell Mol Biol* **42**:498-505.

Barker N, van Es JH, Kuipers J, Kujala P, van den Born M, Cozijnsen M, Haegebarth A, Korving J, Begthel H, Peters PJ and Clevers H (2007) Identification of stem cells in small intestine and colon by marker gene Lgr5. *Nature* **449**:1003-1007.

Barker PM, Nguyen MS, Gatzy JT, Grubb B, Norman H, Hummler E, Rossier B, Boucher RC and Koller B (1998) Role of gammaENaC subunit in lung liquid clearance and electrolyte balance in newborn mice. Insights into perinatal adaptation and pseudohypoaldosteronism. *J Clin Invest* **102**:1634-1640.

Bartis D, Mise N, Mahida RY, Eickelberg O and Thickett DR (2014) Epithelial-mesenchymal transition in lung development and disease: does it exist and is it important? *Thorax* **69**:760-765.

Barton VA, Hall MA, Hudson KR and Heath JK (2000) Interleukin-11 signals through the formation of a hexameric receptor complex. *Journal of Biological Chemistry* **275**:36197-36203.

Baumgart E (2000) Stiffness--an unknown world of mechanical science? *Injury* **31 Suppl 2**:S-B14-23.

Beers MF and Moodley Y (2017) When Is an Alveolar Type 2 Cell an Alveolar Type 2 Cell? A Conundrum for Lung Stem Cell Biology and Regenerative Medicine. *Am J Respir Cell Mol Biol* **57**:18-27.

Beltrán-Heredia E, Almendro-Vedia VG, Monroy F and Cao FJ (2017) Modeling the Mechanics of Cell Division: Influence of Spontaneous Membrane Curvature, Surface Tension, and Osmotic Pressure. *Front Physiol* **8**:312.

Ben-Shahar Y (2011) Sensory functions for degenerin/epithelial sodium channels (DEG/ENaC). *Advances in genetics* **76**:1-26.

Benali R, Tournier JM, Chevillard M, Zahm JM, Klossek JM, Hinnrasky J, Gaillard D, Maquart FX and Puchelle E (1993) Tubule formation by human surface respiratory epithelial cells cultured in a three-dimensional collagen lattice. *American Journal of Physiology-Lung Cellular and Molecular Physiology* **264**:L183-L192.

Berdiev BK, Prat AG, Cantiello HF, Ausiello DA, Fuller CM, Jovov B, Benos DJ and Ismailov II (1996) Regulation of Epithelial Sodium Channels by Short Actin Filaments*. *Journal of Biological Chemistry* **271**:17704-17710.

Bergeron C, Al-Ramli W and Hamid Q (2009) Remodeling in asthma. *Proc Am Thorac Soc* **6**:301-305.

Berhan A, Harris T, Jaffar J, Jativa F, Langenbach S, Lonnstedt I, Alhamdoosh M, Ng M, Lee P, Westall G, Wilson N, Wilson M and Stewart AG (2020) Cellular Microenvironment Stiffness Regulates Eicosanoid Production and Signaling Pathways. *Am J Respir Cell Mol Biol* **63**:819-830.

Bhalla V and Hallows KR (2008) Mechanisms of ENaC regulation and clinical implications. *Journal of the American Society of Nephrology : JASN* **19**:1845-1854.

Bhatia V, Kim SOK, Aronson JF, Chao C, Hellmich MR and Falzon M (2012) Role of parathyroid hormone-related protein in the pro-inflammatory and pro-fibrogenic response associated with acute pancreatitis. *Regul Pept* **175**:49-60.

Birket SE, Chu KK, Liu L, Houser GH, Diephuis BJ, Wilsterman EJ, Dierksen G, Mazur M, Shastry S, Li Y, Watson JD, Smith AT, Schuster BS, Hanes J, Grizzle WE, Sorscher EJ, Tearney GJ and Rowe SM (2014) A functional anatomic defect of the cystic fibrosis airway. *Am J Respir Crit Care Med* **190**:421-432.

Blanco-Melo D, Nilsson-Payant BE, Liu WC, Uhl S, Hoagland D, Moller R, Jordan TX, Oishi K, Panis M, Sachs D, Wang TT, Schwartz RE, Lim JK, Albrecht RA and tenOever BR (2020) Imbalanced Host Response to SARS-CoV-2 Drives Development of COVID-19. *Cell* **181**:1036-1045 e1039.

Boers JE, Ambergen AW and Thunnissen FB (1999) Number and proliferation of clara cells in normal human airway epithelium. *American journal of respiratory and critical care medicine* **159**:1585-1591.

Boj SF, Vonk AM, Statia M, Su J, Vries RR, Beekman JM and Clevers H (2017) Forskolin-induced Swelling in Intestinal Organoids: An In Vitro Assay for Assessing Drug Response in Cystic Fibrosis Patients. *J Vis Exp*.

Bonny O and Hummler E (2000) Dysfunction of epithelial sodium transport: from human to mouse. *Kidney Int* **57**:1313-1318.

Booth AJ, Hadley R, Cornett AM, Dreffs AA, Matthes SA, Tsui JL, Weiss K, Horowitz JC, Fiore VF, Barker TH, Moore BB, Martinez FJ, Niklason LE and White ES (2012) Acellular normal and fibrotic human lung matrices as a culture system for in vitro investigation. *Am J Respir Crit Care Med* **186**:866-876.

Bossé Y and Rola-Pleszczynski M (2007) Controversy surrounding the increased expression of TGF beta 1 in asthma. *Respiratory research* **8**:66-66.

Boulanger MJ, Chow D-c, Brevnova EE and Garcia KC (2003) Hexameric structure and assembly of the interleukin-6/IL-6 α-receptor/gp130 complex. *Science* **300**:2101-2104.

Bourke JE, Li X, Foster SR, Wee E, Dagher H, Ziogas J, Harris T, Bonacci JV and Stewart AG (2011) Collagen remodelling by airway smooth muscle is resistant to steroids and beta(2)-agonists. *Eur Respir J* **37**:173-182.

Brackel HJ, Pedersen OF, Mulder PG, Overbeek SE, Kerrebijn KF and Bogaard JM (2000a) Central airways behave more stiffly during forced expiration in patients with asthma. *American journal of respiratory and critical care medicine* **162**:896-904.

Brackel HJL, Pedersen OF, Mulder PGH, Overbeek SE, Kerrebijn KF and Bogaard JM (2000b) Central Airways Behave More Stiffly during Forced Expiration in Patients with Asthma. *American Journal of Respiratory and Critical Care Medicine* **162**:896-904.

Bradding P, Richardson M, Hinks TSC, Howarth PH, Choy DF, Arron JR, Wenzel SE and Siddiqui S (2020) ACE2, TMPRSS2, and furin gene expression in the airways of people with asthma-implications for COVID-19. *J Allergy Clin Immunol* **146**:208-211.

Brake SJ, Barnsley K, Lu W, McAlinden KD, Eapen MS and Sohal SS (2020) Smoking Upregulates Angiotensin-Converting Enzyme-2 Receptor: A Potential Adhesion Site for Novel Coronavirus SARS-CoV-2 (Covid-19). *J Clin Med* **9**.

Broutier L, Andersson-Rolf A, Hindley CJ, Boj SF, Clevers H, Koo BK and Huch M (2016) Culture and establishment of self-renewing human and mouse adult liver and pancreas 3D organoids and their genetic manipulation. *Nat Protoc* **11**:1724-1743.

Brown AC, Fiore VF, Sulchek TA and Barker TH (2013) Physical and chemical microenvironmental cues orthogonally control the degree and duration of fibrosis-associated epithelial-to-mesenchymal transitions. *J Pathol* **229**:25-35.

Brown NJ, Salome CM, Berend N, Thorpe CW and King GG (2007) Airway Distensibility in Adults with Asthma and Healthy Adults, Measured by Forced Oscillation Technique. *American Journal of Respiratory and Critical Care Medicine* **176**:129-137.

Bruns JB, Carattino MD, Sheng S, Maarouf AB, Weisz OA, Pilewski JM, Hughey RP and Kleyman TR (2007) Epithelial Na+ channels are fully activated by furin- and prostasin-dependent release of an inhibitory peptide from the gamma-subunit. *J Biol Chem* **282**:6153-6160.

Butcher DT, Alliston T and Weaver VM (2009) A tense situation: forcing tumour progression. *Nat Rev Cancer* **9**:108-122.

Callaghan Patrick J, Ferrick B, Rybakovsky E, Thomas S and Mullin James M (2020) Epithelial barrier function properties of the 16HBE14o- human bronchial epithelial cell culture model. *Bioscience Reports* **40**.

Calvén J, Ax E and Rådinger M (2020) The Airway Epithelium-A Central Player in Asthma Pathogenesis. *Int J Mol Sci* **21**.

Calvo F, Ege N, Grande-Garcia A, Hooper S, Jenkins RP, Chaudhry SI, Harrington K, Williamson P, Moeendarbary E, Charras G and Sahai E (2013) Mechanotransduction and YAP-dependent matrix remodelling is required for the generation and maintenance of cancer-associated fibroblasts. *Nat Cell Biol* **15**:637-646.

Canessa CM, Schild L, Buell G, Thorens B, Gautschi I, Horisberger JD and Rossier BC (1994) Amiloride-sensitive epithelial Na+ channel is made of three homologous subunits. *Nature* **367**:463-467.

Cannalire R, Stefanelli I, Cerchia C, Beccari AR, Pelliccia S and Summa V (2020) SARS-CoV-2 Entry Inhibitors: Small Molecules and Peptides Targeting Virus or Host Cells. *Int J Mol Sci* **21**.

Cantiello HF, Stow JL, Prat AG and Ausiello DA (1991) Actin filaments regulate epithelial Na+ channel activity. *American Journal of Physiology-Cell Physiology* **261**:C882-C888.

Cao X, Coyle JP, Xiong R, Wang Y, Heflich RH, Ren B, Gwinn WM, Hayden P and Rojanasakul L (2021) Invited review: human air-liquid-interface organotypic airway tissue models derived from primary tracheobronchial epithelial cells-overview and perspectives. *In Vitro Cell Dev Biol Anim* **57**:104-132.

Chen JH, Stoltz DA, Karp PH, Ernst SE, Pezzulo AA, Moninger TO, Rector MV, Reznikov LR, Launspach JL, Chaloner K, Zabner J and Welsh MJ (2010) Loss of anion transport without increased sodium absorption characterizes newborn porcine cystic fibrosis airway epithelia. *Cell* **143**:911-923.

Chen MX, Gatfield K, Ward E, Downie D, Sneddon HF, Walsh S, Powell AJ, Laine D, Carr M and Trezise D (2015) Validation and optimization of novel high-throughput assays for human epithelial sodium channels. *J Biomol Screen* **20**:242-253.

Chen S and Schoen J (2019) Air-liquid interface cell culture: From airway epithelium to the female reproductive tract. *Reprod Domest Anim* **54 Suppl 3**:38-45.

Chen YW, Huang SX, de Carvalho A, Ho SH, Islam MN, Volpi S, Notarangelo LD, Ciancanelli M, Casanova JL, Bhattacharya J, Liang AF, Palermo LM, Porotto M, Moscona A and Snoeck HW (2017) A three-dimensional model of human lung development and disease from pluripotent stem cells. *Nat Cell Biol* **19**:542-549.

Chetta A, Zanini A, Foresi A, Del Donno M, Castagnaro A, D'Ippolito R, Baraldo S, Testi R, Saetta M and Olivieri D (2003) Vascular component of airway remodeling in asthma is reduced by high dose of fluticasone. *Am J Respir Crit Care Med* **167**:751-757.

Chhiba KD, Patel GB, Vu THT, Chen MM, Guo A, Kudlaty E, Mai Q, Yeh C, Muhammad LN, Harris KE, Bochner BS, Grammer LC, Greenberger PA, Kalhan R, Kuang FL, Saltoun CA, Schleimer RP, Stevens WW and Peters AT (2020) Prevalence and characterization of asthma in hospitalized and nonhospitalized patients with COVID-19. *J Allergy Clin Immunol* **146**:307-314 e304.

Choudhury A and Mukherjee S (2020) In silico studies on the comparative characterization of the interactions of SARS-CoV-2 spike glycoprotein with ACE-2 receptor homologs and human TLRs. *J Med Virol* **92**:2105-2113.

Christmas P (2010) Toll-Like Receptors: Sensors that Detect Infection, in *Nature Education* p 85.

Chu H, Chan JF-W, Yuen TT-T, Shuai H, Yuan S, Wang Y, Hu B, Yip CC-Y, Tsang JO-L, Huang X, Chai Y, Yang D, Hou Y, Chik KK-H, Zhang X, Fung AY-F, Tsoi H-W, Cai J-P, Chan W-M, Ip JD, Chu AW-H, Zhou J, Lung DC, Kok K-H, To KK-W, Tsang OT-Y, Chan K-H and Yuen K-Y (2020) Comparative tropism, replication kinetics, and cell damage profiling of SARS-CoV-2 and SARS-CoV with implications for clinical manifestations, transmissibility, and laboratory studies of COVID-19: an observational study. *The Lancet Microbe* **1**:e14-e23.

Chu HW, Balzar S, Seedorf GJ, Westcott JY, Trudeau JB, Silkoff P and Wenzel SE (2004) Transforming growth factor-beta2 induces bronchial epithelial mucin expression in asthma. *The American journal of pathology* **165**:1097-1106.

Chua CW, Shibata M, Lei M, Toivanen R, Barlow LJ, Bergren SK, Badani KK, McKiernan JM, Benson MC and Hibshoosh H (2014) Single luminal epithelial progenitors can generate prostate organoids in culture. *Nature cell biology* **16**:951-961.

Chung KF (2005) The role of airway smooth muscle in the pathogenesis of airway wall remodeling in chronic obstructive pulmonary disease. *Proc Am Thorac Soc* **2**:347-354; discussion 371-342.

Claassen DA, Desler MM and Rizzino A (2009) ROCK inhibition enhances the recovery and growth of cryopreserved human embryonic stem cells and human induced pluripotent stem cells. *Mol Reprod Dev* **76**:722-732.

Collawn JF, Lazrak A, Bebok Z and Matalon S (2012) The CFTR and ENaC debate: how important is ENaC in CF lung disease? *American journal of physiology Lung cellular and molecular physiology* **302**:L1141-L1146.

Collawn JF and Matalon S (2014) CFTR and lung homeostasis. *Am J Physiol Lung Cell Mol Physiol* **307**:L917-923.

Colombo C, Burgel P-R, Gartner S, van Koningsbruggen-Rietschel S, Naehrlich L, Sermet-Gaudelus I and Southern KW (2020) Impact of COVID-19 on people with cystic fibrosis. *The Lancet Respiratory Medicine* **8**:e35-e36.

Comer DM, Kidney JC, Ennis M and Elborn JS (2013) Airway epithelial cell apoptosis and inflammation in COPD, smokers and nonsmokers. *European Respiratory Journal* **41**:1058.

Cook D, Brown D, Alexander R, March R, Morgan P, Satterthwaite G and Pangalos MN (2014) Lessons learned from the fate of AstraZeneca's drug pipeline: a five-dimensional framework. *Nature reviews Drug discovery* **13**:419-431.

Cook DI, Dinudom A, Komwatana P, Kumar S and Young JA (2002) Patch-clamp studies on epithelial sodium channels in salivary duct cells. *Cell Biochem Biophys* **36**:105-113.

Coppola S, Carnevale I, Danen EHJ, Peters GJ, Schmidt T, Assaraf YG and Giovannetti E (2017) A mechanopharmacology approach to overcome chemoresistance in pancreatic cancer. *Drug resistance updates : reviews and commentaries in antimicrobial and anticancer chemotherapy* **31**:43-51.

Corning (2019) Corning Matrigel matrix. Frequently asked questions. *Corning Incorporated Life Sciences*.

Cozens AL, Yezzi MJ, Kunzelmann K, Ohrui T, Chin L, Eng K, Finkbeiner WE, Widdicombe JH and Gruenert DC (1994) CFTR expression and chloride secretion in polarized immortal human bronchial epithelial cells. *Am J Respir Cell Mol Biol* **10**:38-47.

Crespo M, Vilar E, Tsai SY, Chang K, Amin S, Srinivasan T, Zhang T, Pipalia NH, Chen HJ, Witherspoon M, Gordillo M, Xiang JZ, Maxfield FR, Lipkin S, Evans T and Chen S (2017) Colonic organoids derived from human induced pluripotent stem cells for modeling colorectal cancer and drug testing. *Nat Med* **23**:878-884.

Crystal RG, Randell SH, Engelhardt JF, Voynow J and Sunday ME (2008) Airway epithelial cells: current concepts and challenges. *Proc Am Thorac Soc* **5**:772-777.

Cukierman E, Pankov R, Stevens DR and Yamada KM (2001) Taking cell-matrix adhesions to the third dimension. *Science* **294**:1708-1712.

Cummings MJ, Baldwin MR, Abrams D, Jacobson SD, Meyer BJ, Balough EM, Aaron JG, Claassen J, Rabbani LE, Hastie J, Hochman BR, Salazar-Schicchi J, Yip NH, Brodie D and O'Donnell MR (2020) Epidemiology, clinical course, and outcomes of critically ill adults with COVID-19 in New York City: a prospective cohort study. *The Lancet* **395**:1763-1770.

Curtis AS, Forrester JV, McInnes C and Lawrie F (1983) Adhesion of cells to polystyrene surfaces. *The Journal of cell biology* **97**:1500-1506.

da Silva da Costa FA, Soares MR, Malagutti-Ferreira MJ, da Silva GR, Livero F and Ribeiro-Paes JT (2021) Three-Dimensional Cell Cultures as a Research Platform in Lung Diseases and COVID-19. *Tissue Eng Regen Med*.

Danahay H, Pessotti AD, Coote J, Montgomery BE, Xia D, Wilson A, Yang H, Wang Z, Bevan L, Thomas C, Petit S, London A, LeMotte P, Doelemeyer A, Velez-Reyes GL, Bernasconi P, Fryer CJ, Edwards M, Capodieci P, Chen A, Hild M and Jaffe AB (2015) Notch2 is required for inflammatory cytokine-driven goblet cell metaplasia in the lung. *Cell Rep* **10**:239-252.

Daniels CE, Lasky JA, Limper AH, Mieras K, Gabor E, Schroeder DR and Imatinib IPFSI (2010) Imatinib treatment for idiopathic pulmonary fibrosis: Randomized placebo-controlled trial results. *Am J Respir Crit Care Med* **181**:604-610.

Daniels CE, Wilkes MC, Edens M, Kottom TJ, Murphy SJ, Limper AH and Leof EB (2004) Imatinib mesylate inhibits the profibrogenic activity of TGF-beta and prevents bleomycin-mediated lung fibrosis. *J Clin Invest* **114**:1308-1316.

Davenport EA and Nettesheim P (1996) Regulation of mucociliary differentiation of rat tracheal epithelial cells by type I collagen gel substratum. *American Journal of Respiratory Cell and Molecular Biology* **14**:19-26.

Davis GE (1992) Affinity of integrins for damaged extracellular matrix: αvβ3 binds to denatured collagen type I through RGD sites. *Biochemical and biophysical research communications* **182**:1025-1031.

De Boeck K and Amaral MD (2016) Progress in therapies for cystic fibrosis. *Lancet Respir Med* **4**:662-674.

De Rose V, Molloy K, Gohy S, Pilette C and Greene CM (2018) Airway Epithelium Dysfunction in Cystic Fibrosis and COPD. *Mediators of Inflammation* **2018**:1309746.

Dekkers JF, Alieva M, Wellens LM, Ariese HCR, Jamieson PR, Vonk AM, Amatngalim GD, Hu H, Oost KC, Snippert HJG, Beekman JM, Wehrens EJ, Visvader JE, Clevers H and Rios AC (2019) High-resolution 3D imaging of fixed and cleared organoids. *Nat Protoc* **14**:1756-1771.

Dekkers JF, Wiegerinck CL, de Jonge HR, Bronsveld I, Janssens HM, de Winter-de Groot KM, Brandsma AM, de Jong NW, Bijvelds MJ, Scholte BJ, Nieuwenhuis EE, van den Brink S, Clevers H, van der Ent CK, Middendorp S and Beekman JM (2013) A functional CFTR assay using primary cystic fibrosis intestinal organoids. *Nat Med* **19**:939-945.

Demers CJ, Soundararajan P, Chennampally P, Cox GA, Briscoe J, Collins SD and Smith RL (2016) Development-on-chip: in vitro neural tube patterning with a microfluidic device. *Development* **143**:1884-1892.

Den Beste KA, Hoddeson EK, Parkos CA, Nusrat A and Wise SK (2013) Epithelial permeability alterations in an in vitro air-liquid interface model of allergic fungal rhinosinusitis. *Int Forum Allergy Rhinol* **3**:19-25.

Dennler S, Itoh S, Vivien D, ten Dijke P, Huet S and Gauthier JM (1998) Direct binding of Smad3 and Smad4 to critical TGF β - inducible elements in the promoter of human plasminogen activator inhibitor - type 1 gene. *The EMBO journal* **17**:3091-3100.

Deprez M, Zaragosi L-E, Truchi M, Becavin C, Ruiz García S, Arguel M-J, Plaisant M, Magnone V, Lebrigand K, Abelanet S, Brau F, Paquet A, Pe'er D, Marquette C-H, Leroy S and Barbry P (2020) A Single-Cell Atlas of the Human Healthy Airways. *American Journal of Respiratory and Critical Care Medicine* **202**:1636-1645.

Diaz AA, Come CE, Ross JC, Estépar RSJ, Han MK, Loring SH, Silverman EK, Washko GR and Investigators C (2012) Association between airway caliber changes with lung inflation and emphysema assessed by volumetric CT scan in subjects with COPD. *Chest* **141**:736-744.

Dijkman R, Jebbink MF, Koekkoek SM, Deijs M, Jonsdottir HR, Molenkamp R, Ieven M, Goossens H, Thiel V and van der Hoek L (2013) Isolation and characterization of

current human coronavirus strains in primary human epithelial cell cultures reveal differences in target cell tropism. *J Virol* **87**:6081-6090.

Discher D, Dong C, Fredberg JJ, Guilak F, Ingber D, Janmey P, Kamm RD, Schmid-Schonbein GW and Weinbaum S (2009) Biomechanics: cell research and applications for the next decade. *Annals of biomedical engineering* **37**:847-859.

Discher DE, Janmey P and Wang Y-l (2005a) Tissue cells feel and respond to the stiffness of their substrate. *Science* **310**:1139-1143.

Discher DE, Janmey P and Wang YL (2005b) Tissue cells feel and respond to the stiffness of their substrate. *Science* **310**:1139-1143.

Doss MX and Sachinidis A (2019) Current Challenges of iPSC-Based Disease Modeling and Therapeutic Implications. *Cells* **8**.

Dowden H and Munro J (2019) Trends in clinical success rates and therapeutic focus. *Nature reviews Drug discovery* **18**:495-496.

Drost J, Karthaus WR, Gao D, Driehuis E, Sawyers CL, Chen Y and Clevers H (2016) Organoid culture systems for prostate epithelial and cancer tissue. *Nature protocols* **11**:347-358.

Drummond HA, Gebremedhin D and Harder DR (2004) Degenerin/epithelial Na+ channel proteins: components of a vascular mechanosensor. *Hypertension (Dallas, Tex : 1979)* **44**:643-648.

Du Toit J, Woolcock AJ, Salome C, Sundrum R and Black J (1986) Characteristics of bronchial hyperresponsiveness in smokers with chronic air-flow limitation. *American review of respiratory disease* **134**:498-501.

Du Y, Days E, Romaine I, Abney KK, Kaufmann K, Sulikowski G, Stauffer S, Lindsley CW and Weaver CD (2015) Development and validation of a thallium flux-based functional assay for the sodium channel NaV1.7 and its utility for lead discovery and compound profiling. *ACS chemical neuroscience* **6**:871-878.

Dupont S, Morsut L, Aragona M, Enzo E, Giulitti S, Cordenonsi M, Zanconato F, Le Digabel J, Forcato M, Bicciato S, Elvassore N and Piccolo S (2011) Role of YAP/TAZ in mechanotransduction. *Nature* **474**:179-183.

Dutta D, Heo I and Clevers H (2017) Disease Modeling in Stem Cell-Derived 3D Organoid Systems. *Trends Mol Med* **23**:393-410.

Dye BR, Dedhia PH, Miller AJ, Nagy MS, White ES, Shea LD and Spence JR (2016) A bioengineered niche promotes in vivo engraftment and maturation of pluripotent stem cell derived human lung organoids. *eLife* **5**.

Dye BR, Hill DR, Ferguson MA, Tsai YH, Nagy MS, Dyal R, Wells JM, Mayhew CN, Nattiv R, Klein OD, White ES, Deutsch GH and Spence JR (2015) In vitro generation of human pluripotent stem cell derived lung organoids. *eLife* **4**.

Ebina M, Takahashi T, Chiba T and Motomiya M (1993a) Cellular hypertrophy and hyperplasia of airway smooth muscle underlying bronchial asthma. *The American review of respiratory disease* **148**:720-726.

Ebina M, Takahashi T, Chiba T and Motomiya M (1993b) Cellular hypertrophy and hyperplasia of airway smooth muscles underlying bronchial asthma. A 3-D morphometric study. *The American review of respiratory disease* **148**:720-726.

Edelheit O, Hanukoglu I, Dascal N and Hanukoglu A (2011) Identification of the roles of conserved charged residues in the extracellular domain of an epithelial sodium channel (ENaC) subunit by alanine mutagenesis. *Am J Physiol Renal Physiol* **300**:F887-897.

Ehrig S, Schamberger B, Bidan CM, West A, Jacobi C, Lam K, Kollmannsberger P, Petersen A, Tomancak P, Kommareddy K, Fischer FD, Fratzl P and Dunlop JWC (2019) Surface tension determines tissue shape and growth kinetics. *Science Advances* **5**:eaav9394.

Eitzman DT, McCoy RD, Zheng X, Fay WP, Shen T, Ginsburg D and Simon RH (1996) Bleomycin-induced pulmonary fibrosis in transgenic mice that either lack or overexpress the murine plasminogen activator inhibitor-1 gene. *The Journal of clinical investigation* **97**:232-237.

Ekberg-Jansson A, Amin K, Bake B, Rosengren A, Tylén U, Venge P and Löfdahl C-G (2005) Bronchial mucosal mast cells in asymptomatic smokers relation to structure, lung function and emphysema. *Respiratory medicine* **99**:75-83.

El-Mohri H, Wu Y, Mohanty S and Ghosh G (2017) Impact of matrix stiffness on fibroblast function. *Materials science & engineering C, Materials for biological applications* **74**:146-151.

Elias JA, Zheng T, Einarsson O, Landry M, Trow T, Rebert N and Panuska J (1994) Epithelial interleukin-11. Regulation by cytokines, respiratory syncytial virus, and retinoic acid. *Journal of Biological Chemistry* **269**:22261-22268.

Engler AJ, Sen S, Sweeney HL and Discher DE (2006) Matrix elasticity directs stem cell lineage specification. *Cell* **126**:677-689.

Evans CM, Kim K, Tuvim MJ and Dickey BF (2009) Mucus hypersecretion in asthma: causes and effects. *Current opinion in pulmonary medicine* **15**:4-11.

Farinha CM and Matos P (2016) Repairing the basic defect in cystic fibrosis - one approach is not enough. *Febs j* **283**:246-264.

FDA (2020) FDA Approves First Treatment for COVID-19, U.S. FOOD & DRUG ADMINISTRATION.

FDA (2021) Coronavirus (COVID-19) Update: FDA Authorizes Monoclonal Antibodies for Treatment of COVID-19, U.S. FOOD & DRUG ADMINISTRATION.

Fehrenbach H, Wagner C and Wegmann M (2017) Airway remodeling in asthma: what really matters. *Cell Tissue Res* **367**:551-569.

Feldman MB, Wood M, Lapey A and Mou H (2019) SMAD Signaling Restricts Mucous Cell Differentiation in Human Airway Epithelium. *Am J Respir Cell Mol Biol* **61**:322-331.

Felix JP, Williams BS, Priest BT, Brochu RM, Dick IE, Warren VA, Yan L, Slaughter RS, Kaczorowski GJ, Smith MM and Garcia ML (2004) Functional Assay of Voltage-Gated Sodium Channels Using Membrane Potential-Sensitive Dyes. *Assay and drug development technologies* **2**:260-268.

Feng X, Degese MS, Iglesias-Bartolome R, Vaque JP, Molinolo AA, Rodrigues M, Zaidi MR, Ksander BR, Merlino G, Sodhi A, Chen Q and Gutkind JS (2014) Hippo-independent activation of YAP by the GNAQ uveal melanoma oncogene through a trio-regulated rho GTPase signaling circuitry. *Cancer Cell* **25**:831-845.

Fernandes DJ, Bonacci JV and Stewart AG (2006) Extracellular matrix, integrins, and mesenchymal cell function in the airways. *Curr Drug Targets* **7**:567-577.

Finney LJ, Glanville N, Farne H, Aniscenko J, Fenwick P, Kemp SV, Trujillo-Torralbo MB, Loo SL, Calderazzo MA, Wedzicha JA, Mallia P, Bartlett NW, Johnston SL and Singanayagam A (2021) Inhaled corticosteroids downregulate the SARS-CoV-2 receptor ACE2 in COPD through suppression of type I interferon. *J Allergy Clin Immunol* **147**:510-519 e515.

Fischer-Friedrich E, Hyman AA, Jülicher F, Müller DJ and Helenius J (2014) Quantification of surface tension and internal pressure generated by single mitotic cells. *Scientific Reports* **4**:6213.

Foster CT, Gualdrini F and Treisman R (2017) Mutual dependence of the MRTF-SRF and YAP-TEAD pathways in cancer-associated fibroblasts is indirect and mediated by cytoskeletal dynamics. *Genes Dev* **31**:2361-2375.

Frank J, Roux J, Kawakatsu H, Su G, Dagenais A, Berthiaume Y, Howard M, Canessa CM, Fang X, Sheppard D, Matthay MA and Pittet JF (2003) Transforming growth factor-beta1 decreases expression of the epithelial sodium channel alphaENaC and alveolar epithelial vectorial sodium and fluid transport via an ERK1/2-dependent mechanism. *J Biol Chem* **278**:43939-43950.

Freedman BS, Brooks CR, Lam AQ, Fu H, Morizane R, Agrawal V, Saad AF, Li MK, Hughes MR and Vander Werff R (2015) Modelling kidney disease with CRISPR-mutant kidney organoids derived from human pluripotent epiblast spheroids. *Nature communications* **6**:1-13.

Fuchs S, Hollins AJ, Laue M, Schaefer UF, Roemer K, Gumbleton M and Lehr CM (2003) Differentiation of human alveolar epithelial cells in primary culture: morphological characterization and synthesis of caveolin-1 and surfactant protein-C. *Cell Tissue Res* **311**:31-45.

Fujita J (1999) Cold shock response in mammalian cells. *J Mol Microbiol Biotechnol* **1**:243-255.

Fulcher ML, Gabriel S, Burns KA, Yankaskas JR and Randell SH (2005) Well-differentiated human airway epithelial cell cultures. *Methods Mol Med* **107**:183-206.

Fung Y-c (1993) *Biomechanics: mechanical properties of living tissues*, Springer Science & Business Media.

Fustin JM, Li M, Gao B, Chen Q, Cheng T and Stewart AG (2019) Rhythm on a chip: circadian entrainment in vitro is the next frontier in body-on-a chip technology. *Curr Opin Pharmacol* **48**:127-136.

Gagliardo R, Chanez P, Gjomarkaj M, La Grutta S, Bonanno A, Montalbano AM, Di Sano C, Albano GD, Gras D, Anzalone G, Riccobono L and Profita M (2013) The role of transforming growth factor-β1 in airway inflammation of childhood asthma. *Int J Immunopathol Pharmacol* **26**:725-738.

Garty H and Palmer LG (1997) Epithelial sodium channels: function, structure, and regulation. *Physiol Rev* **77**:359-396.

Geiser M, Jeannet N, Fierz M and Burtscher H (2017) Evaluating Adverse Effects of Inhaled Nanoparticles by Realistic In Vitro Technology. *Nanomaterials (Basel)* **7**.

Gentzsch M, Boyles SE, Cheluvaraju C, Chaudhry IG, Quinney NL, Cho C, Dang H, Liu X, Schlegel R and Randell SH (2016) Pharmacological Rescue of Conditionally Reprogrammed Cystic Fibrosis Bronchial Epithelial Cells. *American Journal of Respiratory Cell and Molecular Biology* **56**:568-574.

Ghosh AK and Vaughan DE (2012) PAI‐1 in tissue fibrosis. *Journal of cellular physiology* **227**:493-507.

Gianotti A, Delpiano L and Caci E (2018) In vitro Methods for the Development and Analysis of Human Primary Airway Epithelia. *Frontiers in pharmacology* **9**:1176-1176.

Gibbs JE, Beesley S, Plumb J, Singh D, Farrow S, Ray DW and Loudon AS (2009) Circadian timing in the lung; a specific role for bronchiolar epithelial cells. *Endocrinology* **150**:268-276.

Gillespie PG and Walker RG (2001) Molecular basis of mechanosensory transduction. *Nature* **413**:194-202.

Gimenez A, Duch P, Puig M, Gabasa M, Xaubet A and Alcaraz J (2017) Dysregulated Collagen Homeostasis by Matrix Stiffening and TGF-beta1 in Fibroblasts from Idiopathic Pulmonary Fibrosis Patients: Role of FAK/Akt. *Int J Mol Sci* **18**.

GINA (2020) Global Strategy for Asthma Management and Prevention, 2020, Global Initiative for Asthma.

Gindele JA, Kiechle T, Benediktus K, Birk G, Brendel M, Heinemann F, Wohnhaas CT, LeBlanc M, Zhang H, Strulovici-Barel Y, Crystal RG, Thomas MJ, Stierstorfer B, Quast K and Schymeinsky J (2020) Intermittent exposure to whole cigarette smoke alters the differentiation of primary small airway epithelial cells in the air-liquid interface culture. *Scientific Reports* **10**:6257.

Giraldez T, Rojas P, Jou J, Flores C and Alvarez de la Rosa D (2012) The epithelial sodium channel δ-subunit: new notes for an old song. *American Journal of Physiology-Renal Physiology* **303**:F328-F338.

Gjorevski N, Sachs N, Manfrin A, Giger S, Bragina ME, Ordonez-Moran P, Clevers H and Lutolf MP (2016) Designer matrices for intestinal stem cell and organoid culture. *Nature* **539**:560-564.

GOLD (2020) Global strategy for the diagnosis, management, and prevention of chronic obstructive pulmonary disease 2020 report, Global Initiative for Chronic Obstructive Lung Disease.

Gomi K, Arbelaez V, Crystal RG and Walters MS (2015) Activation of NOTCH1 or NOTCH3 signaling skews human airway basal cell differentiation toward a secretory pathway. *PloS one* **10**:e0116507-e0116507.

Goss BC, McGee KP, Ehman EC, Manduca A and Ehman RL (2006) Magnetic resonance elastography of the lung: technical feasibility. *Magnetic resonance in medicine* **56**:1060-1066.

Graham A, Hasani A, Alton EW, Martin GP, Marriott C, Hodson ME, Clarke SW and Geddes DM (1993) No added benefit from nebulized amiloride in patients with cystic fibrosis. *Eur Respir J* **6**:1243-1248.

Grainger CI, Greenwell LL, Lockley DJ, Martin GP and Forbes B (2006) Culture of Calu-3 cells at the air interface provides a representative model of the airway epithelial barrier. *Pharm Res* **23**:1482-1490.

Gras D, Chanez P, Vachier I, Petit A and Bourdin A (2013) Bronchial epithelium as a target for innovative treatments in asthma. *Pharmacol Ther* **140**:290-305.

Graul AI, Dulsat C, Pina P, Cruces E and Tracy M (2019) The year's new drugs and biologics 2018: Part II - News that shaped the industry in 2018. *Drugs Today (Barc)* **55**:131-160.

Graul AI, Dulsat C, Pina P, Tracy M and D'Souza P (2018) The year's new drugs & biologics, 2017, part II - News that shaped the industry in 2017. *Drugs Today (Barc)* **54**:137-167.

Graul AI, Dulsat C, Tracy M and Cruces E (2017) The year's new drugs & biologics 2016: Part II - Trends and highlights of an unforgettable year. *Drugs Today (Barc)* **53**:117-158.

Graul AI, Pina P, Tracy M and Sorbera L (2020) The year's new drugs and biologics 2019. *Drugs of Today (Barcelona, Spain: 1998)* **56**:47-103.

Graul AI and Sorbera LA (2021) The year's new drugs and biologics 2020. *Drugs of Today (Barcelona, Spain: 1998)* **57**:101-177.

Gray TE, Guzman K, Davis CW, Abdullah LH and Nettesheim P (1996) Mucociliary differentiation of serially passaged normal human tracheobronchial epithelial cells. *Am J Respir Cell Mol Biol* **14**:104-112.

Greenburg G and Hay ED (1982) Epithelia suspended in collagen gels can lose polarity and express characteristics of migrating mesenchymal cells. *J Cell Biol* **95**:333-339.

Group RC, Horby P, Lim WS, Emberson JR, Mafham M, Bell JL, Linsell L, Staplin N, Brightling C, Ustianowski A, Elmahi E, Prudon B, Green C, Felton T, Chadwick D, Rege K, Fegan C, Chappell LC, Faust SN, Jaki T, Jeffery K, Montgomery A, Rowan K, Juszczak E, Baillie JK, Haynes R and Landray MJ (2021) Dexamethasone in Hospitalized Patients with Covid-19. *N Engl J Med* **384**:693-704.

Gudas LJ and Wagner JA (2011) Retinoids regulate stem cell differentiation. *Journal of cellular physiology* **226**:322-330.

Gumz ML, Cheng KY, Lynch IJ, Stow LR, Greenlee MM, Cain BD and Wingo CS (2010) Regulation of alphaENaC expression by the circadian clock protein Period 1 in mpkCCD(c14) cells. *Biochim Biophys Acta* **1799**:622-629.

Gumz ML, Stow LR, Lynch IJ, Greenlee MM, Rudin A, Cain BD, Weaver DR and Wingo CS (2009) The circadian clock protein Period 1 regulates expression of the renal epithelial sodium channel in mice. *J Clin Invest* **119**:2423-2434.

Gunst JD, Staerke NB, Pahus MH, Kristensen LH, Bodilsen J, Lohse N, Dalgaard LS, Brønnum D, Fröbert O, Hønge B, Johansen IS, Monrad I, Erikstrup C, Rosendal R, Vilstrup E, Mariager T, Bove DG, Offersen R, Shakar S, Cajander S, Jørgensen NP, Sritharan SS, Breining P, Jespersen S, Mortensen KL, Jensen ML, Kolte L, Frattari GS, Larsen CS, Storgaard M, Nielsen LP, Tolstrup M, Sædder EA, Østergaard LJ, Ngo HTT, Jensen MH, Højen JF, Kjolby M and Søgaard OS (2021) Efficacy of the TMPRSS2 inhibitor camostat mesilate in patients hospitalized with Covid-19-a double-blind randomized controlled trial. *EClinicalMedicine*.

Ha EV and Rogers DF (2016) Novel Therapies to Inhibit Mucus Synthesis and Secretion in Airway Hypersecretory Diseases. *Pharmacology* **97**:84-100.

Hackett TL, Shaheen F, Johnson A, Wadsworth S, Pechkovsky DV, Jacoby DB, Kicic A, Stick SM and Knight DA (2008) Characterization of side population cells from human airway epithelium. *Stem cells (Dayton, Ohio)* **26**:2576-2585.

Haghi M, Young PM, Traini D, Jaiswal R, Gong J and Bebawy M (2010) Time- and passage-dependent characteristics of a Calu-3 respiratory epithelial cell model. *Drug Development and Industrial Pharmacy* **36**:1207-1214.

Hajj R, Baranek T, Le Naour R, Lesimple P, Puchelle E and Coraux C (2007) Basal cells of the human adult airway surface epithelium retain transit-amplifying cell properties. *Stem cells (Dayton, Ohio)* **25**:139-148.

Halder G, Dupont S and Piccolo S (2012) Transduction of mechanical and cytoskeletal cues by YAP and TAZ. *Nat Rev Mol Cell Biol* **13**:591-600.

Halwani R, Al-Muhsen S, Al-Jahdali H and Hamid Q (2011) Role of transforming growth factor-beta in airway remodeling in asthma. *Am J Respir Cell Mol Biol* **44**:127-133.

Han Y, Duan X, Yang L, Nilsson-Payant BE, Wang P, Duan F, Tang X, Yaron TM, Zhang T, Uhl S, Bram Y, Richardson C, Zhu J, Zhao Z, Redmond D, Houghton S, Nguyen DT, Xu D, Wang X, Jessurun J, Borczuk A, Huang Y, Johnson JL, Liu Y, Xiang J, Wang H, Cantley LC, tenOever BR, Ho DD, Pan FC, Evans T, Chen HJ, Schwartz RE and Chen S (2021) Identification of SARS-CoV-2 inhibitors using lung and colonic organoids. *Nature* **589**:270-275.

Haque A, Engel J, Teichmann SA and Lönnberg T (2017) A practical guide to single-cell RNA-sequencing for biomedical research and clinical applications. *Genome Medicine* **9**:75.

Hardie WD, Glasser SW and Hagood JS (2009) Emerging concepts in the pathogenesis of lung fibrosis. *Am J Pathol* **175**:3-16.

Harris WT, Muhlebach MS, Oster RA, Knowles MR, Clancy JP and Noah TL (2011) Plasma TGF-β_1 in pediatric cystic fibrosis: potential biomarker of lung disease and response to therapy. *Pediatr Pulmonol* **46**:688-695.

Harris WT, Muhlebach MS, Oster RA, Knowles MR and Noah TL (2009) Transforming growth factor-beta(1) in bronchoalveolar lavage fluid from children with cystic fibrosis. *Pediatr Pulmonol* **44**:1057-1064.

Harrison RG, Greenman M, Mall FP and Jackson C (1907) Observations of the living developing nerve fiber. *The Anatomical Record* **1**:116-128.

Harrison RK (2016) Phase II and phase III failures: 2013-2015. *Nature reviews Drug discovery* **15**:817-818.

Harutyunyan M, Huang Y, Mun K-S, Yang F, Arora K and Naren AP (2018) Personalized medicine in CF: from modulator development to therapy for cystic fibrosis patients with rare CFTR mutations. *American journal of physiology Lung cellular and molecular physiology* **314**:L529-L543.

Hewitt RJ and Lloyd CM (2021) Regulation of immune responses by the airway epithelial cell landscape. *Nat Rev Immunol*:1-16.

Hikmet F, Mear L, Edvinsson A, Micke P, Uhlen M and Lindskog C (2020) The protein expression profile of ACE2 in human tissues. *Mol Syst Biol* **16**:e9610.

Hild M and Jaffe AB (2016) Production of 3-D Airway Organoids From Primary Human Airway Basal Cells and Their Use in High-Throughput Screening. *Current protocols in stem cell biology* **37**:IE 9 1-IE 9 15.

Hillyer P, Shepard R, Uehling M, Krenz M, Sheikh F, Thayer KR, Huang L, Yan L, Panda D, Luongo C, Buchholz UJ, Collins PL, Donnelly RP and Rabin RL (2018) Differential Responses by Human Respiratory Epithelial Cell Lines to Respiratory Syncytial Virus Reflect Distinct Patterns of Infection Control. *J Virol* **92**.

Hinz B (2015) The extracellular matrix and transforming growth factor-beta1: Tale of a strained relationship. *Matrix Biol* **47**:54-65.

Hirsh AJ, Sabater JR, Zamurs A, Smith RT, Paradiso AM, Hopkins S, Abraham WM and Boucher RC (2004) Evaluation of second generation amiloride analogs as therapy for cystic fibrosis lung disease. *J Pharmacol Exp Ther* **311**:929-938.

Hirst SJ, Martin JG, Bonacci JV, Chan V, Fixman ED, Hamid QA, Herszberg B, Lavoie JP, McVicker CG, Moir LM, Nguyen TT, Peng Q, Ramos-Barbon D and Stewart AG (2004) Proliferative aspects of airway smooth muscle. *J Allergy Clin Immunol* **114**:S2-17.

Hobbs CA, Blanchard MG, Alijevic O, Tan CD, Kellenberger S, Bencharit S, Cao R, Kesimer M, Walton WG, Henderson AG, Redinbo MR, Stutts MJ and Tarran R (2013) Identification of the SPLUNC1 ENaC-inhibitory domain yields novel strategies to treat sodium hyperabsorption in cystic fibrosis airway epithelial cultures. *Am J Physiol Lung Cell Mol Physiol* **305**:L990-l1001.

Hoffmann K, Berger H, Kulbe H, Thillainadarasan S, Mollenkopf HJ, Zemojtel T, Taube E, Darb‐Esfahani S, Mangler M and Sehouli J (2020a) Stable expansion of high‐grade serous ovarian cancer organoids requires a low‐Wnt environment. *The EMBO journal* **39**:e104013.

Hoffmann M, Hofmann-Winkler H, Smith JC, Kruger N, Arora P, Sorensen LK, Sogaard OS, Hasselstrom JB, Winkler M, Hempel T, Raich L, Olsson S, Danov O, Jonigk D, Yamazoe T, Yamatsuta K, Mizuno H, Ludwig S, Noe F, Kjolby M, Braun A, Sheltzer JM and Pohlmann S (2021) Camostat mesylate inhibits SARS-CoV-2 activation by TMPRSS2-related proteases and its metabolite GBPA exerts antiviral activity. *EBioMedicine* **65**:103255.

Hoffmann M, Kleine-Weber H, Schroeder S, Kruger N, Herrler T, Erichsen S, Schiergens TS, Herrler G, Wu NH, Nitsche A, Muller MA, Drosten C and Pohlmann S (2020b) SARS-CoV-2 Cell Entry Depends on ACE2 and TMPRSS2 and Is Blocked by a Clinically Proven Protease Inhibitor. *Cell* **181**:271-280 e278.

Hofmann H, Pyrc K, van der Hoek L, Geier M, Berkhout B and Pöhlmann S (2005) Human coronavirus NL63 employs the severe acute respiratory syndrome coronavirus receptor for cellular entry. *Proc Natl Acad Sci U S A* **102**:7988-7993.

Hojyo S, Uchida M, Tanaka K, Hasebe R, Tanaka Y, Murakami M and Hirano T (2020) How COVID-19 induces cytokine storm with high mortality. *Inflamm Regen* **40**:37.

Holguin F, Cardet JC, Chung KF, Diver S, Ferreira DS, Fitzpatrick A, Gaga M, Kellermeyer L, Khurana S, Knight S, McDonald VM, Morgan RL, Ortega VE, Rigau D, Subbarao P, Tonia T, Adcock IM, Bleecker ER, Brightling C, Boulet L-P, Cabana M, Castro M, Chanez P, Custovic A, Djukanovic R, Frey U, Frankemolle B, Gibson P, Hamerlijnck D, Jarjour N, Konno S, Shen H, Vitary C and Bush A (2019) Management of Severe

Asthma: a European Respiratory Society/American Thoracic Society Guideline. *European Respiratory Journal*:1900588.

Horani A, Nath A, Wasserman MG, Huang T and Brody SL (2013) Rho-associated protein kinase inhibition enhances airway epithelial Basal-cell proliferation and lentivirus transduction. *American journal of respiratory cell and molecular biology* **49**:341-347.

Hoshino M, Takahashi M, Takai Y, Sim J and Aoike N (2001) Inhaled corticosteroids decrease vascularity of the bronchial mucosa in patients with asthma. *Clin Exp Allergy* **31**:722-730.

Hotary K, Allen E, Punturieri A, Yana I and Weiss SJ (2000) Regulation of cell invasion and morphogenesis in a three-dimensional type I collagen matrix by membrane-type matrix metalloproteinases 1, 2, and 3. *The Journal of cell biology* **149**:1309-1323.

Howat WJ, Barabás T, Holmes JA, Holgate ST and Lackie PM (2002) Distribution of basement membrane pores in bronchus revealed by microscopy following epithelial removal. *Journal of Structural Biology* **139**:137-145.

Howat WJ, Holmes JA, Holgate ST and Lackie PM (2001) Basement membrane pores in human bronchial epithelium: a conduit for infiltrating cells? *Am J Pathol* **158**:673-680.

Huang G, Li F, Zhao X, Ma Y, Li Y, Lin M, Jin G, Lu TJ, Genin GM and Xu F (2017) Functional and Biomimetic Materials for Engineering of the Three-Dimensional Cell Microenvironment. *Chem Rev* **117**:12764-12850.

Huang J, Hume AJ, Abo KM, Werder RB, Villacorta-Martin C, Alysandratos KD, Beermann ML, Simone-Roach C, Lindstrom-Vautrin J, Olejnik J, Suder EL, Bullitt E, Hinds A, Sharma A, Bosmann M, Wang R, Hawkins F, Burks EJ, Saeed M, Wilson AA, Muhlberger E and Kotton DN (2020a) SARS-CoV-2 Infection of Pluripotent Stem Cell-Derived Human Lung Alveolar Type 2 Cells Elicits a Rapid Epithelial-Intrinsic Inflammatory Response. *Cell Stem Cell* **27**:962-973 e967.

Huang J, Lam H, Koziol-White C, Limjunyawong N, Kim D, Kim N, Karmacharya N, Rajkumar P, Firer D, Dalesio NM, Jude J, Kurten RC, Pluznick JL, Deshpande DA, Penn RB, Liggett SB, Panettieri RA, Jr., Dong X and An SS (2020b) The odorant receptor OR2W3 on airway smooth muscle evokes bronchodilation via a cooperative chemosensory tradeoff between TMEM16A and CFTR. *Proc Natl Acad Sci U S A* **117**:28485-28495.

Huang J, Olivenstein R, Taha R, Hamid Q and Ludwig M (1999) Enhanced proteoglycan deposition in the airway wall of atopic asthmatics. *American journal of respiratory and critical care medicine* **160**:725-729.

Huang SX, Islam MN, O'Neill J, Hu Z, Yang YG, Chen YW, Mumau M, Green MD, Vunjak-Novakovic G, Bhattacharya J and Snoeck HW (2014) Efficient generation of lung and airway epithelial cells from human pluripotent stem cells. *Nat Biotechnol* **32**:84-91.

Huang W-T, Vayalil PK, Miyata T, Hagood J and Liu R-M (2012a) Therapeutic Value of Small Molecule Inhibitor to Plasminogen Activator Inhibitor–1 for Lung Fibrosis. *American journal of respiratory cell and molecular biology* **46**:87-95.

Huang X, Yang N, Fiore VF, Barker TH, Sun Y, Morris SW, Ding Q, Thannickal VJ and Zhou Y (2012b) Matrix stiffness-induced myofibroblast differentiation is mediated by intrinsic mechanotransduction. *Am J Respir Cell Mol Biol* **47**:340-348.

Hubert CG, Rivera M, Spangler LC, Wu Q, Mack SC, Prager BC, Couce M, McLendon RE, Sloan AE and Rich JN (2016) A three-dimensional organoid culture system derived from human glioblastomas recapitulates the hypoxic gradients and cancer stem cell heterogeneity of tumors found in vivo. *Cancer research* **76**:2465-2477.

Hughey RP, Bruns JB, Kinlough CL, Harkleroad KL, Tong Q, Carattino MD, Johnson JP, Stockand JD and Kleyman TR (2004) Epithelial sodium channels are activated by furin-dependent proteolysis. *J Biol Chem* **279**:18111-18114.

Huh D, Fujioka H, Tung Y-C, Futai N, Paine R, 3rd, Grotberg JB and Takayama S (2007) Acoustically detectable cellular-level lung injury induced by fluid mechanical stresses in microfluidic airway systems. *Proceedings of the National Academy of Sciences of the United States of America* **104**:18886-18891.

Huh D, Matthews BD, Mammoto A, Montoya-Zavala M, Hsin HY and Ingber DE (2010) Reconstituting organ-level lung functions on a chip. *Science* **328**:1662-1668.

Hummler E, Barker P, Gatzy J, Beermann F, Verdumo C, Schmidt A, Boucher R and Rossier BC (1996) Early death due to defective neonatal lung liquid clearance in αENaC-deficient mice. *Nature Genetics* **12**:325-328.

Hung IF-N, Lung K-C, Tso EY-K, Liu R, Chung TW-H, Chu M-Y, Ng Y-Y, Lo J, Chan J, Tam AR, Shum H-P, Chan V, Wu AK-L, Sin K-M, Leung W-S, Law W-L, Lung DC, Sin S, Yeung P, Yip CC-Y, Zhang RR, Fung AY-F, Yan EY-W, Leung K-H, Ip JD, Chu AW-H, Chan W-M, Ng AC-K, Lee R, Fung K, Yeung A, Wu T-C, Chan JW-M, Yan W-W, Chan W-M, Chan JF-W, Lie AK-W, Tsang OT-Y, Cheng VC-C, Que T-L, Lau C-S, Chan K-H, To KK-W and Yuen K-Y (2020) Triple combination of interferon beta-1b, lopinavir–ritonavir, and ribavirin in the treatment of patients admitted to hospital with COVID-19: an open-label, randomised, phase 2 trial. *The Lancet* **395**:1695-1704.

Hunt L, Hacker DL, Grosjean F, De Jesus M, Uebersax L, Jordan M and Wurm FM (2005) Low-temperature pausing of cultivated mammalian cells. *Biotechnol Bioeng* **89**:157-163.

Inman GJ, Nicolás FJ, Callahan JF, Harling JD, Gaster LM, Reith AD, Laping NJ and Hill CS (2002) SB-431542 is a potent and specific inhibitor of transforming growth factor-β superfamily type I activin receptor-like kinase (ALK) receptors ALK4, ALK5, and ALK7. *Molecular pharmacology* **62**:65-74.

Ioannidis I, Ye F, McNally B, Willette M and Flano E (2013) Toll-like receptor expression and induction of type I and type III interferons in primary airway epithelial cells. *J Virol* **87**:3261-3270.

Isaacs C, Robert NJ, Bailey FA, Schuster MW, Overmoyer B, Graham M, Cai B, Beach KJ, Loewy JW and Kaye JA (1997) Randomized placebo-controlled study of recombinant human interleukin-11 to prevent chemotherapy-induced thrombocytopenia in patients with breast cancer receiving dose-intensive cyclophosphamide and doxorubicin. *Journal of Clinical Oncology* **15**:3368-3377.

Itani OA, Chen JH, Karp PH, Ernst S, Keshavjee S, Parekh K, Klesney-Tait J, Zabner J and Welsh MJ (2011) Human cystic fibrosis airway epithelia have reduced Cl- conductance but not increased Na+ conductance. *Proc Natl Acad Sci U S A* **108**:10260-10265.

Iwasaki A, Foxman EF and Molony RD (2017) Early local immune defences in the respiratory tract. *Nat Rev Immunol* **17**:7-20.

James AL, Elliot JG, Jones RL, Carroll ML, Mauad T, Bai TR, Abramson MJ, McKay KO and Green FH (2012) Airway smooth muscle hypertrophy and hyperplasia in asthma. *American journal of respiratory and critical care medicine* **185**:1058-1064.

Jansen KA, Atherton P and Ballestrem C (2017) Mechanotransduction at the cell-matrix interface. *Semin Cell Dev Biol* **71**:75-83.

Jasti J, Furukawa H, Gonzales EB and Gouaux E (2007) Structure of acid-sensing ion channel 1 at 1.9 A resolution and low pH. *Nature* **449**:316-323.

Jayaraman S, Song Y, Vetrivel L, Shankar L and Verkman AS (2001) Noninvasive in vivo fluorescence measurement of airway-surface liquid depth, salt concentration, and pH. *The Journal of Clinical Investigation* **107**:317-324.

Jeffery KP, Gizycki JM and Rogers VA (1997) Airway wall structure, in *Allergy and Allergic Diseases: The New Mechanisms and Therapeutics* (Denburg JA ed), Humana Press Inc., Human Press.

Jeffery PK (2004) Remodeling and inflammation of bronchi in asthma and chronic obstructive pulmonary disease. *Proc Am Thorac Soc* **1**:176-183.

Jeffery PK and Haahtela T (2006) Allergic rhinitis and asthma: inflammation in a one-airway condition. *BMC Pulmonary Medicine* **6**:S5.

Jia HP, Look DC, Shi L, Hickey M, Pewe L, Netland J, Farzan M, Wohlford-Lenane C, Perlman S and McCray PB, Jr. (2005) ACE2 receptor expression and severe acute respiratory syndrome coronavirus infection depend on differentiation of human airway epithelia. *J Virol* **79**:14614-14621.

Jia HP, Look DC, Tan P, Shi L, Hickey M, Gakhar L, Chappell MC, Wohlford-Lenane C and McCray PB, Jr. (2009) Ectodomain shedding of angiotensin converting enzyme 2 in human airway epithelia. *Am J Physiol Lung Cell Mol Physiol* **297**:L84-96.

Jin B-J, Battula S, Zachos N, Kovbasnjuk O, Fawlke-Abel J, In J, Donowitz M and Verkman AS (2014) Microfluidics platform for measurement of volume changes in immobilized intestinal enteroids. *Biomicrofluidics* **8**:024106.

Jin Y, Kim J, Lee JS, Min S, Kim S, Ahn D-H, Kim Y-G and Cho S-W (2018) Vascularized Liver Organoids Generated Using Induced Hepatic Tissue and Dynamic Liver-Specific Microenvironment as a Drug Testing Platform. *Advanced Functional Materials* **28**.

Johnson LA, Rodansky ES, Haak AJ, Larsen SD, Neubig RR and Higgins PD (2013) Novel Rho/MRTF/SRF inhibitors block matrix-stiffness and TGF-β–induced fibrogenesis in human colonic myofibroblasts. *Inflammatory bowel diseases* **20**:154-165.

Johnson PR, Black JL, Carlin S, Ge Q and Underwood PA (2000) The production of extracellular matrix proteins by human passively sensitized airway smooth-muscle cells in culture: the effect of beclomethasone. *Am J Respir Crit Care Med* **162**:2145-2151.

Jones RL, Noble PB, Elliot JG and James AL (2016) Airway remodelling in COPD: It's not asthma! *Respirology (Carlton, Vic)* **21**:1347-1356.

Jonsdottir HR and Dijkman R (2016) Coronaviruses and the human airway: a universal system for virus-host interaction studies. *Virol J* **13**:24.

Joubert P and Hamid Q (2005) Role of airway smooth muscle in airway remodeling. *J Allergy Clin Immunol* **116**:713-716.

Kashlan OB, Adelman JL, Okumura S, Blobner BM, Zuzek Z, Hughey RP, Kleyman TR and Grabe M (2011) Constraint-based, homology model of the extracellular domain of the epithelial Na+ channel α subunit reveals a mechanism of channel activation by proteases. *J Biol Chem* **286**:649-660.

Keenan CR, Langenbach SY, Jativa F, Harris T, Li M, Chen Q, Xia Y, Gao B, Schuliga MJ, Jaffar J, Prodanovic D, Tu Y, Berhan A, Lee PVS, Westall GP and Stewart AG (2018) Casein Kinase 1delta/epsilon Inhibitor, PF670462 Attenuates the Fibrogenic Effects of Transforming Growth Factor-beta in Pulmonary Fibrosis. *Front Pharmacol* **9**:738.

Keenan CR, Mok JS, Harris T, Xia Y, Salem S and Stewart AG (2014) Bronchial epithelial cells are rendered insensitive to glucocorticoid transactivation by transforming growth factor-beta1. *Respir Res* **15**:55.

Keenan CR, Radojicic D, Li M, Radwan A and Stewart AG (2015) Heterogeneity in mechanisms influencing glucocorticoid sensitivity: the need for a systems biology approach to treatment of glucocorticoid-resistant inflammation. *Pharmacol Ther* **150**:81-93.

Keenan CR, Salem S, Fietz ER, Gualano RC and Stewart AG (2012) Glucocorticoid-resistant asthma and novel anti-inflammatory drugs. *Drug Discov Today* **17**:1031-1038.

Keeratichamroen S, Lirdprapamongkol K and Svasti J (2018) Mechanism of ECM-induced dormancy and chemoresistance in A549 human lung carcinoma cells. *Oncology reports* **39**:1765-1774.

Kessler M, Hoffmann K, Brinkmann V, Thieck O, Jackisch S, Toelle B, Berger H, Mollenkopf H-J, Mangler M and Sehouli J (2015) The Notch and Wnt pathways regulate stemness and differentiation in human fallopian tube organoids. *Nature communications* **6**:1-11.

Khan MA, Ellis R, Inman MD, Bates JH, Sanderson MJ and Janssen LJ (2010) Influence of airway wall stiffness and parenchymal tethering on the dynamics of bronchoconstriction. *Am J Physiol Lung Cell Mol Physiol* **299**:L98-l108.

Kılıç A, Ameli A, Park J-A, Kho AT, Tantisira K, Santolini M, Cheng F, Mitchel JA, McGill M, O'Sullivan MJ, De Marzio M, Sharma A, Randell SH, Drazen JM, Fredberg JJ and Weiss ST (2020) Mechanical forces induce an asthma gene signature in healthy airway epithelial cells. *Scientific Reports* **10**:966.

Kim JY, Sajjan US, Krasan GP and LiPuma JJ (2005) Disruption of tight junctions during traversal of the respiratory epithelium by Burkholderia cenocepacia. *Infect Immun* **73**:7107-7112.

Kim KK, Kugler MC, Wolters PJ, Robillard L, Galvez MG, Brumwell AN, Sheppard D and Chapman HA (2006) Alveolar epithelial cell mesenchymal transition develops in vivo during pulmonary fibrosis and is regulated by the extracellular matrix. *Proc Natl Acad Sci U S A* **103**:13180-13185.

Kim T, Hwang D, Lee D, Kim JH, Kim SY and Lim DS (2017) MRTF potentiates TEAD-YAP transcriptional activity causing metastasis. *EMBO J* **36**:520-535.

Kirby TJ and Lammerding J (2018) Emerging views of the nucleus as a cellular mechanosensor. *Nat Cell Biol* **20**:373-381.

Kleinman HK, McGarvey ML, Hassell JR, Star VL, Cannon FB, Laurie GW and Martin GR (1986) Basement membrane complexes with biological activity. *Biochemistry* **25**:312-318.

Kleinman HK, McGarvey ML, Liotta LA, Robey PG, Tryggvason K and Martin GR (1982) Isolation and characterization of type IV procollagen, laminin, and heparan sulfate proteoglycan from the EHS sarcoma. *Biochemistry* **21**:6188-6193.

Kleyman TR, Carattino MD and Hughey RP (2009) ENaC at the cutting edge: regulation of epithelial sodium channels by proteases. *J Biol Chem* **284**:20447-20451.

Knight DA and Holgate ST (2003) The airway epithelium: structural and functional properties in health and disease. *Respirology (Carlton, Vic)* **8**:432-446.

Knowles MR, Church NL, Waltner WE, Yankaskas JR, Gilligan P, King M, Edwards LJ, Helms RW and Boucher RC (1990) A pilot study of aerosolized amiloride for the treatment of lung disease in cystic fibrosis. *N Engl J Med* **322**:1189-1194.

Koblinski JE, Wu M, Demeler B, Jacob K and Kleinman HK (2005) Matrix cell adhesion activation by non-adhesion proteins. *Journal of cell science* **118**:2965-2974.

Kohri K, Ueki IF, Shim JJ, Burgel PR, Oh YM, Tam DC, Dao-Pick T and Nadel JA (2002) Pseudomonas aeruginosa induces MUC5AC production via epidermal growth factor receptor. *Eur Respir J* **20**:1263-1270.

Kong X-B, Ma H-G, Li H-G and Xiong C-L (2009) Blockade of epithelial sodium channels improves sperm motility in asthenospermia patients. *International Journal of Andrology* **32**:330-336.

Konishi S, Gotoh S, Tateishi K, Yamamoto Y, Korogi Y, Nagasaki T, Matsumoto H, Muro S, Hirai T, Ito I, Tsukita S and Mishima M (2016) Directed Induction of Functional Multi-ciliated Cells in Proximal Airway Epithelial Spheroids from Human Pluripotent Stem Cells. *Stem Cell Reports* **6**:18-25.

Konstas A-A, Mavrelos D and Korbmacher C (2000) Conservation of pH sensitivity in the epithelial sodium channel (ENaC) with Liddle's syndrome mutation. *Pflügers Archiv* **441**:341-350.

Kramer EL and Clancy JP (2018) TGFbeta as a therapeutic target in cystic fibrosis. *Expert Opin Ther Targets* **22**:177-189.

Kreft ME, Jerman UD, Lasič E, Hevir-Kene N, Rižner TL, Peternel L and Kristan K (2015) The characterization of the human cell line Calu-3 under different culture conditions and its use as an optimized in vitro model to investigate bronchial epithelial function. *European Journal of Pharmaceutical Sciences* **69**:1-9.

Krishnan R, Park JA, Seow CY, Lee PV and Stewart AG (2016) Cellular Biomechanics in Drug Screening and Evaluation: Mechanopharmacology. *Trends Pharmacol Sci* **37**:87-100.

Kuek LE, Griffin P, Martinello P, Graham AN, Kalitsis P, Robinson PJ and Mackay GA (2018) Identification of an Immortalized Human Airway Epithelial Cell Line with Dyskinetic Cilia. *Am J Respir Cell Mol Biol* **59**:375-382.

Kuhn JH, Li W, Choe H and Farzan M (2004) Angiotensin-converting enzyme 2: a functional receptor for SARS coronavirus. *Cellular and molecular life sciences : CMLS* **61**:2738-2743.

Kuo JC (2014) Focal adhesions function as a mechanosensor. *Prog Mol Biol Transl Sci* **126**:55-73.

Kuperman DA, Huang X, Koth LL, Chang GH, Dolganov GM, Zhu Z, Elias JA, Sheppard D and Erle DJ (2002) Direct effects of interleukin-13 on epithelial cells cause airway hyperreactivity and mucus overproduction in asthma. *Nature medicine* **8**:885-889.

Lachapelle P, Li M, Douglass J and Stewart A (2018) Safer approaches to therapeutic modulation of TGF-beta signaling for respiratory disease. *Pharmacol Ther* **187**:98-113.

Lamers MM, van der Vaart J, Knoops K, Riesebosch S, Breugem TI, Mykytyn AZ, Beumer J, Schipper D, Bezstarosti K, Koopman CD, Groen N, Ravelli RBG, Duimel HQ, Demmers JAA, Verjans G, Koopmans MPG, Muraro MJ, Peters PJ, Clevers H and Haagmans BL (2020) An organoid-derived bronchioalveolar model for SARS-CoV-2 infection of human alveolar type II-like cells. *EMBO J*:e105912.

Lancaster MA and Knoblich JA (2014) Organogenesis in a dish: modeling development and disease using organoid technologies. *Science* **345**:1247125.

Lancaster MA, Renner M, Martin C-A, Wenzel D, Bicknell LS, Hurles ME, Homfray T, Penninger JM, Jackson AP and Knoblich JA (2013) Cerebral organoids model human brain development and microcephaly. *Nature* **501**:373-379.

Laoukili J, Perret E, Willems T, Minty A, Parthoens E, Houcine O, Coste A, Jorissen M, Marano F and Caput D (2001) IL-13 alters mucociliary differentiation and ciliary beating of human respiratory epithelial cells. *The Journal of clinical investigation* **108**:1817-1824.

Lazarovici P, Lahiani A, Gincberg G, Haham D, Fluksman A, Benny O, Marcinkiewicz C and Lelkes PI (2018) Nerve Growth Factor-Induced Angiogenesis: 1. Endothelial Cell Tube Formation Assay, in *Neurotrophic Factors: Methods and Protocols* (Skaper SD ed) pp 239-250, Springer New York, New York, NY.

LeBleu VS, MacDonald B and Kalluri R (2007) Structure and function of basement membranes. *Experimental biology and medicine* **232**:1121-1129.

Leight JL, Wozniak MA, Chen S, Lynch ML and Chen CS (2012) Matrix rigidity regulates a switch between TGF-β1-induced apoptosis and epithelial-mesenchymal transition. *Mol Biol Cell* **23**:781-791.

Leisman DE, Ronner L, Pinotti R, Taylor MD, Sinha P, Calfee CS, Hirayama AV, Mastroiani F, Turtle CJ, Harhay MO, Legrand M and Deutschman CS (2020) Cytokine elevation in severe and critical COVID-19: a rapid systematic review, meta-analysis, and comparison with other inflammatory syndromes. *Lancet Respir Med* **1**.

Levardon H, Yonker LM, Hurley BP and Mou H (2018) Expansion of Airway Basal Cells and Generation of Polarized Epithelium. *Bio Protoc* **8**.

Li M, Keenan CR, Lopez-Campos G, Mangum JE, Chen Q, Prodanovic D, Xia YC, Langenbach SY, Harris T, Hofferek V, Reid GE and Stewart AG (2019) A Non-canonical Pathway with Potential for Safer Modulation of Transforming Growth Factor-beta1 in Steroid-Resistant Airway Diseases. *iScience* **12**:232-246.

Li MO, Wan YY, Sanjabi S, Robertson AK and Flavell RA (2006) Transforming growth factor-beta regulation of immune responses. *Annu Rev Immunol* **24**:99-146.

Li T and Folkesson HG (2006) RNA interference for α-ENaC inhibits rat lung fluid absorption in vivo. *American Journal of Physiology-Lung Cellular and Molecular Physiology* **290**:L649-L660.

Li X, Xu S, Yu M, Wang K, Tao Y, Zhou Y, Shi J, Zhou M, Wu B, Yang Z, Zhang C, Yue J, Zhang Z, Renz H, Liu X, Xie J, Xie M and Zhao J (2020) Risk factors for severity and mortality in adult COVID-19 inpatients in Wuhan. *J Allergy Clin Immunol* **146**:110-118.

Liang M, Yu M, Xia R, Song K, Wang J, Luo J, Chen G and Cheng J (2017) Yap/Taz Deletion in Gli(+) Cell-Derived Myofibroblasts Attenuates Fibrosis. *Journal of the American Society of Nephrology : JASN* **28**:3278-3290.

Lieber M, Todaro G, Smith B, Szakal A and Nelson-Rees W (1976) A continuous tumor-cell line from a human lung carcinoma with properties of type II alveolar epithelial cells. *International Journal of Cancer* **17**:62-70.

Lin C-C and Anseth KS (2009) PEG Hydrogels for the Controlled Release of Biomolecules in Regenerative Medicine. *Pharmaceutical Research* **26**:631-643.

Lindahl GE, Stock CJ, Shi-Wen X, Leoni P, Sestini P, Howat SL, Bou-Gharios G, Nicholson AG, Denton CP and Grutters JC (2013) Microarray profiling reveals suppressed interferon stimulated gene program in fibroblasts from scleroderma-associated interstitial lung disease. *Respiratory research* **14**:1-14.

Linde-Medina M and Marcucio R (2018) Living tissues are more than cell clusters: The extracellular matrix as a driving force in morphogenesis. *Progress in biophysics and molecular biology* **137**:46-51.

Lingueglia E, Renard S, Voilley N, Waldmann R, Chassande O, Lazdunski M and Barbry P (1993a) Molecular cloning and functional expression of different molecular forms of rat amiloride-binding proteins. *Eur J Biochem* **216**:679-687.

Lingueglia E, Voilley N, Waldmann R, Lazdunski M and Barbry P (1993b) Expression cloning of an epithelial amiloride-sensitive Na+ channel. A new channel type with homologies to Caenorhabditis elegans degenerins. *FEBS Lett* **318**:95-99.

Linnemann JR, Miura H, Meixner LK, Irmler M, Kloos UJ, Hirschi B, Bartsch HS, Sass S, Beckers J and Theis FJ (2015) Quantification of regenerative potential in primary human mammary epithelial cells. *Development* **142**:3239-3251.

Liu F, Lagares D, Choi KM, Stopfer L, Marinkovic A, Vrbanac V, Probst CK, Hiemer SE, Sisson TH, Horowitz JC, Rosas IO, Fredenburgh LE, Feghali-Bostwick C, Varelas X, Tager AM and Tschumperlin DJ (2015) Mechanosignaling through YAP and TAZ drives fibroblast activation and fibrosis. *Am J Physiol Lung Cell Mol Physiol* **308**:L344-357.

Liu F, Mih JD, Shea BS, Kho AT, Sharif AS, Tager AM and Tschumperlin DJ (2010) Feedback amplification of fibrosis through matrix stiffening and COX-2 suppression. *J Cell Biol* **190**:693-706.

Lloyd CM and Marsland BJ (2017) Lung Homeostasis: Influence of Age, Microbes, and the Immune System. *Immunity* **46**:549-561.

Lloyd CM and Robinson DS (2007) Allergen-induced airway remodelling. *The European respiratory journal* **29**:1020-1032.

Lochbaum R, Schilpp C, Nonnenmacher L, Frick M, Dietl P and Wittekindt OH (2020) Retinoic acid signalling adjusts tight junction permeability in response to air-liquid interface conditions. *Cellular Signalling* **65**:109421.

Long QX, Tang XJ, Shi QL, Li Q, Deng HJ, Yuan J, Hu JL, Xu W, Zhang Y, Lv FJ, Su K, Zhang F, Gong J, Wu B, Liu XM, Li JJ, Qiu JF, Chen J and Huang AL (2020) Clinical and immunological assessment of asymptomatic SARS-CoV-2 infections. *Nat Med* **26**:1200-1204.

Lovinsky-Desir S, Deshpande DR, De A, Murray L, Stingone JA, Chan A, Patel N, Rai N, DiMango E, Milner J and Kattan M (2020) Asthma among hospitalized patients with COVID-19 and related outcomes. *J Allergy Clin Immunol* **146**:1027-1034 e1024.

Lu T, Cao Y, Zhao P, Shen S and Xi Y (2021) Organoid: a powerful tool to study lung regeneration and disease. *Cell Regen* **10**:21.

Luengen AE, Kniebs C, Buhl EM, Cornelissen CG, Schmitz-Rode T, Jockenhoevel S and Thiebes AL (2020) Choosing the Right Differentiation Medium to Develop Mucociliary Phenotype of Primary Nasal Epithelial Cells In Vitro. *Sci Rep* **10**:6963.

Lukassen S, Chua RL, Trefzer T, Kahn NC, Schneider MA, Muley T, Winter H, Meister M, Veith C, Boots AW, Hennig BP, Kreuter M, Conrad C and Eils R (2020) SARS-CoV-2 receptor ACE2 and TMPRSS2 are primarily expressed in bronchial transient secretory cells. *EMBO J* **39**:e105114.

Maitra R, Sivashanmugam P and Warner K (2013) A rapid membrane potential assay to monitor CFTR function and inhibition. *J Biomol Screen* **18**:1132-1137.

Mak JC, Chan-Yeung MM, Ho SP, Chan KS, Choo K, Yee KS, Chau CH, Cheung AH, Ip MS and Members of Hong Kong Thoracic Society CSG (2009) Elevated plasma TGF-beta1 levels in patients with chronic obstructive pulmonary disease. *Respir Med* **103**:1083-1089.

Mall M, Grubb BR, Harkema JR, O'Neal WK and Boucher RC (2004) Increased airway epithelial Na+ absorption produces cystic fibrosis-like lung disease in mice. *Nat Med* **10**:487-493.

Malsure S, Wang Q, Charles R-P, Sergi C, Perrier R, Christensen BM, Maillard M, Rossier BC and Hummler E (2014) Colon-specific deletion of epithelial sodium channel causes sodium loss and aldosterone resistance. *Journal of the American Society of Nephrology : JASN* **25**:1453-1464.

Marinelli JP, Levin DL, Vassallo R, Carter RE, Hubmayr RD, Ehman RL and McGee KP (2017) Quantitative assessment of lung stiffness in patients with interstitial lung disease using MR elastography. *J Magn Reson Imaging* **46**:365-374.

Marsh GA, McAuley AJ, Brown S, Pharo EA, Crameri S, Au GG, Baker ML, Barr JA, Bergfeld J, Bruce MP, Burkett K, Durr PA, Holmes C, Izzard L, Layton R, Lowther S, Neave MJ, Poole T, Riddell SJ, Rowe B, Soldani E, Stevens V, Suen WW, Sundaramoorthy V, Tachedjian M, Todd S, Trinidad L, Williams SM, Druce JD, Drew TW and Vasan SS (2021) In vitro characterisation of SARS-CoV-2 and susceptibility of domestic ferrets (Mustela putorius furo). *Transbound Emerg Dis*.

Masilamani S, Kim GH, Mitchell C, Wade JB and Knepper MA (1999) Aldosterone-mediated regulation of ENaC alpha, beta, and gamma subunit proteins in rat kidney. *J Clin Invest* **104**:R19-23.

Mason RJ and Crystal RG (1998) Pulmonary Cell Biology. *American Journal of Respiratory and Critical Care Medicine* **157**:S72-S81.

Massaro GD, Singh G, Mason R, Plopper CG, Malkinson AM and Gail DB (1994) Biology of the Clara cell. *Am J Physiol* **266**:L101-106.

Matalon S, Bartoszewski R and Collawn JF (2015) Role of epithelial sodium channels in the regulation of lung fluid homeostasis. *Am J Physiol Lung Cell Mol Physiol* **309**:L1229-1238.

Matalon S and O'Brodovich H (1999) Sodium channels in alveolar epithelial cells: molecular characterization, biophysical properties, and physiological significance. *Annual review of physiology* **61**:627-661.

Matsui H, Randell SH, Peretti SW, Davis CW and Boucher RC (1998) Coordinated clearance of periciliary liquid and mucus from airway surfaces. *J Clin Invest* **102**:1125-1131.

Mattes C, Laube M and Thome UH (2014) Rapid elevation of sodium transport through insulin is mediated by AKT in alveolar cells. *Physiological Reports* **2**:e00269.

Matthay MA, Folkesson HG and Verkman AS (1996) Salt and water transport across alveolar and distal airway epithelia in the adult lung. *American Journal of Physiology-Lung Cellular and Molecular Physiology* **270**:L487-L503.

Mazzochi C, Bubien JK, Smith PR and Benos DJ (2006) The Carboxyl Terminus of the α-Subunit of the Amiloride-sensitive Epithelial Sodium Channel Binds to F-actin*. *Journal of Biological Chemistry* **281**:6528-6538.

McCauley KB, Hawkins F, Serra M, Thomas DC, Jacob A and Kotton DN (2017) Efficient Derivation of Functional Human Airway Epithelium from Pluripotent Stem Cells via Temporal Regulation of Wnt Signaling. *Cell Stem Cell* **20**:844-857 e846.

McGraw MD, Kim SY, Reed C, Hernady E, Rahman I, Mariani TJ and Finkelstein JN (2020) Airway basal cell injury after acute diacetyl (2,3-butanedione) vapor exposure. *Toxicol Lett* **325**:25-33.

Meng Q (2010) Three-dimensional culture of hepatocytes for prediction of drug-induced hepatotoxicity. *Expert Opin Drug Metab Toxicol* **6**:733-746.

Meyer-Berg H, Zhou Yang L, Pilar de Lucas M, Zambrano A, Hyde SC and Gill DR (2020) Identification of AAV serotypes for lung gene therapy in human embryonic stem cell-derived lung organoids. *Stem Cell Res Ther* **11**:448.

Mezey RJ, Cohn MA, Fernandez RJ, Januszkiewicz AJ and Wanner A (1978) Mucociliary transport in allergic patients with antigen-induced bronchospasm. *The American review of respiratory disease* **118**:677-684.

Mih JD, Sharif AS, Liu F, Marinkovic A, Symer MM and Tschumperlin DJ (2011) A multiwell platform for studying stiffness-dependent cell biology. *PLoS One* **6**:e19929.

Miller K, Mattey D, Measures H, Hopkins C and Garrod D (1987) Localisation of the protein and glycoprotein components of bovine nasal epithelial desmosomes by immunoelectron microscopy. *EMBO J* **6**:885-889.

Mills RJ, Humphrey SJ, Fortuna PRJ, Lor M, Foster SR, Quaife-Ryan GA, Johnston RL, Dumenil T, Bishop C, Rudraraju R, Rawle DJ, Le T, Zhao W, Lee L, Mackenzie-Kludas C, Mehdiabadi NR, Halliday C, Gilham D, Fu L, Nicholls SJ, Johansson J, Sweeney M, Wong NCW, Kulikowski E, Sokolowski KA, Tse BWC, Devilée L, Voges HK, Reynolds LT, Krumeich S, Mathieson E, Abu-Bonsrah D, Karavendzas K, Griffen B, Titmarsh D, Elliott DA, McMahon J, Suhrbier A, Subbarao K, Porrello ER, Smyth MJ, Engwerda CR, MacDonald KPA, Bald T, James DE and Hudson JE (2021) BET inhibition blocks inflammation-induced cardiac dysfunction and SARS-CoV-2 infection. *Cell* **184**:2167-2182.e2122.

Minshall E, Chakir J, Laviolette M, Molet S, Zhu Z, Olivenstein R, Elias JA and Hamid Q (2000) IL-11 expression is increased in severe asthma: association with epithelial cells and eosinophils. *Journal of allergy and clinical immunology* **105**:232-238.

Mirrakhimov AE (2015) Hypercalcemia of Malignancy: An Update on Pathogenesis and Management. *N Am J Med Sci* **7**:483-493.

Morachevskaya EA and Sudarikova AV (2021) Actin dynamics as critical ion channel regulator: ENaC and Piezo in focus. *American journal of physiology Cell physiology* **320**:C696-C702.

Mroue R and Bissell MJ (2012) Three-dimensional cultures of mouse mammary epithelial cells, in *Epithelial Cell Culture Protocols* pp 221-250, Springer.

Munitz A, Brandt EB, Mingler M, Finkelman FD and Rothenberg ME (2008) Distinct roles for IL-13 and IL-4 via IL-13 receptor alpha1 and the type II IL-4 receptor in asthma pathogenesis. *Proc Natl Acad Sci U S A* **105**:7240-7245.

Murthy SE, Dubin AE and Patapoutian A (2017) Piezos thrive under pressure: mechanically activated ion channels in health and disease. *Nat Rev Mol Cell Biol* **18**:771-783.

Myerburg MM, Harvey PR, Heidrich EM, Pilewski JM and Butterworth MB (2010) Acute regulation of the epithelial sodium channel in airway epithelia by proteases and trafficking. *American journal of respiratory cell and molecular biology* **43**:712-719.

Nakahari T (2007) Regulation of ciliary beat frequency in airways: shear stress, ATP action, and its modulation. *Am J Physiol Lung Cell Mol Physiol* **292**:L612-613.

Narkhede AA, Crenshaw JH, Manning RM and Rao SS (2018) The influence of matrix stiffness on the behavior of brain metastatic breast cancer cells in a biomimetic hyaluronic acid hydrogel platform. *Journal of biomedical materials research Part A* **106**:1832-1841.

Nesterov V, Dahlmann A, Bertog M and Korbmacher C (2008) Trypsin can activate the epithelial sodium channel (ENaC) in microdissected mouse distal nephron. *American Journal of Physiology-Renal Physiology* **295**:F1052-F1062.

Nesterov V, Dahlmann A, Krueger B, Bertog M, Loffing J and Korbmacher C (2012) Aldosterone-dependent and -independent regulation of the epithelial sodium channel (ENaC) in mouse distal nephron. *American Journal of Physiology-Renal Physiology* **303**:F1289-F1299.

Nesterov V, Krueger B, Bertog M, Dahlmann A, Palmisano R and Korbmacher C (2016) In Liddle Syndrome, Epithelial Sodium Channel Is Hyperactive Mainly in the Early Part of the Aldosterone-Sensitive Distal Nephron. *Hypertension (Dallas, Tex : 1979)* **67**:1256-1262.

Ng B, Dong J, D'Agostino G, Viswanathan S, Widjaja AA, Lim WW, Ko NSJ, Tan J, Chothani SP, Huang B, Xie C, Pua CJ, Chacko AM, Guimaraes-Camboa N, Evans SM, Byrne AJ, Maher TM, Liang J, Jiang D, Noble PW, Schafer S and Cook SA (2019) Interleukin-11 is a therapeutic target in idiopathic pulmonary fibrosis. *Science translational medicine* **11**.

Noreng S, Bharadwaj A, Posert R, Yoshioka C and Baconguis I (2018) Structure of the human epithelial sodium channel by cryo-electron microscopy. *eLife* **7**.

O'Riordan TG, Donn KH, Hodsman P, Ansede JH, Newcomb T, Lewis SA, Flitter WD, White VS, Johnson MR, Montgomery AB, Warnock DG and Boucher RC (2014) Acute hyperkalemia associated with inhalation of a potent ENaC antagonist: Phase 1 trial of GS-9411. *J Aerosol Med Pulm Drug Deliv* **27**:200-208.

Olivia MY, Miyamoto S and Brown JH (2016) Myocardin-related transcription factor a and yes-associated protein exert dual control in G protein-coupled receptor-and RhoA-mediated transcriptional regulation and cell proliferation. *Molecular and cellular biology* **36**:39-49.

Olman MA, Mackman N, Gladson CL, Moser KM and Loskutoff DJ (1995) Changes in procoagulant and fibrinolytic gene expression during bleomycin-induced lung injury in the mouse. *The Journal of clinical investigation* **96**:1621-1630.

Olson EN and Nordheim A (2010) Linking actin dynamics and gene transcription to drive cellular motile functions. *Nat Rev Mol Cell Biol* **11**:353-365.

Oran DP and Topol EJ (2020) Prevalence of Asymptomatic SARS-CoV-2 Infection : A Narrative Review. *Ann Intern Med* **173**:362-367.

Oswald H, Phelan PD, Lanigan A, Hibbert M, Bowes G and Olinsky A (1994) Outcome of childhood asthma in mid-adult life. *BMJ* **309**:95-96.

Ott HC, Clippinger B, Conrad C, Schuetz C, Pomerantseva I, Ikonomou L, Kotton D and Vacanti JP (2010) Regeneration and orthotopic transplantation of a bioartificial lung. *Nat Med* **16**:927-933.

Ott HC, Matthiesen TS, Goh SK, Black LD, Kren SM, Netoff TI and Taylor DA (2008) Perfusion-decellularized matrix: using nature's platform to engineer a bioartificial heart. *Nat Med* **14**:213-221.

Owen MJ (2017) Silicone Hydrophobicity and Oleophilicity. *Silicon* **9**:651-655.

Palmer LG and Frindt G (1986) Epithelial sodium channels: characterization by using the patch-clamp technique. *Fed Proc* **45**:2708-2712.

Pan D (2010) The hippo signaling pathway in development and cancer. *Dev Cell* **19**:491-505.

Panciera T, Azzolin L, Cordenonsi M and Piccolo S (2017) Mechanobiology of YAP and TAZ in physiology and disease. *Nat Rev Mol Cell Biol* **18**:758-770.

Park BK, Kim D, Park S, Maharjan S, Kim J, Choi JK, Akauliya M, Lee Y and Kwon HJ (2021) Differential Signaling and Virus Production in Calu-3 Cells and Vero Cells upon SARS-CoV-2 Infection. *Biomol Ther (Seoul)*.

Park J-A, Sharif AS, Tschumperlin DJ, Lau L, Limbrey R, Howarth P and Drazen JM (2012) Tissue factor–bearing exosome secretion from human mechanically stimulated bronchial epithelial cells in vitro and in vivo. *Journal of allergy and clinical immunology* **130**:1375-1383.

Park J-A and Tschumperlin DJ (2009) Chronic intermittent mechanical stress increases MUC5AC protein expression. *American journal of respiratory cell and molecular biology* **41**:459-466.

Park SE, Georgescu A and Huh D (2019) Organoids-on-a-chip. *Science* **364**:960-965.

Passero CJ, Mueller GM, Rondon-Berrios H, Tofovic SP, Hughey RP and Kleyman TR (2008) Plasmin activates epithelial Na+ channels by cleaving the gamma subunit. *The Journal of biological chemistry* **283**:36586-36591.

Paul SR, Bennett F, Calvetti JA, Kelleher K, Wood CR, O'Hara RM, Jr., Leary AC, Sibley B, Clark SC, Williams DA and et al. (1990) Molecular cloning of a cDNA encoding interleukin 11, a stromal cell-derived lymphopoietic and hematopoietic cytokine. *Proc Natl Acad Sci U S A* **87**:7512-7516.

Peters DM, Vadász I, Wujak L, Wygrecka M, Olschewski A, Becker C, Herold S, Papp R, Mayer K, Rummel S, Brandes RP, Günther A, Waldegger S, Eickelberg O, Seeger W and Morty RE (2014) TGF-β directs trafficking of the epithelial sodium channel ENaC which has implications for ion and fluid transport in acute lung injury. *Proc Natl Acad Sci U S A* **111**:E374-383.

Peters MC, Sajuthi S, Deford P, Christenson S, Rios CL, Montgomery MT, Woodruff PG, Mauger DT, Erzurum SC, Johansson MW, Denlinger LC, Jarjour NN, Castro M, Hastie AT, Moore W, Ortega VE, Bleecker ER, Wenzel SE, Israel E, Levy BD, Seibold MA and Fahy JV (2020) COVID-19-related Genes in Sputum Cells in Asthma. Relationship to Demographic Features and Corticosteroids. *Am J Respir Crit Care Med* **202**:83-90.

Petersen TH, Calle EA, Zhao L, Lee EJ, Gui L, Raredon MB, Gavrilov K, Yi T, Zhuang ZW, Breuer C, Herzog E and Niklason LE (2010) Tissue-engineered lungs for in vivo implantation. *Science* **329**:538-541.

Pharo EA, Williams SM, Boyd V, Sundaramoorthy V, Durr PA and Baker ML (2020) Host–Pathogen Responses to Pandemic Influenza H1N1pdm09 in a Human Respiratory Airway Model. *Viruses* **12**.

Piccolo S, Dupont S and Cordenonsi M (2014) The biology of YAP/TAZ: hippo signaling and beyond. *Physiol Rev* **94**:1287-1312.

Pizzorno A, Padey B, Julien T, Trouillet-Assant S, Traversier A, Errazuriz-Cerda E, Fouret J, Dubois J, Gaymard A, Lescure FX, Duliere V, Brun P, Constant S, Poissy J, Lina B, Yazdanpanah Y, Terrier O and Rosa-Calatrava M (2020) Characterization and Treatment of SARS-CoV-2 in Nasal and Bronchial Human Airway Epithelia. *Cell Rep Med* **1**:100059.

Plopper CG, Mariassy AT and Hill LH (1980) Ultrastructure of the nonciliated bronchiolar epithelial (Clara) cell of mammalian lung: I. A comparison of rabbit, guinea pig, rat, hamster, and mouse. *Exp Lung Res* **1**:139-154.

Plow EF, Haas TA, Zhang L, Loftus J and Smith JW (2000) Ligand binding to integrins. *Journal of Biological Chemistry* **275**:21785-21788.

Pollard TD (2007) Regulation of actin filament assembly by Arp2/3 complex and formins. *Annu Rev Biophys Biomol Struct* **36**:451-477.

Poniatowski LA, Wojdasiewicz P, Gasik R and Szukiewicz D (2015) Transforming growth factor Beta family: insight into the role of growth factors in regulation of fracture healing biology and potential clinical applications. *Mediators Inflamm* **2015**:137823.

Prodanovic D, Keenan CR, Langenbach S, Li M, Chen Q, Lew MJ and Stewart AG (2017) Cortisol limits selected actions of synthetic glucocorticoids in the airway epithelium. *The FASEB Journal*:fj. 201700730R.

Pruniéras M, Régnier M and Woodley D (1983) Methods for cultivation of keratinocytes with an air-liquid interface. *J Invest Dermatol* **81**:28s-33s.

Qadri YJ, Rooj AK and Fuller CM (2012) ENaCs and ASICs as therapeutic targets. *American journal of physiology Cell physiology* **302**:C943-965.

Qiao Y, Tam JKC, Tan SSL, Tai YK, Chin CY, Stewart AG, Ashman L, Sekiguchi K, Langenbach SY, Stelmack G, Halayko AJ, Tran T and Melbourne Epidemiological Study of Childhood Asthma g (2017) CD151, a laminin receptor showing increased expression in asthmatic patients, contributes to airway hyperresponsiveness through calcium signaling. *J Allergy Clin Immunol* **139**:82-92 e85.

Quaranta V (2000) Cell migration through extracellular matrix: membrane-type metalloproteinases make the way. *The Journal of cell biology* **149**:1167-1170.

Ramaiahgari SC, den Braver MW, Herpers B, Terpstra V, Commandeur JN, van de Water B and Price LS (2014) A 3D in vitro model of differentiated HepG2 cell spheroids with improved liver-like properties for repeated dose high-throughput toxicity studies. *Arch Toxicol* **88**:1083-1095.

Ramsey WS, Hertl W, Nowlan ED and Binkowski NJ (1984) Surface treatments and cell attachment. *In Vitro* **20**:802-808.

Randrianarison N, Clerici C, Ferreira C, Fontayne A, Pradervand S, Fowler-Jaeger N, Hummler E, Rossier BC and Planes C (2008) Low expression of the beta-ENaC subunit impairs lung fluid clearance in the mouse. *Am J Physiol Lung Cell Mol Physiol* **294**:L409-416.

Rayner RE, Makena P, Prasad GL and Cormet-Boyaka E (2019) Optimization of Normal Human Bronchial Epithelial (NHBE) Cell 3D Cultures for in vitro Lung Model Studies. *Sci Rep* **9**:500.

Reddel RR, Ke Y, Gerwin BI, McMenamin MG, Lechner JF, Su RT, Brash DE, Park J-B, Rhim JS and Harris CC (1988) Transformation of Human Bronchial Epithelial Cells by Infection with SV40 or Adenovirus-12 SV40 Hybrid Virus, or Transfection via Strontium Phosphate Coprecipitation with a Plasmid Containing SV40 Early Region Genes. *Cancer Research* **48**:1904-1909.

Redington AE, Madden J, Frew AJ, Djukanovic R, Roche WR, Holgate ST and Howarth PH (1997) Transforming growth factor-beta 1 in asthma. Measurement in bronchoalveolar lavage fluid. *Am J Respir Crit Care Med* **156**:642-647.

Reynolds SD, Giangreco A, Power JH and Stripp BR (2000) Neuroepithelial bodies of pulmonary airways serve as a reservoir of progenitor cells capable of epithelial regeneration. *Am J Pathol* **156**:269-278.

Reynolds SD and Malkinson AM (2010) Clara cell: progenitor for the bronchiolar epithelium. *The international journal of biochemistry & cell biology* **42**:1-4.

Reynolds SD, Rios C, Wesolowska-Andersen A, Zhuang Y, Pinter M, Happoldt C, Hill CL, Lallier SW, Cosgrove GP, Solomon GM, Nichols DP and Seibold MA (2016) Airway Progenitor Clone Formation Is Enhanced by Y-27632-Dependent Changes in the Transcriptome. *American journal of respiratory cell and molecular biology* **55**:323-336.

Richards J, Greenlee MM, Jeffers LA, Cheng KY, Guo L, Eaton DC and Gumz ML (2012) Inhibition of alphaENaC expression and ENaC activity following blockade of the circadian clock-regulatory kinases CK1delta/epsilon. *Am J Physiol Renal Physiol* **303**:F918-927.

Roche WR, Montefort S, Baker J and Holgate ST (1993) Cell adhesion molecules and the bronchial epithelium. *The American review of respiratory disease* **148**:S79-82.

Rock JR, Gao X, Xue Y, Randell SH, Kong Y-Y and Hogan BLM (2011) Notch-dependent differentiation of adult airway basal stem cells. *Cell stem cell* **8**:639-648.

Rock JR and Hogan BL (2011) Epithelial progenitor cells in lung development, maintenance, repair, and disease. *Annual review of cell and developmental biology* **27**:493-512.

Rock JR, Onaitis MW, Rawlins EL, Lu Y, Clark CP, Xue Y, Randell SH and Hogan BL (2009) Basal cells as stem cells of the mouse trachea and human airway epithelium. *Proc Natl Acad Sci U S A* **106**:12771-12775.

Rogers DF (2007) Physiology of airway mucus secretion and pathophysiology of hypersecretion. *Respiratory care* **52**:1134-1146; discussion 1146-1139.

Rokicki W, Rokicki M, Wojtacha J and Dzeljijli A (2016) The role and importance of club cells (Clara cells) in the pathogenesis of some respiratory diseases. *Kardiochir Torakochirurgia Pol* **13**:26-30.

Rosol TJ and Capen CC (1992) Mechanisms of cancer-induced hypercalcemia. *Laboratory investigation; a journal of technical methods and pathology* **67**:680-702.

Ross TD, Coon BG, Yun S, Baeyens N, Tanaka K, Ouyang M and Schwartz MA (2013) Integrins in mechanotransduction. *Curr Opin Cell Biol* **25**:613-618.

Rossi G, Manfrin A and Lutolf MP (2018) Progress and potential in organoid research. *Nature reviews Genetics* **19**:671-687.

Sachs N, Papaspyropoulos A, Zomer-van Ommen DD, Heo I, Bottinger L, Klay D, Weeber F, Huelsz-Prince G, Iakobachvili N, Amatngalim GD, de Ligt J, van Hoeck A, Proost N, Viveen MC, Lyubimova A, Teeven L, Derakhshan S, Korving J, Begthel H, Dekkers JF, Kumawat K, Ramos E, van Oosterhout MF, Offerhaus GJ, Wiener DJ, Olimpio EP, Dijkstra KK, Smit EF, van der Linden M, Jaksani S, van de Ven M, Jonkers J, Rios AC, Voest EE, van Moorsel CH, van der Ent CK, Cuppen E, van Oudenaarden A, Coenjaerts FE, Meyaard L, Bont LJ, Peters PJ, Tans SJ, van Zon JS, Boj SF, Vries RG, Beekman JM and Clevers H (2019) Long-term expanding human airway organoids for disease modeling. *EMBO J* **38**.

Salahudeen AA, Choi SS, Rustagi A, Zhu J, van Unen V, de la OS, Flynn RA, Margalef-Catala M, Santos AJM, Ju J, Batish A, Usui T, Zheng GXY, Edwards CE, Wagar LE, Luca V, Anchang B, Nagendran M, Nguyen K, Hart DJ, Terry JM, Belgrader P, Ziraldo SB, Mikkelsen TS, Harbury PB, Glenn JS, Garcia KC, Davis MM, Baric RS, Sabatti C, Amieva MR, Blish CA, Desai TJ and Kuo CJ (2020) Progenitor identification and SARS-CoV-2 infection in human distal lung organoids. *Nature* **588**:670-675.

Salem S, Harris T, Mok JS, Li MY, Keenan CR, Schuliga MJ and Stewart AG (2012) Transforming growth factor-beta impairs glucocorticoid activity in the A549 lung adenocarcinoma cell line. *Br J Pharmacol* **166**:2036-2048.

Samarakoon R, Higgins CE, Higgins SP, Kutz SM and Higgins PJ (2005) Plasminogen activator inhibitor type‐1 gene expression and induced migration in TGF‐β1‐stimulated smooth muscle cells is pp60c‐src/MEK‐dependent. *Journal of cellular physiology* **204**:236-246.

Sasaki S, Yui N and Noda Y (2014) Actin directly interacts with different membrane channel proteins and influences channel activities: AQP2 as a model. *Biochimica et Biophysica Acta (BBA) - Biomembranes* **1838**:514-520.

Satlin LM, Sheng S, Woda CB and Kleyman TR (2001) Epithelial Na+ channels are regulated by flow. *American Journal of Physiology-Renal Physiology* **280**:F1010-F1018.

Sato T, Stange DE, Ferrante M, Vries RG, Van Es JH, Van Den Brink S, Van Houdt WJ, Pronk A, Van Gorp J and Siersema PD (2011) Long-term expansion of epithelial organoids from human colon, adenoma, adenocarcinoma, and Barrett's epithelium. *Gastroenterology* **141**:1762-1772.

Sato T, Vries RG, Snippert HJ, van de Wetering M, Barker N, Stange DE, van Es JH, Abo A, Kujala P, Peters PJ and Clevers H (2009) Single Lgr5 stem cells build crypt-villus structures in vitro without a mesenchymal niche. *Nature* **459**:262-265.

Schafer JA (2002) Abnormal regulation of ENaC: syndromes of salt retention and salt wasting by the collecting duct. *American Journal of Physiology-Renal Physiology* **283**:F221-F235.

Schafer S, Viswanathan S, Widjaja AA, Lim WW, Moreno-Moral A, DeLaughter DM, Ng B, Patone G, Chow K, Khin E, Tan J, Chothani SP, Ye L, Rackham OJL, Ko NSJ, Sahib NE, Pua CJ, Zhen NTG, Xie C, Wang M, Maatz H, Lim S, Saar K, Blachut S, Petretto E, Schmidt S, Putoczki T, Guimaraes-Camboa N, Wakimoto H, van Heesch S, Sigmundsson K, Lim SL, Soon JL, Chao VTT, Chua YL, Tan TE, Evans SM, Loh YJ, Jamal MH, Ong KK, Chua KC, Ong BH, Chakaramakkil MJ, Seidman JG, Seidman CE, Hubner N, Sin KYK and Cook SA (2017) IL-11 is a crucial determinant of cardiovascular fibrosis. *Nature* **552**:110-115.

Scheinman RI, Gualberto A, Jewell CM, Cidlowski JA and Baldwin AS (1995) Characterization of mechanisms involved in transrepression of NF-kappa B by activated glucocorticoid receptors. *Molecular and Cellular Biology* **15**:943-953.

Scherrer U, Rexhaj E, Jayet P-Y, Allemann Y and Sartori C (2010) New Insights in the Pathogenesis of High-Altitude Pulmonary Edema. *Progress in Cardiovascular Diseases* **52**:485-492.

Schogler A, Blank F, Brugger M, Beyeler S, Tschanz SA, Regamey N, Casaulta C, Geiser T and Alves MP (2017) Characterization of pediatric cystic fibrosis airway epithelial cell cultures at the air-liquid interface obtained by non-invasive nasal cytology brush sampling. *Respir Res* **18**:215.

Schögler A, Blank F, Brügger M, Beyeler S, Tschanz SA, Regamey N, Casaulta C, Geiser T and Alves MP (2017) Characterization of pediatric cystic fibrosis airway epithelial cell cultures at the air-liquid interface obtained by non-invasive nasal cytology brush sampling. *Respiratory Research* **18**:215.

Schuliga M, Ong SC, Soon L, Zal F, Harris T and Stewart AG (2010) Airway smooth muscle remodels pericellular collagen fibrils: implications for proliferation. *Am J Physiol Lung Cell Mol Physiol* **298**:L584-592.

Schuliga MJ, See I, Ong SC, Soon L, Camoretti-Mercado B, Harris T and Stewart AG (2009) Fibrillar collagen clamps lung mesenchymal cells in a nonproliferative and noncontractile phenotype. *Am J Respir Cell Mol Biol* **41**:731-741.

Scichilone N, La Sala A, Bellia M, Fallano K, Togias A, Brown RH, Midiri M and Bellia V (2008) The airway response to deep inspirations decreases with COPD severity and is associated with airway distensibility assessed by computed tomography. *Journal of applied physiology* **105**:832-838.

Sender R, Fuchs S and Milo R (2016) Revised Estimates for the Number of Human and Bacteria Cells in the Body. *PLoS Biol* **14**:e1002533.

Senoo T, Hattori N, Tanimoto T, Furonaka M, Ishikawa N, Fujitaka K, Haruta Y, Murai H, Yokoyama A and Kohno N (2010) Suppression of plasminogen activator inhibitor-1 by RNA interference attenuates pulmonary fibrosis. *Thorax* **65**:334-340.

Shamir ER and Ewald AJ (2014) Three-dimensional organotypic culture: experimental models of mammalian biology and disease. *Nat Rev Mol Cell Biol* **15**:647-664.

Sharma V, Dogra N, Saikia UN and Khullar M (2017) Transcriptional regulation of endothelial-to-mesenchymal transition in cardiac fibrosis: role of myocardin-related transcription factor A and activating transcription factor 3. *Can J Physiol Pharmacol* **95**:1263-1270.

Shei RJ, Peabody JE, Kaza N and Rowe SM (2018) The epithelial sodium channel (ENaC) as a therapeutic target for cystic fibrosis. *Curr Opin Pharmacol* **43**:152-165.

Shigaev A, Asher C, Latter H, Garty H and Reuveny E (2000) Regulation of sgk by aldosterone and its effects on the epithelial Na(+) channel. *Am J Physiol Renal Physiol* **278**:F613-619.

Shkumatov A, Thompson M, Choi KM, Sicard D, Baek K, Kim DH, Tschumperlin DJ, Prakash YS and Kong H (2015) Matrix stiffness-modulated proliferation and secretory function of the airway smooth muscle cells. *Am J Physiol Lung Cell Mol Physiol* **308**:L1125-1135.

Sirenko O, Mitlo T, Hesley J, Luke S, Owens W and Cromwell EF (2015) High-content assays for characterizing the viability and morphology of 3D cancer spheroid cultures. *Assay and drug development technologies* **13**:402-414.

Song S, Liu B, Habibie H, van den Bor J, Smit MJ, Gosens R, Wu X, Brandsma CA, Cool RH, Haisma HJ, Poelarends GJ and Melgert BN (2021) D-dopachrome tautomerase contributes to lung epithelial repair via atypical chemokine receptor 3-dependent Akt signaling. *EBioMedicine* **68**:103412.

Sont JK, Willems LN, Bel EH, van Krieken JH, Vandenbroucke JP and Sterk PJ (1999) Clinical control and histopathologic outcome of asthma when using airway hyperresponsiveness as an additional guide to long-term treatment. The AMPUL Study Group. *Am J Respir Crit Care Med* **159**:1043-1051.

Sorrentino G, Rezakhani S, Yildiz E, Nuciforo S, Heim MH, Lutolf MP and Schoonjans K (2020) Mechano-modulatory synthetic niches for liver organoid derivation. *Nature Communications* **11**:3416.

Soundararajan R, Zhang TT, Wang J, Vandewalle A and Pearce D (2005) A Novel Role for Glucocorticoid-induced Leucine Zipper Protein in Epithelial Sodium Channel-mediated Sodium Transport*. *Journal of Biological Chemistry* **280**:39970-39981.

Speight P, Kofler M, Szászi K and Kapus A (2016) Context-dependent switch in chemo/mechanotransduction via multilevel crosstalk among cytoskeleton-regulated MRTF and TAZ and TGFβ-regulated Smad3. *Nature communications* **7**:11642.

Springer J, Scholz FR, Peiser C, Groneberg DA and Fischer A (2004) SMAD-signaling in chronic obstructive pulmonary disease: transcriptional down-regulation of inhibitory SMAD 6 and 7 by cigarette smoke. *Biol Chem* **385**:649-653.

Srinivasan B, Kolli AR, Esch MB, Abaci HE, Shuler ML and Hickman JJ (2015) TEER measurement techniques for in vitro barrier model systems. *J Lab Autom* **20**:107-126.

Staruschenko A, Adams E, Booth RE and Stockand JD (2005) Epithelial Na+ channel subunit stoichiometry. *Biophys J* **88**:3966-3975.

Stellato C (2007) Glucocorticoid actions on airway epithelial responses in immunity: functional outcomes and molecular targets. *J Allergy Clin Immunol* **120**:1247-1263; quiz 1264-1245.

STEMCELL (2015) Sphere Culture of Differentiated HBECs with PneumaCultTM-ALI. *STEMCELL Technologies*.

Stepp MA, Spurr-Michaud S, Tisdale A, Elwell J and Gipson IK (1990) Alpha 6 beta 4 integrin heterodimer is a component of hemidesmosomes. *Proc Natl Acad Sci U S A* **87**:8970-8974.

Stewart AG, Thomas B and Koff J (2018) TGF-beta: Master regulator of inflammation and fibrosis. *Respirology (Carlton, Vic)* **23**:1096-1097.

Stewart AP, Haerteis S, Diakov A, Korbmacher C and Edwardson JM (2011) Atomic force microscopy reveals the architecture of the epithelial sodium channel (ENaC). *J Biol Chem* **286**:31944-31952.

Stewart CE, Torr EE, Mohd Jamili NH, Bosquillon C and Sayers I (2012a) Evaluation of Differentiated Human Bronchial Epithelial Cell Culture Systems for Asthma Research. *Journal of Allergy* **2012**:943982.

Stewart CE, Torr EE, Mohd Jamili NH, Bosquillon C and Sayers I (2012b) Evaluation of differentiated human bronchial epithelial cell culture systems for asthma research. *J Allergy (Cairo)* **2012**:943982.

Strikoudis A, Cieślak A, Loffredo L, Chen Y-W, Patel N, Saqi A, Lederer DJ and Snoeck H-W (2019) Modeling of fibrotic lung disease using 3D organoids derived from human pluripotent stem cells. *Cell reports* **27**:3709-3723. e3705.

Suchyna TM, Tape SE, Koeppe RE, 2nd, Andersen OS, Sachs F and Gottlieb PA (2004) Bilayer-dependent inhibition of mechanosensitive channels by neuroactive peptide enantiomers. *Nature* **430**:235-240.

Sudarikova AV, Tsaplina OA, Chubinskiy-Nadezhdin VI, Morachevskaya EA and Negulyaev YA (2015) Amiloride-insensitive sodium channels are directly regulated by actin cytoskeleton dynamics in human lymphoma cells. *Biochemical and biophysical research communications* **461**:54-58.

Suissa S, Patenaude V, Lapi F and Ernst P (2013) Inhaled corticosteroids in COPD and the risk of serious pneumonia. *Thorax* **68**:1029-1036.

Suki B, Ito S, Stamenovic D, Lutchen KR and Ingenito EP (2005) Biomechanics of the lung parenchyma: critical roles of collagen and mechanical forces. *Journal of applied physiology (Bethesda, Md : 1985)* **98**:1892-1899.

Sun M, Chi G, Xu J, Tan Y, Xu J, Lv S, Xu Z, Xia Y, Li L and Li Y (2018) Extracellular matrix stiffness controls osteogenic differentiation of mesenchymal stem cells mediated by integrin α5. *Stem Cell Research & Therapy* **9**:52.

Sun Z, Guo SS and Fassler R (2016) Integrin-mediated mechanotransduction. *J Cell Biol* **215**:445-456.

Surjit M, Ganti KP, Mukherji A, Ye T, Hua G, Metzger D, Li M and Chambon P (2011) Widespread negative response elements mediate direct repression by agonist-liganded glucocorticoid receptor. *Cell* **145**:224-241.

Surolia R, Li FJ, Wang Z, Li H, Liu G, Zhou Y, Luckhardt T, Bae S, Liu R-m and Rangarajan S (2017) 3D pulmospheres serve as a personalized and predictive multicellular model for assessment of antifibrotic drugs. *JCI insight* **2**.

Tadokoro T, Wang Y, Barak LS, Bai Y, Randell SH and Hogan BL (2014) IL-6/STAT3 promotes regeneration of airway ciliated cells from basal stem cells. *Proc Natl Acad Sci U S A* **111**:E3641-3649.

Taglauer ES, Wachman EM, Juttukonda L, Klouda T, Kim J, Wang Q, Ishiyama A, Hackam DJ, Yuan K and Jia H (2021) Acute SARS-CoV-2 infection in pregnancy is associated with placental ACE-2 shedding. *bioRxiv*.

Takada Y, Ye X and Simon S (2007) The integrins. *Genome biology* **8**:1-9.

Takasato M, Pei XE, Chiu HS, Maier B, Baillie GJ, Ferguson C, Parton RG, Wolvetang EJ, Roost MS and de Sousa Lopes SMC (2015) Kidney organoids from human iPS cells contain multiple lineages and model human nephrogenesis. *Nature* **526**:564-568.

Takizawa H, Tanaka M, Takami K, Ohtoshi T, Ito K, Satoh M, Okada Y, Yamasawa F, Nakahara K and Umeda A (2001) Increased expression of transforming growth factor-beta1 in small airway epithelium from tobacco smokers and patients with chronic obstructive pulmonary disease (COPD). *Am J Respir Crit Care Med* **163**:1476-1483.

Tan KS, Lim RL, Liu J, Ong HH, Tan VJ, Lim HF, Chung KF, Adcock IM, Chow VT and Wang Y (2020) Respiratory Viral Infections in Exacerbation of Chronic Airway Inflammatory Diseases: Novel Mechanisms and Insights From the Upper Airway Epithelium. *Front Cell Dev Biol* **8**:99.

Tan Q, Choi KM, Sicard D and Tschumperlin DJ (2017) Human airway organoid engineering as a step toward lung regeneration and disease modeling. *Biomaterials* **113**:118-132.

Tang ML, Wilson JW, Stewart AG and Royce SG (2006) Airway remodelling in asthma: current understanding and implications for future therapies. *Pharmacol Ther* **112**:474-488.

Tang W, Yang L, Yang Y-C, Leng SX and Elias JA (1998) Transforming Growth Factor-β Stimulates Interleukin-11 Transcription via Complex Activating Protein-1-dependent Pathways. *Journal of Biological Chemistry* **273**:5506-5513.

Tarran R, Button B and Boucher RC (2006) Regulation of normal and cystic fibrosis airway surface liquid volume by phasic shear stress. *Annual review of physiology* **68**:543-561.

Tay B, Stewart TA, Davis FM, Deuis JR and Vetter I (2019) Development of a high-throughput fluorescent no-wash sodium influx assay. *PLoS One* **14**:e0213751.

Thannickal VJ and Horowitz JC (2006) Evolving concepts of apoptosis in idiopathic pulmonary fibrosis. *Proc Am Thorac Soc* **3**:350-356.

Thomson A, Smart K, Somerville MS, Lauder SN, Appanna G, Horwood J, Sunder Raj L, Srivastava B, Durai D, Scurr MJ, Keita ÅV, Gallimore AM and Godkin A (2019) The Ussing chamber system for measuring intestinal permeability in health and disease. *BMC Gastroenterology* **19**:98.

Thurner PJ (2009) Atomic force microscopy and indentation force measurement of bone. *Wiley interdisciplinary reviews Nanomedicine and nanobiotechnology* **1**:624-649.

Tilly TB, Nelson MT, Chakravarthy KB, Shira EA, Debrose MC, Grabinski CM, Salisbury RL, Mattie DR and Hussain SM (2020) In Vitro Aerosol Exposure to Nanomaterials: From Laboratory to Environmental Field Toxicity Testing. *Chem Res Toxicol* **33**:1179-1194.

Tojo M, Hamashima Y, Hanyu A, Kajimoto T, Saitoh M, Miyazono K, Node M and Imamura T (2005) The ALK-5 inhibitor A-83-01 inhibits Smad signaling and epithelial-to-mesenchymal transition by transforming growth factor-beta. *Cancer Sci* **96**:791-800.

Torday JS (2003) Parathyroid hormone-related protein is a gravisensor in lung and bone cell biology. *Adv Space Res* **32**:1569-1576.

Torday JS, Torres E and Rehan VK (2003) The role of fibroblast transdifferentiation in lung epithelial cell proliferation, differentiation, and repair in vitro. *Pediatr Pathol Mol Med* **22**:189-207.

Totura AL, Whitmore A, Agnihothram S, Schafer A, Katze MG, Heise MT and Baric RS (2015) Toll-Like Receptor 3 Signaling via TRIF Contributes to a Protective Innate Immune Response to Severe Acute Respiratory Syndrome Coronavirus Infection. *mBio* **6**:e00638-00615.

Tschumperlin DJ, Dai G, Maly IV, Kikuchi T, Laiho LH, McVittie AK, Haley KJ, Lilly CM, So PT and Lauffenburger DA (2004) Mechanotransduction through growth-factor shedding into the extracellular space. *Nature* **429**:83-86.

Tzima E, del Pozo MA, Shattil SJ, Chien S and Schwartz MA (2001) Activation of integrins in endothelial cells by fluid shear stress mediates Rho-dependent cytoskeletal alignment. *EMBO J* **20**:4639-4647.

Urbach V, Verriere V, Grumbach Y, Bousquet J and Harvey BJ (2006) Rapid anti-secretory effects of glucocorticoids in human airway epithelium. *Steroids* **71**:323-328.

Ussing HH and Zerahn K (1951) Active transport of sodium as the source of electric current in the short‐circuited isolated frog skin. *Acta physiologica Scandinavica* **23**:110-127.

Vallath S, Hynds RE, Succony L, Janes SM and Giangreco A (2014) Targeting EGFR signalling in chronic lung disease: therapeutic challenges and opportunities. *Eur Respir J* **44**:513-522.

Vanderheiden A, Ralfs P, Chirkova T, Upadhyay AA, Zimmerman MG, Bedoya S, Aoued H, Tharp GM, Pellegrini KL, Manfredi C, Sorscher E, Mainou B, Lobby JL, Kohlmeier JE, Lowen AC, Shi PY, Menachery VD, Anderson LJ, Grakoui A, Bosinger SE and

Suthar MS (2020) Type I and Type III Interferons Restrict SARS-CoV-2 Infection of Human Airway Epithelial Cultures. *J Virol* **94**.

Vandevyver S, Dejager L, Tuckermann J and Libert C (2013) New insights into the anti-inflammatory mechanisms of glucocorticoids: an emerging role for glucocorticoid-receptor-mediated transactivation. *Endocrinology* **154**:993-1007.

Vareille M, Kieninger E, Edwards MR and Regamey N (2011) The airway epithelium: soldier in the fight against respiratory viruses. *Clin Microbiol Rev* **24**:210-229.

Vartiainen MK, Guettler S, Larijani B and Treisman R (2007) Nuclear actin regulates dynamic subcellular localization and activity of the SRF cofactor MAL. *Science* **316**:1749-1752.

Velasquez LS, Sutherland LB, Liu Z, Grinnell F, Kamm KE, Schneider JW, Olson EN and Small EM (2013) Activation of MRTF-A-dependent gene expression with a small molecule promotes myofibroblast differentiation and wound healing. *Proc Natl Acad Sci U S A* **110**:16850-16855.

Vernardis SI, Terzoudis K, Panoskaltsis N and Mantalaris A (2017) Human embryonic and induced pluripotent stem cells maintain phenotype but alter their metabolism after exposure to ROCK inhibitor. *Scientific Reports* **7**:42138.

Verrecchia F and Mauviel A (2002) Transforming growth factor-beta signaling through the Smad pathway: role in extracellular matrix gene expression and regulation. *J Invest Dermatol* **118**:211-215.

Vickaryous MK and Hall BK (2006) Human cell type diversity, evolution, development, and classification with special reference to cells derived from the neural crest. *Biol Rev Camb Philos Soc* **81**:425-455.

Vieira Braga FA, Kar G, Berg M, Carpaij OA, Polanski K, Simon LM, Brouwer S, Gomes T, Hesse L, Jiang J, Fasouli ES, Efremova M, Vento-Tormo R, Talavera-López C, Jonker MR, Affleck K, Palit S, Strzelecka PM, Firth HV, Mahbubani KT, Cvejic A, Meyer KB, Saeb-Parsy K, Luinge M, Brandsma C-A, Timens W, Angelidis I, Strunz M, Koppelman GH, van Oosterhout AJ, Schiller HB, Theis FJ, van den Berge M, Nawijn MC and Teichmann SA (2019) A cellular census of human lungs identifies novel cell states in health and in asthma. *Nature Medicine* **25**:1153-1163.

Visser J, Melchels FP, Jeon JE, van Bussel EM, Kimpton LS, Byrne HM, Dhert WJ, Dalton PD, Hutmacher DW and Malda J (2015) Reinforcement of hydrogels using three-dimensionally printed microfibres. *Nat Commun* **6**:6933.

Volpato V and Webber C (2020) Addressing variability in iPSC-derived models of human disease: guidelines to promote reproducibility. *Dis Model Mech* **13**.

Wadsworth SJ, Yang SJ and Dorscheid DR (2012) IL-13, Asthma and Glycosylation in Airway Epithelial Repair, in *Carbohydrates-Comprehensive Studies on Glycobiology and Glycotechnology*, InTech.

Wagner A, Liu Q, Rose OL, Eden A, Vijay A, Rojanasakul Y and Dinu CZ (2019) Toxicity screening of two prevalent metal organic frameworks for therapeutic use in human lung epithelial cells. *Int J Nanomedicine* **14**:7583-7591.

Waldmann R, Champigny G, Bassilana F, Voilley N and Lazdunski M (1995) Molecular cloning and functional expression of a novel amiloride-sensitive Na+ channel. *J Biol Chem* **270**:27411-27414.

Walters MS, Gomi K, Ashbridge B, Moore MA, Arbelaez V, Heldrich J, Ding BS, Rafii S, Staudt MR and Crystal RG (2013) Generation of a human airway epithelium derived basal cell line with multipotent differentiation capacity. *Respir Res* **14**:135.

Wang DZ, Li S, Hockemeyer D, Sutherland L, Wang Z, Schratt G, Richardson JA, Nordheim A and Olson EN (2002) Potentiation of serum response factor activity by a family of myocardin-related transcription factors. *Proc Natl Acad Sci U S A* **99**:14855-14860.

Wang HB, Dembo M and Wang YL (2000) Substrate flexibility regulates growth and apoptosis of normal but not transformed cells. *American journal of physiology Cell physiology* **279**:C1345-1350.

Wang J, Zhu Z, Nolfo R and Elias JA (1999) Dexamethasone regulation of lung epithelial cell and fibroblast interleukin-11 production. *American Journal of Physiology-Lung Cellular and Molecular Physiology* **276**:L175-L185.

Wang K, Gheblawi M, Nikhanj A, Munan M, MacIntyre E, O'Neil C, Poglitsch M, Colombo D, Del Nonno F, Kassiri Z, Sligl W and Oudit GY (2022) Dysregulation of ACE (Angiotensin-Converting Enzyme)-2 and Renin-Angiotensin Peptides in SARS-CoV-2 Mediated Mortality and End-Organ Injuries. *Hypertension (Dallas, Tex : 1979)* **79**:365-378.

Wang KC, Yeh YT, Nguyen P, Limqueco E, Lopez J, Thorossian S, Guan KL, Li YJ and Chien S (2016) Flow-dependent YAP/TAZ activities regulate endothelial phenotypes and atherosclerosis. *Proc Natl Acad Sci U S A* **113**:11525-11530.

Wang Y, Wang H, Deng P, Chen W, Guo Y, Tao T and Qin J (2018a) In situ differentiation and generation of functional liver organoids from human iPSCs in a 3D perfusable chip system. *Lab on a chip* **18**:3606-3616.

Wang Y, Wang L, Zhu Y and Qin J (2018b) Human brain organoid-on-a-chip to model prenatal nicotine exposure. *Lab on a chip* **18**:851-860.

Ward C, Johns DP, Bish R, Pais M, Reid DW, Ingram C, Feltis B and Walters EH (2001) Reduced airway distensibility, fixed airflow limitation, and airway wall remodeling in asthma. *American journal of respiratory and critical care medicine* **164**:1718-1721.

Ward JE, Harris T, Bamford T, Mast A, Pain MC, Robertson C, Smallwood D, Tran T, Wilson J and Stewart AG (2008) Proliferation is not increased in airway myofibroblasts isolated from asthmatics. *Eur Respir J* **32**:362-371.

Watanabe K, Ueno M, Kamiya D, Nishiyama A, Matsumura M, Wataya T, Takahashi JB, Nishikawa S, Nishikawa S, Muguruma K and Sasai Y (2007) A ROCK inhibitor permits survival of dissociated human embryonic stem cells. *Nat Biotechnol* **25**:681-686.

Wei SC and Yang J (2016) Forcing through Tumor Metastasis: The Interplay between Tissue Rigidity and Epithelial-Mesenchymal Transition. *Trends Cell Biol* **26**:111-120.

Wells RG (2008) The role of matrix stiffness in regulating cell behavior. *Hepatology (Baltimore, Md)* **47**:1394-1400.

Westergren-Thorsson G, Chakir J, Lafrenière-Allard M-J, Boulet L-P and Tremblay GM (2002) Correlation between airway responsiveness and proteoglycan production by bronchial fibroblasts from normal and asthmatic subjects. *The international journal of biochemistry & cell biology* **34**:1256-1267.

Whitcutt MJ, Adler KB and Wu R (1988) A biphasic chamber system for maintaining polarity of differentiation of cultured respiratory tract epithelial cells. *In Vitro Cell Dev Biol* **24**:420-428.

WHO (2020) WHO Director-General's opening remarks at the media briefing on COVID-19 - 11 March 2020, World Health Organization.

Wichmann L and Althaus M (2020) Evolution of epithelial sodium channels: current concepts and hypotheses. *American journal of physiology Regulatory, integrative and comparative physiology* **319**:R387-R400.

Widdicombe JG (1997) Airway liquid: a barrier to drug diffusion? *Eur Respir J* **10**:2194-2197.

Willis BC and Borok Z (2007) TGF-beta-induced EMT: mechanisms and implications for fibrotic lung disease. *Am J Physiol Lung Cell Mol Physiol* **293**:L525-534.

Wilson JW and Li X (1997) The measurement of reticular basement membrane and submucosal collagen in the asthmatic airway. *Clin Exp Allergy* **27**:363-371.

Wilson JW, Li X and Pain MC (1993a) The lack of distensibility of asthmatic airways. *American Review of Respiratory Disease* **148**:806-809.

Wilson JW, Li X and Pain MCF (1993b) The Lack of Distensibility of Asthmatic Airways. *American Review of Respiratory Disease* **148**:806-809.

Winters SL, Davis CW and Boucher RC (2007) Mechanosensitivity of mouse tracheal ciliary beat frequency: roles for Ca2+, purinergic signaling, tonicity, and viscosity. *Am J Physiol Lung Cell Mol Physiol* **292**:L614-624.

Wipff PJ, Rifkin DB, Meister JJ and Hinz B (2007) Myofibroblast contraction activates latent TGF-beta1 from the extracellular matrix. *J Cell Biol* **179**:1311-1323.

Wiseman OJ, Fowler CJ and Landon DN (2003) The role of the human bladder lamina propria myofibroblast. *BJU Int* **91**:89-93.

Wolf S, Perez GF, Mukharesh L, Isaza N, Preciado D, Freishtat RJ, Pillai D, Rose MC and Nino G (2017) Conditional reprogramming of pediatric airway epithelial cells: A new human model to investigate early-life respiratory disorders. *Pediatr Allergy Immunol* **28**:810-817.

Wolfel R, Corman VM, Guggemos W, Seilmaier M, Zange S, Muller MA, Niemeyer D, Jones TC, Vollmar P, Rothe C, Hoelscher M, Bleicker T, Brunink S, Schneider J, Ehmann R, Zwirglmaier K, Drosten C and Wendtner C (2020) Virological assessment of hospitalized patients with COVID-2019. *Nature* **581**:465-469.

Wong JY, Velasco A, Rajagopalan P and Pham Q (2003) Directed Movement of Vascular Smooth Muscle Cells on Gradient-Compliant Hydrogels†. *Langmuir* **19**:1908-1913.

Woodruff PG, Boushey HA, Dolganov GM, Barker CS, Yang YH, Donnelly S, Ellwanger A, Sidhu SS, Dao-Pick TP, Pantoja C, Erle DJ, Yamamoto KR and Fahy JV (2007) Genome-wide profiling identifies epithelial cell genes associated with asthma and with treatment response to corticosteroids. *Proc Natl Acad Sci U S A* **104**:15858-15863.

Woodruff PG, Dolganov GM, Ferrando RE, Donnelly S, Hays SR, Solberg OD, Carter R, Wong HH, Cadbury PS and Fahy JV (2004) Hyperplasia of smooth muscle in mild to moderate asthma without changes in cell size or gene expression. *American journal of respiratory and critical care medicine* **169**:1001-1006.

Woodruff PG, Wolff M, Hohlfeld JM, Krug N, Dransfield MT, Sutherland ER, Criner GJ, Kim V, Prasse A, Nivens MC, Tetzlaff K, Heilker R and Fahy JV (2010) Safety and efficacy of an inhaled epidermal growth factor receptor inhibitor (BIBW 2948 BS) in chronic obstructive pulmonary disease. *Am J Respir Crit Care Med* **181**:438-445.

Woolcock AJ, Salome C and Yan K (1984) The shape of the dose-response curve to histamine in asthmatic and normal subjects. *American Review of Respiratory Disease* **130**:71-75.

Wu NH, Yang W, Beineke A, Dijkman R, Matrosovich M, Baumgartner W, Thiel V, Valentin-Weigand P, Meng F and Herrler G (2016) The differentiated airway epithelium infected by influenza viruses maintains the barrier function despite a dramatic loss of ciliated cells. *Sci Rep* **6**:39668.

Wu X, Peters-Hall JR, Bose S, Pena MT and Rose MC (2011) Human bronchial epithelial cells differentiate to 3D glandular acini on basement membrane matrix. *Am J Respir Cell Mol Biol* **44**:914-921.

Wu Z and McGoogan JM (2020) Characteristics of and Important Lessons From the Coronavirus Disease 2019 (COVID-19) Outbreak in China: Summary of a Report of 72314 Cases From the Chinese Center for Disease Control and Prevention. *JAMA* **323**:1239-1242.

Wynn TA (2008) Cellular and molecular mechanisms of fibrosis. *J Pathol* **214**:199-210.

Wynne BM, Zou L, Linck V, Hoover RS, Ma HP and Eaton DC (2017) Regulation of Lung Epithelial Sodium Channels by Cytokines and Chemokines. *Frontiers in immunology* **8**:766.

Xia YC, Radwan A, Keenan CR, Langenbach SY, Li M, Radojicic D, Londrigan SL, Gualano RC and Stewart AG (2017) Glucocorticoid Insensitivity in Virally Infected Airway Epithelial Cells Is Dependent on Transforming Growth Factor-beta Activity. *PLoS Pathog* **13**:e1006138.

Yaghi A and Dolovich MB (2016) Airway Epithelial Cell Cilia and Obstructive Lung Disease. *Cells* **5**.

Yang IA, Clarke MS, Sim EH and Fong KM (2012) Inhaled corticosteroids for stable chronic obstructive pulmonary disease. *Cochrane Database Syst Rev*:Cd002991.

Yang L, Han Y, Nilsson-Payant BE, Gupta V, Wang P, Duan X, Tang X, Zhu J, Zhao Z, Jaffre F, Zhang T, Kim TW, Harschnitz O, Redmond D, Houghton S, Liu C, Naji A, Ciceri G, Guttikonda S, Bram Y, Nguyen DT, Cioffi M, Chandar V, Hoagland DA, Huang Y, Xiang J, Wang H, Lyden D, Borczuk A, Chen HJ, Studer L, Pan FC, Ho DD, tenOever BR, Evans T, Schwartz RE and Chen S (2020) A Human Pluripotent Stem Cell-based Platform to Study SARS-CoV-2 Tropism and Model Virus Infection in Human Cells and Organoids. *Cell Stem Cell* **27**:125-136 e127.

Yeung T, Georges PC, Flanagan LA, Marg B, Ortiz M, Funaki M, Zahir N, Ming W, Weaver V and Janmey PA (2005) Effects of substrate stiffness on cell morphology, cytoskeletal structure, and adhesion. *Cell Motility* **60**:24-34.

Yin JJ, Selander K, Chirgwin JM, Dallas M, Grubbs BG, Wieser R, Massagué J, Mundy GR and Guise TA (1999) TGF-beta signaling blockade inhibits PTHrP secretion by breast cancer cells and bone metastases development. *The Journal of clinical investigation* **103**:197-206.

Yin X, Mead BE, Safaee H, Langer R, Karp JM and Levy O (2016) Engineering stem cell organoids. *Cell stem cell* **18**:25-38.

Yohan Payan JO (2017) *Biomechanics of Living Organs*, Academic Press.

Yoon JH, Gray T, Guzman K, Koo JS and Nettesheim P (1997) Regulation of the secretory phenotype of human airway epithelium by retinoic acid, triiodothyronine, and extracellular matrix. *Am J Respir Cell Mol Biol* **16**:724-731.

Yu FX, Zhao B and Guan KL (2015) Hippo Pathway in Organ Size Control, Tissue Homeostasis, and Cancer. *Cell* **163**:811-828.

Yu HB, Li M, Wang WP and Wang XL (2016) High throughput screening technologies for ion channels. *Acta Pharmacol Sin* **37**:34-43.

Yu L, Helms MN, Yue Q and Eaton DC (2008) Single-channel analysis of functional epithelial sodium channel (ENaC) stability at the apical membrane of A6 distal kidney cells. *American journal of physiology Renal physiology* **295**:F1519-F1527.

Zeisberg M and Neilson EG (2009) Biomarkers for epithelial-mesenchymal transitions. *J Clin Invest* **119**:1429-1437.

Zhang H, Rostami MR, Leopold PL, Mezey JG, O'Beirne SL, Strulovici-Barel Y and Crystal RG (2020a) Expression of the SARS-CoV-2 ACE2 Receptor in the Human Airway Epithelium. *Am J Respir Crit Care Med* **202**:219-229.

Zhang JJ, Dong X, Cao YY, Yuan YD, Yang YB, Yan YQ, Akdis CA and Gao YD (2020b) Clinical characteristics of 140 patients infected with SARS-CoV-2 in Wuhan, China. *Allergy* **75**:1730-1741.

Zhang W and Gunst SJ (2008) Interactions of airway smooth muscle cells with their tissue matrix: implications for contraction. *Proc Am Thorac Soc* **5**:32-39.

Zhou F, Yu T, Du R, Fan G, Liu Y, Liu Z, Xiang J, Wang Y, Song B, Gu X, Guan L, Wei Y, Li H, Wu X, Xu J, Tu S, Zhang Y, Chen H and Cao B (2020) Clinical course and risk factors for mortality of adult inpatients with COVID-19 in Wuhan, China: a retrospective cohort study. *The Lancet* **395**:1054-1062.

Zhou J, Li C, Sachs N, Chiu MC, Wong BH, Chu H, Poon VK, Wang D, Zhao X, Wen L, Song W, Yuan S, Wong KK, Chan JF, To KK, Chen H, Clevers H and Yuen KY (2018) Differentiated human airway organoids to assess infectivity of emerging influenza virus. *Proc Natl Acad Sci U S A* **115**:6822-6827.

Zhou Y, Huang X, Hecker L, Kurundkar D, Kurundkar A, Liu H, Jin TH, Desai L, Bernard K and Thannickal VJ (2013) Inhibition of mechanosensitive signaling in myofibroblasts ameliorates experimental pulmonary fibrosis. *J Clin Invest* **123**:1096-1108.

Zhu L, Fan X, Wang B, Liu L, Yan X, Zhou L, Zeng Y, Poznansky MC, Wang L, Chen H and Du Y (2017a) Biomechanically primed liver microtumor array as a high-throughput mechanopharmacological screening platform for stroma-reprogrammed combinatorial therapy. *Biomaterials* **124**:12-24.

Zhu N, Wang W, Liu Z, Liang C, Wang W, Ye F, Huang B, Zhao L, Wang H, Zhou W, Deng Y, Mao L, Su C, Qiang G, Jiang T, Zhao J, Wu G, Song J and Tan W (2020) Morphogenesis and cytopathic effect of SARS-CoV-2 infection in human airway epithelial cells. *Nat Commun* **11**:3910.

Zhu Y, Chidekel A and Shaffer TH (2010) Cultured human airway epithelial cells (calu-3): a model of human respiratory function, structure, and inflammatory responses. *Crit Care Res Pract* **2010**.

Zhu Y, Wang L, Yu H, Yin F, Wang Y, Liu H, Jiang L and Qin J (2017b) In situ generation of human brain organoids on a micropillar array. *Lab on a chip* **17**:2941-2950.

SUPPLEMENTS

Video S1-4 Airway organoids cultured from four independent NHBE cultures. Videos were recorded using Olympus IX53 microscope equipped with QImaging optiMOS high speed camera at 100 frames/sec.

Video S5 Native primary human bronchial epithelial cells were isolated from human lung tissue. Videos were recorded 72 h after cells were seeded into collagen coated tissue culture plate.

Video S6 Native primary human bronchial epithelial cell brushings were embedded in Matrigel®. Cells generated spheroid-like structures and kept alive after 14 days.

Video S7 Everted cilia in NHBE cells derived airway organoids.

Video S8 Immunofluorescence staining of acetylated tubulin (magenta), CC10 (green), ACE2 (red), and nucleus (blue) in NHBE cells derived organoid.